

Theory of many-body effects in the Kondo-lattice model: Projection-operator method

DISSERTATION

zur Erlangung des akademischen Grades
doctor rerum naturalium
(Dr. rer. nat.)
im Fach Physik

eingereicht an der
Mathematisch-Naturwissenschaftlichen Fakultät I
Humboldt-Universität zu Berlin

von

Herr Dipl.-Phys. Tilmann Hickel
geboren am 19.10.1974 in Leipzig

Präsident der Humboldt-Universität zu Berlin:
Prof. Dr. Jürgen Mlynek

Dekan der Mathematisch-Naturwissenschaftlichen Fakultät I:
Prof. Thomas Buckhout, PhD

Gutachter:

1. Prof. Dr. Wolfgang Nolting
2. Priv.-Doz. Dr. Michael Potthoff
3. Prof. Dr. Roland Zimmermann

Tag der mündlichen Prüfung: 23. September 2005

Abstract

The magnetic behaviour of various materials is due to an indirect interaction of localized magnetic moments, which is based on itinerant electrons in a conduction band. The Kondo-lattice model is an elegant approach for a quantum-mechanical description of this process. It reduces the relevant physics to an intra-atomic exchange interaction of the localized and the itinerant electrons.

The aim of the present work is a detailed investigation of analytic properties of this model. Here, the interplay of two distinct types of particles, described by Fermi operators and quantum-mechanical spin operators respectively, is a major challenge of the considered model. Previous studies have focused on one of these subsystems only. Using the projection-operator method, we suggest an efficient way to describe both subsystems on the same level of approximation. With this method common shortcomings such as the mapping on the Heisenberg model or the use of classical spin operators can be avoided.

An evaluation of the subsystem of itinerant electrons yields an expression for the self-energy, which describes linear and quadratic interaction effects exactly. The densities of states derived with this theory show strong correlation effects. We were able to assess results obtained with less systematic approaches and to predict new many-particle effects.

The application of the projection-operator method to the subsystem of localized magnetic moments results in a detailed analysis of the RPA (random phase approximation). The dependence of magnon spectra and Curie temperatures on model parameters are investigated systematically. Previously unknown drawbacks of the RPA are revealed, which prevent the combination of these results with theories for the itinerant subsystem. Improvements beyond RPA and alternative approximations are discussed.

Keywords:

Kondo lattice, Mori formalism, RPA, magnons

Zusammenfassung

Das magnetische Verhalten zahlreicher Materialien lässt sich auf eine indirekte Wechselwirkung lokalisierter magnetischer Momente, vermittelt durch die Elektronen eines Leitungsbandes, zurückführen. Das Kondo-Gitter-Modell hat sich als elegante Möglichkeit bewährt, diesen Prozess quantenmechanisch zu beschreiben. Es reduziert die Physik auf eine intra-atomare Wechselwirkung der Spins von lokalisierten und itineranten Elektronen.

Die vorliegende Arbeit ist den analytischen Eigenschaften dieses Modells gewidmet. Die besondere Herausforderung des Kondo-Gitter-Modells besteht dabei im Zusammenwirken zweier verschiedener Teilchensorten, beschrieben durch Fermi-Operatoren sowie quantenmechanische Spins. Zahlreiche bisherige Untersuchungen haben sich in der Regel nur auf eine der beiden Teilchensorten konzentriert. Mit der Projektions-Operator-Methode stellen wir nun eine systematische und effektive Möglichkeit vor, beide Teilsysteme in gleicher Qualität zu behandeln. Die in dieser Form erstmalige Anwendung der Projektions-Operator Methode auf das Kondo-Gitter-Modell kommt ganz ohne eine Abbildung auf das Heisenberg-Modell oder ein Zurückgreifen auf klassische lokalisierte Spins aus.

Die Auswertung des Teilsystems der itineranten Elektronen führt auf einen Ausdruck für die Selbstenergie, der lineare und quadratische Effekte in der Wechselwirkung exakt beschreibt. Die resultierenden Zustandsdichten weisen starke Korrelationseffekte auf. Deren Untersuchung dient sowohl der Bestätigung von Ergebnissen weniger systematischer Zugänge als auch dem Aufzeigen neuer Vielteilchen-Phänomene.

Die Anwendung der Projektions-Operator-Methode auf das System der lokalisierten Momente führt zwangsläufig zu einer Analyse der häufig verwendeten RPA (random phase approximation). Zu diesem Zweck werden die Magnonenspektren und die Curie-Temperaturen systematisch untersucht. Dabei treten bisher unbekannte Schwachpunkte der RPA zu Tage, die auch die Kombination mit Theorien für das itinerante Teilsystem verhindern. Verbesserungen und Alternativen zur RPA werden diskutiert.

Schlagwörter:

Kondo-Gitter-Modell, Projektions-Operator-Methode, RPA, Magnonen

Contents

1	Motivation	1
1.1	The inevitable reduction	1
1.2	The challenges of the Kondo-lattice model	2
1.3	The advantages of the projection-operator method	5
1.4	The intention of the present work	5
2	Current knowledge of the Kondo-lattice model	7
2.1	Many-body Hamiltonian	7
2.2	Exact statements	9
2.3	Approximative theories	14
3	The projection-operator method	23
3.1	Dynamics within the Liouville space	23
3.2	Separation of time scales	25
3.3	Expansion using continued fractions	27
3.4	Application to the Hubbard model	31
4	The subsystem of itinerant carriers	37
4.1	The ferromagnetically saturated semiconductor	37
4.2	The zero-bandwidth limit	48
4.3	Weak-coupling approach to the KLM	51
4.4	The modified perturbation theory	60
4.5	Possibility of ferromagnetic order	72
5	The subsystem of local moments	81
5.1	Application of the projection-operator method	81
5.2	Alternative POM for the subsystem of local moments	87
5.3	The random-phase approximation	98
6	Concluding remarks	113
6.1	Assessment of the POM	113
6.2	Weak-coupling results for the KLM	116
6.3	Perspectives	119
A	Basic operator relations	133

B	A remarkable equality	135
C	The Laplace transformation	137
	C.1 A special Fourier transformation	137
	C.2 Application to the Mori equation	138
D	Details of calculations in Sec. 4.1	139
E	Depolarization effects in the conduction band	143
	E.1 The conventional SOPT	143
	E.2 The SOPT relative to Hartree-Fock	145
	E.3 Conclusion	146
F	Details of calculations in Sec. 5.1	149
G	The POM with a two-dimensional basis	153

List of Figures

2.1	Curie temperature vs. coupling strength in MCDA	18
4.1	DOS in mean-field approximation	52
4.2	DOS in second-order perturbation theory	55
4.3	Possibilities for complete polarization	56
4.4	SOPT with Brillouin function	57
4.5	conventional SOPT vs. SOPT-HF	59
4.6	Comparison of MPT approaches for moderate J	66
4.7	Comparison of MPT approaches for large J	68
4.8	Dependence on band occupation for sc MPT	69
4.9	Dependence on magnetization for sc MPT	70
4.10	Dependence on magnetization for half-filling	71
4.11	Behaviour of QDOS close to exact limits	73
4.12	Behaviour of QDOS close to exact limits	74
4.13	Ground state energy	75
4.14	Curie temperature vs. coupling strength in SOPT	78
5.1	MPT with mean-field input for $\langle S^z \rangle$	83
5.2	Magnetization for two-dimensional basis	93
5.3	Magnon dispersion for the RPA	99
5.4	Curie temperatures for the spin wave approximation	102
5.5	Temperature dependent magnon dispersions	103
5.6	Effect of the Stoner continuum in various directions	103
5.7	RPA magnon dispersion for different magnetizations	104
5.8	Spectral density for negative magnon energies	105
5.9	Magnetization and Curie temperature within the RPA	106
5.10	Dispersion of Lindhard function	108
5.11	Spin Waves with different input for self-energy	111

Chapter 1

Motivation

1.1 The inevitable reduction

Most fascinating about physics is its purpose to describe complex processes in simple terms. It distinguishes a physicist from other scientists that he or she is able to reduce a given system to its most relevant aspects, rather than taking all details into consideration. *The earth, for example, is a system of so many parameters, that it is impossible to simultaneously grasp everything what happens on it. However, in order to explain the motion of this planet around the sun, the physicist reduces everything on earth to a single mass point. The gravitational law and some simple theorems are sufficient to predict the relevant parameters, e.g., the period of a year.*

Such a reduction has two major advantages: It is the prerequisite for the calculability of complex processes and secondly it implies universality. *If the earth is reduced to a mass point, there is nothing special about it any more. Hence, doing the same with the moon, one can readily understand how long it takes for the latter to orbit around the earth. There is no need for new considerations or theorems. We just have to accept that it is the same basic law which applies to both cases.*

It goes without saying, that the degree of simplification has to be related to a physical question. *In order to explain tides on earth, it does not make sense to consider this planet as a mass point. Similarly, for an understanding of a solar eclipse a problem of three celestial bodies has to be solved; and for a prediction of its starting time the radii of these bodies are also relevant.*

The problems of gravitational astronomy might be considered relatively simple ones, due to our knowledge of their straightforward solutions. By contrast, the phenomenon of magnetism, the spontaneous collective order of magnetic moments in some materials, is much more exciting for us. Despite the fact, that it has inspired mankind for thousands of years, there is still no completely satisfactory theory available. This alone, makes magnetism very attractive for theoretical research. In addition, magnetic properties are of increasing importance for technology and computer applications. Modern data storage devices, such as MRAMs, make explicitly use of magnetic effects. The functionality and performance of these devices could be further enhanced, if more were known about the processes that lead to magnetic order.

Some steps towards an understanding of the phenomenon of spontaneous magnetiza-

tion have already been taken. A lot of papers and several outstanding books on this topic have been published. Now it is known, that the effect is necessarily of quantum mechanical origin (Bohr-van Leeuwen theorem [110]). More importantly, there is no doubt that this phenomenon is a many-particle effect. The high number of contributing particles is the reason for the complexity of magnetism. For its description, simplifications cannot be avoided. In fact, in no other area of physics has the reduction to simple models been performed as consequently as in many-particle physics.

The requirement, that the many-body character must not be destroyed by the approximation, is a major difference to the two-body problem of the earth and the sun. The fundamentals of quantum statistics allow a subdivision into classes of indistinguishable particles. Nevertheless, there are a lot of interactions among particles of the same class and between particles of different classes. This is the point, where simplifications can be performed. In solid state physics the Coulomb attraction and repulsion is the only important interaction in many cases. Density functional theory is one way of treating this interaction, retaining its spatial dependence. In the theory of strongly correlated electrons, important for an understanding of magnetism, another approach is pursued.

The Hubbard model is a typical example of a Hamiltonian for strongly correlated electrons. Hubbard [54, 55] claimed that for some materials the repulsion of two electrons with opposite spin located on the same atom of a regular lattice is stronger than any other energy of the system. Therefore, a positive energy, called U , is allocated to this process. No further interaction is considered, which is, of course, a drastic oversimplification. There is little doubt that the model is too simple to faithfully describe actual solids [156].

Nevertheless, the Hubbard model fulfills two important criteria: On the one hand, it is believed to exhibit various interesting phenomena including the one we are interested in: it exhibits spontaneous ferromagnetic order. It is commonly accepted, that principle mechanisms governing the behaviour of the Hubbard model also play an important role in a certain class of real materials. In this sense, understanding the physics of the Hubbard model is a prerequisite for getting an idea of the origin of itinerant ferromagnetism and for purposefully and meaningfully modify these materials. On the other hand, despite its simplicity, the Hamiltonian is not exactly solvable. Therefore, generations of theoretical physicists had their “fun” in developing new approximation schemes for this model. As for other famous problems (Fermat’s last theorem, Ising model, . . .) the techniques developed were of use for many more applications other than the Hubbard model.

1.2 The challenges of the Kondo-lattice model

The Kondo-lattice model (KLM) embodies a similar universality as the Hubbard model. Again, its main purpose is the understanding of ferromagnetism in a certain class of materials. However, the focus is on another process. Instead of attributing ferromagnetism to the Coulomb repulsion directly, a Hund’s rule coupling is considered the most important interaction.

Hund’s rules determine the electron occupation of the orbitals of an atom. According to these rules, a certain spin orientation of an electron that enters a partly filled shell is energetically preferred. This process can be modelled: The complex system of the atom

is reduced to a single quantum mechanical operator, the localized spin. The interaction energy of an additional electron is solely determined by the orientation of its spin with respect to the localized spin of the atom.

Besides the dispersion of the itinerant electrons in the conduction band, this Hund's rule coupling is the only physical process considered in the Kondo-lattice model. Mathematically, it is described by an intra-atomic exchange interaction. The model does not include interactions between the localized electrons or Coulomb interaction within the conduction-electron band. It reduces the multiband scenario to a single s-band. It also neglects a possible \mathbf{k} -dependence of the coupling constant. It does not take into account superexchange of localized moments or other possible inter-atomic interaction mechanisms. It does not incorporate anisotropy or disorder.

The only prerequisite of the KLM is the existence of these two groups of electrons: localized electrons in a partly filled shell and itinerant electrons in a conduction band. A microscopic explanation why this is an appropriate description of transition metals can be found in early works of Zener [179, 180], Anderson and Hasegawa [3] or Vonsovskij and Izyumov [164]. Despite its oversimplified structure, the Kondo-lattice model has been used successfully for a quantitative description of the magnetism in classical local moment metals (Gd, Dy, Tb) as well as in magnetic semiconductors (EuO, EuS, EuTe, ...) [143, 61, 102].

The KLM has already been applied to many other materials. We do not wish to repeat more detailed overviews given elsewhere [115, 92]. However, the topics that have attracted substantial attention are briefly mentioned here:

- Already since the end of the 1970s heavy-fermion systems, which are characterized by large values of the Sommerfeld coefficient and the Pauli susceptibility (Refs. in [44, 37]), have been discussed intensively in context of the Kondo-lattice model.
- Based on bandstructure calculations for Heusler alloys, de Groot [22] predicted the existence of half-metallic ferromagnets in 1983. These are characterized by metallic majority-spin and semiconducting minority-spin electrons (Refs. in [58]). One year later a shape-memory effect was observed in Heusler alloys [168]. Since these alloys are ideal local moment systems [75, 179], the Kondo-lattice model is well suited for studying the magnetism in both cases.
- Towards the end of last century, a lot of effort was expended on describing manganese perovskites (Refs. in [39]). The interest has arisen due to the discovery of the colossal magneto-resistance effect (Refs. in [62]) in these materials.

In recent years the KLM experienced a revival due to the observation of high Curie temperatures in semiconductors that have been doped with a few percent of magnetic atoms [121, 122]. This discovery inspired the idea of using diluted magnetic semiconductors (DMS) for new spin-based electronic devices [170, 123, 120]. A "diluted" Kondo-lattice model was used to predict most promising materials for room temperature ferromagnetism [24]. Many improved theoretical approaches have already been published (Refs. in [74, 21]). It turned out that for a realistic description of DMS, further effects such as disorder and spin-orbit coupling are important. Nevertheless, there is no doubt, that the

magnetic order in DMS is due to the indirect interaction of the doped magnetic moments via itinerant conduction electrons. Therefore, a proper approximation of this interaction is essential. Many authors use a mean-field theory for the determination of the Curie temperature. Any improvement of the mean-field description should first of all be applied to the translational invariant model. Only if such a system is completely understood is it possible to deal with the additional challenge of dilution and disorder.

Hence, we consider it important to keep the Kondo-lattice model as it is: the simplest possible structure incorporating a coupling of localized and itinerant electrons. It is not our intention to introduce further parameters for fitting some experimental data. Similar to the situation of the Hubbard model, we believe that it is the universality of the exchange coupling and the abundance of physical phenomena, which make this model so interesting.

The Kondo-lattice model also fulfills the second criterion mentioned in connection with the Hubbard model: It is sufficiently complex, to evade an exact solution. It is our impression, that much less is known about its analytical properties than for the Hubbard model. An overview of known results is presented in Chap. 2. However, a particular challenge of the Kondo-lattice model can already be emphasized: Since being confronted with two subsystems of electrons, at least twice the effort has to be invested to obtain the same quality of approximation as for the Hubbard model. In the literature most approaches avoid this effort, only focus on one subsystem and treat the second in a very simple approximation. The aim of our work is to provide a formalism which treats both subsystems equally well.

The second mathematical difficulty of the KLM is related to the nature of localized spins. Compared to Fermi operators, these spins are described using a much more difficult algebra, defined by the commutation relations. Therefore, many theorems and methods, that work well for the Hubbard model, are not applicable to the Kondo lattice. In particular this concerns diagrammatic perturbation theory. The summation rules for diagrams are based on Wick's theorem which is only defined for Fermions and Bosons. There are some trials of an extension of this method to spin operators reported in the literature [60, 43], but none of them has become an accepted formalism.

A common loophole is a classical treatment of localized spins. Based on this assumption, substantial results have been obtained using dynamical mean field theory [39, 45] or Monte Carlo techniques [72]. However, this might be considered as dealing with a different model. Many investigations have shown, that the quantum-mechanical character of the spins has indeed a substantial impact on the electronic properties of the materials concerned [25, 96]. Therefore, an analytical and numerical treatment of the KLM, which retains the quantum nature of spins, should be aspired to.

Another possibility suggested in the literature [114] is the mapping of the local-moment subsystem onto an effective Heisenberg model. This implies the danger to observe magnetic properties of this model, rather than of the KLM. Furthermore, there are a few attempts to restrict the Green's function hierarchy of equations of motion by a decoupling scheme. From an analytical point of view, such a kind of approximation always suffers from a lack of controllability. To overcome these shortcomings is an ambition of our alternative method.

1.3 The advantages of the projection-operator method

The projection-operator method (POM), also known as the Mori-formalism, incorporates all the properties we would like to have for an approximation technique. We wish to highlight some of the advantages of this method, with the details to be explained in the various chapters of this thesis.

The most important concept is the projection of the dynamics onto a relevant subspace. Therefore, as compared to other approximation methods, it takes seriously the philosophy mentioned at the beginning of reducing the complexity of a system. In this sense, it is a natural continuation of a simplification that has already been started with the construction of the model. The subspace considered to be relevant, can be continuously enlarged. Mathematically, this results in a continued fraction for the one-particle Green's function. The approximation is controlled in the sense that the length of the continued fraction, or similarly the size of the considered subspace, can be fixed. This does not automatically imply a Taylor expansion in the coupling constant. Nevertheless, we treat the method such, that the results are correct in second order perturbation theory.

In contrast to Wick's theorem, the POM is not limited to a certain kind of operator. It can be applied equally well to spin operators that obey the commutation relations of angular momentum. This offers the chance, to treat the localized and the itinerant subsystem of the Kondo-lattice model with the same technique. There is another property of the POM, that makes its application so attractive: It allows for a variety of different approaches by modifying the relevant subspace and the way, in which it is enlarged. When "playing" with these possibilities, one gets a feeling for the analytical properties of the KLM. A further advantage of the POM is the compact notation of all necessary transformations. Although, this is first of all an aesthetic aspect, we believe that there is a relation between the "beauty" and the quality of a theory.

Using the projection operator method we introduce a technique to many-body theory which until now has mainly been applied to transport theory. There are already a few applications to the Hubbard [16] and the Heisenberg model [11]. However, it is not yet an established alternative to widely used decoupling techniques for the hierarchy of equations of motion of retarded Green's functions. In this thesis we would like to emphasize the advantages and limitations of the projection operator method, which shall be applied to the Kondo-lattice model for the first time.

1.4 The intention of the present work

From the previous remarks it is clear, that the intention of this thesis is twofold: On the one hand, we are going to evaluate the projection-operator method as a technique to treat many-body Green's functions. On the other hand, we would like to provide an insight into the analytical properties of the KLM.

In order to fulfill our first objective, the philosophy of the projection-operator method will be thoroughly explained in Chap. 3. For a deeper understanding we consider it equally important to demonstrate several variations of this technique by calculating some explicit examples. A couple of exactly solvable limits of the KLM are very appropriate

for this purpose. For example, in Sec. 4.1, the motivation for deriving the result for the ferromagnetically saturated semiconductor in several different ways is to illustrate how the projection-operator method can be modified for a better generalization, rather than to ascertain that no mistake has occurred in the calculations.

The POM can be used in order to study several aspects of the KLM. For this thesis we have decided to focus on its weak-coupling behaviour for a ferromagnetic Hund's coupling. Our aim is to find an expression for the Green's function, where the memory matrix is exact up to second order in the coupling constant. This approach is particularly suited for a comparison with the widely used mean-field approximations, which is of linear order. Using the POM, we will show that it is indeed possible to treat both subsystems of the KLM on the same footing. Nevertheless, due to their different physical properties the subsequent analysis of the obtained expressions depends on the subsystem. For the subsystem of itinerant conduction electrons, the second-order result (Sec. 4.3) will be improved such that exactly solvable limiting cases of the KLM are fulfilled (Sec. 4.4). Following the labelling of a similar procedure for the Hubbard model we call this approach the modified perturbation theory (MPT). Chapter 5 is devoted to the subsystem of localized moments. Here, already the second-order result (Sec. 5.1) is too complicated for a numerical evaluation. Therefore, a further simplification is discussed (Sec. 5.2). The result, which is known from decoupling techniques as the random phase approximation (RPA), is evaluated in Sec. 5.3.

For an explanation of the POM a substantial amount of formulae cannot be avoided. However, for the sake of readability we will try to limit their number such that an interested reader can still follow the gist of the calculation. Whenever it is required to provide intermediate steps, we will shift this information to an appendix. The same applies to the discussion of aspects, which do not belong to the main stream of this thesis. Furthermore, we have abandoned explanations concerning the basics of many-body theory and Green's function techniques. For more information on these issues the interested reader is referred to standard text books [107, 85, 40].

We will use Chap. 6 to summarize the systematic investigation of the Kondo-lattice model based on the projection operator method. We will conclude, that the POM is indeed an interesting and compact formalism to investigate the properties of the KLM and other many-body problems. Our hope is to convey this impression throughout the whole thesis and to share with the reader the pleasure of using this method. A greatest success of this thesis would be to inspire someone else by the work presented here into continuing the investigations and answering the outstanding questions.

Chapter 2

Current knowledge of the Kondo-lattice model

The physical motivation for the Kondo-lattice model (KLM), its assumptions and applications, have already been introduced in Chap. 1. Now, in order to perform calculations which employ temperature-dependent statistics, the model has to be implemented using a Hamiltonian. The subsequent approximate evaluation is going to be guided by mathematical aspects. Accordingly, the following two questions will dominate this chapter: Under which conditions does an exact solution of this Hamiltonian exist? For all other cases, which strategies are already available to obtain approximate solutions? Whatever the approach, at the end we will always try to draw physical conclusions from these results.

2.1 Many-body Hamiltonian

The desired Hamiltonian has to combine the effect of two different groups of electrons, itinerant and localized. The physics of s-conduction electrons is most effectively described in second quantization. The first (Wannier) representation of their kinetic energy

$$H_s = \sum_{i,j} \sum_{\sigma} T_{ij} c_{i\sigma}^{\dagger} c_{j\sigma} = \sum_{\mathbf{k}} \varepsilon_{\mathbf{k}} \hat{n}_{\mathbf{k}\sigma} \quad (2.1)$$

has a very physical interpretation: an electron with spin σ , which is annihilated via $c_{j\sigma}$ at a lattice site \mathbf{R}_j , hops with a certain probability T_{ij} to an adjacent site \mathbf{R}_i without changing its spin. In fact, the itinerant electron cannot be allocated to certain lattice sites, but rather it belongs to different Bloch states of energy $\varepsilon_{\mathbf{k}}$. This is expressed by the second (Bloch) representation in (2.1), where $\hat{n}_{\mathbf{k}\sigma}$ denotes the occupation number operator. The transformation is given by:¹

$$T_{ij} = \frac{1}{N} \sum_{\mathbf{k}} \varepsilon_{\mathbf{k}} e^{i\mathbf{k}(\mathbf{R}_i - \mathbf{R}_j)}, \quad (2.2)$$

with N being the number of lattice sites.

¹For a list of all Fourier transformations see appendix A.

For localized electrons, on the other hand, the hybridization between neighbouring atoms is negligible. The combined effect of electrons at a certain lattice site \mathbf{R}_i is commonly described by quantum-mechanical spin-operators \mathbf{S}_i . Zener [179, 180] recognized that a Heisenberg-like interaction between these spins is not able to explain the magnetic behaviour of transition metals. Instead Vonsovskij and Izyumov [164] considered an intra-atomic interaction

$$H_{sf} = -\frac{J}{\hbar} \sum_i \boldsymbol{\sigma}_i \cdot \mathbf{S}_i \quad (2.3)$$

between the spins of the itinerant electrons $\boldsymbol{\sigma}_i$ and the localized spins \mathbf{S}_i . This is the Hund's rule coupling mentioned in Chap. 1, which is either called *sf*- or *sd*-interaction. With the conduction electron bandwidth W and the coupling constant J we therefore have two energy scales² in the system. Following Zener's terminology [180, 3] the combined Hamiltonian $H_s + H_{sf}$ is nowadays labelled *double exchange* if the limit $J \gg W$ is considered. This is a valid assumption for manganites [76, 27, 39].

In the opposite limit $J \ll W$ Kasuya [66] and Yosida [177] were able to show perturbatively that the ground state of $H_s + H_{sf}$ has again the structure of a Heisenberg Hamiltonian. This indirect spin-spin coupling is named after Rudermann and Kittel [138] and the above mentioned physicists the RKKY-mechanism and is often used in an approximate description of experimental results.

However, for general J a convincing name for this Hamiltonian has still not been established in the literature. One can formally derive the Kondo model [73] by an exact transformation [146] of the Single Impurity Anderson Model [2] in the limit of small hybridization energies or large on-site Coulomb repulsions [154]. This transformation yields negative exchange interactions J and describes a situation of a single magnetic impurity in a non-magnetic host. It established *Kondo physics* as a separate branch in condensed matter physics [48], a topic closely related to the concept of heavy fermions [44, 37].

Nevertheless, the periodic extension of this Hamiltonian,

$$H_{\text{KLM}} = H_s + H_{sf} = \sum_{i,j} \sum_{\sigma} T_{ij} c_{i\sigma}^{\dagger} c_{j\sigma} - \frac{J}{\hbar} \sum_i \boldsymbol{\sigma}_i \cdot \mathbf{S}_i, \quad (2.4)$$

for evident reasons often called *Kondo-lattice model*, is usually – in particular if positive values of J are considered – devoted to a different set of physical problems. The magnetic behaviour of classical local moment metals (Gd, Dy, Tb) as well as that of magnetic semiconductors (EuO, EuS, EuTe, ...) is believed to be dominated by such an indirect exchange interaction via conduction electrons [79, 165]. Indeed, the Kondo-lattice model has successfully been applied to these materials [143, 61, 102].

The physics of the model, most clearly seen in the notation

$$H = \sum_{i,j} \sum_{\sigma} T_{ij} c_{i\sigma}^{\dagger} c_{j\sigma} - \frac{J}{2} \sum_i \sum_{\sigma} \left(z_{\sigma} S_i^z \hat{n}_{i\sigma} + S_i^{\sigma} c_{i-\sigma}^{\dagger} c_{i\sigma} \right), \quad (2.5)$$

²To be precise, the notation (2.3) implies that only $J\hbar$ has the dimension of an energy. In our work this is implicitly meant, whenever we identify J with an energy.

with $z_\sigma = \delta_{\sigma\uparrow} - \delta_{\sigma\downarrow}$ and $S^\sigma = S^x + iz_\sigma S^y$, can be considered from two perspectives: On the one hand, on their way through the lattice conduction electrons experience an Ising-type potential, caused by the z -component of the localized spins. Additionally, they are scattered by local moments such that their spin flips. Both processes drastically affect electrical conductivity and the density of states within the conduction-electron band. The localized moments, on the other hand, try to minimize their energy in the bath of electrons. There is a possibility of an indirect communication between them, since the itinerant electrons are polarized whenever they pass a lattice site and act as carriers of information. This can lead to magnetically ordered states, magnons, spin waves etc.

A problem of most many-body approaches to the KLM is the consideration of only a single Green's function. This automatically implies that the focus is on only one of the above mentioned perspectives. However, due to the mutual dependence of both subsystems, a combination of results from both perspectives is essential for a complete description of the KLM.

2.2 Exact statements

Despite its simplicity, the Kondo-lattice model cannot be solved exactly. For necessary approximations the knowledge of exact statements for the Kondo-lattice model is particularly important [49]. They can, a priori, serve as a starting point for simplifications and are, a posteriori, essential for an assessment of these approaches. It is clear that only a constrained model has an exact solution. Therefore, we will discuss some meaningful constraints on the KLM and provide the principle structure of exact solutions.

Constraints on model parameters

In (2.4) the model parameters are the hopping amplitudes T_{ij} and the coupling constant J . If the latter is set to zero, the solution is the trivial result of free electrons. Even the first order (Hartree-Fock) correction in J does not give rise to any correlation effects. As can be seen from the retarded Green's function

$$G_{\mathbf{k}\sigma}^{(\text{MF})}(E) = \frac{\hbar}{E - \varepsilon_{\mathbf{k}} + \frac{1}{2}Jz_\sigma \langle S^z \rangle + i0^+}, \quad (2.6)$$

it yields a rigid spin-dependent shift of the free density of states.

The situation is much more interesting, if the hopping T_{ij} of the conduction electrons is suppressed. Depending on whether the Wannier or the Bloch representation of (2.1) is considered this limit is called *atomic* or *zero bandwidth limit*, respectively. As expected for a finite system, the excitation spectrum is discrete. The mathematical implication is a closed system of equations of motion. For the single-electron Green's function

$$G_\sigma(E) = \langle\langle c_\sigma; c_\sigma^\dagger \rangle\rangle_E = \hbar \sum_{i=1}^4 \frac{\alpha_{i\sigma}}{E - E_i + i0^+} \quad (2.7)$$

a short, but non-trivial evaluation yields four energy poles and corresponding spectral

weights [112]:

$$\begin{aligned}
 E_1 &= -\frac{1}{2}J\hbar S & \alpha_{1\sigma} &= \frac{1}{2S+1} \left\{ S + 1 + \frac{z_\sigma}{\hbar} \langle S^z \rangle - \frac{1}{\hbar} p_\sigma - (S + 1) \langle \hat{n}_{-\sigma} \rangle \right\} \\
 E_2 &= +\frac{1}{2}J\hbar(S + 1) & \alpha_{2\sigma} &= \frac{1}{2S+1} \left\{ S - \frac{z_\sigma}{\hbar} \langle S^z \rangle + \frac{1}{\hbar} p_\sigma - S \langle \hat{n}_{-\sigma} \rangle \right\} \\
 E_3 &= -\frac{1}{2}J\hbar(S + 1) & \alpha_{3\sigma} &= \frac{1}{2S+1} \left\{ S \langle \hat{n}_{-\sigma} \rangle + \frac{1}{\hbar} p_\sigma \right\} \\
 E_4 &= +\frac{1}{2}J\hbar S & \alpha_{4\sigma} &= \frac{1}{2S+1} \left\{ (S + 1) \langle \hat{n}_{-\sigma} \rangle - \frac{1}{\hbar} p_\sigma \right\}.
 \end{aligned} \tag{2.8}$$

The correlation function $\langle \hat{n}_{-\sigma} \rangle$ as well as $p_\sigma := z_\sigma \langle S^z \hat{n}_{-\sigma} \rangle - \langle S^{-\sigma} c_\sigma^\dagger c_{-\sigma} \rangle$ can be calculated selfconsistently. Only the magnetization $\langle S^z \rangle$ remains as an external parameter in the sense that it cannot be obtained from the involved Green's functions using a spectral theorem. However, the assumption of a $\langle S^z \rangle$ -value different from zero leads to inconsistencies for the other correlation functions [49]. This agrees with the Mermin-Wagner theorem [90], which applies in less than three dimensions (see p. 12).

For a more physical description, the atomic-limit result can be used in form of an alloy analogy [55] as input for a CPA (coherent-potential approximation). As a consequence, the δ -peaks in the density of states are replaced by four energy bands. Ferromagnetic order is allowed [109, 27, 96]. However, such an approach has several shortcomings. For example, it does not consider repeated spin exchange with the local-moment subsystem. Furthermore, this approach is not appropriate for the description of antiferromagnetic order within the localized moment subsystem.

A natural extension of the atomic limit is the analytical calculation of a two-site cluster. With a non-zero intersite hopping integral, a motion of electrons between different lattice sites is allowed. The resulting finite energy dispersion is a first step towards bulk material. Further, two lattice sites can serve as a limit for an antiferromagnet. We were able to obtain an exact and analytical solution for all Green's functions related to a two-site cluster [49, 51]. As the full solution consists of more than 100 energy poles, this result can already be used to study the formation of bands and investigate the dependence of spectral weights on system parameters.

Nevertheless, it was also apparent from these calculations that a two site Kondo-lattice Hamiltonian is at the limit of what can be done analytically. On the one hand, the step from one site (4 energy poles) to two sites (102 energy poles) was connected with a massive increase of mathematical effort. On the other hand, the solution obtained shows such a high level of complexity that an evaluation is only sensible if the cluster is again limited to some special situations.³ Hence, we do not believe that further constraints on model parameters will provide any additional insight.

Constraints on expectation values

The two most important expectation values that enter the calculations are the electron occupation number $\langle \hat{n}_\uparrow + \hat{n}_\downarrow \rangle$ and the magnetization $\langle S^z \rangle$. For certain physical situations both values can be expressed by fixed c-numbers.

For many materials of interest for experimental investigations each of the local-moment atoms provides a single itinerant electron ($\langle \hat{n}_\uparrow + \hat{n}_\downarrow \rangle = 1$) leading to a half-filled con-

³For example, the case of a two-site cluster with an empty conduction band (6 energy poles) is instructive.

duction band. Usually, these atoms also form a bipartite lattice.⁴ For such situations there exists the exact theorem [150, 158, 159] that the ground state is unique and a spin singlet.⁵ The proof is based on the spin-reflection positivity initially proposed for the Hubbard model [81] and has the essential precondition that the local moment is formed by just one electron. Hence, the additional limitation $S = 1/2$ is assumed.

With the class of magnetic semiconductors the KLM describes materials particularly important with respect to spintronics applications. For these materials the conduction-electron band is almost empty ($\langle \hat{n}_\uparrow + \hat{n}_\downarrow \rangle = 0$). If ferromagnetic saturation ($\langle S^z \rangle = \hbar S$) is assumed at $T = 0$ K, one can evaluate the eigenenergies of single-electron excitations [149, 151]. Hence, exact expressions for the one-electron Green's functions can be provided [107, 113]. For an excess electron with a spin direction parallel to the local-moment magnetization we obtain⁶

$$G_{\mathbf{k}\uparrow}(\omega) = \frac{\hbar}{\hbar\omega - \varepsilon_{\mathbf{k}} + \frac{1}{2}J\hbar S}. \quad (2.9)$$

The equivalence to the mean-field result (2.6) is due to the fact that spin-flip processes are not possible in this configuration. If $\rho_0(E)$ denotes the free density of states (DOS), the \uparrow -electron can propagate according to the DOS $\rho_\uparrow(E) = \rho_0(E + \frac{1}{2}J\hbar S)$ as a quasi-free particle through the lattice.

The situation is completely different, if the single excess electron in the otherwise empty conduction band has its spin direction antiparallel to the local-moment magnetization axis. This yields a Green's function

$$G_{\mathbf{k}\downarrow}(\omega) = \frac{\hbar}{\hbar\omega - \varepsilon_{\mathbf{k}} - \Sigma_\downarrow(\omega)} \quad \text{with} \quad \Sigma_\downarrow(\omega) = \frac{J}{2} \hbar S \left(1 + \frac{J\hbar B(\omega)}{1 - \frac{1}{2}J\hbar B(\omega)} \right). \quad (2.10)$$

For the evaluation of the lifetime of the corresponding quasi-particle the imaginary part

$$I_B(E + i0^+) = \Im B(\omega) = -\pi\rho_0(E + \frac{1}{2}J\hbar S) = -\pi\rho_\uparrow(E) \quad (2.11)$$

of the function

$$B(\omega) = \frac{1}{N} \sum_{\mathbf{q}} \{ \hbar\omega + \frac{1}{2}J\hbar S - \varepsilon_{\mathbf{q}} \}^{-1} \quad (2.12)$$

is important. There are two possibilities: If the energy of the \downarrow -electron lies within a region where the \uparrow -electrons have a finite density of states, then it will be damped due to the possibility of spin-flip processes. The imaginary part of the self-energy

$$\Im \Sigma_\downarrow(\omega) \sim \rho_\uparrow(E) \quad (2.13)$$

has a finite value and hence the DOS for the \downarrow -electrons is non-zero. This part of the spectrum is called the *scattering part*. However, for energies outside the $\rho_\uparrow(E) \neq 0$ region

⁴ A bipartite lattice is a lattice that can be divided into two sublattices such that for each site nearest neighbours belong to the other sublattice.

⁵To be precise, this is for $J > 0$ only true, if the number of sites N_A of sublattice A is equal to the corresponding number N_B of sublattice B . Otherwise $S_{\text{tot}} = |N_A - N_B|$.

⁶From this point on we will repeatedly use the complex variable $\omega = E/\hbar + i0^+$ in our equations. This includes a change to frequency representation, which is more common for the projection-operator formalism.

the \downarrow -electrons will have a non-zero DOS, if

$$\Im G_{\mathbf{k}\downarrow}(\omega) = \delta(\hbar\omega - \varepsilon_{\mathbf{k}} - \Re \Sigma_{\downarrow}(\omega)) \iff \rho_{\downarrow}(E) = \rho_0(E - \Re \Sigma_{\downarrow}(\omega)) \quad (2.14)$$

does not vanish. For these energies with $\Im \Sigma_{\downarrow}(\omega) = 0$ the corresponding quasi-particle has an infinite lifetime. We call this a *magnetic polaron*, since on its way through the lattice this conduction electron carries a cloud of magnons, which are virtually emitted and absorbed, with it.⁷ We will discuss the exact result in more detail in Sec. 4.1, when it will be derived explicitly using the projection-operator method.

Constraints on lattice dimensions

The reduction of dimensionality is apparently attractive for an investigation of the KLM [159, 160], since exact diagonalization and density matrix renormalization group techniques can be applied. Nevertheless, provided no anisotropy is included, the Mermin-Wagner theorem [90] also applies to the KLM [23]. Therefore, for $T \neq 0$ K the KLM shows no spontaneous magnetization in less than three dimensions. This limits the value of another exact statement on the one-dimensional KLM: Sigrist et al. [152] have proven the existence of a ferromagnetic ground state ($T = 0$ K) in the strong-coupling limit for all conduction electron densities. To our knowledge, the investigations in 1D and 2D have not lead to further rigorous results. In contrast to the impurity problem, even the Bethe ansatz is apparently not successful for the 1D lattice.

The opposite limit of infinite dimensionality is even more interesting, since one can prove rigorously that in this case the self-energy is local [42, 91]. Nevertheless, the locality of the self-energy is not sufficient to provide its exact expression. In addition, within the scheme of a dynamical mean-field theory (DMFT) it is necessary to solve the impurity problem (see p. 20). For an empty conduction band, there seems to be an analytical solution of this problem [139]. However, the generalization of this approach to arbitrary band occupations is unlikely. Instead, many authors [39, 45] combine DMFT with the assumption of classical local spins. These results will be discussed in Sec. 2.3.

The concept of dimensionality becomes meaningless, if an infinite range hopping of the form $T_{ij} = \hat{T} \forall i \neq j$ is assumed. This exceptional situation allows for an exact solution of the ground state energy for arbitrary band occupations [166]. For the applied cluster expansion of the grand-canonical potential a fermionization of the local spin operators is necessary. This limits the applicability to $S = 1/2$. It remains unclear if the main result, a metal-insulator phase transition at half filling, is an artifact of the unphysical nature of the hopping.

Constraints on the energy scale

Retarded Green's functions can be defined in several ways [107, 85]. The version based on the spectral density function $A_{\mathbf{k}\sigma}(E)$ implies a high-energy expansion of the Green's

⁷ The physical situation is comparable to the well-known concept of polarons in semiconductors [36], where electrons are surrounded by a virtual cloud of phonons.

function

$$G_{\mathbf{k}\sigma}(\omega) = \int_{-\infty}^{+\infty} dE' \frac{A_{\mathbf{k}\sigma}(E')}{E - E' + i0^+} = \frac{1}{\hbar\omega} \sum_{n=0}^{\infty} \int_{-\infty}^{+\infty} dE' \left(\frac{E'}{\hbar\omega} \right)^n A_{\mathbf{k}\sigma}(E') = \hbar \sum_{n=0}^{\infty} \frac{m_{\mathbf{k}\sigma}^{(n)}}{(\hbar\omega)^{n+1}}. \quad (2.15)$$

The spectral moments of $A_{\mathbf{k}\sigma}(E)$ thus defined have the integral representation

$$m_{\mathbf{k}\sigma}^{(n)} = \frac{1}{\hbar} \int_{-\infty}^{+\infty} dE E^n A_{\mathbf{k}\sigma}(E). \quad (2.16)$$

What makes this expansion so interesting is the fact, that these moments can be calculated analytically up to an (in principle arbitrary) order n [107]. This is possible by means of an equation of motion, leading to the following commutators with the Hamiltonian

$$m_{\mathbf{k}\sigma}^{(n)} = m_{\mathbf{k}\sigma}^{(n,x)} = \frac{1}{N} \sum_{i,j} e^{i\mathbf{k}(\mathbf{R}_i - \mathbf{R}_j)} \left\langle \left[\underbrace{[\dots [c_{i\sigma}, H]_-, \dots, H]_-}_{(n-x)\text{-times}}, \underbrace{[H, \dots, [H, c_{j\sigma}^\dagger]_- \dots]_-}_{x\text{-times}} \right]_+ \right\rangle, \quad (2.17)$$

where the result is independent of x . In a so-called spectral density approach (SDA) [108] one essentially truncates (2.15) and reduces the calculation of the Green's function to the first four moments. This is certainly a good approximation for the high-energy region and turned out to be successful for the Hubbard model [47]. To incorporate the undoubtedly important low-energy part of the spectrum, Mancini et al. [5, 161] suggested a modification of the SDA using composite operators.

The fact that the moments (2.17) can be determined analytically belongs to the class of exact statements on the KLM. The precise expressions of the first moments

$$m_{\mathbf{k}\sigma}^{(0)} = 1 \quad (2.18)$$

$$m_{\mathbf{k}\sigma}^{(1)} = \varepsilon_{\mathbf{k}} - \frac{J}{2} z_{\sigma} \langle S^z \rangle \quad (2.19)$$

$$m_{\mathbf{k}\sigma}^{(2)} = \varepsilon_{\mathbf{k}}^2 - \varepsilon_{\mathbf{k}} J z_{\sigma} \langle S^z \rangle + \frac{J^2}{4} \hbar \left\{ 2z_{\sigma} \langle S^z \hat{n}_{-\sigma} \rangle - 2 \langle S^{-\sigma} c_{\sigma}^\dagger c_{-\sigma} \rangle + \hbar S(S+1) - z_{\sigma} \langle S^z \rangle \right\} \quad (2.20)$$

exemplify their principle structure for the KLM. Via the Dyson-equation

$$\hbar\omega G_{\mathbf{k}\sigma}(\omega) = \hbar + [\varepsilon_{\mathbf{k}} + \Sigma_{\mathbf{k}\sigma}(\omega)] G_{\mathbf{k}\sigma}(\omega), \quad \implies \quad \Sigma_{\mathbf{k}\sigma}(\omega) = \sum_{m=0}^{\infty} \frac{C_{\mathbf{k}\sigma}^{(m)}}{(\hbar\omega)^m}. \quad (2.21)$$

a high-energy expansion of the Green's function implies such an expansion for the self-energy, too. A comparison of coefficients yields the following relationships

$$\begin{aligned} \frac{1}{E} : \quad C_{\mathbf{k}\sigma}^{(0)} &= m_{\mathbf{k}\sigma}^{(1)} - \varepsilon_{\mathbf{k}} \\ \frac{1}{E^2} : \quad C_{\mathbf{k}\sigma}^{(1)} &= m_{\mathbf{k}\sigma}^{(2)} - [m_{\mathbf{k}\sigma}^{(1)}]^2 \\ \frac{1}{E^3} : \quad C_{\mathbf{k}\sigma}^{(2)} &= m_{\mathbf{k}\sigma}^{(3)} - 2m_{\mathbf{k}\sigma}^{(2)}m_{\mathbf{k}\sigma}^{(1)} + [m_{\mathbf{k}\sigma}^{(1)}]^3 \end{aligned} \quad (2.22)$$

The coefficients $C_{\mathbf{k}\sigma}^{(m)}$ of the self-energy will become important for the projection-operator method.

As mentioned above, one can show rigorously that the moments (2.17) do not depend on the choice of x . This fact can be exploited when the moment $m_{\mathbf{k}\sigma}^{(3)}$ is calculated. As a consequence the following relationship must hold between several correlation functions [50]:

$$\begin{aligned} \sum_j T_{ij} \left(\langle S_i^\sigma c_{i-\sigma}^\dagger c_{j\sigma} \rangle - \langle S_i^\sigma c_{j-\sigma}^\dagger c_{i\sigma} \rangle \right) \\ = \frac{J}{2} \left(\hbar \langle S_i^\sigma c_{i-\sigma}^\dagger c_{i\sigma} \rangle + 2z_\sigma \langle S_i^\sigma S_i^z c_{i-\sigma}^\dagger c_{i\sigma} \rangle \right. \\ \left. - 2z_\sigma \hbar \langle S_i^z \hat{n}_{i-\sigma} \hat{n}_{i\sigma} \rangle + \langle S_i^\sigma S_i^{-\sigma} \hat{n}_{i-\sigma} \rangle - \langle S_i^{-\sigma} S_i^\sigma \hat{n}_{i\sigma} \rangle \right) \end{aligned} \quad (2.23)$$

A detailed proof of this remarkable equality can be found in appendix B. The concept used for the proof can be generalized to obtain further exact relations. However, it is not clear, whether these relations have any practical implication.

For relation (2.23) one cannot argue that both sides of the equation have to vanish independently, even though they depend on different model parameters. This arises because the correlation functions do implicitly depend on T_{ij} and J , too. However, it can be simplified in the limit $\langle S^z \rangle \rightarrow \hbar S$ of an assumed ferromagnetic saturation of the local-moment system and leads to $\langle \hat{n}_\downarrow \rangle = \langle \hat{n}_\downarrow \hat{n}_\uparrow \rangle$. Hence, in average each \downarrow -electron is sitting on a doubly occupied site.⁸ A similar effect can be observed in the atomic limit (2.8), where the lowest energy E_3 is bound to a double occupancy of the respective lattice site [96] and has a spectral weight proportional to the number of \downarrow -electrons: $\alpha_{3\uparrow}(\langle S^z \rangle = \hbar S) = \frac{2S}{2S+1} \langle \hat{n}_\downarrow \rangle$. Both statements contradict the physical picture that due to Coulomb repulsion double occupancy should be avoided. This artifact of the KLM can be removed if a sufficiently large Hubbard term is added to the model Hamiltonian [68, 45].

2.3 Approximative theories

To go beyond a constrained physical situation, the Kondo-lattice model has to be solved approximately. Several theoretical concepts have already been applied to the KLM. We do not intend to review all of them, but want to explain the (from our perspective) most important concepts in some detail. In principle, one can subdivide these concepts into two classes. There are those theories that obey the quantum commutation relations of the localized spin operators. In other papers it is assumed that these spins can be treated classically. We will concentrate on approaches belonging to the first of these classes.

An interpolating self-energy approach

A straightforward idea for an approximative theory is an interpolation between all the constrained physical situations mentioned in the previous section. The structure of the

⁸The decoupling $\langle \hat{n}_\downarrow \hat{n}_\uparrow \rangle \rightarrow \langle \hat{n}_\downarrow \rangle \langle \hat{n}_\uparrow \rangle$ would imply $\langle \hat{n}_\downarrow \rangle = 0$ for $n < 1$, but is not an exact transformation.

electronic self-energy for the ferromagnetically saturated semiconductor (2.10) is similar to that of the atomic limit (2.7) for $n = 0$. This motivates the ansatz [115]:

$$\Sigma_\sigma(\omega) = -\frac{J}{2} z_\sigma \langle S^z \rangle + \frac{J^2}{4} \frac{a_\sigma \frac{1}{N} \sum_{\mathbf{q}} G_{\mathbf{q}-\sigma}^{(\text{MF})}(\omega)}{1 - b_\sigma \frac{1}{N} \sum_{\mathbf{q}} G_{\mathbf{q}-\sigma}^{(\text{MF})}(\omega)}. \quad (2.24)$$

If the fitting parameters are chosen as

$$a_\sigma = \hbar S(S+1) - z_\sigma \langle S^z \rangle (z_\sigma \langle S^z \rangle / \hbar + 1) \quad \text{and} \quad b_\sigma = \frac{J}{2}, \quad (2.25)$$

then the self-energy fulfils, in addition to the two limits mentioned above, the first four spectral moments and the second-order perturbation theory, both for $n=0$. The ansatz can even be improved such, that the same limits are fulfilled for $n=2$, too [117]. For this purpose a Hubbard interaction is introduced, which triggers the splitting of the Green's function into two effective medium propagators. The effective media of the propagators are related to the empty and completely filled conduction band, respectively.

The quasiparticle density of states (QDOS) resulting from the Green's function of the interpolating self-energy approach (ISA) shows a lot of correlation effects. Here we only want to note, that several subbands are observed for each spin-direction. Depending on the parameters, their number varies between one and three. The positions are determined by the zero-bandwidth result, which seems to dominate the physics of this approach.

A moment-conserving decoupling approach

For the many-body concept of Green's functions the notation of equations of motion is another straightforward approach. Each equation of motion results in higher-order Green's functions and spectral moments (its inhomogeneities). To truncate this hierarchy a decoupling is necessary. Ideally, it is performed such that for each included correlation function the compatible Green's function for an application of the spectral theorem is also considered in the system of equations. To our knowledge, the most sophisticated decoupling procedure, which follows this rule, is given by the moment-conserving decoupling approach (MCDA) of Nolting et al. [114]. They suggest three different types of treatments for the Green's functions emerging in the third order of the hierarchy of equations.

1. Some non-diagonal Green's functions are expressed by lower-order Green's functions

$$\left\langle\left\langle S_i^{-\sigma} [c_{k-\sigma}, H_{sf}]_- ; c_{j\sigma}^\dagger \right\rangle\right\rangle_E \xrightarrow{i \neq k} \Sigma_{kl-\sigma}(E) \left\langle\left\langle S_i^{-\sigma} c_{l-\sigma} ; c_{j\sigma}^\dagger \right\rangle\right\rangle_E, \quad (2.26)$$

analogous to the definition of the site-dependent self-energy $\Sigma_{kl\sigma}$ via the Dyson equation

$$\left\langle\left\langle [c_{k\sigma}, H_{sf}]_- ; c_{j\sigma}^\dagger \right\rangle\right\rangle_E =: \Sigma_{kl\sigma}(E) \left\langle\left\langle c_{l\sigma} ; c_{j\sigma}^\dagger \right\rangle\right\rangle_E. \quad (2.27)$$

It also follows from their spectral representations [32] that both Green's functions in (2.26) must have the same pole structure.

2. If the time dependence of localized spin operators is in demand, H_{sf} is replaced by an effective Heisenberg model (2.33), followed by a Tyablikov approximation [12]:

$$\begin{aligned} & \left\langle \left\langle [S_i^{-\sigma}, H_{sf}]_- c_{k-\sigma}; c_{j\sigma}^\dagger \right\rangle \right\rangle_E \xrightarrow{i \neq k} \left\langle \left\langle [S_i^{-\sigma}, H_{ff}]_- c_{k-\sigma}; c_{j\sigma}^\dagger \right\rangle \right\rangle_E \\ & \longrightarrow 2\hbar z_\sigma \langle S^z \rangle \left(\hat{J}_{il} \left\langle \left\langle S_l^{-\sigma} c_{k-\sigma}; c_{j\sigma}^\dagger \right\rangle \right\rangle_E - \hat{J}_0 \left\langle \left\langle S_i^{-\sigma} c_{k-\sigma}; c_{j\sigma}^\dagger \right\rangle \right\rangle_E \right). \end{aligned} \quad (2.28)$$

3. Due to the strong intra-atomic correlations a modified treatment of diagonal Green's functions is required. Again, they are expressed by lower-order Green's functions, e.g.

$$\left\langle \left\langle S_i^{-\sigma} S_k^\sigma c_{k\sigma}; c_{j\sigma}^\dagger \right\rangle \right\rangle_E \xrightarrow{i=k} \alpha_\sigma \left\langle \left\langle c_{i\sigma}; c_{j\sigma}^\dagger \right\rangle \right\rangle_E + \beta_\sigma \left\langle \left\langle S_i^z c_{i\sigma}; c_{j\sigma}^\dagger \right\rangle \right\rangle_E. \quad (2.29)$$

In contrast to the above mentioned treatments, the parameters α_σ and β_σ are determined such that the first and second spectral moment of the expressions on both sides of (2.29) are identical.⁹ This ansatz is exact in certain limiting cases ($S = 1/2$ or $n = 0$).

The combination of these approximations yields an implicit equation for the self-energy

$$\Sigma_{\mathbf{k}\sigma}(\omega) = -\frac{J}{2} z_\sigma \langle S^z \rangle + \frac{J^2}{4} D_{\mathbf{k}\sigma}(\omega, J). \quad (2.30)$$

The second term in (2.30) is a correction to the mean-field result, which is predominantly determined by spin-exchange processes [116]. The included correlation functions

$$\langle \hat{n}_\sigma \rangle, \langle S^z \hat{n}_\sigma \rangle, \langle S^{-\sigma} c_\sigma^\dagger c_{-\sigma} \rangle, \langle S^{-\sigma} S^\sigma \hat{n}_\sigma \rangle, \langle S^{-\sigma} S^z c_\sigma^\dagger c_{-\sigma} \rangle \text{ and } \langle S^z \hat{n}_{-\sigma} \hat{n}_\sigma \rangle, \quad (2.31)$$

which are of ‘‘mixed s-f character’’ [114], can be determined self-consistently from the involved Green's functions. Their large number is the major advantage of this method. Additionally, there is a class of further correlation functions

$$\langle S^z \rangle, \langle (S^z)^2 \rangle \text{ and } \langle (S^z)^3 \rangle, \quad (2.32)$$

which are exclusively connected to the localized subsystem of the KLM and cannot be determined self-consistently within the MCDA. Using simple approximations for (2.32), the MCDA has successfully been applied to several physical aspects and materials [144, 145, 133, 113].

A modified RKKY interaction

For a more serious treatment of the correlation functions (2.32) Nolting et al. suggest the mapping of the H_{sf} -Hamiltonian onto an effective Heisenberg model [114, 140, 141]. This is possible by averaging out the band electron degrees of freedom:

$$H_{sf} \longrightarrow \langle H_{sf} \rangle^{(c)} \equiv H_{ff} = - \sum_{ij} \hat{J}_{ij} \mathbf{S}_i \cdot \mathbf{S}_j. \quad (2.33)$$

⁹For numerical reasons it seems to be more convenient, to define all Green's functions such that their first moment vanishes [140, 83]. Anyhow, this does not change the analytical properties of the approximation.

The trace in the expectation value is performed such that the operators of the localized spins are not affected. On the one hand, these operators can be removed from the angular brackets in (2.33) and treated as pre-factors. On the other hand, their contribution to the Hilbert space used for the thermodynamical average is considered in the form of c -numbers.

The restricted Green's function corresponding to this restricted Hilbert space is given by the implicit equation

$$\begin{aligned} \hat{G}_{\mathbf{k}\sigma, \mathbf{k}+\mathbf{q}\sigma'}(E) = & - \frac{J}{2N\hbar} \sum_{i\mathbf{k}'\sigma''} e^{i(\mathbf{k}-\mathbf{k}')\cdot\mathbf{R}_i} G_{\mathbf{k}}^{(0)}(\mathbf{S}_i \cdot \hat{\boldsymbol{\sigma}})_{\sigma\sigma''} \hat{G}_{\mathbf{k}'\sigma'', \mathbf{k}+\mathbf{q}\sigma'} + \\ & + \delta_{\mathbf{q},0} \delta_{\sigma\sigma'} G_{\mathbf{k}}^{(0)} - \frac{J}{2N\hbar} \sum_{i\mathbf{k}'\sigma''} e^{i(\mathbf{k}'-(\mathbf{k}+\mathbf{q}))\cdot\mathbf{R}_i} \hat{G}_{\mathbf{k}\sigma, \mathbf{k}'\sigma''}(\mathbf{S}_i \cdot \hat{\boldsymbol{\sigma}})_{\sigma''\sigma'} G_{\mathbf{k}+\mathbf{q}}^{(0)}. \end{aligned} \quad (2.34)$$

Here, the components of $\hat{\boldsymbol{\sigma}}$ are the Pauli spin matrices and $G_{\mathbf{k}}^{(0)}(E)$ is the Green's function of a free electron gas. If the restricted Green's functions on the right hand side of Eq. (2.34) were also replaced by free Green's functions¹⁰, the averaging procedure would result into the following (Fourier-transformed) effective exchange integrals:

$$\hat{J}_{\mathbf{k}}^{(\text{RKKY})} = -\frac{J^2}{2N} \sum_{\mathbf{q}} \frac{f_-(\varepsilon_{\mathbf{q}+\mathbf{k}}) - f_-(\varepsilon_{\mathbf{q}})}{\varepsilon_{\mathbf{q}+\mathbf{k}} - \varepsilon_{\mathbf{q}}}. \quad (2.35)$$

This is the expression of the *conventional* RKKY [66, 177, 138] exchange interaction of localized spins via spin-polarized conduction electrons. It depends on the square of the interband exchange J and via μ on the conduction electron density n . Evaluated in real space the exchange integrals \hat{J}_{ij} show an oscillatory behaviour as a function of the distance R_{ij} .

In order to incorporate to higher order the spin polarization of conduction electrons, the restricted Green's functions on the right of Eq. (2.34) can be replaced by the full Green's functions $G_{\mathbf{k}\sigma}(E)$, as for instance obtained by the MCDA above. Then the averaging procedure yields a *modified* RKKY interaction with effective exchange integrals

$$\hat{J}_{\mathbf{k}}^{(\text{MRKKY})} = -\frac{J^2}{2\hbar} \int_{-\infty}^{\infty} dE f_-(E) \frac{1}{N} \sum_{\mathbf{q}\sigma} \left\{ -\frac{1}{\pi} \Im (G_{\mathbf{q}}^{(0)}(E) G_{\mathbf{k}+\mathbf{q},\sigma}(E)) \right\}. \quad (2.36)$$

Due to the dependence on $G_{\mathbf{k}\sigma}(E)$, these exchange integrals include the full self-energy of the electronic subsystem. Therefore, the dependence on J, n and further correlation functions is much more sophisticated as in the conventional RKKY. Nevertheless, the exchange integrals \hat{J}_{ij} still have oscillating values as a function of the distance R_{ij} . [141]

Combination of MCDA and modified RKKY theory

The modified RKKY theory allows the application of standard decoupling techniques for the Heisenberg model [17] to obtain the expectation values (2.32) of localized spin

¹⁰This corresponds to a first order approximation in the iteration scheme of Eq. (2.34).

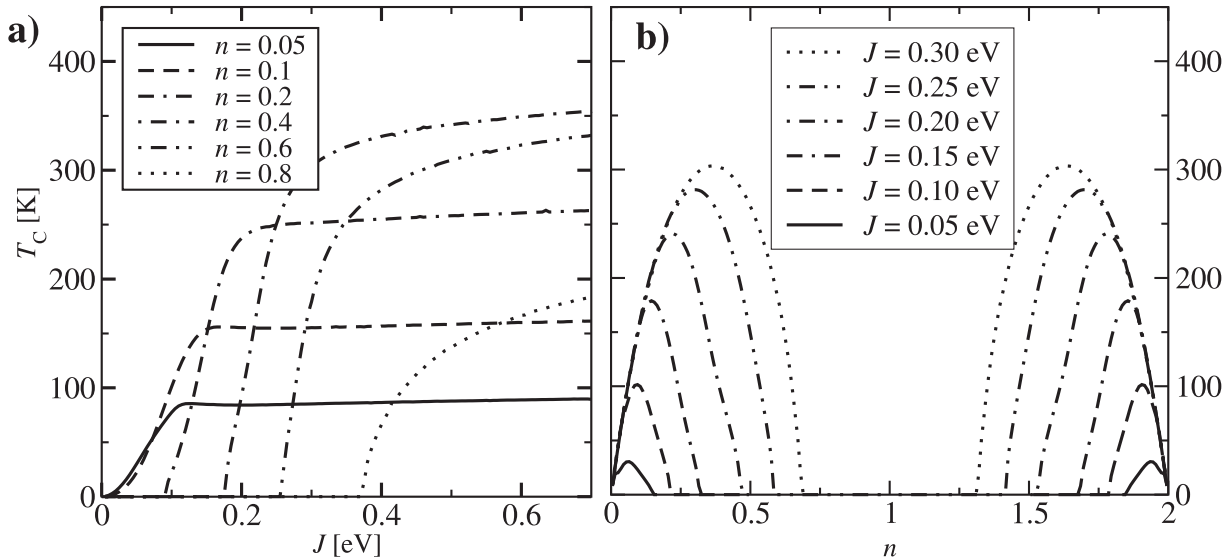


Figure 2.1: Curie temperatures obtained by the modified RKKY theory using a self-energy as obtained by MCDA. **a)** For several band occupations n the dependence on coupling strength J is plotted. **b)** For several coupling strengths J the dependence on the band occupation n is plotted. Other parameters: $S = 7/2, W = 1.0$ eV for a simple-cubic lattice. [142, 141]

operators. Its exchange integrals (2.36) are determined by an electronic self-energy. In turn, the MCDA needs the expectation values (2.32) as an input for the self-energy (2.30). Therefore, the combination of these two approaches forms a fully self-consistent theory for the KLM, which has been analyzed intensively by Santos, Nolting [141, 140] and co-workers. Out of the wide range of results the obtained Curie temperatures are particularly interesting. A ferromagnetic order of the localized spin system is certainly due to the interband coupling J . Nevertheless, the results of the modified RKKY theory in Fig. 2.1a demonstrate the existence of qualitatively different parameter regimes.

For small values of J the Curie temperature increases quadratically with the coupling. This behaviour has also been predicted by conventional RKKY, which is particularly reliable in this parameter range due to its perturbational character. Therefore, it is at the first sight surprising to observe in Fig. 2.1a, that for band occupations larger than $n_c = 0.13$ the J^2 -dependence is replaced by a behaviour with a critical J_c below which no ferromagnetism occurs [141]. However, this is not in contrast to perturbation theory. Conventional RKKY predicts that regardless of the coupling, ferromagnetism is limited to band occupations $n < n_c$. The modified RKKY theory obeys this rule such that for $n > n_c$ ferromagnetism is only possible for coupling strengths J outside the range of applicability of conventional RKKY.

That the modified RKKY allows a finite Curie temperature for almost all band occupations, can also be observed in Fig. 2.1b. According to these findings, ferromagnetism is only excluded for a small region around $n = 1$. Nevertheless, systems with an almost half-filled conduction band have to experience a very large intra-atomic coupling in order to show ferromagnetism. This result is consistent with the $T = 0$ K phase diagram for

the KLM [19, 46].

For increasing coupling strengths the T_C lines in Fig. 2.1a run into saturation. The explanation of this effect is probably related to the electronic subsystem. A large coupling strength yields a separation of the QDOS into two subbands. A further increase of J mainly increases the distance between these subbands, but does not change the magnetic behaviour of the local moment system very much. For $J \rightarrow \infty$, where the KLM is often called double-exchange model, the magnetic behaviour is dominated by the itinerant subsystem. Theories therefore predict a scaling of the Curie temperature with the conduction bandwidth. This trend is confirmed by the combined theory of MCDA and modified RKKY.

A random-phase approximation

If one is interested in the spin-wave dynamics of the KLM, one could resort to the Heisenberg model, as it has been done by the RKKY theory. A more general approach is the formulation of the equations of motion for the one-magnon Green's function [167]:

$$\begin{aligned} \hbar\omega \langle\langle S_{-\mathbf{k}}^\sigma; S_{\mathbf{k}}^{-\sigma} \rangle\rangle_E &= 2\hbar z_\sigma \langle S_0^z \rangle - z_\sigma \frac{J\hbar}{N} \sum_{\mathbf{qp}} \langle\langle S_{\mathbf{q}-\mathbf{k}}^z c_{\mathbf{p}+\mathbf{q},-\sigma}^\dagger c_{\mathbf{p},\sigma}; S_{\mathbf{k}}^{-\sigma} \rangle\rangle_E \\ &+ \frac{J\hbar}{2N} \sum_{\mathbf{qp}} \left\{ \langle\langle S_{\mathbf{q}-\mathbf{k}}^\sigma c_{\mathbf{p}+\mathbf{q},\sigma}^\dagger c_{\mathbf{p},\sigma}; S_{\mathbf{k}}^{-\sigma} \rangle\rangle_E - \langle\langle S_{\mathbf{q}-\mathbf{k}}^\sigma c_{\mathbf{p}+\mathbf{q},-\sigma}^\dagger c_{\mathbf{p},-\sigma}; S_{\mathbf{k}}^{-\sigma} \rangle\rangle_E \right\}. \end{aligned} \quad (2.37)$$

A random-phase approximation (RPA), similar to the Tyablikov approximation [12] for the Heisenberg model, is given by the following decoupling procedure:

$$\langle\langle S_{\mathbf{q}-\mathbf{k}}^z c_{\mathbf{p}+\mathbf{q},-\sigma}^\dagger c_{\mathbf{p},\sigma}; S_{\mathbf{k}}^{-\sigma} \rangle\rangle_E \approx \langle S_{\mathbf{q}-\mathbf{k}}^z \rangle \langle\langle c_{\mathbf{p}+\mathbf{q},-\sigma}^\dagger c_{\mathbf{p},\sigma}; S_{\mathbf{k}}^{-\sigma} \rangle\rangle_E, \quad (2.38)$$

$$\langle\langle S_{\mathbf{q}-\mathbf{k}}^\sigma c_{\mathbf{p}+\mathbf{q},\hat{\sigma}}^\dagger c_{\mathbf{p},\hat{\sigma}}; S_{\mathbf{k}}^{-\sigma} \rangle\rangle_E \approx \langle c_{\mathbf{p}+\mathbf{q},\hat{\sigma}}^\dagger c_{\mathbf{p},\hat{\sigma}} \rangle \langle\langle S_{\mathbf{q}-\mathbf{k}}^\sigma; S_{\mathbf{k}}^{-\sigma} \rangle\rangle_E. \quad (2.39)$$

The only higher order Green's function considered in the RPA appears on the right hand side of (2.38). If the equation of motion of this function is decoupled similarly to (2.38) and (2.39) it yields:

$$\langle\langle c_{\mathbf{p}+\mathbf{k},-\sigma}^\dagger c_{\mathbf{p},\sigma}; S_{\mathbf{k}}^{-\sigma} \rangle\rangle_E = \frac{J}{2} \frac{\langle \hat{n}_{\mathbf{p},-\sigma} \rangle - \langle \hat{n}_{\mathbf{p}+\mathbf{k},\sigma} \rangle}{\hbar\omega - Jz_\sigma \langle S^z \rangle - (\varepsilon_{\mathbf{p}} - \varepsilon_{\mathbf{p}+\mathbf{k}})} \langle\langle S_{-\mathbf{k}}^\sigma; S_{\mathbf{k}}^{-\sigma} \rangle\rangle_E. \quad (2.40)$$

This closes the system of equations. We will discuss extensively the expression for the one-magnon Green's function and its properties in Sec. 5.3.

Dynamical mean-field theory

Within the last decade dynamical mean-field theory (DMFT) has developed to one of the most promising approaches for strongly-correlated electron systems (for reviews see [42, 131]). It is based on the observation that in the limit of infinite spatial dimensions the self-energy of a lattice model with on-site interactions becomes local [91]. This property is

connected to the fact, that the self-energy functional (the dependence of the self-energy on the respective propagators) for the lattice-model is equivalent to that of a corresponding impurity model. The observation gives rise to an iteration scheme for the self-energy of the lattice model [131]:

0. Start with an initial choice for the local self-energy $\Sigma_\sigma(\omega)$.
1. Calculate the local one-particle Green's function:

$$G_\sigma(\omega) = \frac{1}{N} \sum_{\mathbf{k}} \frac{\hbar}{\hbar\omega - \varepsilon_{\mathbf{k}} - \Sigma_\sigma(\omega)} = \int_{-\infty}^{\infty} dx \frac{\hbar\rho_0(x)}{\hbar\omega - x - \Sigma_\sigma(\omega)} \quad (2.41)$$

2. Determine an effective medium by the so-called Weiss propagator

$$[\mathcal{G}_\sigma(\omega)]^{-1} = [G_\sigma(\omega)]^{-1} + \Sigma_\sigma(\omega), \quad (2.42)$$

an analogue to the mean-field of Weiß's theory for the Ising model.

3. Solve the impurity problem defined by the effective medium and the local interaction at a single site. This yields a local Green's function

$$G_\sigma^{(\text{imp})}(\omega) = \frac{\hbar}{\hbar\omega - \Delta_\sigma(\omega) - \Sigma_\sigma^{(\text{imp})}(\omega)} \quad \text{with} \quad \Delta_\sigma(\omega) = \hbar\omega - \hbar [\mathcal{G}_\sigma(\omega)]^{-1}. \quad (2.43)$$

4. Identify the impurity self-energy with that of the lattice model, $\Sigma_\sigma(\omega) = \Sigma_\sigma^{(\text{imp})}(\omega)$, and continue with step 1 until self-consistency is obtained.

The iteration scheme of DMFT cannot be applied directly to spin models such as the Kondo-lattice model. As explained in more detail by Meyer [92], neither a heuristic derivation of the DMFT condition in terms of Feynman diagrams nor the strict mathematical prove based on the cavity method [42] can be transferred to this model. The problem is that there exist no Wick's theorem and no Grassmann numbers for spin-operators.

There are two possibilities to circumvent these difficulties. For $S = 1/2$, the operators for localized spins can be expressed in terms of auxiliary Fermi operators [88, 96]:

$$\mathbf{S}_i = \sum_{\alpha,\beta} f_{i\alpha}^\dagger \hat{\sigma}_{\alpha,\beta} f_{i\beta} \quad \text{with} \quad \sum_{\alpha} f_{i\alpha}^\dagger f_{i\alpha} = 1 \quad \forall i, \quad (2.44)$$

where $\hat{\sigma}_{\alpha,\beta}$ represent the Pauli spin matrices. The resulting Hamiltonian is very similar to that of the periodic Anderson model [48] for which the concepts of DMFT are known [42]. The impurity problem can be solved by returning to spin operators and performing a decoupling of the equations of motion similar to (2.26) [96]. The second possibility to perform a DMFT for the KLM is the limit $S \rightarrow \infty$. Then the localized spins can be treated classically and the determination of the impurity Green's function is essentially reduced to a two-dimensional integration over all angles for the impurity spin [39, 18]. Replacing the Hund's rule coupling by an Ising-type interaction [45] is, in the paramagnetic region,

equivalent to the assumption of classical local spins. Based on this approach, a Monte-Carlo calculation has been performed, in order to solve the impurity problem [45].

The DMFT results for $S = 1/2$ and $S \rightarrow \infty$ show remarkable differences implying a strong impact of the quantum-mechanical character of the localized spins on the electronic properties of the KLM. Although, in particular for manganites, the optical conductivity is of major interest [18], we will only make a few remarks on the quasiparticle density of states (QDOS) obtained. First, we consider the classical limit $S \rightarrow \infty$ (cf Fig. 5 in [39]). At $T = 0$ K the QDOS shows just the mean-field shift of the \uparrow - and the \downarrow -band. Such a situation would give rise to a complete spin-polarization, a property which is also addressed in appendix E. For finite temperatures, there are two subbands in each spin-channel, again separated by the mean-field distance. Therefore, the only effect of an increasing temperature is a re-distribution of spectral weight to energies belonging to the $T = 0$ K band of the opposite spin direction.

The situation is completely different for the quantum-mechanical spin $S = 1/2$ (cf Figs. 3 and 4 in [96]), where the QDOS shows strong correlation effects already at $T = 0$ K. Firstly, there is a broadening of the QDOS with increasing coupling strength. Furthermore, the onset of the splitting of the band can be observed, which yields two subbands in the \downarrow - as well as in the \uparrow -channel for moderate values of J . In particular, the pronounced correlation effect for \uparrow -electrons at $T = 0$ K is a feature not observed in the MCDA. For \downarrow -electrons the effects are consistent with the situation of the ferromagnetically saturated semiconductor. At temperatures close to the Curie temperature the QDOS of the DMFT and the MCDA do coincide for all coupling strengths. Here, one observes a broad structure with a dip indicating the onset of a band splitting.

Kogan et al. [70] were successful in using the DMFT equations for $S \rightarrow \infty$ to derive an explicit expression for the Curie temperature T_C . Plotted as a function of band occupation (cf Fig. 1 in [70]) the qualitative similarities of the results as compared to the MCDA-results in Fig. 2.1b are surprising. Also in their calculations, finite Curie temperatures are obtained for small band occupations. An increasing J yields larger Curie temperatures and the possibility of ferromagnetism for an increasing region of band occupations. Furthermore, Michaelis et al. [97] conclude from their DMFT calculations that, in contrast to previous observations, already moderate values of the coupling constant J are sufficient to describe the experimental situation in pseudocubic manganites.

Conclusions

The provided list of approximate approaches to the KLM is by no means exhaustive. However, it is sufficient to be informed about important trends in this field. All the mentioned approximations have their shortcomings. Decoupling techniques are often considered to be uncontrollable and intuitive [83]. The interpolating self-energy approach has the problem that the local moment magnetization has to come into play only as an external parameter. Most of the DMFT calculations have to assume classical local spins. The alternative DMFT approach with a fermionization of spin operators suffers from numerical inconsistencies in some parameter regions [139].

From our perspective, the combination of the moment-conserving decoupling approach (MCDA) with the modified RKKY theory provides the most reliable method for a study of

the KLM. However, one can also note some drawbacks of this method: Although the conservation of the first spectral moments reduces the drawbacks of decoupling approaches, the variety of techniques to treat third-order Green's functions still evokes the danger of arbitrariness. A resulting spin-dependence of the correlation function $\langle S^\sigma c_{-\sigma}^\dagger c_\sigma \rangle$ pinpoints inconsistencies within the MCDA. However, the probably most serious approximation is given by the mapping of the local-moment subsystem. As a consequence, the resulting magnetic behaviour is essentially that of a Heisenberg ferromagnet. The method cannot cover magnetic excitations that are characteristic for the KLM, although they might be essential for the obtained Curie temperatures.

These considerations lead to the following conclusion: An approximation of the KLM, that treats the magnetic and the electronic subsystem with the same Hamiltonian and the same techniques is still missing. We consider such an approximation essential, in order to satisfy the complex physics included in the Kondo-lattice model. The projection-operator method, introduced in the next chapter, is an excellent candidate for this purpose.

Chapter 3

The projection-operator method

The projection-operator method (POM) is characterized by a mixture of favourable features. It is a many-body technique that results in an expression for the desired Green's function. It is an exact formalism which allows systematic approximations by truncations at well-defined levels. It has, in contrast to Wick's theorem, the potential to handle spin operators with their complicated commutation relations. Last but not least, it has a certain beauty in the way the dynamic and static entities are treated. We will use this chapter to substantiate these claims.

3.1 Dynamics within the Liouville space

To explain the projection-operator method one should start with the fundamentals of quantum statistics [33]. Here, the aim of all efforts is the determination of time-dependent correlation functions. This requires the calculation of expectation values, which for an arbitrary observable A are determined by

$$\langle A \rangle(t) = \text{Tr}(\rho(t)A). \quad (3.1)$$

Here, it is the statistical operator ρ , that carries the time dependence of the system. Hilbert states are only needed to calculate the trace. More generally, it turns out that for quantum statistics a formulation of theories in terms of operators is more convenient than considerations within the Hilbert space.

Since linear operators A, B, \dots can be added and multiplied by complex scalars, they may themselves be regarded as elements $|A\rangle, |B\rangle, \dots$ of an abstract vector space. The space of linear operators acting on a Hilbert space is called *Liouville space*. The notion behind the projection-operator method is that only a relatively small set of observables is relevant for the description of the dynamics of the system. These elements span a subspace of the Liouville space, also called *level of description* [132]. The statistical operator contains a lot of additional information which is not related to the dynamics of the observables considered. In this sense the additional information is irrelevant for our calculations. Therefore, a projector is used to filter out only the relevant part of the information.

A necessary condition for the definition of a projector is the existence of a scalar product within the Liouville space. There are several possibilities to define it. Mori [99],

who is one of the pioneers in the formalism using projection-operators, used the definition

$$(A|B) := \frac{1}{\beta} \int_0^\beta \langle e^{\lambda H} A e^{-\lambda H} B^\dagger \rangle d\lambda, \quad (3.2)$$

where H is the Hamiltonian, $\beta = 1/k_B T$ and the angular brackets denote the average over the canonical ensemble.¹ As will become apparent below, the definition

$$(A|B) := \langle [A^\dagger; B]_\eta \rangle \quad (3.3)$$

is closely related to the language of retarded Green's functions. It will be used extensively within our calculations. Here, $\eta = +$ or $-$ if we work with fermions or spin operators, respectively. The angular brackets denote the average over the grand-canonical ensemble. It can easily be shown, that both bilinear forms fulfil the necessary mathematical conditions for a scalar product.

Once provided with a scalar product an operator \mathcal{P} that projects an arbitrary element onto the level of description spanned by the set $\{|A_\nu\rangle$ is given by²

$$\mathcal{P} = |A_\mu\rangle \chi_{\mu\nu}^{-1} \langle A_\nu| \quad \text{with} \quad \chi_{\alpha\beta} = (A_\alpha|A_\beta). \quad (3.4)$$

The representation (3.4) of \mathcal{P} is independent of the chosen basis elements $|A_\nu\rangle$. The matrix of scalar products of these basis elements is called *susceptibility matrix*. $\chi_{\mu\nu}^{-1}$ denotes an element of the inverse matrix χ^{-1} . In this context the latter plays the role of a metric.

Such an operator \mathcal{P} acts on elements $|B\rangle$ of the Liouville space. Its action results in new elements

$$|B_{\mathcal{P}}\rangle = \mathcal{P}|B\rangle = \{\chi_{\mu\nu}^{-1} \langle A_\nu|B\rangle\} |A_\mu\rangle \quad (3.5)$$

of the Liouville space. To distinguish such a projection operator from operators acting in Hilbert space (which are the elements of the Liouville space) \mathcal{P} is referred to as a *superoperator*. We will not discuss the whole spectrum of superoperators that can be found in the literature. However, at least one further example of a superoperator has to be mentioned.

It is the *Liouvillian* \mathcal{L} defined as

$$\mathcal{L}|A\rangle := \hbar^{-1} |[H, A]_-, \quad (3.6)$$

which is very important for the dynamics of the system. In the Schrödinger representation³ the Liouvillian is directly related to the time derivative

$$\frac{d\rho}{dt} = -i\mathcal{L}\rho \quad (3.7)$$

¹ Mori has chosen this scalar product to justify a linearization of the Langevin equation in the stochastic theory of Brownian motion [99]. An extended discussion of its physical significance can be found in [33].

² Here, and in the rest of the chapter we use Einstein's sum convention.

³ In the Heisenberg representation it is related to the time derivative of observables without an explicit time dependence.

of the statistical operator ρ . Written within an exponential \mathcal{L} affects the transformation of operators according to the rule⁴

$$e^{c\mathcal{L}}A = e^{cH/\hbar}Ae^{-cH/\hbar}, \quad (3.8)$$

where c is some number proportional to time. Furthermore, this superoperator can be used for a particularly compact notation

$$m_{ij}^{(n)} = \hbar^n \left(c_{i\sigma}^\dagger \left| \mathcal{L}^n \right| c_{j\sigma}^\dagger \right), \quad (3.9)$$

for the spectral moments (2.16) of the one-particle Green's function. This requires the scalar product to be of the form (3.3). For above mentioned reasons the Liouvillian will dominate the subsequent discussions.

3.2 Separation of time scales

The projection-operator method, now used in several branches of physics, has its roots in (quantum) transport theory. We have already mentioned the pioneering work of Mori [99, 100]; even earlier Nakajima [105] and Zwanzig [182, 183] have published similar approaches.⁵ Zwanzig derived a master equation to study irreversibility. He separated the ensemble density in a *relevant* and an *irrelevant* part by means of a projection, solved the latter part formally in terms of the former one and substituted the solution back into the equation for the relevant part [182]. This exact transformation is particularly suitable for integrating out fast variations in time [183].

The detection and systematic exploitation of a separation of time scales is the basic practical merit of the projection-operator method [132]. The context of transport theory is useful for an illustration. Take, e.g., the Brownian motion of a massive particle within a liquid of small molecules. This process consists of damping on a macroscopic scale due to the viscosity of the liquid and fast vibrations due to stochastic residual forces. Both processes are caused by collisions between the particle and the molecules, but they happen on different time scales. The damping process is for the observable “position of the particle” much more relevant, than the vibrations, which vanish when averaged over time. However, only if these two processes are separated, one can neglect the one and consider the other.

More formally, we study the Heisenberg time dependence of a set $\{A_\nu\}$ of relevant observables. According to (3.8) it is given by

$$|A_\nu(t)\rangle = e^{i\mathcal{L}t} |A_\nu\rangle \quad \iff \quad \left| \dot{A}_\nu(t) \right\rangle = e^{i\mathcal{L}t} \left| \dot{A}_\nu \right\rangle \quad (3.10)$$

where we assume that $|A_\nu\rangle \equiv |A_\nu(0)\rangle$ and \mathcal{L} carry no explicit time dependence and accordingly define $|\dot{A}_\nu\rangle \equiv i\mathcal{L}|A_\nu(0)\rangle$. Even though at $t = 0$ s the relevant observables

⁴Relation (3.8) can be proven using the Baker-Hausdorff theorem [107].

⁵ This is also the reason why the POM is referred to as the *Mori formalism* or the *Nakajima-Zwanzig projection technique*.

span the level of description, there is no reason why $|\dot{A}_\nu\rangle$ should lie within this Liouville subspace. Nevertheless, by inserting $1 = \mathcal{P} + \mathcal{Q}$ in the form

$$|\dot{A}_\nu(t)\rangle = e^{i\mathcal{L}t}\mathcal{P}|\dot{A}_\nu\rangle + e^{i\mathcal{L}t}\mathcal{Q}|\dot{A}_\nu\rangle \quad (3.11)$$

one can distinguish between those parts within the level of description (mediated by \mathcal{P}) and those which belong to the orthogonal complement (mediated by $\mathcal{Q} = 1 - \mathcal{P}$). However, due to the factor $e^{i\mathcal{L}t}$ in front of the second term, it is possible that it describes *relevant* physics. Therefore, with the help of the identity⁶

$$e^{i\mathcal{L}t} \equiv i \int_0^t e^{i\mathcal{L}(t-t')}\mathcal{P}\mathcal{L} e^{i\mathcal{Q}\mathcal{L}t'} dt' + e^{i\mathcal{Q}\mathcal{L}t} \quad (3.12)$$

we replace this factor by an expression which allows for a clearer interpretation.

The resulting expressions, also known as the *Mori equations*,

$$|\dot{A}_\nu(t)\rangle = i\chi_{\mu\rho}^{-1}\Omega_{\rho\nu}|A_\mu(t)\rangle - \int_0^t dt' \chi_{\mu\rho}^{-1}M_{\rho\nu}(t')|A_\mu(t-t')\rangle + f_\mu(t) \quad (3.13)$$

form a system of coupled integro-differential equations for the set $\{A_\nu\}$ of observables $|A_\mu(t)\rangle$. They are of similar structure as the Langevin equation, obtained for the Brownian motion of particles discussed above. We will now discuss each of the three contributing terms, explain their physical meaning and their origins.

The first term, which arises in the transformation

$$e^{i\mathcal{L}t}\mathcal{P}|\dot{A}_\nu\rangle \stackrel{(3.4)}{=} e^{i\mathcal{L}t}|A_\mu\rangle\chi_{\mu\rho}^{-1}\left(A_\rho|\dot{A}_\nu\rangle\right) \stackrel{(3.8)}{=} |A_\mu(t)\rangle i\chi_{\mu\rho}^{-1}\underbrace{(A_\rho|\mathcal{L}|A_\nu)}_{\Omega_{\rho\nu}}, \quad (3.14)$$

is particularly simple to understand. It is well known that a differential equation $\dot{x}(t) = i\omega \cdot x(t)$ describes a harmonic oscillation with frequency ω . If we neglect the contribution of the metric, then $\Omega_{\rho\nu}$ can be understood as the *frequency matrix* of a coupled system of oscillators. Within the picture of Brownian motion this is the set of eigenfrequencies of a particle system entering the liquid.

The third term, which can be written in the form

$$f_\mu(t) \stackrel{(3.12)}{=} e^{i\mathcal{Q}\mathcal{L}t}\mathcal{Q}|\dot{A}_\nu\rangle \stackrel{(3.8)}{=} i e^{i\mathcal{Q}\mathcal{L}t}\mathcal{Q}\mathcal{L}|A_\nu\rangle \stackrel{\mathcal{Q}^2=\mathcal{Q}}{=} i\mathcal{Q} e^{i\mathcal{Q}\mathcal{L}\mathcal{Q}t}\mathcal{L}|A_\nu\rangle, \quad (3.15)$$

has the property that for every time t it belongs to the orthogonal complement of the level of description, and therefore to the irrelevant Liouville subspace. Hence, it is called *residual force*. It is responsible for vibrations in the picture of Brownian motion. One can

⁶The identity is readily proven if one notices that both sides of the equation fulfil the same differential equation $\dot{x}(t) = i\mathcal{L}x(t)$ and the same initial condition $x(0) = 1$.

readily see that the dynamics of $f_\mu(t)$ is driven by $\mathcal{Q}\mathcal{L}\mathcal{Q}$ rather than by the Liouvillian \mathcal{L} . This results in a completely different time scale of this motion.

For the calculation of the remaining second term of (3.13) one needs to know the value of the relevant observables for all times t' with $0 \leq t' < t$. This term is therefore called *memory term*.⁷ Its derivation is as follows:

$$\begin{aligned} i e^{i\mathcal{L}(t-t')} \mathcal{P}\mathcal{L} e^{i\mathcal{Q}\mathcal{L}t'} \mathcal{Q} \left| \dot{A}_\nu \right\rangle &\stackrel{(3.4)}{=} - e^{i\mathcal{L}(t-t')} |A_\mu\rangle \chi_{\mu\rho}^{-1} (A_\rho | \mathcal{L} e^{i\mathcal{Q}\mathcal{L}t'} \mathcal{Q}\mathcal{L} | A_\nu) \\ &\stackrel{(3.8)}{=} - |A_\mu(t-t')\rangle \chi_{\mu\rho}^{-1} \underbrace{(A_\rho | \mathcal{L}\mathcal{Q} e^{i\mathcal{Q}\mathcal{L}\mathcal{Q}t'} \mathcal{L} | A_\nu)}_{M_{\rho\nu}(t')}. \end{aligned} \quad (3.16)$$

A comparison of this result with (3.15) shows that the memory matrix M can be expressed in terms of the residual forces

$$M_{\rho\nu}(t) = (A_\rho | \mathcal{L}\mathcal{Q} e^{i\mathcal{Q}\mathcal{L}\mathcal{Q}t} \mathcal{L} | A_\nu) = (f_\rho(0) | f_\nu(t)), \quad (3.17)$$

where the fact has been used that \mathcal{L} is Hermitian. Hence, the memory term in (3.13) has the structure of a damping with a damping constant (which is actually not constant at all) formed by the same forces that already appeared in the previously discussed term. This is exactly the process which was described above for the Brownian motion of a particle.

We would like to stress again that the dynamics of $|A_\mu(t-t')\rangle$ in the memory term (3.16) is determined by the Liouvillian \mathcal{L} . This is not the case for the residual forces. Hence, we have achieved the desired separation of time scales into a relevant and an irrelevant part.

3.3 Expansion using continued fractions

In the previous section the dynamics of the system is expressed in terms of time-dependent Liouville states and their time derivatives. The description of strongly correlated electrons, however, is usually based on energy-dependent Green's functions. Accordingly, the derivation of the Mori equations has to follow a different line of argumentation [37, 9, 69].

Starting with the definition of a retarded Green's function in Heisenberg representation one can immediately find an expression in terms of the Liouvillian

$$G_{AB}(t) = -\frac{i}{\hbar} \Theta(t) \left\langle [A^\dagger(0); B(-t)]_\eta \right\rangle \stackrel{(3.8)}{=} -\frac{i}{\hbar} \Theta(t) (A | e^{-i\mathcal{L}t} | B), \quad (3.18)$$

using a Liouville scalar product of the form (3.3). The analytical behaviour is dominated by the Heaviside unit step function $\Theta(t)$ with its important integral representation

$$\Theta(t) = \frac{i}{2\pi} \int_{-\infty}^{+\infty} dx \frac{e^{-ixt}}{x + i0^+}. \quad (3.19)$$

⁷One speaks of Markovian processes, if the value of observables depends only on their value at a previous time step. Therefore, the effect of a finite memory is often called *non-Markovian* in transport theory.

Hence, the Green's function is Fourier transformed to

$$G_{AB}(E) = \int_{-\infty}^{+\infty} dt G_{AB}(t) e^{iEt/\hbar} = \left(A \left| \frac{1}{E/\hbar - \mathcal{L} + i0^+} \right| B \right). \quad (3.20)$$

This is the typical structure of a *resolvent*.

Such a structure is convenient for a projection-operator treatment. If $|A_i\rangle$ and $|A_j\rangle$ belong to the level of description and the abbreviation $\omega = E/\hbar + i0^+$ is used, then the following set of straightforward⁸ transformations is possible:

$$R_{ij} = \left(A_i \left| \frac{1}{\omega - \mathcal{L}} \right| A_j \right) = \left(A_i \left| \frac{1}{\omega - \mathcal{L}\mathcal{Q}} + \frac{1}{\omega - \mathcal{L}\mathcal{Q}} \mathcal{L}\mathcal{P} \frac{1}{\omega - \mathcal{L}} \right| A_j \right) \quad (3.21)$$

$$= \frac{1}{\omega} \chi_{ij} + \left(A_i \left| \frac{1}{\omega - \mathcal{L}\mathcal{Q}} \mathcal{L} \right| A_l \right) \chi_{lm}^{-1} R_{mj} \quad (3.22)$$

$$= \frac{1}{\omega} \chi_{ij} + \frac{1}{\omega} (\Omega_{il} + M_{il}(\omega)) \chi_{lm}^{-1} R_{mj}. \quad (3.23)$$

This approach shows a lot of similarities to the concept of separated time scales, discussed in the previous section. First of all, (3.21) is basically a multiplication of the Liouvillian with $1 = \mathcal{P} + \mathcal{Q}$ from the right. This corresponds to the insertion done in (3.11). Secondly, it is not accidental that in (3.23) the same symbols as above have been used for

the susceptibility matrix	$\chi_{ij} = (A_i A_j),$	
the frequency matrix	$\Omega_{ij} = (A_i \mathcal{L} A_j)$	and
the memory matrix	$M_{ij}(\omega) = \left(A_i \left \mathcal{L}\mathcal{Q} \frac{1}{\omega - \mathcal{Q}\mathcal{L}\mathcal{Q}} \mathcal{Q}\mathcal{L} \right A_j \right).$	(3.24)

In the first and the second case they are identical to the expressions defined in (3.4) and (3.14), respectively. For the memory matrix the correspondence to (3.17) is apparent due to the fact that the dynamics is determined by $\mathcal{Q}\mathcal{L}\mathcal{Q}$. A formal equivalence is obtained with the help of a one-sided Fourier transform [16]

$$M_{ij}(\omega) = i \int_0^{\infty} dt e^{i\omega t} M_{ij}(-t). \quad (3.25)$$

But most importantly, it can be proven that the matrix equation (3.23) is nothing but an energy representation of the Mori equation, already given in (3.13). To show this, a Laplace transformation of the *dynamical correlation function* $i(A_i | A_j(t))$ has to be performed, using the integro-differential equation (3.13). The interested reader is referred to appendix C for further details on this point.

⁸ The first line is proven with the help of the identity $\frac{1}{a+b} = \frac{1}{a} - \frac{1}{a} b \frac{1}{a+b}$, the second line is based on the definition of \mathcal{P} in (3.4) and \mathcal{Q} , whereas the third line can be proven with the help of a geometric series.

The advantage of the energy representation (3.23) becomes most apparent, if a compact matrix notation

$$\underline{\mathbf{R}}(\omega) = \frac{1}{\omega \underline{\mathbf{1}} - [\underline{\mathbf{Q}} + \underline{\mathbf{M}}] \underline{\mathbf{X}}^{-1} \underline{\mathbf{X}}} \quad (3.26)$$

and the structural similarity between the memory matrix (3.24) and the Green's function (3.20) are used. Both functions have the form of a resolvent. This allows the application of transformations (3.21)-(3.23) to the Green's function as well as to the memory matrix. A repeated insertion into (3.26) therefore yields a *continued fraction* for the Green's function, which has the following principle structure

$$G(\omega) = \frac{\chi_1}{\omega - \Omega_1 - \frac{\chi_2}{\omega - \Omega_2 - \frac{\chi_3}{\omega - \Omega_3 + \dots}}} \quad (3.27)$$

Hence, the dynamics of the Green's function is explicitly given in terms of the static expectation values included in the susceptibility matrices χ_i and the frequency matrices Ω_i , respectively. What looks like a fantastic possibility for an exact representation of the Green's function, has of course two major drawbacks:

1. For all cases of practical relevance the continued fraction is infinitely long.
2. Expectation values are, like Green's functions, unknown quantities.

The first point implies the necessity of a truncation. In practice, this is usually done by a simplification of the Liouvillian in the memory matrix of a certain level. If, e.g., the interaction part of \mathcal{L} is skipped, the remaining memory matrix might be solved exactly without the necessity of an additional projection. This automatically truncates the continued fraction.

It is important and essential for the POM to note that for each level of the continued fraction the memory matrix is calculated in a different Liouville subspace. The starting point is the level of description formed by the set $\{A_j\}$ of Liouville states $|A_j\rangle$. However, already the first memory matrix is formed by the Liouville states $|\mathcal{QL}A_j\rangle$, which, by construction, are part of the orthogonal complement of the original level of description. States in the second memory matrix

$$\hat{M}_{il}(\omega) = (\mathcal{QL}A_i | \mathcal{QL}Q\hat{Q} \frac{1}{\omega - \hat{Q}Q\mathcal{L}Q\hat{Q}} \hat{Q}Q\mathcal{L}Q | \mathcal{QL}A_l) \quad (3.28)$$

do again belong to none of the previously used levels of description, since they include the projector product $\hat{Q}Q$. Here, \hat{Q} is defined as

$$\hat{Q} = 1 - |\mathcal{QL}A_j\rangle \frac{1}{[\hat{\chi}^{-1}]_{jk}} (\mathcal{QL}A_k | \quad \text{with} \quad \hat{\chi}_{il} = (\mathcal{QL}A_i | \mathcal{QL}A_l). \quad (3.29)$$

Hence, with each step a larger and larger subspace of the Liouville space is considered to be relevant.⁹ A truncation procedure of the continued fraction therefore provides a final decision for a separation of the Liouville space into a relevant and an irrelevant part. In this sense we are dealing with a controlled approximation.

It is worth mentioning, that something similar happens in an equation of motion approach (EOM) for a retarded Green's function. There, with each higher order Green's function of the form $\langle\langle \mathcal{L}^n A; B \rangle\rangle_E$ the Liouville subspace considered is enlarged. However, there are two major differences between the EOM and the POM. Firstly, within EOM one is forced to find the solution of a complete set of Green's functions, whereas in POM one can (but does not have to) concentrate on a single Green's function only. Secondly, the EOM of a high order Green's function always contains a mixture of Green's functions of lower and higher order, what makes the set of equations particularly difficult to solve.¹⁰ Something like this is explicitly excluded in the POM, since the level of description of a higher order subspace is always orthogonal to all previous ones.

The second drawback mentioned above is more serious. Apparently, it is an intrinsic property of Green's functions to depend on several, a priori unknown, expectation values. To find appropriate expressions for them is also a major problem of the EOM. One clearly has to say, that this challenge is not avoided by the POM.

There are interesting suggestions by Becker and Fulde [37] to treat the static aspects in the same formalism as the dynamic entities. They combine the advantages of the POM with those of cumulant expectation values. A Liouville product¹¹ in terms of cumulants is defined as

$$(A|B)_0^c := \langle A^\dagger B \rangle_0^c \quad \text{with} \quad \langle A_1^\alpha \dots A_n^\nu \rangle_0^c = \frac{\partial^\alpha}{\partial \lambda_1^\alpha} \dots \frac{\partial^\nu}{\partial \lambda_n^\nu} \ln \left\langle \Phi_0 \left| \prod_{i=1}^n e^{\lambda_i A_i} \right| \Phi_0 \right\rangle \Big|_{\lambda_1=\lambda_n=0}. \quad (3.30)$$

Here $|\Phi_0\rangle$ is the ground state of an exactly-soluble system H_0 (with corresponding Liouvilian \mathcal{L}_0). A deeper investigation [77, 10] of the relations between cumulants and usual expectation values reveals a correspondence to the linked cluster theorem for Feynman diagrams, where the expectation values are evaluated by operator contractions. As in diagrammatic perturbation theories, this tool helps to limit the number of necessary calculations, to avoid normalization denominators and to ensure size consistency. All these advantages are transferred without the need of Wick's theorem.

For a compact notation Becker et al. introduced the wave operator

$$|\Omega\rangle = \lim_{z \rightarrow 0} \left(1 + \frac{1}{z - (H_1 + \mathcal{L}_0)} H_1 \right), \quad (3.31)$$

which transforms $|\Phi_0\rangle$ into the ground state of a system with an additional perturbation H_1 . For the system $H_0 + H_1$ they can then provide expressions for static quantities such as the ground-state energy shift [10] and general expectation values [9],

$$\delta E_0 = (H_1 |\Omega\rangle) \quad \text{and} \quad \langle A_\nu \rangle = (\Omega | A_\nu | \Omega)_0^c, \quad (3.32)$$

⁹The first hints of this idea can be found in the works of Mori, whereas Zwanzig was apparently not aware of this advantage of the continued fraction.

¹⁰This is a experience of our extensive study of the EOM in context of a two-site Kondo-cluster [49].

¹¹ The suggested product is not a scalar product since it is not positive definite.

and also for dynamic correlation functions [9],

$$\langle \delta A_\nu(\tau) \delta A_\mu \rangle = (\Omega | A_\nu e^{-\tau(\mathcal{L}_0 + H_1)} A_\mu | \Omega)_0^c \quad \text{with} \quad \delta A = A - \langle A \rangle, \quad (3.33)$$

at $T = 0\text{K}$ within the same approach. Even though a Laplace transformation of (3.33) allows for an application of the POM, the extension of the cumulant approach to finite temperatures [71] is from our perspective too difficult for a systematic investigation in terms of the POM.

For our study of the KLM, having the choice to use either cumulants or the POM, we have decided to evaluate a straightforward application of the POM and to not make use of cumulants. It is then most convenient to treat the static expectation values such, that their choice is consistent with the level of approximation used for the dynamics.

3.4 Application to the Hubbard model

We were not aware of any attempts to apply the POM to the KLM, before we started our investigations. However, there are some applications of the POM in the context of the Hubbard model [54, 55]

$$H = \sum_{i,j} \sum_{\sigma} (t_{ij} - \mu \delta_{ij}) c_{i\sigma}^\dagger c_{j\sigma} + \frac{U}{2} \sum_i \sum_{\sigma} \hat{n}_{i\sigma} \hat{n}_{i-\sigma} \quad (3.34)$$

$$= \sum_{\mathbf{k}} (\varepsilon(\mathbf{k}) - \mu) \hat{n}_{\mathbf{k}\sigma} + \frac{U}{N} \sum_{\mathbf{k}_1, \mathbf{k}_2, \mathbf{k}_3, \mathbf{k}_4} \delta_{\mathbf{k}_1 - \mathbf{k}_2, \mathbf{k}_4 - \mathbf{k}_3} c_{\mathbf{k}_1\uparrow}^\dagger c_{\mathbf{k}_2\uparrow} c_{\mathbf{k}_3\downarrow}^\dagger c_{\mathbf{k}_4\downarrow} \quad (3.35)$$

$$\implies \mathcal{L} = \mathcal{L}_0 + \mathcal{L}_1. \quad (3.36)$$

Because of similarities of these two models [124], it is worthwhile to review some of the strategies applied to the Hubbard model. Since these efforts were quite successful for this model, we will make use of them for our treatment of the KLM in the following chapters.

Consideration of weak and strong couplings

A highly relevant paper that should be mentioned in this context has been published by **Kishore** [69]. He was the first to put equal focus on the weak- and the strong-correlation regime of the Hubbard model and used the POM for this purpose. His level of description is formed by the one-dimensional basis $|A\rangle = |c_{j\sigma}^\dagger\rangle$. Then the frequency matrix is already sufficient to obtain the Hartree-Fock result.

In the weak-correlation regime Kishore truncates the continued fraction by neglecting the contribution of \mathcal{L}_1 in the denominator of the memory matrix. Since $\mathcal{L}_1 \sim U$, those parts of the self-energy, which are proportional to U^3 or higher powers of U are therefore not taken into account. The intention to be correct in order U^2 also assists in the evaluation of static expectation values, which are obtained using the set of eigenstates of H_0 . Therefore, Kishore obtains for the memory matrix

$$M_{\mathbf{k}\sigma}(\omega) = \left(\frac{U}{N}\right)^2 \sum_{\mathbf{k}_1, \mathbf{k}_2} \frac{\hat{n}_{\mathbf{k}_1-\sigma} (1 - \hat{n}_{\mathbf{k}_2-\sigma}) + (\hat{n}_{\mathbf{k}_2-\sigma} - \hat{n}_{\mathbf{k}_1-\sigma}) \hat{n}_{\mathbf{k}+\mathbf{k}_1-\mathbf{k}_2\sigma}}{\omega + \varepsilon_{\mathbf{k}_1} - \varepsilon_{\mathbf{k}_2} - \varepsilon_{\mathbf{k}+\mathbf{k}_1-\mathbf{k}_2}}. \quad (3.37)$$

Before studying Kishore's strategy for the strongly correlated regime, one should mention the precursor work of **Fedro and Wilson** [30]. In this limit Fedro and Wilson investigated several levels of approximation for the memory matrix. The first level is analogous to Kishore's weak-correlation strategy. If the contribution of \mathcal{L}_0 is completely neglected in the memory matrix,

$$M_{\mathbf{k}\sigma}(\omega) = \frac{U^2 n_{-\sigma}(1 - n_{-\sigma})}{\omega + \mu - U(1 - n_{-\sigma})} \quad (3.38)$$

it is identical to the Hubbard-I-solution [54]. The similarity is not accidental, since in the latter only those higher-order Green's functions are decoupled which have the hopping integral t_{ij} as a prefactor in the equation of motion. It is possible to factor out t_{ij} , and this single contribution of the hopping corresponds to the frequency matrix in POM. On the other hand the U -contribution is treated exactly in both approaches.

The second level of approximation in the work of Fedro and Wilson consists of an equation of motion for the memory matrix, obtained from the time derivative of the time-dependent memory matrix. This strategy is similar¹² to a second level in the continued fraction as obtained by the POM. It yields a correlation function in the memory matrix which is proportional to t_{ij} . For this correlation function one has to replace the Liouvillian \mathcal{L} again by the interaction part \mathcal{L}_1 to obtain the expression

$$\begin{aligned} B_{\mathbf{k}\sigma} &= \sum_{ij} t_{ij} \left\langle c_{i-\sigma}^\dagger c_{j-\sigma} \right\rangle - \sum_j t_{ij} \left\langle \left(c_{i-\sigma}^\dagger c_{j-\sigma} + c_{j-\sigma}^\dagger c_{i-\sigma} \right) \hat{n}_{j\sigma} \right\rangle \\ &- \sum_{(i-j)} e^{-i\mathbf{k}(\mathbf{R}_i - \mathbf{R}_j)} t_{ij} \left(\left\langle \delta \hat{n}_{i-\sigma} \delta \hat{n}_{j-\sigma} \right\rangle + \left\langle c_{j\sigma}^\dagger c_{j-\sigma} c_{i-\sigma}^\dagger c_{i\sigma} \right\rangle - \left\langle c_{j\sigma}^\dagger c_{j-\sigma} c_{i-\sigma} c_{i\sigma} \right\rangle \right), \end{aligned} \quad (3.39)$$

which enters the memory matrix as follows:

$$M_{\mathbf{k}\sigma}(\omega) = \frac{U^2 n_{-\sigma}(1 - n_{-\sigma})}{\omega + \mu - U(1 - n_{-\sigma})} - \frac{U^2 B_{\mathbf{k}\sigma}}{(\omega + \mu - U(1 - n_{-\sigma}))^2}. \quad (3.40)$$

The result resembles a Taylor expansion of the self-energy as obtained by Esterling et al. [29] and the spectral-density approach (SDA) of Nolting et al. [111]. For the latter, an identical expression for $B_{\mathbf{k}\sigma}$ is obtained.

In a third level of approximation the same kind of equation of motion is now applied to the correlation function which lead to $B_{\mathbf{k}\sigma}$. This yields another correlation function of the same order in t_{ij} . One therefore has to conclude, that (3.40) does not include all contributions proportional to t_{ij} . Fedro and Wilson claim that this problem is an inherent difficulty of expanding around the atomic limit. This was pointed out earlier by Bari [7] and Esterling [28].

Kishore comes to the conclusion that in the atomic limit the two-level structure of the quasiparticle-spectrum is responsible for these difficulties in the strong-correlation regime. He therefore suggests as an alternative approach a Hubbard-III-like splitting of the Green's function [55],

$$G_{ij\sigma} = \sum_{\alpha=\pm} \left\langle \left\langle \hat{n}_{i-\sigma}^\alpha c_{i\sigma}; c_{j\sigma}^\dagger \right\rangle \right\rangle_E \quad \text{with} \quad \hat{n}_{i-\sigma}^+ = \hat{n}_{i-\sigma} \quad / \quad \hat{n}_{i-\sigma}^- = 1 - \hat{n}_{i-\sigma}. \quad (3.41)$$

¹² The strategy is not equivalent to the POM. Note, for example, that the time derivative of the memory matrix performed in [30] does not have the structure of a Dyson equation.

To each of these single-poled partial Green's functions the projection-operator method is applied, using the projector

$$\mathcal{P}_\sigma^\alpha := \left| c_{j\sigma}^\dagger \right\rangle \frac{1}{n_{-\sigma}^\alpha} \langle \hat{n}_{i-\sigma}^\alpha c_{i\sigma} |. \quad (3.42)$$

The expression obtained for the memory matrix is particularly convenient for an expansion in terms of $\varepsilon_{\mathbf{k}}$, since it is already sufficient to neglect the contribution of \mathcal{L}_0 in the denominator of the memory matrix to obtain the first order result

$$M_{\mathbf{k}\sigma}^\alpha = -n_{-\sigma}^{(-\alpha)} \varepsilon_{\mathbf{k}} - \frac{B_{\mathbf{k}\sigma}}{n_{-\sigma}^\alpha}. \quad (3.43)$$

Here, $B_{\mathbf{k}\sigma}$ is identical with the expression of Fedro and Wilson (3.39). However, in contrast to their result the memory matrix (3.43) does not show an ω -dependence. The combined Green's function is therefore

$$G_{\mathbf{k}\sigma}(w) = \frac{n_{-\sigma}}{\omega - n_{-\sigma} \varepsilon_{\mathbf{k}} - U + \frac{B_{\mathbf{k}\sigma}}{n_{-\sigma}}} + \frac{1 - n_{-\sigma}}{\omega - (1 - n_{-\sigma}) \varepsilon_{\mathbf{k}} + \frac{B_{\mathbf{k}\sigma}}{1 - n_{-\sigma}}}. \quad (3.44)$$

This result has similar features to the SDA of Nolting et al. [111], but it is not identical to it.

Iteration of the POM

An interesting improvement of Kishore's weak-coupling results has been suggested by **Bulk and Jelitto** [15, 16]. It consists in an *iterated partitioning of the Hamiltonian*. The initial partitioning is given in (3.36). Bulk and Jelitto suggest that for the next and every following order in perturbation the sum of all self-energy contributions of the preceding orders should be added to the unperturbed part:

$$\left. \begin{aligned} H_0^{(N)} &= H_0^{(N-1)} + V^{(N-1)}(\omega) \\ H_1^{(N)} &= H - H_0^{(N)}(\omega) \end{aligned} \right\} V^{(N-1)}(\omega) = \sum_{\mathbf{k}\sigma} M_{\mathbf{k}\sigma}^{(N-1)}(\omega) \hat{n}_{\mathbf{k}\sigma} \quad (3.45)$$

The partitioning of the Hubbard Hamiltonian enters the POM in three different ways. Firstly, due to the structure of the Hamiltonian, the \mathcal{L}_0 -part of the Liouville states $\left| \mathcal{Q}\mathcal{L}c_{j\sigma}^\dagger \right\rangle$ vanishes. Secondly, in terms of a weak-correlation perturbation theory the effect of \mathcal{L}_1 is neglected in the denominator of the memory matrix. Thirdly, expectation values for all correlation functions are determined in the unperturbed system defined by H_0 . The last two effects are most important. To add here a lower order self-energy is similar to a perturbation *around Hartree-Fock* in diagrammatic approaches. As a result the following expression of the memory-matrix is obtained:

$$M_{\mathbf{k}\sigma}(\omega) = \left(\frac{U}{N} \right)^2 \sum_{\mathbf{q}\mathbf{p}} \frac{(1 - f_{\mathbf{q}\sigma})(1 - f_{\mathbf{p}-\sigma}) f_{\mathbf{p}+\mathbf{q}-\mathbf{k},-\sigma} + f_{\mathbf{q}\sigma} f_{\mathbf{p}-\sigma} (1 - f_{\mathbf{p}+\mathbf{q}-\mathbf{k},-\sigma})}{\omega - \varepsilon_{\mathbf{q}} - \varepsilon_{\mathbf{p}} + \varepsilon_{\mathbf{p}+\mathbf{q}-\mathbf{k}} - U n_{-\sigma} + \mu}. \quad (3.46)$$

The f 's abbreviate the Fermi-distribution functions

$$f_{\mathbf{q}\sigma} = \langle n_{\mathbf{q}\sigma} \rangle_0 = \frac{1}{\exp[\beta(\varepsilon_{\mathbf{q}} + Un_{-\sigma} - \mu)] + 1}. \quad (3.47)$$

The emergence of U is the third effect of the partitioning mentioned above.

Of course, there are structural similarities to the result (3.37) of Kishore. However, the appearance of U in the denominator renders the result much closer¹³ to the structure of the solution (3.38) of the strong-correlation regime, which includes the atomic limit. A comparison with other methods shows that the iteration of Bulk and Jelitto yields a more complex structure of the energy dependence of the self-energy. Most importantly, a splitting of the free Bloch band occurs into two quasiparticle sub-bands approximately at T_0 and $T_0 + U$. This is well-known from the strong-correlation regime. However, there is no gap. The bands are linked by a small but finite density of states due to damping effects. Concerning the question of ferromagnetism the description is a clear improvement of the Stoner results. One not only obtains a critical value U_c , but also an n_c above which ferromagnetism might occur. A comparison with strong-coupling SDA-results [111] yields the remarkable conclusion that in its range of applicability the second-order perturbation theory of Bulk and Jelitto is not restricted to parameter constellations with $U \leq W$, but also leads to rather plausible results for larger values of U .

Enlargement of the relevant Liouville subspace

In principle there are two ways to improve results within the POM. 1) Consider further steps in the continued fraction. 2) Increase the dimensionality of the relevant Liouville subspace already for the first step of the POM. **B. Mehlig, H. Eskes, R. Hayn and M. Meinders** [89] applied this second approach to the Hubbard model. The basis of their subspace is given by

$$\begin{aligned} |A_1\rangle &= \left| c_{\mathbf{k}\sigma}^\dagger \right\rangle &= \frac{1}{\sqrt{N}} \sum_j e^{i\mathbf{k}\mathbf{R}_j} \left| c_{j\sigma}^\dagger \right\rangle \\ |A_2\rangle &= \left| \mathcal{Q}_1 \mathcal{L} c_{\mathbf{k}\sigma}^\dagger \right\rangle &\sim \frac{1}{\sqrt{N}} \sum_j e^{i\mathbf{k}\mathbf{R}_j} \left| c_{j\sigma}^\dagger \delta \hat{n}_{j-\sigma} \right\rangle \\ &\vdots \\ |A_\nu\rangle &= \left| \mathcal{Q}_{\nu-1} \cdots \mathcal{Q}_1 \mathcal{L}^{\nu-1} A_1 \right\rangle \end{aligned} \quad (3.48)$$

with $\mathcal{Q}_\nu = 1 - |A_\nu\rangle \frac{1}{\langle A_\nu | A_\nu \rangle} \langle A_\nu |$. A two-pole approximation corresponds to taking $\nu_{\max} = 2$ and yields the same set of operators as the Hubbard-I approximation [54]. The 2×2 susceptibility and frequency matrix are calculated. The memory matrix, however, is not considered. The elements of the frequency matrix are closely related to the moments $M_{\mathbf{k}\sigma}^{(n)}$ of the spectral density [111] as defined in (3.9). For instance

$$\begin{aligned} (A_2 | \mathcal{L} | A_2) &= \left(c_{\mathbf{k}\sigma}^\dagger \mathcal{L} \mathcal{Q} \left| \mathcal{L} \left| \mathcal{Q} \mathcal{L} c_{\mathbf{k}\sigma}^\dagger \right\rangle \right. \right) \quad \text{with} \quad \mathcal{Q} = 1 - \left| c_{\mathbf{k}\sigma}^\dagger \right\rangle \left(c_{\mathbf{k}\sigma}^\dagger \left| \right. \right) \\ &= \left(c_{\mathbf{k}\sigma}^\dagger \left| \mathcal{L}^3 c_{\mathbf{k}\sigma}^\dagger \right\rangle \right) + 2 \left(c_{\mathbf{k}\sigma}^\dagger \left| \mathcal{L} c_{\mathbf{k}\sigma}^\dagger \right\rangle \right) \left(c_{\mathbf{k}\sigma}^\dagger \left| \mathcal{L}^2 c_{\mathbf{k}\sigma}^\dagger \right\rangle \right) + \left(c_{\mathbf{k}\sigma}^\dagger \left| \mathcal{L} c_{\mathbf{k}\sigma}^\dagger \right\rangle \right)^3 \\ &= M_{\mathbf{k}\sigma}^{(3)} + 2M_{\mathbf{k}\sigma}^{(1)} M_{\mathbf{k}\sigma}^{(2)} + \left(M_{\mathbf{k}\sigma}^{(1)} \right)^3. \end{aligned} \quad (3.49)$$

¹³ It is even identical with the Hubbard-I solution at half filling.

Hence,

$$\Omega_{\mathbf{k}\sigma} = \begin{pmatrix} M_{\mathbf{k}\sigma}^{(1)} & M_{\mathbf{k}\sigma}^{(2)} + \left(M_{\mathbf{k}\sigma}^{(1)}\right)^2 \\ M_{\mathbf{k}\sigma}^{(2)} + \left(M_{\mathbf{k}\sigma}^{(1)}\right)^2 & M_{\mathbf{k}\sigma}^{(3)} + 2M_{\mathbf{k}\sigma}^{(1)}M_{\mathbf{k}\sigma}^{(2)} + \left(M_{\mathbf{k}\sigma}^{(1)}\right)^3 \end{pmatrix}. \quad (3.50)$$

It is not surprising that there are similarities to SDA calculations [111]. Mehlig et al. [89] claim that these results are improved by the inclusion of antiferromagnetic correlations. This is particularly related to the calculation of the correlation functions in $B_{\mathbf{k}\sigma}$ given by (3.39) and which are contributing to $M_{\mathbf{k}\sigma}^{(3)}$. They are determined by additional Green's functions $(B_\nu | \frac{1}{w-\mathcal{L}} A_1)$ with some given Liouville states $|B_1\rangle, \dots, |B_4\rangle$, instead of using simplifying assumptions as in [111]. These Green's functions are approximated by projecting the $|B_\nu\rangle$ onto the subspace spanned by $|A_1\rangle$ and $|A_2\rangle$. This approximation corresponds to Roth's method [134] of treating the two-particle correlation functions. It allows the self-consistent calculation of all expectation values and gives a closed set of equations for the single-particle Green's function.

The results for the single-particle spectral density are compared to numerical spectra of finite Hubbard rings and of a 4×4 cluster given by Leung et al. [80]. Global features of these spectra are reproduced both qualitatively and quantitatively by the two-pole ansatz. In particular, it succeeds in describing the change of dispersion of the Hubbard bands upon doping.

Further strategies

Of course, the number of papers mentioned above is not exhaustive. In recent times, there have been further attempts of a POM approach to the Hubbard model. One could mention the works of S. Onoda and M. Imada [125], who claim that the continued-fraction expansion of the Mori formalism is particularly suited for systematically evaluating the energy hierarchy structure from high to low energies. Also the works of Y. Kakehashi and P. Fulde [64] are very interesting, since they show an equivalence of their combination of the POM with a many-body coherent potential approximation (CPA) on the one hand, and the dynamical mean-field theory (DMFT) on the other. However, since we do not use their strategies for our investigations into the KLM, we refrain from a more detailed discussion.

Chapter 4

The subsystem of itinerant carriers

As already pointed out, the Kondo-lattice model can be approached from two sides. The itinerant subsystem is studied more successfully in the literature than its local-moment counterpart. However, even for this subsystem the POM is by construction more systematic than the approximations provided in Sec. 2.3 and can therefore be used for an assessment of those results. We will start the investigation with a couple of limiting cases, for which definite statements can be made. This is probably the best way to develop and explain approaches, which can subsequently be applied to arbitrary parameter constellations. However, those readers that are merely interested in new results can skip Secs. 4.1 and 4.2. A useful indicator for our purpose is the structure of the density of states, as obtained from the one-electron retarded Green's function. Therefore, our evaluations will focus on this function.

4.1 The ferromagnetically saturated semiconductor

The ferromagnetically saturated semiconductor has already been characterized as a limiting case with constrained expectation values $\langle \hat{n}_\uparrow \rangle = \langle \hat{n}_\downarrow \rangle = 0$ and $\langle S^z \rangle = \hbar S$ in section 2.2. These simplifications allow for the exact determination of expressions (2.9) and (2.10) for the one-electron Green's function. However, a derivation of these results has not yet been given. We will do this with the help of the POM, since this limit is particularly appropriate for studying different aspects of this method. This is also the reason, why we start with approximations and provide more than one exact calculation.¹

Preliminaries

To begin with, the relevant Liouville subspace has to be identified. Since our goal is the one-particle Green's function, this subspace has to contain single-electron excitations $|c_{l\sigma}^\dagger\rangle$. For a start, we stay with this one-dimensional² basis. If this choice is combined

¹ The presentation given here should allow to follow the principle steps of the calculations. A more detailed derivation of some of the equations obtained will be provided in appendix D.

² The classification as a "one-dimensional" basis is based on the Bloch representation $|c_{\mathbf{k}\sigma}^\dagger\rangle$. In real space it actually consists of N elements.

with a convenient scalar product as provided in (3.3), the *susceptibility matrix* $\chi_{ij} = \delta_{ij}$ and the projectors

$$\mathcal{P}_\sigma = \sum_{j=1}^N \left| c_{j\sigma}^\dagger \right\rangle \left\langle c_{j\sigma}^\dagger \right| \quad \text{and} \quad \mathcal{Q}_\sigma = 1 - \mathcal{P}_\sigma \quad (4.1)$$

are particularly simple. Our aim is the representation of the Green's function as a continued fraction. According to the rules presented in the previous chapter (p. 28), we next need to know the action of the Liouvillian on the basis elements

$$\mathcal{L} \left| c_{l\sigma}^\dagger \right\rangle = \frac{1}{\hbar} \left[\left[H, c_{l\sigma}^\dagger \right]_- \right] = \frac{1}{\hbar} \sum_j T_{jl} \left| c_{j\sigma}^\dagger \right\rangle - \frac{J}{2\hbar} \left\{ z_\sigma S_l^z \left| c_{l\sigma}^\dagger \right\rangle + S_l^\sigma \left| c_{l-\sigma}^\dagger \right\rangle \right\}, \quad (4.2)$$

in order to obtain an expression for the single-electron *frequency matrix*:

$$\Omega_{il\sigma} = \frac{1}{\hbar} T_{il} - \frac{J}{2\hbar} z_\sigma \langle S_i^z \rangle \delta_{il} \quad \Longrightarrow \quad \Omega_{\mathbf{k}\sigma} = \frac{1}{\hbar} \varepsilon_{\mathbf{k}} - \frac{J}{2} z_\sigma S. \quad (4.3)$$

Evidently, this is already the full mean-field contribution (2.6) to the self-energy – a general feature of the POM.

The more demanding memory matrix should be evaluated in terms of the geometric series

$$M_{il\sigma} = \sum_{m=0}^{\infty} \frac{1}{\omega^{m+1}} \left(\mathcal{Q}\mathcal{L} c_{i\sigma}^\dagger \left| \left(\mathcal{Q}\mathcal{L}\mathcal{Q} \right)^m \right| \mathcal{Q}\mathcal{L} c_{l\sigma}^\dagger \right). \quad (4.4)$$

A necessary condition for the evaluation of this infinite sum is the possibility to express the effect of $(\mathcal{Q}\mathcal{L}\mathcal{Q})^m$ for arbitrary m . This is the actual challenge of the memory matrix. Even though the idempotence of \mathcal{Q} makes some of these operators in (4.4) superfluous³, a notation in this form has the advantage of a Liouville state

$$\left| \mathcal{Q}\mathcal{L} c_{l\sigma}^\dagger \right\rangle = -\frac{J}{2\hbar} \left\{ z_\sigma [S_l^z - \langle S^z \rangle] \left| c_{l\sigma}^\dagger \right\rangle + S_l^\sigma \left| c_{l-\sigma}^\dagger \right\rangle \right\}, \quad (4.5)$$

which scales with the interaction J . Since the same is true for the bra-state $\left(\mathcal{Q}\mathcal{L} c_{i\sigma}^\dagger \left| \right.$ the memory matrix is at least of order J^2 . For example, for the first term of (4.4) one obtains the scalar product

$$\left(\mathcal{Q}\mathcal{L} c_{i\sigma}^\dagger \left| \mathcal{Q}\mathcal{L} c_{l\sigma}^\dagger \right. \right) = \frac{1}{2} J^2 S \delta_{\sigma\downarrow} \delta_{il}. \quad (4.6)$$

Therefore, the prefactor of J^2 vanishes for \uparrow -electrons and is the positive number $\frac{1}{2} S \hbar^2$ for \downarrow -electrons. The other terms in (4.4) will yield higher order expressions in J or $\varepsilon_{\mathbf{k}}$, respectively. The structure is particularly convenient for an expansion of the self-energy. Similar to the investigations of Kishore [69] for the Hubbard model we can study the strong- and weak-coupling limit with the same level of approximation.

³We omit the index σ at \mathcal{Q}_σ due to the fact that $M_{i\uparrow}$ vanishes identically and only $\sigma = \downarrow$ needs to be considered.

Strong-coupling limit

In the strong-coupling limit an expansion of the self-energy in terms of the hopping matrix T_{il} is of interest. This is obtained if only the contribution of \mathcal{L}_{sf} is considered in the denominator of the geometric series (4.4). Its effect on the state (4.5) is given by the commutator

$$\mathcal{L}_{sf} \left| \mathcal{Q} \mathcal{L} c_{l\sigma}^\dagger \right\rangle = \frac{J^2}{4\hbar^2} \sum_i \sum_{\sigma'} \left[\left[z_{\sigma'} S_i^z \hat{n}_{i\sigma'} + S_i^{\sigma'} c_{i-\sigma'}^\dagger c_{i\sigma'}, z_\sigma \delta(S_l^z) c_{l\sigma}^\dagger + S_l^\sigma c_{l-\sigma}^\dagger \right]_- \right], \quad (4.7)$$

which yields a sum of four non-trivial operator products. Here, the abbreviation $\delta(A) = A - \langle A \rangle$ has been introduced. However, the result of (4.7) is only an intermediate step. We are actually interested in the projection onto the orthogonal complement of the original Liouville subspace. After a couple of transformations provided in appendix D the result can be expressed in the form

$$\mathcal{Q} \mathcal{L}_{sf} \left| \mathcal{Q} \mathcal{L} c_{l\sigma}^\dagger \right\rangle = \frac{J}{2} (1 + z_\sigma S) \left| \mathcal{Q} \mathcal{L} c_{l\sigma}^\dagger \right\rangle. \quad (4.8)$$

The fact that the original Liouville state $\left| \mathcal{Q} \mathcal{L} c_{l\sigma}^\dagger \right\rangle$ is reproduced when applying the superoperator $(\mathcal{Q} \mathcal{L}_{sf} \mathcal{Q})$ is a nice mathematical feature. However, it is also essential for the summation of the entire geometric series, since the expression for the general term of this series

$$\left(\mathcal{Q} \mathcal{L} c_{i\sigma}^\dagger \left| (\mathcal{Q} \mathcal{L}_{sf} \mathcal{Q})^m \left| \mathcal{Q} \mathcal{L} c_{l\sigma}^\dagger \right\rangle \right. \right) = \left(\mathcal{Q} \mathcal{L} c_{i\sigma}^\dagger \left| \left(\frac{1}{2} J \right)^m (1 + z_\sigma S)^m \left| \mathcal{Q} \mathcal{L} c_{l\sigma}^\dagger \right\rangle \right) \quad (4.9)$$

can now be provided. For this reason there is, of course, no need to proceed with the concept of a continued fraction. In combination with the previous result (4.6) for the scalar product it is now rather simple to obtain the full expression for the *memory matrix* directly

$$M_{il}^{(1)}(\omega) = \frac{\frac{1}{2} J^2 S}{\omega - \frac{1}{2} J(1 - S)} \delta_{il} \quad \Longrightarrow \quad M_{\mathbf{k}\downarrow}^{(1)}(\omega) = \frac{\frac{1}{2} J^2 S}{\omega - \frac{1}{2} J(1 - S)}. \quad (4.10)$$

What does this approximated result mean in terms of Green's functions? For \uparrow -electrons the memory matrix does not contribute to the self-energy and the mean-field Green's function is the complete result. For \downarrow -electrons one has to insert the result into the representation (3.26)

$$G_{\mathbf{k}\downarrow}^{(1)}(\omega) = \frac{1}{\omega - \frac{1}{\hbar} \varepsilon_{\mathbf{k}} - \frac{1}{2} JS - M_{\mathbf{k}\downarrow}^{(1)}(\omega)} = \frac{1}{\omega_1 - \omega_2} \left(\frac{\omega_1 - \frac{1}{2} J(1 - S)}{\omega - \omega_1} - \frac{\omega_2 - \frac{1}{2} J(1 - S)}{\omega - \omega_2} \right) \quad (4.11)$$

and one obtains a structure with two energy poles

$$\omega_{1,2} = \frac{1}{2\hbar} \varepsilon_{\mathbf{k}} + \frac{1}{4} J \pm \frac{1}{2} \sqrt{\left(\frac{1}{\hbar} \varepsilon_{\mathbf{k}} - \frac{1}{2} J + JS \right)^2 + \lambda 2J^2 S}. \quad (4.12)$$

Here, we have introduced the parameter λ to visualize the corrections of higher orders in J . Taking $\lambda = 0$ yields the mean-field result for the \downarrow -Green's function. The energy pole $\omega_2(\lambda = 0) = \frac{1}{2}J(1 - S)$ has vanishing spectral weight. Switching on λ leads to an increase of the spectral weight of this pole and simultaneously to a decrease of the spectral weight of ω_1 , such that their sum remains 1. The full contribution of \mathcal{L}_{sf} in the memory matrix corresponds to $\lambda = 1$. How the spectral weight is actually distributed between the two poles depends on the interplay of the energy scales W and J . In the zero-bandwidth limit ($W = 0$) we have a ratio of the spectral weights $\alpha_1 : \alpha_2 = 2S : 1$.

Weak-coupling limit

In analogy to the strong-coupling limit we treat the weak coupling by neglecting the interaction \mathcal{L}_{sf} in the denominator of the memory matrix (4.4). It is the kinetic energy H_s which plays the dominant role in this limit. In the previously discussed limit it was essential, that the application of $(\mathcal{Q}\mathcal{L}_{sf}\mathcal{Q})$ does not change the relevant Liouville subspace. The same is not true for $(\mathcal{Q}\mathcal{L}_s\mathcal{Q})$, since a sum⁴ over the index of the Fermi-operator is introduced:

$$(\mathcal{Q}\mathcal{L}_s\mathcal{Q})^1 \left| \mathcal{Q}\mathcal{L} c_{l\sigma}^\dagger \right\rangle = -\frac{J}{2\hbar} \frac{1}{\hbar^1} T_{k_1 l} \left| z_\sigma \delta(S_l^z) c_{k_1 \sigma}^\dagger + S_l^\sigma c_{k_1 - \sigma}^\dagger \right\rangle \quad (4.13)$$

$$(\mathcal{Q}\mathcal{L}_s\mathcal{Q})^2 \left| \mathcal{Q}\mathcal{L} c_{l\sigma}^\dagger \right\rangle = -\frac{J}{2\hbar} \frac{1}{\hbar^2} T_{k_2 k_1} T_{k_1 l} \left| z_\sigma \delta(S_l^z) c_{k_2 \sigma}^\dagger + S_l^\sigma c_{k_2 - \sigma}^\dagger \right\rangle \quad (4.14)$$

⋮

$$(\mathcal{Q}\mathcal{L}_s\mathcal{Q})^m \left| \mathcal{Q}\mathcal{L} c_{l\sigma}^\dagger \right\rangle = -\frac{J}{2\hbar} \frac{1}{\hbar^m} [\underline{\mathbb{T}}^m]_{k_m l} \left| z_\sigma \delta(S_l^z) c_{k_m \sigma}^\dagger + S_l^\sigma c_{k_m - \sigma}^\dagger \right\rangle \quad (4.15)$$

Here, $\underline{\mathbb{T}}$ is the hopping matrix composed of the elements T_{kl} . Accordingly, $[\underline{\mathbb{T}}^m]_{kl}$ is an element of the matrix $\underline{\mathbb{T}}^m$. Nevertheless, this is a generalization that can still be handled. The reason is a scalar product with the bra-state that is almost identical to (4.6). The additional index label only yields a further δ_{ik} -function, but has no other implications.

The matrix identities are best expressed in the Fourier transformed representation

$$\left(\mathcal{Q}\mathcal{L} c_{\mathbf{k}\sigma}^\dagger \left| (\mathcal{Q}\mathcal{L}_s\mathcal{Q})^m \left| \mathcal{Q}\mathcal{L} c_{\mathbf{k}\sigma}^\dagger \right\rangle \right. \right) = \frac{1}{2} J^2 S \delta_{\sigma\downarrow} \frac{1}{N} \sum_{\mathbf{q}} \frac{1}{\hbar^m} \varepsilon_{\mathbf{k}-\mathbf{q}}^m, \quad (4.16)$$

which allows for a direction calculation of the geometric series. For the memory matrix in the weak-coupling limit we obtain:

$$M_{\mathbf{k}\sigma}^{(2)}(\omega) = \frac{1}{2} J^2 S \delta_{\sigma\downarrow} \frac{1}{N} \sum_{\mathbf{q}} \frac{\hbar}{\hbar\omega - \varepsilon_{\mathbf{k}-\mathbf{q}}} = \frac{1}{2} J^2 S \delta_{\sigma\downarrow} \frac{1}{N} \sum_{\mathbf{q}} G_{\mathbf{q}}^{(0)}(\omega), \quad (4.17)$$

where $G_{\mathbf{q}}^{(0)}(\omega)$ denotes the free Green's function. Reconsidering the assumptions of this limit, it is clear that the result derived here for the self-energy differs from an exact

⁴Einstein's sum convention is used.

calculation only in terms which are at least of order J^3 . Hence,

$$\Sigma_{\mathbf{k}\sigma}^{(2)}(\omega) = -\frac{J}{2} z_\sigma \hbar S + \frac{J^2}{4} \cdot \frac{2\hbar S}{N} \sum_{\mathbf{q}} G_{\mathbf{q}}^{(0)}(\omega) \delta_{\sigma\downarrow}, \quad (4.18)$$

is, up to order J^2 , the exact expression for the self-energy of the ferromagnetically saturated semiconductor. In contrast to the strong-coupling limit it is not possible to separate the respective Green's function into two energy poles. Due to the \mathbf{q} -summation in $M_{\mathbf{k}\sigma}^{(2)}$ already the spectral density shows a continuum.

All-coupling strategy I: In the spirit of weak and strong couplings

As mentioned in section 2.2 even an exact solution for the Green's function of the ferromagnetically saturated semiconductor is known. Of course, this can also be obtained with the help of the POM. There are – and this is what makes the work with the projection-operator method so interesting – at least four different possibilities to derive it. According to the aim of this section to study different aspects of the POM, we will briefly explain each of them.

The first strategy is based on the following idea: Since the geometric series (4.4) can be calculated exactly with $(\mathcal{Q}\mathcal{L}_s\mathcal{Q})$ and with $(\mathcal{Q}\mathcal{L}_{sf}\mathcal{Q})$ in the denominator, the same could be possible for the sum $(\mathcal{Q}\mathcal{L}_s\mathcal{Q}) + (\mathcal{Q}\mathcal{L}_{sf}\mathcal{Q})$. Unfortunately, one is then confronted with terms such as

$$(\mathcal{Q}\mathcal{L}_s\mathcal{Q})^p (\mathcal{Q}\mathcal{L}_{sf}\mathcal{Q}) (\mathcal{Q}\mathcal{L}_s\mathcal{Q})^q \left| \mathcal{Q}\mathcal{L}c_{l\sigma}^\dagger \right\rangle. \quad (4.19)$$

First, $(\mathcal{Q}\mathcal{L}_s\mathcal{Q})^q$ changes the ket-state at the right to a version with different indices for the spin- and the Fermi-operators, then the application of $(\mathcal{Q}\mathcal{L}_{sf}\mathcal{Q})$ destroys the repetitive structure, since a simplification as in (4.8) has equal indices as a precondition and finally $(\mathcal{Q}\mathcal{L}_s\mathcal{Q})^p$ yields a highly non-trivial product of operators.

However, one should keep in mind that at the end the scalar product with the bra-state $\langle \mathcal{Q}\mathcal{L}c_{i\sigma}^\dagger |$ needs to be evaluated for the memory matrix. The fact, that during the calculation of the expectation value a lot of operator combinations vanish, is borne in mind by introducing the Liouville state

$$|_{k_n \dots k_1} A_{lj} \rangle = -\frac{J}{2\hbar} \left(\frac{J}{2} z_\sigma \right)^n \left| S_{k_n}^z \cdot S_{k_{n-1}}^z \cdots S_{k_2}^z \cdot S_{k_1}^z \cdot S_l^\sigma c_{j-\sigma}^\dagger \right\rangle. \quad (4.20)$$

It incorporates all the operators which remain essential in the limit considered. For example one does not make a mistake if one identifies the Liouville state $|\mathcal{Q}\mathcal{L}c_{i\sigma}^\dagger\rangle$ just with $|A_{ll}\rangle$. Using this notation all further calculations can be reduced to the following rules:

$$(A_{ii} |_{k_n \dots k_1} A_{lj} \rangle) \stackrel{(4.6)}{=} \frac{1}{2} J^2 S \delta_{\sigma\downarrow} \delta_{il} \delta_{ij} \prod_{x=1}^n \frac{1}{2} J \hbar (\delta_{ik_x} - S), \quad (4.21)$$

$$(A_{ii} | (\mathcal{Q}\mathcal{L}_{sf}\mathcal{Q})^m |_{k_n \dots k_1} A_{lj} \rangle) \stackrel{(4.7)}{=} \frac{1}{\hbar^m} (A_{ii} | \underbrace{j \dots j}_{m \times} |_{k_n \dots k_1} A_{lj} \rangle), \quad (4.22)$$

$$(A_{ii} | (\mathcal{Q}\mathcal{L}_s\mathcal{Q})^m |_{k_n \dots k_1} A_{lj} \rangle) \stackrel{(4.15)}{=} (A_{ii} |_{k_n \dots k_1} A_{lk} \rangle) \frac{1}{\hbar^m} [\mathbf{T}^m]_{kj}. \quad (4.23)$$

These are generalizations of corresponding calculations in the previous limits.

Now, the problem of an expression like (4.19) becomes apparent as the δ_{ik_x} -function in the scalar product (4.21). This term is the reason why the structure for the first terms

$$(A_{ii} | (\mathcal{QLQ})^m | A_{ll}) = \frac{1}{2} J^2 S \delta_{\sigma\downarrow} \delta_{il} \left[\left(\frac{1}{\hbar} \mathbb{T} + \frac{1}{2} J \mathbb{1} - \frac{1}{2} J S \mathbb{1} \right)^m \right]_{il} \quad m = 0, 1, 2. \quad (4.24)$$

of the geometric series (4.4) cannot be generalized to $m \geq 3$. Instead, we separate out all terms without this δ -function and define a modified hopping matrix

$$\underline{U} = \left[\frac{1}{\hbar} \mathbb{T} - \frac{1}{2} J S \mathbb{1} \right]. \quad (4.25)$$

Interestingly⁵, this corresponds to a partitioning of the Hamiltonian into the Hartree-Fock contribution ($H_{\text{MF}} \leftrightarrow \underline{U}$) and the rest of the interaction ($H_{\text{I}} = H - H_{\text{MF}} \leftrightarrow \frac{1}{2} J \delta_{ik_x}$). It turns out that this is a very convenient separation for further calculations. One can immediately accept that the term $(\mathcal{QL}_{\text{MF}}\mathcal{Q})^m$ yields a contribution $[\underline{U}^m]_{il}$ in the memory matrix. And if we are now confronted with terms such as $(\mathcal{QL}_{\text{MF}}\mathcal{Q})^p (\mathcal{QL}_{\text{I}}\mathcal{Q})^1 (\mathcal{QL}_{\text{MF}}\mathcal{Q})^q$ the result simply becomes $\frac{1}{2} J [\underline{U}^p]_{il} [\underline{U}^q]_{il}$. Hence, the first terms of the geometric series with $m \geq 3$ have the structure

$$(A_{ii} | (\mathcal{QLQ})^3 | A_{ll}) = \frac{1}{2} J^2 S \delta_{\sigma\downarrow} \delta_{il} \left\{ [\underline{U}^3]_{il} + \frac{J}{2} (2[\underline{U}^2]_{il} + [\underline{U}^1]_{il}^2) + \frac{J^2}{4} 3[\underline{U}^1]_{il} + \frac{J^3}{8} \right\}, \quad (4.26)$$

$$(A_{ii} | (\mathcal{QLQ})^4 | A_{ll}) = \frac{1}{2} J^2 S \delta_{\sigma\downarrow} \delta_{il} \left\{ [\underline{U}^4]_{il} + \frac{J}{2} (2[\underline{U}^3]_{il} + 2[\underline{U}^2]_{il} [\underline{U}^1]_{il}) + \frac{J^2}{4} (3[\underline{U}^2]_{il} + 3[\underline{U}^1]_{il}^2) + \frac{J^3}{8} 4[\underline{U}^1]_{il} + \frac{J^4}{16} \right\}. \quad (4.27)$$

With the help of some combinatorial analysis, all these terms can be combined to

$$M_{il\sigma} = \frac{1}{2} J^2 S \delta_{\sigma\downarrow} \delta_{il} \sum_{n=0}^{\infty} \left[\frac{J}{2} \right]^n \left(\frac{1}{\omega} \sum_{m=0}^{\infty} \left[\left(\frac{\underline{U}}{\omega} \right)^m \right]_{il} \right)^{n+1}. \quad (4.28)$$

The Fourier transformation of the expressions within the parenthesis

$$\frac{1}{N} \sum_{il} e^{-i\mathbf{k}(\mathbf{R}_i - \mathbf{R}_l)} \frac{1}{\omega} \sum_{m=0}^{\infty} \left[\left(\frac{\underline{U}}{\omega} \right)^m \right]_{il} \delta_{il} = \frac{1}{N} \sum_{\mathbf{q}} \frac{\hbar}{\hbar\omega - \varepsilon_{\mathbf{k}-\mathbf{q}} + \frac{1}{2} J \hbar S} = \frac{1}{N} \sum_{\mathbf{q}} G_{\mathbf{q}\uparrow}^{(\text{MF})}(\omega) \quad (4.29)$$

leads to the memory matrix

$$M_{\mathbf{k}\sigma} = \frac{1}{2} J^2 S \delta_{\sigma\downarrow} \frac{\frac{1}{N} \sum_{\mathbf{q}} G_{\mathbf{q}\uparrow}^{(\text{MF})}(\omega)}{1 - \frac{1}{2} J \frac{1}{N} \sum_{\mathbf{q}} G_{\mathbf{q}\uparrow}^{(\text{MF})}(\omega)}. \quad (4.30)$$

In contrast to the calculation in the previous subsections, the resulting expression for the memory matrix is derived with the full Liouvillian. Hence, it is the exact result of this limit, which is indeed in agreement with the result (2.10) of an equation-of-motion approach.

⁵The fact that the separation of the mean-field result simplifies the calculation of the ferromagnetically saturated semiconductor gives a hint for perturbational approaches presented below.

All-coupling strategy II: A perturbational expansion

The previous strategy results in an expression (4.30) for the memory matrix $M_{\mathbf{k}\sigma}$ that consists of terms with different powers of J . However, this notation does not match a Taylor expansion in J . This is due to the fact, that the definition of the modified hopping matrix (4.25) yields mean-field Green's functions which by definition contain an explicit J -dependence. To get a perturbation expansion

$$M_{\mathbf{k}\sigma}(\omega) =: \frac{1}{2} J^2 S \delta_{\sigma\downarrow} \sum_{m=0}^{\infty} \left[\frac{1}{2} J\right]^m \mathcal{M}_m \quad (4.31)$$

of the memory matrix (and therefore the self-energy) a modified strategy is necessary.

The clue for this problem is to rewrite the memory matrix (4.4) as

$$M_{il\sigma} = \sum_{m=0}^{\infty} \left(Q\mathcal{L}c_{i\sigma}^\dagger \left| \frac{1}{\omega - Q\mathcal{L}_s Q} \left([Q\mathcal{L}_{sf} Q] \frac{1}{\omega - Q\mathcal{L}_s Q} \right)^m \right| Q\mathcal{L}c_{l\sigma}^\dagger \right) \quad (4.32)$$

$$= \sum_{m=0}^{\infty} \sum_{n_0} \cdots \sum_{n_m} \frac{1}{\omega^{n_0+1}} \cdots \frac{1}{\omega^{n_m+1}} \cdot \quad (4.33)$$

$$\begin{aligned} & \cdot \left(Q\mathcal{L}c_{i\sigma}^\dagger \left| (Q\mathcal{L}_s Q)^{n_0} (Q\mathcal{L}_{sf} Q) (Q\mathcal{L}_s Q)^{n_1} \cdots (Q\mathcal{L}_{sf} Q) (Q\mathcal{L}_s Q)^{n_m} \right| Q\mathcal{L}c_{l\sigma}^\dagger \right) \\ & = \frac{1}{2} J^2 S \delta_{\sigma\downarrow} \delta_{il} \sum_{m=0}^{\infty} \left[\frac{1}{2} J\right]^m \sum_{n_0} \cdots \sum_{n_m} \frac{1}{\hbar^{n_0+\dots+n_m}} \cdot \frac{1}{\omega^{n_0+1}} \cdots \frac{1}{\omega^{n_m+1}} \cdots \quad (4.34) \\ & \cdot [\underline{\mathbb{T}}^{n_0}]_{ik_1} (\delta_{ik_1} - S) [\underline{\mathbb{T}}^{n_1}]_{k_1 k_2} (\delta_{ik_2} - S) [\underline{\mathbb{T}}^{n_2}]_{k_2 k_3} \cdots (\delta_{ik_m} - S) [\underline{\mathbb{T}}^{n_m}]_{k_m l}, \end{aligned}$$

where for the last line again rules (4.21)-(4.23) have been used⁶.

In order to obtain the expansion (4.31) we define the Fourier transformation of the n -fold product of the hopping matrix $\underline{\mathbb{T}}$ as

$$\Gamma_n := (-S)^{n-1} \frac{1}{N} \sum_{\mathbf{q}} \left(\frac{\hbar}{\hbar\omega - \varepsilon_{\mathbf{q}}} \right)^n = -\frac{1}{NS} \sum_{\mathbf{q}} (-SG_{\mathbf{q}\sigma}^{(0)}(\omega))^n. \quad (4.35)$$

On the right hand side it is formulated in terms of the free Green's function $G_{\mathbf{q}\sigma}^{(0)}(\omega)$. For fixed m in (4.34) the expansion coefficients \mathcal{M}_m consist of several combinations of these Γ 's, depending on whether the contribution δ_{ik_x} or $(-S)$ of the Liouvillian \mathcal{L}_{sf} is considered. The first coefficients

$$\begin{aligned} \text{"}\mathcal{L}_s\text{"} & \longrightarrow \mathcal{M}_0 = \Gamma_1, \\ \text{"}\mathcal{L}_s \mathcal{L}_{sf} \mathcal{L}_s\text{"} & \longrightarrow \mathcal{M}_1 = \Gamma_1^2 + \Gamma_2, \\ \text{"}\mathcal{L}_s \mathcal{L}_{sf} \mathcal{L}_s \mathcal{L}_{sf} \mathcal{L}_s\text{"} & \longrightarrow \mathcal{M}_2 = \Gamma_1^3 + 2\Gamma_1 \Gamma_2 + \Gamma_3, \\ \text{"}\mathcal{L}_s \mathcal{L}_{sf} \mathcal{L}_s \mathcal{L}_{sf} \mathcal{L}_s \mathcal{L}_{sf} \mathcal{L}_s\text{"} & \longrightarrow \mathcal{M}_3 = \Gamma_1^4 + 3\Gamma_1^2 \Gamma_2 + 2\Gamma_1 \Gamma_3 + \Gamma_2^2 + \Gamma_4 \end{aligned} \quad (4.36)$$

can readily be derived. The recursive formula

$$\mathcal{M}_m = \mathcal{M}_{m-1} \Gamma_1 + \mathcal{M}_{m-2} \Gamma_2 + \mathcal{M}_{m-3} \Gamma_3 + \dots + \mathcal{M}_0 \Gamma_m + \Gamma_{m+1}, \quad (4.37)$$

⁶If the Liouvillian were again split into the parts \mathcal{L}_{MF} and \mathcal{L}_I , then (4.33) would directly lead to (4.28) without the need of combinatorial considerations.

can be obtained. Even though an explicit formula for any arbitrary coefficients \mathcal{M}_m cannot be provided, this result allows the computation of all terms of the J -expansion of the memory-matrix (4.31) and hence the self-energy of the itinerant electrons.

One can easily check that the second order is identical to the previously derived expression (4.18). The next (third) order in the expansion of the self-energy is provided by the coefficient

$$\mathcal{M}_1 = \left[\frac{1}{N} \sum_{\mathbf{q}} G_{\mathbf{q}\sigma}^{(0)}(\omega) \right]^2 - \frac{S}{N} \sum_{\mathbf{q}} [G_{\mathbf{q}\sigma}^{(0)}(\omega)]^2. \quad (4.38)$$

However, the second term of (4.38) creates difficulties. Its imaginary part

$$\begin{aligned} \Im \left(\frac{1}{N} \sum_{\mathbf{q}} \left[\frac{1}{E - \varepsilon_{\mathbf{q}} + i0^+} \right]^2 \right) &= \Im \int dx \frac{\rho_0(x)}{(E - x + i0^+)^2} = \int dx \frac{-20^+(E - x)\rho_0(x)}{[(E - x)^2 + (0^+)^2]^2} \\ &= -2 \int dx \frac{0^+}{(E - x)^2 + (0^+)^2} \cdot \frac{(E - x)\rho_0(x)}{(E - x)^2 + (0^+)^2} = -2 \int dx \delta(E - x) \cdot \frac{\rho_0(x)}{E - x} \end{aligned}$$

apparently diverges for all energies E , for which the free DOS $\rho_0(E)$ is non-zero. Since the imaginary part of the self-energy enters e.g. the formula for the density of states, this divergence is of great physical relevance. It is clear that it will cancel with the contribution of higher order coefficients, but still one has to conclude that the expansion of the self-energy in powers of J higher than two might not be desirable.

Nevertheless, this does not render useless the whole strategy provided here. On the contrary, it is possible to obtain a compact notation for the sum $\sum_m [\frac{1}{2}J]^m \mathcal{M}_m$, by using a formula which is equivalent⁷ to the recursion relation (4.37):

$$\frac{J}{2} \left(\sum_{m=0}^{\infty} [\frac{1}{2}J]^m \mathcal{M}_m \right) \cdot \left(\sum_{n=1}^{\infty} [\frac{1}{2}J]^n \Gamma_n - 1 \right) + \sum_{n=1}^{\infty} [\frac{1}{2}J]^n \Gamma_n = 0. \quad (4.39)$$

Using the structure (4.35) of Γ_n the involved geometric series is readily obtained and (4.39) can be solved for the memory matrix

$$M_{\mathbf{k}\sigma}(\omega) = JS\delta_{\sigma\downarrow} \frac{1 - \frac{1}{N} \sum_{\mathbf{q}} \frac{1}{1 + \frac{1}{2}JSG_{\mathbf{q}}^{(0)}(\omega)}}{S - 1 + \frac{1}{N} \sum_{\mathbf{q}} \frac{1}{1 + \frac{1}{2}JSG_{\mathbf{q}}^{(0)}(\omega)}}. \quad (4.40)$$

Although not being identical to (4.30), this is again an exact solution for the ferromagnetically saturated semiconductor. In contrast to the first strategy, where the propagators are mean-field Green's functions, the self-energy is now expressed in terms of free Green's functions. This is obtained at the expense of a more complicated structure of the memory matrix.

⁷The equivalence can be shown by a comparison of coefficients.

All-coupling strategy III: The philosophy of continued fractions

The strategies presented above are uncommon for the POM in the sense that they aim at a direct solution of the exact geometric series. According to the philosophy of the POM, the solution is approached by a continued fraction. The limit of the ferromagnetically saturated semiconductor can also be used to study this strategy.

The general formulae for a representation of the memory matrix in the form

$$\underline{M}(\omega) = \frac{1}{\omega \underline{\mathbf{1}} - [\underline{\hat{\Omega}} + \underline{\hat{M}}] \underline{\hat{\chi}}^{-1} \underline{\hat{\chi}}} \quad (4.41)$$

have already been provided in Chap. 3.3 (p. 29). The essential difference is the level of description, now formed by $|\mathcal{QL}c_{i\sigma}^\dagger\rangle$. This has consequences for the higher-level susceptibility and frequency matrix,

$$\hat{\chi}_{il} = \left(\mathcal{QL}c_{i\sigma}^\dagger \left| \mathcal{QL}c_{i\sigma}^\dagger \right. \right) \stackrel{(4.6)}{=} \frac{1}{2} J^2 S \delta_{\sigma\downarrow} \delta_{il} \quad \text{and} \quad (4.42)$$

$$\hat{\Omega}_{il} = \left(\mathcal{QL}c_{i\sigma}^\dagger \left| \mathcal{QLQ} \left| \mathcal{QL}c_{i\sigma}^\dagger \right. \right. \right) \stackrel{(4.24)}{=} \frac{1}{2} J^2 S \delta_{\sigma\downarrow} \delta_{il} \left[\frac{1}{\hbar} T_{ii} + \frac{1}{2} J - \frac{1}{2} JS \right]. \quad (4.43)$$

For the higher-level memory matrix

$$\hat{M}_{il}(\omega) = \left(\mathcal{QL}c_{i\sigma}^\dagger \left| \mathcal{QLQ}\hat{Q} \frac{1}{\omega - \hat{Q}\mathcal{QLQ}\hat{Q}} \hat{Q}\mathcal{QLQ} \left| \mathcal{QL}c_{i\sigma}^\dagger \right. \right. \right) \quad (4.44)$$

a treatment with the full Liouvillian \mathcal{L} in the denominator might be successful. However, to follow the philosophy of the POM, we truncate the continued fraction by the replacement $\mathcal{L} \rightarrow \mathcal{L}_s$. This has the advantage that only a certain part of the Liouville state

$$\hat{Q}\mathcal{QLQ} \left| \mathcal{QL}c_{i\sigma}^\dagger \right. \rangle \rightarrow \frac{1}{\hbar} T_{kl} (1 - \delta_{kl}) |A_{lk}\rangle =: |B_l\rangle \quad (4.45)$$

yields a finite contribution to the memory matrix. Its expansion into a geometric series

$$\left[\hat{\underline{M}}(\omega) \hat{\underline{\chi}}^{-1} \right]_{\mathbf{k}} = \frac{1}{\omega} \sum_{m=0}^{\infty} \frac{1}{\omega^m} \hat{\mathcal{M}}_m = \frac{1}{\omega} \sum_{m=0}^{\infty} \frac{\omega}{\omega^m} \hat{\mathcal{M}}_{m-1} - \hat{\mathcal{M}}_{-1} \quad (4.46)$$

hence consists of coefficients

$$\hat{\mathcal{M}}_m = (B_i | (\hat{Q}\mathcal{QL}_s\hat{Q})^m | B_j) \hat{\chi}_{jl}^{-1} = \frac{1}{\hbar^m} T_{ik_m} (1 - \delta_{k_m i}) T_{k_m k_{m-1}} \cdots T_{k_1 k_0} (1 - \delta_{k_0 i}) T_{k_0 l} \delta_{il} \quad (4.47)$$

determined by the Liouville state $|B_l\rangle$. The additional element $\hat{\mathcal{M}}_{-1} := \frac{1}{\hbar} T_{ii} \delta_{il}$ has been included for mathematical reasons. Similar to (4.37) the multiple sum (4.47) can be expressed as a recursion relation

$$\hat{\mathcal{M}}_m = \delta_{il} \frac{1}{\hbar^2} [\underline{\mathbf{T}}^{m+2}]_{ii} - \sum_{x=-1}^{m-1} \hat{\mathcal{M}}_x \frac{1}{\hbar^{m-x}} [\underline{\mathbf{T}}^{m-x}]_{ii} \quad (4.48)$$

Again one can prove by comparing coefficients, that this recursion is equivalent to an explicit formula

$$\delta_{il} \sum_{n=1}^{\infty} \frac{1}{(\hbar\omega)^n} [\mathbb{T}^n]_{ii} = \frac{1}{\omega} \left(\sum_{m=0}^{\infty} \frac{1}{\omega^m} \hat{\mathcal{M}}_{m-1} \right) \left(1 + \delta_{il} \sum_{n=1}^{\infty} \frac{1}{(\hbar\omega)^n} [\mathbb{T}^n]_{ii} \right). \quad (4.49)$$

Hence, after Fourier transformation, Eq. (4.46) can be evaluated as

$$\left[\hat{\mathbb{M}}(\omega) \hat{\chi}^{-1} \right]_{\mathbf{k}} = \omega \cdot \frac{\frac{\omega}{N} \sum_{\mathbf{q}} G_{\mathbf{q}}^{(0)}(\omega) - 1}{1 + \frac{\omega}{N} \sum_{\mathbf{q}} G_{\mathbf{q}}^{(0)}(\omega) - 1} - \frac{1}{N\hbar} \sum_{\mathbf{q}} \varepsilon_{\mathbf{q}}. \quad (4.50)$$

Once the higher order memory matrix has been derived, one can enter the result into the expression for the continued fraction (4.41):

$$M_{\mathbf{k}\sigma}(\omega) = \frac{1}{2} J^2 S \delta_{\sigma\downarrow} \frac{\frac{1}{N} \sum_{\mathbf{q}} G_{\mathbf{q}}^{(0)}(\omega)}{1 - \frac{1}{2} J (1 - S) \frac{1}{N} \sum_{\mathbf{q}} G_{\mathbf{q}}^{(0)}(\omega)} \quad (4.51)$$

One can immediately see that this result is not identical to the exact expression (4.30). This is not surprising since in (4.47) we have approximated the Liouvillian \mathcal{L} by its free part \mathcal{L}_s . Nevertheless, (4.30) and (4.51) have a very similar structure. It is a self-evident observation, that a replacement $\mathcal{L} \rightarrow \mathcal{L}_{\text{MF}}$ would yield the exact result. Indeed, when doing so all calculations remain identical with the only exception that the modified hopping \underline{U} , as defined in (4.25), has to be used. Then the previous free Green's functions will become mean-field Green's functions. Furthermore, the factor $\frac{1}{2}JS$ in the denominator of (4.51) vanishes due to the fact, that the \mathcal{M}_{-1} -contribution in (4.50) has to be extended by this term.

Hence, a projection-operator method for the ferromagnetically saturated ferromagnet which approximates the Liouvillian \mathcal{L} in the second level of the continued fraction by its mean-field part \mathcal{L}_{MF} yields a result

$$M_{\mathbf{k}\sigma} = \frac{1}{2} J^2 S \delta_{\sigma\downarrow} \frac{\frac{1}{N} \sum_{\mathbf{q}} G_{\mathbf{q}\uparrow}^{(\text{MF})}(\omega)}{1 - \frac{1}{2} J \frac{1}{N} \sum_{\mathbf{q}} G_{\mathbf{q}\uparrow}^{(\text{MF})}(\omega)}, \quad (4.52)$$

that has already been shown to be exact in (4.30). Why does the approximation not influence the correctness of the result? Apparently, the neglected contribution \mathcal{L}_1 is not relevant for the physics in this limit. Or more precisely, we have chosen a Liouville subspace which describes the whole physical situation in this limit. All processes that move out of this subspace do not contribute to the one-electron Green's function.

All-coupling strategy IV: An extended basis

If, as concluded above, the choice for the relevant subspace is essential to obtain the exact result, one should consequently start with this subspace from the very beginning. This is done by considering a space spanned by

$$\left| c_{l\sigma}^\dagger \right\rangle =: |B_{1l}\rangle \quad \text{and} \quad \left| \mathcal{Q}\mathcal{L}c_{l\sigma}^\dagger \right\rangle \rightarrow |A_{ll}\rangle =: |B_{2l}\rangle \quad (4.53)$$

and respective projection operators $\bar{\mathcal{P}}$ and $\bar{\mathcal{Q}}$. This choice allows us to use the result of strategy III to determine the susceptibility and the frequency matrix

$$\bar{\underline{\chi}} = \begin{pmatrix} 1 & 0 \\ 0 & \frac{1}{2}J^2S \end{pmatrix} \quad \text{and} \quad \bar{\underline{\Omega}}\bar{\underline{\chi}}^{-1} = \begin{pmatrix} \frac{1}{\hbar}\varepsilon_{\mathbf{k}} + \frac{1}{2}JS & 1 \\ \frac{1}{2}J^2S & \frac{1}{\hbar}T_0 + \frac{1}{2}J(1-S) \end{pmatrix}, \quad (4.54)$$

already given in its Fourier transformed form. Even for the memory matrix

$$\bar{M}_{il}(\omega) = (B_{1/2i} | \mathcal{L}\bar{\mathcal{Q}} \frac{1}{\omega - \bar{\mathcal{Q}}\mathcal{L}\bar{\mathcal{Q}}} \bar{\mathcal{Q}}\mathcal{L} | B_{1/2l}), \quad (4.55)$$

again with an approximated denominator, results obtained previously can be used. This is because, $\bar{\mathcal{Q}} = \hat{\mathcal{Q}}\mathcal{Q}$. Therefore, $\bar{\mathcal{Q}}\mathcal{L}|B_{1l}\rangle = 0$ and the only non-vanishing contribution of the memory matrix is identical to (4.44). Hence, depending on the approximation of the Liouvillian in (4.55) either the expression (4.50) or the version with modified hopping can be used in this strategy, too. If \mathcal{L} is replaced by \mathcal{L}_s we finally obtain the matrix equation

$$\begin{pmatrix} 1 & 0 \\ 0 & \frac{1}{2}J^2S \end{pmatrix} = \begin{pmatrix} \omega - \frac{1}{\hbar}\varepsilon_{\mathbf{k}} - \frac{1}{2}JS & -1 \\ -\frac{1}{2}J^2S & [\frac{1}{N}\sum_{\mathbf{q}} G_{\mathbf{q}}^{(0)}(\omega)]^{-1} - \frac{1}{2}J(1-S) \end{pmatrix} \begin{pmatrix} G_{\mathbf{k}\downarrow} & * \\ * & * \end{pmatrix}. \quad (4.56)$$

The asterisks in the Green's function matrix point out that we are only interested in $G_{\mathbf{k}\downarrow}$. The other contributions do not belong to single-particle excitations. By inversion and matrix multiplication we obtain

$$\boxed{G_{\mathbf{k}\downarrow}(\omega) = \frac{1}{\omega - \frac{1}{\hbar}\varepsilon_{\mathbf{k}} - \frac{1}{2}JS - M_{\mathbf{k}\downarrow}(\omega)},} \quad (4.57)$$

with exactly the same $M_{\mathbf{k}\downarrow}(\omega)$ as given in (4.51) or (4.52), respectively.

What has been shown here in the context of the KLM for the ferromagnetically saturated semiconductor can be generalized to a statement for the POM: The quality of the expression obtained for the Green's function is uniquely determined by the level of description (the chosen relevant Liouville subspace). A strategy that starts with a basis set $\{A_i\}$ of Liouville states $|A_i\rangle$ and truncates the calculations in the second level of the continued fraction is equivalent to a strategy that works from the very beginning with a basis formed by $|A_i\rangle$ and $|\mathcal{Q}\mathcal{L}A_i\rangle$ and restricts itself to the first fraction. The advantage of the latter is the possibility to obtain several Green's functions at once. The disadvantage is the higher complexity of calculations. The actual choice for a strategy depends on the physical problem.

4.2 The zero-bandwidth limit

The assumption of a vanishing conduction bandwidth is a second valuable limit of the KLM. It implies that the coupling (the remaining energy scale of the model) can be considered as comparatively strong – a good starting point for perturbational approaches. For an investigation of the KLM by means of the POM, it is therefore desirable that the limit is tractable with this method. That this is indeed the case, will be shown below.

The generic basis of the atomic limit

It is well known [112] that a set of four Green's functions is sufficient to get a closed equation-of-motion system for the zero-bandwidth/atomic limit. Therefore, the four basis elements⁸

$$\begin{aligned} |B_1\rangle &:= |c_\sigma^\dagger\rangle, & |B_3\rangle &:= \left| z_\sigma S^z c_\sigma^\dagger + S^\sigma c_{-\sigma}^\dagger \right\rangle, \\ |B_2\rangle &:= |\hat{n}_{-\sigma} c_\sigma^\dagger\rangle, & |B_4\rangle &:= \left| z_\sigma S^z \hat{n}_{-\sigma} c_\sigma^\dagger + S^\sigma \hat{n}_\sigma c_{-\sigma}^\dagger \right\rangle. \end{aligned} \quad (4.58)$$

related to these Green's functions describe the whole physics relevant in this context. Since the action of the Liouvillian in the atomic limit⁹ (AL),

$$\begin{aligned} \mathcal{L}_{\text{AL}} |B_1\rangle &= -\frac{1}{2\hbar} J |B_3\rangle, & \mathcal{L}_{\text{AL}} |B_3\rangle &= -\frac{1}{2} J \hbar S(S+1) |B_1\rangle + \frac{1}{2} J |B_3\rangle - J |B_4\rangle, \\ \mathcal{L}_{\text{AL}} |B_2\rangle &= -\frac{1}{2\hbar} J |B_4\rangle, & \mathcal{L}_{\text{AL}} |B_4\rangle &= -\frac{1}{2} J \hbar S(S+1) |B_2\rangle - \frac{1}{2} J |B_4\rangle, \end{aligned} \quad (4.59)$$

remains within the subspace spanned by $|B_1\rangle, \dots, |B_4\rangle$, the choice (4.58) is already the basis for the complete Liouville space L_{AL} , relevant to this situation.

This has two remarkable consequences: First, the memory matrix vanishes automatically. Secondly, the frequency matrix can be separated into the susceptibility matrix $\underline{\chi}$, containing the expectation values, and a further matrix \underline{L} , composed of the prefactors of (4.59):

$$\underline{\Omega} = \underline{\chi} \cdot \underline{L} \quad \text{with} \quad \underline{L} = \begin{pmatrix} 0 & 0 & -\frac{1}{2} J \hbar S(S+1) & 0 \\ 0 & 0 & 0 & -\frac{1}{2} J \hbar S(S+1) \\ -\frac{1}{2\hbar} J & 0 & \frac{1}{2} J & 0 \\ 0 & -\frac{1}{2\hbar} J & -J & -\frac{1}{2} J \end{pmatrix} \quad (4.60)$$

Hence, the set of Green's functions is the result of the following matrix product

$$\underline{G} = [\omega \mathbf{1} - \underline{\Omega} \cdot \underline{\chi}^{-1}]^{-1} \cdot \underline{\chi} = \underline{\chi} \cdot [\omega \mathbf{1} - \underline{L}]^{-1}. \quad (4.61)$$

There is no need to invert $\underline{\chi}$. The determinant of $[\omega \mathbf{1} - \underline{L}]$, which composes the denominator of the Green's functions, is the product of the four energy poles, which are provided

⁸Site indices can be omitted, since only one lattice site is relevant in the atomic limit.

⁹An on-site hopping integral T_0 set to zero, but can be included as a constant energy shift in the result. The approach remains the same, if a local Hubbard interaction is also considered.

explicitly in Eq. (2.8). The respective spectral weights are determined mainly by the susceptibility matrix, which is given as:

$$\underline{\chi} = \begin{pmatrix} 1 & \langle \hat{n}_{-\sigma} \rangle & z_{\sigma} \langle S^z \rangle & p_{\sigma} \\ \langle \hat{n}_{-\sigma} \rangle & \langle \hat{n}_{-\sigma} \rangle & p_{\sigma} & p_{\sigma} \\ z_{\sigma} \langle S^z \rangle & p_{\sigma} & q_{\sigma} & x_{\sigma} \\ p_{\sigma} & p_{\sigma} & x_{\sigma} & x_{\sigma} \end{pmatrix} \quad \text{with} \quad \begin{cases} p_{\sigma} = z_{\sigma} \langle S^z \hat{n}_{-\sigma} \rangle - \langle S^{-\sigma} c_{\sigma}^{\dagger} c_{-\sigma} \rangle, \\ q_{\sigma} = \hbar^2 S(S+1) - z_{\sigma} \hbar \langle S^z \rangle + 2\hbar p_{\sigma}, \\ x_{\sigma} = \hbar^2 S(S+1) \langle \hat{n}_{-\sigma} \rangle + \hbar p_{\sigma}. \end{cases} \quad (4.62)$$

A lengthy but straightforward calculation of the matrix entries χ_{34} and χ_{44} yields expressions with several expectation values. Here, the exact relation (2.23) explained in appendix B is used, to obtain the expression x_{σ} .

One can easily convince oneself that the results for the Green's functions obtained with this method are identical to those obtained using the equations of motion [112]. In addition, the POM provides six further Green's functions for the atomic limit.

Consequences of an adapted basis

A four-dimensional basis, as suggested above, is probably not appropriate for a generalization to arbitrary bandwidths. A finite hopping matrix element yields contributions in $\mathcal{L}|B_i\rangle$ which do not belong to the subspace spanned by the basis; the frequency matrix cannot be factorized as in (4.60). The inversion of the susceptibility matrix yields long expressions with a combination of expectation values.

Instead, a two-dimensional basis is chosen such that it reduces to the choice (4.53) if the constraints of the ferromagnetically saturated semiconductor are applied. Such a basis could be used for an interpolation between these two limiting cases. Its explicit form is

$$|C_1\rangle := |c_{\sigma}^{\dagger}\rangle = |B_1\rangle, \quad (4.63)$$

$$|C_2\rangle := \{1 - |C_1\rangle\langle C_1|\} \mathcal{L}_{\text{AL}} |C_1\rangle = -\frac{J}{2\hbar} \left\{ |B_3\rangle - z_{\sigma} \langle S^z \rangle |B_1\rangle \right\}. \quad (4.64)$$

The Liouville state $|C_2\rangle$ is already constructed such that the susceptibility matrix becomes diagonal. The complete set of contributing matrices is given by

$$\underline{\chi} = \begin{pmatrix} 1 & 0 \\ 0 & \chi_{22} \end{pmatrix}, \quad \underline{\Omega} = \begin{pmatrix} -\frac{J}{2\hbar} z_{\sigma} \langle S^z \rangle & \chi_{22} \\ \chi_{22} & \Omega_{22} \end{pmatrix} \quad \text{and} \quad \underline{M} = \begin{pmatrix} 0 & 0 \\ 0 & M_{22} \end{pmatrix}. \quad (4.65)$$

Based on the calculations using the basis (4.58) one obtains

$$\chi_{22} = \frac{J^2}{4\hbar^2} \{q_{\sigma} - \langle S^z \rangle^2\} \quad \text{and} \quad (4.66)$$

$$\Omega_{22} = -\frac{J^3}{8\hbar^3} \{z_{\sigma} \langle S^z \rangle^3 + \hbar^2 S(S+1) z_{\sigma} \langle S^z \rangle - (\hbar + 2z_{\sigma} \langle S^z \rangle) q_{\sigma} + 2\hbar x_{\sigma}\}. \quad (4.67)$$

Of course, the memory matrix is not zero anymore. Even the fact that it has only one non-vanishing entry is an accidental feature of the KLM in the atomic limit¹⁰. To

¹⁰All matrix elements are non-zero if in addition a Hubbard interaction is taken into consideration.

determine

$$M_{22} = \langle C_2 | \mathcal{L}_{AL} \mathcal{Q} \frac{1}{\omega - \mathcal{Q} \mathcal{L}_{AL} \mathcal{Q}} \mathcal{Q} \mathcal{L}_{AL} | C_2 \rangle \quad \text{with} \quad \mathcal{Q} = 1 - |C_1\rangle \langle C_1| - \frac{1}{\chi_{22}} |C_2\rangle \langle C_2|, \quad (4.68)$$

one has to perform a further step of the POM.

Again, the decision for the most appropriate basis is crucial for the calculations. It is decisive that it belongs to the orthogonal complement of the first two basis elements, since then

$$[L_{AL} \cap \text{span}\{|C_1\rangle, |C_2\rangle\}] \cap \text{span}\{|C_3\rangle, |C_4\rangle\} = L_{AL} \cap \text{span}\{|C_1\rangle, \dots, |C_4\rangle\}. \quad (4.69)$$

The right hand side of this equation is an empty set, provided that the basis states are linearly independent. Consequently, the memory matrix vanishes in this step of the POM. This truncates the series of continued fractions. Accordingly, we set

$$|C_3\rangle := \mathcal{Q} |B_4\rangle = \frac{2\hbar}{J^2} \mathcal{Q} \mathcal{L}_{AL} |C_2\rangle \quad (4.70)$$

$$|C_4\rangle := \mathcal{Q} \left\{ |B_2\rangle - \alpha |B_4\rangle \right\}. \quad (4.71)$$

The choice of $|C_3\rangle$ directly yields M_{22} as the solution of the resolvent given in (4.68). The remaining basis state $|C_4\rangle$ is (apart from normalization) given in its most general form. To ensure a diagonal susceptibility matrix also in this Liouville subspace the adjustable parameter α has to be taken as

$$\alpha = \frac{p_\sigma (1 - \langle \hat{n}_{-\sigma} \rangle) (q_\sigma - \langle S^z \rangle^2) - (p_\sigma - z_\sigma \langle S^z \rangle \langle \hat{n}_{-\sigma} \rangle) (x_\sigma - z_\sigma \langle S^z \rangle p_\sigma)}{(x_\sigma - p_\sigma^2) (q_\sigma - \langle S^z \rangle^2) - (x_\sigma - z_\sigma \langle S^z \rangle p_\sigma)^2}. \quad (4.72)$$

Due to the lengthy expression, the following calculations of the susceptibility and the frequency are a bit cumbersome. If, on the other hand, $\alpha = 0$ is chosen, the two matrix inversions, which are necessary for obtaining the resolvent from the susceptibility and the frequency matrix,¹¹ yield lengthy expressions, too. It should not be forgotten that finally the result for M_{22} has to be inserted into

$$G_{11} = \langle\langle c_\sigma; c_\sigma^\dagger \rangle\rangle_E = \frac{1}{\omega - \frac{1}{2} J z_\sigma \langle S^z \rangle - \frac{\chi_{22}}{\omega - \Omega_{22} \chi_{22}^{-1} - M_{22} \chi_{22}^{-1}}} \quad (4.73)$$

in order to obtain the desired Green's function.

These calculations can be performed and indeed give the exact solution for the one-electron Green's function in the atomic limit. In comparison to the treatment based on the four-dimensional basis (4.58) it is more challenging to consider the various expectation values. On the other hand, a smaller basis is more appropriate for generalizing to arbitrary bandwidths. Nevertheless, there is no reason to favour the two-dimensional basis in the following calculations. To obtain (4.73), one can also start with the one-dimensional basis $|c_\sigma^\dagger\rangle$ and extend the Liouville subspace in the second step of the POM. The formulae remain the same, since only the level of description is important.

¹¹A separation of the frequency matrix as suggested in (4.60) cannot be used in this step, since the application of the Liouvillian on the basis states yields contributions outside this subspace.

4.3 Weak-coupling approach to the KLM

Based on the experiences with limiting cases, we will now move to situations with arbitrary parameters. Here, we cannot expect that the POM will provide an exact solution for the self-energy of the conduction electrons. Instead we can draw on the experience of strong (p. 39) and weak coupling (p. 40) in the limit of the magnetic polaron in order to perform approximations. It is of physical interest to study the influence of the sf-interaction J as compared to the situation of free electrons. Our aim is an expression for the electronic self-energy, which is correct to first and second order in J .

First order: The frequency matrix

Since we consider deviations from the free electron situation we use the Bloch representation

$$H = \sum_{\mathbf{k}} \sum_{\sigma} \varepsilon_{\mathbf{k}} \hat{n}_{\mathbf{k}\sigma} - \frac{J}{2N} \sum_{\mathbf{q}, \mathbf{p}} \sum_{\sigma} \left(z_{\sigma} S_{\mathbf{q}}^z c_{\mathbf{p}, \sigma}^{\dagger} c_{\mathbf{p}-\mathbf{q}, \sigma} + S_{\mathbf{q}}^{\sigma} c_{\mathbf{p}, -\sigma}^{\dagger} c_{\mathbf{p}-\mathbf{q}, \sigma} \right) \quad (4.74)$$

of the Hamiltonian (2.5). To obtain the one-particle Green's function it is sufficient to start the POM with an one-dimensional Liouville subspace, formed by the basis state $|c_{\mathbf{k}\sigma}^{\dagger}\rangle$:

$$G_{\mathbf{k}\sigma}(\omega) = \left(c_{\mathbf{k}\sigma}^{\dagger} \left| \frac{1}{\omega - \mathcal{L}} \right| c_{\mathbf{k}\sigma}^{\dagger} \right) = \frac{1}{\omega - \Omega_{\mathbf{k}\sigma} - M_{\mathbf{k}\sigma}(\omega)} = \frac{\hbar}{E - \varepsilon_{\mathbf{k}} - \Sigma_{\mathbf{k}\sigma}(E) + i0^+}. \quad (4.75)$$

In the zero bandwidth limit and for a ferromagnetically saturated semiconductor we have noticed that a two-dimensional basis allows a more compact derivation of exact results. Nevertheless, such a strategy also implies the calculation of additional Green's functions, which at the moment are not needed for our calculations.

The frequency matrix is a generalization of the version obtained in Sec. 4.1:

$$\Omega_{\mathbf{k}\sigma} = \left(c_{\mathbf{k}\sigma}^{\dagger} \left| \mathcal{L} \right| c_{\mathbf{k}\sigma}^{\dagger} \right) = \frac{1}{\hbar} \varepsilon_{\mathbf{k}} - \frac{J}{2\hbar} z_{\sigma} \langle S^z \rangle \quad (4.76)$$

and, as already mentioned before, contains the full mean-field contribution (2.6) to the self-energy. The energy independence of $\frac{1}{2} J z_{\sigma} \langle S^z \rangle$ yields a rigid shift of the previously free density of states (DOS), as can be seen in Fig. 4.1. In particular, there is no dependence on the band-occupation n . If an arbitrary value such as $n = 0.8$ is chosen, then the part of the DOS highlighted in Fig. 4.1 will be occupied. It corresponds to a chemical potential of $\mu = -0.064$ eV and an electron polarization of $\langle \hat{n}_{\uparrow} - \hat{n}_{\downarrow} \rangle / n = 62\%$. However, for the chosen set of parameters a band occupation $n < 0.33$ implies a completely polarized conduction band. Alternatively, even for $n = 0.8$ an exchange coupling $J > 1.3$ eV yields the same effect. If this were correct, it would be highly relevant for spintronics applications, where one of the major issues is the predictability of the electron spin polarization. We will keep this effect in mind for subsequent discussions.

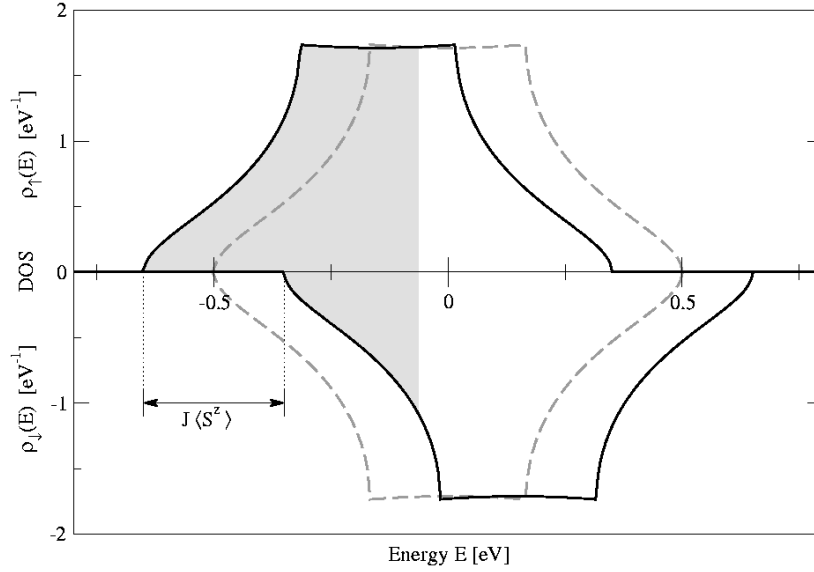


Figure 4.1: Density of states of the conduction electrons in mean-field approximation (solid line) as compared to the free DOS (dashed line). The hatched area displays the occupied part at $T = 0$ K. The parameters are: $J = 0.6$ eV, $n = 0.8$, $\langle S^z \rangle = 0.5$ and $W = 1.0$ eV for a simple-cubic lattice.

Second order: The memory matrix

The memory matrix in (4.75) will now be approximated by

$$M_{\mathbf{k}\sigma}(\omega) \approx \left(\mathcal{Q} \mathcal{L} c_{\mathbf{k}\sigma}^{\dagger} \left| \frac{1}{\omega - \mathcal{Q} \mathcal{L}_{\text{MF}} \mathcal{Q}} \right| \mathcal{Q} \mathcal{L} c_{\mathbf{k}\sigma}^{\dagger} \right) = \left(\mathcal{Q} \mathcal{L}_{sf} c_{\mathbf{k}\sigma}^{\dagger} \left| \frac{1}{\omega - \mathcal{L}_{\text{MF}}} \right| \mathcal{Q} \mathcal{L}_{sf} c_{\mathbf{k}\sigma}^{\dagger} \right). \quad (4.77)$$

The expression on the left hand side includes a truncation of the Liouvillian, as it is common for the POM. The expression on the right hand side needs further explanation. First we note, that one does not have to consider the \mathcal{L}_s -part in the Liouville state, since it belongs to the subspace which is projected out by \mathcal{Q} . Instead, as for (4.5) one obtains:

$$\left| \mathcal{Q} \mathcal{L} c_{\mathbf{k}\sigma}^{\dagger} \right) = \left| \mathcal{Q} \mathcal{L}_{sf} c_{\mathbf{k}\sigma}^{\dagger} \right) = -\frac{J}{2\hbar N} \sum_{\mathbf{q}} \left\{ z_{\sigma} (S_{\mathbf{q}}^z - \langle S_{\mathbf{q}}^z \rangle \delta_{\mathbf{q},0}) \left| c_{\mathbf{q}+\mathbf{k},\sigma}^{\dagger} \right) + S_{\mathbf{q}}^{\sigma} \left| c_{\mathbf{q}+\mathbf{k},-\sigma}^{\dagger} \right) \right\}. \quad (4.78)$$

The fact, that these states are proportional to J , implies that every term in a geometric-series representation of the memory matrix is at least of order J^2 . If a second-order perturbation theory for the electronic self-energy is desired, it is therefore sufficient to consider only the J -independent term \mathcal{L}_s in the denominator of (4.77). With writing \mathcal{L}_{MF} we convey the idea of an iterated partitioning of the Hamiltonian, as suggested by Bulk and Jelitto [16] for the Hubbard model, to the KLM. In this sense, we go beyond second order, although we can always reduce the results to the J^2 -contribution.

Secondly, it is important to note that $(c_{\mathbf{k}\sigma}^{\dagger} | \mathcal{L}_{\text{MF}}^m \mathcal{Q} \mathcal{L}_{sf} | c_{\mathbf{k}\sigma}^{\dagger}) = 0$, independent of the

actual value of m . This can easily be verified, using the result

$$\begin{aligned} \mathcal{L}_{\text{MF}}^m \left| \mathcal{Q} \mathcal{L}_{sf} c_{\mathbf{k}\sigma}^\dagger \right\rangle = & -\frac{J}{2\hbar N} \sum_{\mathbf{q}} \left\{ z_\sigma \left[\frac{1}{\hbar} \varepsilon_{\mathbf{k}+\mathbf{q}} - z_\sigma \frac{J}{2\hbar} \langle S^z \rangle \right]^m \left(S_{\mathbf{q}}^z - \langle S_{\mathbf{q}}^z \rangle \delta_{\mathbf{q},\mathbf{0}} \right) \left| c_{\mathbf{q}+\mathbf{k},\sigma}^\dagger \right\rangle \right. \\ & \left. + \left[\frac{1}{\hbar} \varepsilon_{\mathbf{k}+\mathbf{q}} - z_{-\sigma} \frac{J}{2\hbar} \langle S^z \rangle \right]^m S_{\mathbf{q}}^\sigma \left| c_{\mathbf{q}+\mathbf{k},-\sigma}^\dagger \right\rangle \right\}. \end{aligned} \quad (4.79)$$

We take the geometric-series representation of the fraction

$$\frac{1}{\omega - \mathcal{Q} \mathcal{L}_{\text{MF}} \mathcal{Q}} \left| \mathcal{Q} \mathcal{L}_{sf} c_{\mathbf{k}\sigma}^\dagger \right\rangle = \sum_{m=0}^{\infty} \frac{(\mathcal{Q} \mathcal{L}_{\text{MF}} \mathcal{Q})^m}{\omega^{m+1}} \left| \mathcal{Q} \mathcal{L}_{sf} c_{\mathbf{k}\sigma}^\dagger \right\rangle = \sum_{m=0}^{\infty} \frac{\mathcal{L}_{\text{MF}}^m}{\omega^{m+1}} \left| \mathcal{Q} \mathcal{L}_{sf} c_{\mathbf{k}\sigma}^\dagger \right\rangle. \quad (4.80)$$

Therefore, it is clear that the projectors in the denominator of (4.77) can be omitted. Furthermore, the repetitive structure of (4.79) is well suited for calculating the complete sum given in (4.80). The expressions in the squared brackets can again be treated as a geometric series, resulting in mean-field Green's functions (2.6).

To complete the derivation of the memory matrix one also needs to know the scalar product of the Liouville state (4.78) with itself. According to definition (3.3) this includes two steps. In a first step the anticommutator of operators has to be evaluated. This yields a set of correlation functions

$$\left\langle \left[c_{\mathbf{q}'+\mathbf{k},\sigma} S_{-\mathbf{q}'}^z; S_{\mathbf{q}}^z c_{\mathbf{q}+\mathbf{k},\sigma}^\dagger \right]_+ \right\rangle = \langle S_{-\mathbf{q}}^z S_{\mathbf{q}}^z \rangle \delta_{\mathbf{q}',\mathbf{q}} \quad (4.81)$$

$$\left\langle \left[c_{\mathbf{q}'+\mathbf{k},\sigma} S_{-\mathbf{q}'}^z; S_{\mathbf{q}}^\sigma c_{\mathbf{q}+\mathbf{k},-\sigma}^\dagger \right]_+ \right\rangle = -z_\sigma \hbar \langle S_{\mathbf{q}-\mathbf{q}'}^\sigma c_{\mathbf{q}+\mathbf{k},-\sigma}^\dagger c_{\mathbf{q}'+\mathbf{k},\sigma} \rangle \quad (4.82)$$

$$\left\langle \left[c_{\mathbf{q}'+\mathbf{k},-\sigma} S_{-\mathbf{q}'}^{-\sigma}; S_{\mathbf{q}}^\sigma c_{\mathbf{q}+\mathbf{k},-\sigma}^\dagger \right]_+ \right\rangle = \langle S_{-\mathbf{q}}^{-\sigma} S_{\mathbf{q}}^\sigma \rangle \delta_{\mathbf{q}',\mathbf{q}} + 2\hbar z_\sigma \langle S_{\mathbf{q}-\mathbf{q}'}^z c_{\mathbf{q}+\mathbf{k},-\sigma}^\dagger c_{\mathbf{q}'+\mathbf{k},-\sigma} \rangle \quad (4.83)$$

that have to be evaluated in a second step. Our goal is to obtain the electronic self-energy correct to second-order in J . Already the prefactor in (4.78) ensures a J^2 contribution. Hence, any J -dependence in the expectation values (4.81)-(4.83) yields higher order contributions. To avoid these higher orders in J one has to evaluate the expectation values using the eigenstates of the free-electron system H_s . However, if the mean-field Liouvillian is used in (4.77) also the calculation of the expectation values should be based on the eigenstates of H_{MF} . In any case, (4.82) will vanish and both terms in (4.83) will be proportional to $\delta_{\mathbf{q}',\mathbf{q}}$.

In summary, all these considerations result in the following expression for the memory matrix:

$$\boxed{M_{\mathbf{k}\sigma}(\omega) \approx \frac{J^2}{4\hbar^2} \left[-\langle S^z \rangle^2 G_{\mathbf{k}\sigma}^{(\text{MF})}(\omega) + \frac{1}{N^2} \sum_{\mathbf{q}} \langle S_{-\mathbf{q}}^z S_{\mathbf{q}}^z \rangle G_{\mathbf{k}+\mathbf{q},\sigma}^{(\text{MF})}(\omega) + \frac{1}{N^2} \sum_{\mathbf{q}} \{ \langle S_{-\mathbf{q}}^{-\sigma} S_{\mathbf{q}}^\sigma \rangle + 2\hbar z_\sigma \langle S_{\mathbf{0}}^z \hat{n}_{\mathbf{q}+\mathbf{k},-\sigma} \rangle \} G_{\mathbf{k}+\mathbf{q},-\sigma}^{(\text{MF})}(\omega) \right]}. \quad (4.84)$$

All approximations that have been done so far, concern contributions to the self-energy of order J^m with $m > 2$. Eq. (4.84) is therefore the exact result in second order perturbation theory (SOPT).

Discussion of the SOPT result

Even though the derivation of (4.84) “only” ensures the correctness to second order in J , it already exhibits a quite complex structure and illustrates nicely the mutual influence of the two subsystems of a Kondo lattice. On the one hand, the memory-term of a conduction electron is apparently strongly influenced by all other electrons. Therefore, Green’s functions at different wave vectors and for both spin directions contribute. On the other hand, we have several correlation functions, which uniquely describe the local-moment system. In contrast to the first-order result, that enters the frequency matrix, it is not only the net magnetization of the localized spins which is important, but also the spin-dynamics and the mutual influence of the spins at different lattice sites. Both aspects are combined in unifying \mathbf{q} -summations.

Nevertheless, in this section the focus is on the itinerant subsystem of the KLM. This implies the necessity to use approximations for the local-moment correlation functions. To assume their locality is equivalent to a local self-energy of conduction electrons. The latter approximation is widely accepted in many-body theory [42, 93] and is exact for infinite dimensions [91, 103]. For the KLM it is particularly justified since it is proven to be correct in the non-trivial limit of a ferromagnetically saturated semiconductor, as can be seen in Eq. (4.30). To obtain a local self-energy, one has to average (4.84) over \mathbf{k} . As a consequence the itinerant and the local contributions decouple¹² and the \mathbf{q} -summation renders the correlation functions local¹³.

If we now combine the frequency and the memory matrix to the self-energy, the following weak-coupling expansion can be obtained:

$$\begin{aligned}
 \Sigma_\sigma(E) &= -\tilde{J} z_\sigma \langle S^z \rangle + \tilde{J}^2 \gamma_\sigma(E) + \dots && \text{with } \tilde{J} = \frac{J}{2} \\
 \text{and } \hbar \gamma_\sigma(E) &= -\langle S^z \rangle^2 \frac{1}{N} \sum_{\mathbf{k}} G_{\mathbf{k}\sigma}^{(0)} + \langle (S^z)^2 \rangle \frac{1}{N} \sum_{\mathbf{k}} G_{\mathbf{k},\sigma}^{(0)} \\
 &+ \langle S^{-\sigma} S^\sigma \rangle \frac{1}{N} \sum_{\mathbf{k}} G_{\mathbf{k},-\sigma}^{(0)} + 2\hbar z_\sigma \langle S^z \rangle \frac{1}{N} \sum_{\mathbf{k}} \langle \hat{n}_{\mathbf{k},-\sigma} \rangle^{(0)} G_{\mathbf{k},-\sigma}^{(0)}.
 \end{aligned} \tag{4.85}$$

By using free propagators, we have ensured that γ_σ is a factor in the J -expansion and does not carry a J -dependence itself. For the same reason a mean-field decoupling of $\langle S_0^z \hat{n}_{\mathbf{q}+\mathbf{k},-\sigma} \rangle$ is allowed.

¹²E.g.: $\frac{1}{N^3} \sum_{\mathbf{q}} \langle S_{-\mathbf{q}}^z S_{\mathbf{q}}^z \rangle \sum_{\mathbf{k}} G_{\mathbf{k}+\mathbf{q},\sigma}^{(\text{MF})} = \frac{1}{N^2} \sum_{\mathbf{q}} \langle S_{-\mathbf{q}}^z S_{\mathbf{q}}^z \rangle \frac{1}{N} \sum_{\mathbf{k}} G_{\mathbf{k},\sigma}^{(\text{MF})} = \left(\frac{1}{N^2} \sum_{\mathbf{q}} \langle S_{-\mathbf{q}}^z S_{\mathbf{q}}^z \rangle \right) \left(\frac{1}{N} \sum_{\mathbf{k}} G_{\mathbf{k},\sigma}^{(\text{MF})} \right)$

¹³E.g.: $\frac{1}{N^2} \sum_{\mathbf{q}} \langle S_{-\mathbf{q}}^z S_{\mathbf{q}}^z \rangle = \frac{1}{N^2} \sum_{i,j} \sum_{\mathbf{q}} \langle S_i^z S_j^z \rangle e^{i\mathbf{q}(\mathbf{R}_i - \mathbf{R}_j)} = \frac{1}{N} \sum_{i,j} \langle S_i^z S_j^z \rangle \delta_{ij} = \frac{1}{N} \sum_i \langle (S_i^z)^2 \rangle = \langle (S^z)^2 \rangle$

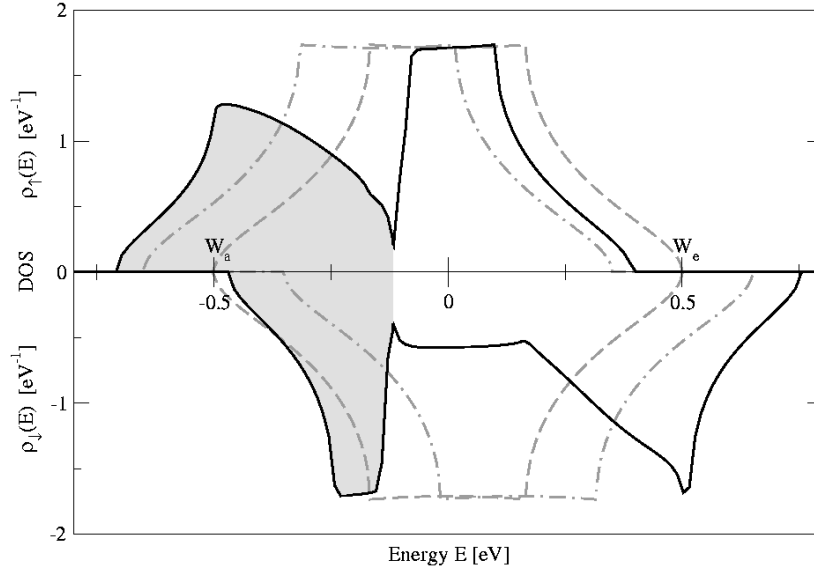


Figure 4.2: Density of states of the conduction electrons in second-order perturbation theory (solid line) as compared to the free DOS (dashed line) and the mean-field result (dash-dotted line). The hatched area displays the occupied part at $T = 0$ K. The parameters are: $J = 0.6$ eV, $n = 0.8$, $S = \langle S^z \rangle = 0.5$, $\mu = -0.12$ eV and $W = 1.0$ eV for a simple-cubic lattice. Resulting polarization: 20 %.

The local-moment correlation functions are trivial if we assume ferromagnetic saturation (which can only exist for $T = 0$ K). Then

$$\gamma_{\uparrow}(E) = \frac{2S\hbar}{N} \sum_{\mathbf{k}} \langle \hat{n}_{\mathbf{k}} \rangle^{(0)} G_{\mathbf{k}}^{(0)}(E) \quad \text{and} \quad \gamma_{\downarrow}(E) = \frac{2S\hbar}{N} \sum_{\mathbf{k}} \left\{ 1 - \langle \hat{n}_{\mathbf{k}} \rangle^{(0)} \right\} G_{\mathbf{k}}^{(0)}(E) \quad (4.86)$$

and the second-order self-energy is dominated by the Fermi distribution function.¹⁴ As a consequence, the density of states

$$\rho_{\sigma}(E) = -\frac{1}{\pi} \cdot \begin{cases} \rho_0(E - \Re \Sigma_{\sigma}(E)) \cdot (-\pi), & \Im \Sigma_{\sigma}(E) = 0 \\ \Im \Sigma_{\sigma}(E) \cdot \int \frac{\rho_0(x) dx}{(E-x-\Re \Sigma_{\sigma})^2 + (\Im \Sigma_{\sigma})^2}, & \Im \Sigma_{\sigma}(E) \neq 0 \end{cases} \quad (4.87)$$

has a clear minimum at the Fermi energy.¹⁵ The depth of this minimum varies. For the set of parameters chosen in Fig. 4.2 we have a $\rho_{\sigma}(\mu) > 0$ and the QDOS is connected for both spin directions, though the band width is larger than in the mean-field case. For

¹⁴Eq. (4.86) is valid without the assumption of a local self-energy and mean-field decoupled expectation values.

¹⁵ The J^2 -contribution of $\Re \Sigma_{\uparrow}$ goes with $\Pr \int_{-\infty}^{\mu} \frac{\rho_0(x)}{E-x} dx = \Pr \int_{E-\mu}^{\infty} \frac{\rho_0(E-y)}{y} dy$. It therefore has its maximum at $E = \mu$. $\Im \Sigma_{\uparrow}$ is proportional to the free DOS for $E < \mu$ and vanishes for $E > \mu$. The opposite is true for Σ_{\downarrow} , where the real part has a minimum at $E = \mu$ and the imaginary part vanishes for $E < \mu$.

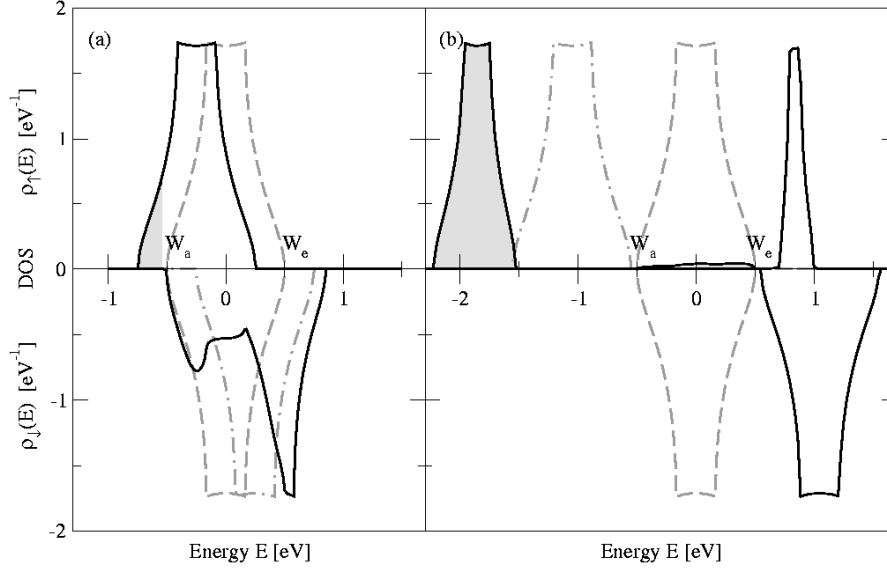


Figure 4.3: Possibilities to obtain a 100% polarized conduction band within SOPT. The figure is structured as in Fig. 4.2. The specific parameters are (a): $J = 0.33$ eV, $n = 0.08$, $\mu = -0.54$ eV and (b): $J = 1.4$ eV, $n = 0.72$, $\mu = 0.54$ eV. For both cases $S = \langle S^z \rangle = 1.5$ and $W = 1.0$ eV.

sufficiently large coupling constants J , given by the relation¹⁶

$$E - \Re \Sigma_{\downarrow}^{E=\mu} \mu - \tilde{J}S\hbar - \tilde{J}^2 2S\hbar^2 \text{Pr} \int_{\mu}^{W_e} \frac{\rho_0(x)}{\mu - x} dx \stackrel{!}{>} W_e, \quad (4.88)$$

a gap will open in the \downarrow -QDOS. For \uparrow -electrons the critical J has a different value. More importantly, the position of the chemical potential μ within the gap differs. For \uparrow -electrons μ forms the upper edge of the lower energy subband, for \downarrow -electrons it is situated at the lower edge of the upper subband. As a consequence, the opening of a gap implies that the conduction electrons close to the Fermi energy are only of \uparrow -type, similar to the situation envisaged for half-metallic ferromagnets [22, 126].

We would like to investigate¹⁷, whether or not such a 100% electron polarization can also be obtained for the whole conduction band. When doing so, we continue an analogous discussion of the mean-field situation and verify the claim of Irkhin and Katsnelson [58] that this is indeed possible within the KLM. Again, this question is only meaningful at $T = 0$ K. Any deviation from a saturated local-moment system can cause spin-flip processes that immediately imply a depolarization. The answer is: Yes, there are certain conditions under which the SOPT approach allows for all conduction electrons to be of the same spin direction. One strategy is to choose a small number of conduction electrons

¹⁶ W_a and W_e are the lower and upper edge of the free DOS (see Fig. 4.2).

¹⁷Details are given in appendix E.

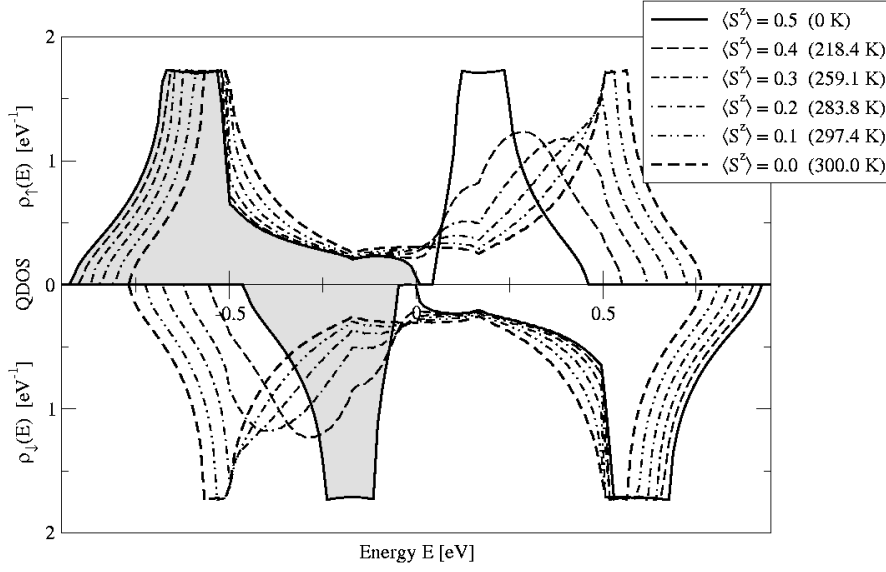


Figure 4.4: Temperature dependence of the QDOS as obtained by SOPT. The expectation value $\langle S^z \rangle$ is taken from a Brillouin function. The hatched area displays the occupied part at $T = 0$ K. The parameters are: $J = 1.0$ eV, $n = 1.0$, $\mu = 0.0$ eV, $S = 0.5$, $T_C = 300$ eV and $W = 1.0$ eV for a simple-cubic lattice. Resulting polarization respectively: 20%, 16%, 12%, 8%, 4% and 0%.

n . As soon as $\mu \leq W_a$, the condition for a vanishing \downarrow -QDOS is given by

$$E - \Re \Sigma_{\downarrow} = E - \tilde{J}S\hbar - \tilde{J}^2 2S\hbar^2 \text{Pr} \int_{W_a}^{W_e} \frac{\rho_0(x)}{E-x} dx \stackrel{!}{<} W_a. \quad (4.89)$$

The integral becomes minimal at $E = W_a$. Hence, all coupling strengths smaller than the corresponding critical J are sufficient¹⁸ to guarantee a vanishing of the QDOS for minority \downarrow -electrons in the relevant energy range $E < \mu$. The situation is plotted in Fig. 4.3a. There is also a strategy that allows for larger numbers of majority electrons. One has to choose a chemical potential such that the second order contribution to $\Re \Sigma_{\downarrow}(E)$ vanishes and only the mean-field contribution accomplishes (4.89): $W_e < \mu < W_a + JS\hbar$. This implies a complete polarization as can be seen in Fig. 4.3b. However, in order to fulfil this inequality J has to be larger than $2W/S\hbar$, what renders perturbation theory in J to be unreliable. Within our theory all other choices of the chemical potential lead to a depolarization of the conduction band.

Apart from the $T = 0$ K statement a study of the temperature dependence of the QDOS is, of course, of interest. For this purpose it is still necessary to have a separate theory for the local-moment subsystem. Suggestions will be presented in Secs. 4.5 and

¹⁸It fulfils condition (4.89) at $E = W_a$ and therefore $\forall E < W_a$.

5.3. For the moment, we shall assume that it is given by a Brillouin function [110]:

$$\langle S^z \rangle = \hbar S \cdot B_D \left(\frac{3S}{S+1} \frac{T_C}{T} \frac{\langle S^z \rangle}{\hbar S} \right) \quad (4.90)$$

$$\text{with } B_D(x) = \frac{2D+1}{2D} \coth \left(\frac{(2D+1)x}{2D} \right) - \frac{1}{2D} \coth \left(\frac{x}{2D} \right). \quad (4.91)$$

For $S = 1/2$ one benefits from the fact that such a temperature dependence has to be provided only for the magnetization. For all higher spin quantum numbers S one can use the RPA formula [114, 17]

$$\langle S^z \rangle = \hbar \frac{(1+S+\varphi)\varphi^{2S+1} + (S-\varphi)(1+\varphi)^{2S+1}}{(1+\varphi)^{2S+1} - \varphi^{2S+1}} \quad (4.92)$$

to transform the magnetization $\langle S^z \rangle$ to an average magnon number $\varphi(S)$, which in turn can be used for the calculation of the correlation functions

$$\langle S^- S^+ \rangle = 2\hbar \langle S^z \rangle \varphi(S) \implies \langle (S^z)^2 \rangle = \hbar^2 S(S+1) - \hbar \langle S^z \rangle (1 + 2\varphi(S)). \quad (4.93)$$

An additional temperature dependence via the spectral theorem is included in the expectation value $\langle \hat{n}_{\mathbf{k}\sigma} \rangle$. However, the effects on the QDOS that can be observed in Fig. 4.4 are mainly due to the change of the magnetization from its ferromagnetic ($\langle S^z \rangle = \hbar S$) to its paramagnetic ($\langle S^z \rangle = 0$) value. The deformations of the QDOS with rising temperature are not surprising. A two-band structure with strong differences for \uparrow - and \downarrow -electrons at $T = 0$ K continuously crosses over to a structure which is identical for both kinds of spin directions at $T = T_C$. The effects are an increase of the total bandwidth and less pronounced peaks in the QDOS. For a better visualization the parameters of Fig. 4.4 are chosen such that for $T = 0$ K the gap is really open. Nevertheless, the temperature dependence of $\langle S^z \rangle$ as well as that of $\langle \hat{n}_{\mathbf{k}\sigma} \rangle$ causes a closing of the gap already for moderate temperatures¹⁹. Furthermore, the particular choice of the chemical potential nicely demonstrates the particle-hole symmetry of the system. As a consequence Fig. 4.4 is point-symmetric with respect to the point of origin.

Discussion of the SOPT relative to Hartree-Fock

When writing down the expression for γ_σ in (4.85) we made sure that it does not carry any J -dependence. This was due to our desire to only consider exactly contributions to the self-energy up to second-order²⁰ without any interference from higher orders in J . On the other hand, for the derivation of the memory matrix (4.84) we used, instead of the free Liouvillian \mathcal{L}_s , a Liouvillian \mathcal{L}_{MF} that includes the mean-field contribution to the self-energy. In the propagator formalism of Feynman diagrams [84] this corresponds to a perturbation treatment around the Hartree-Fock solution. Since this is a systematic extension, which does not affect the J^2 contribution, one has the impression that such a treatment improves the result for the self-energy.

¹⁹Already a temperature of $T = T_C/3$, where $\langle S^z \rangle$ is still close to saturation, results in the closing of the gap.

²⁰In order to distinguish the approach from other concepts we will name it the ‘‘conventional SOPT’’.

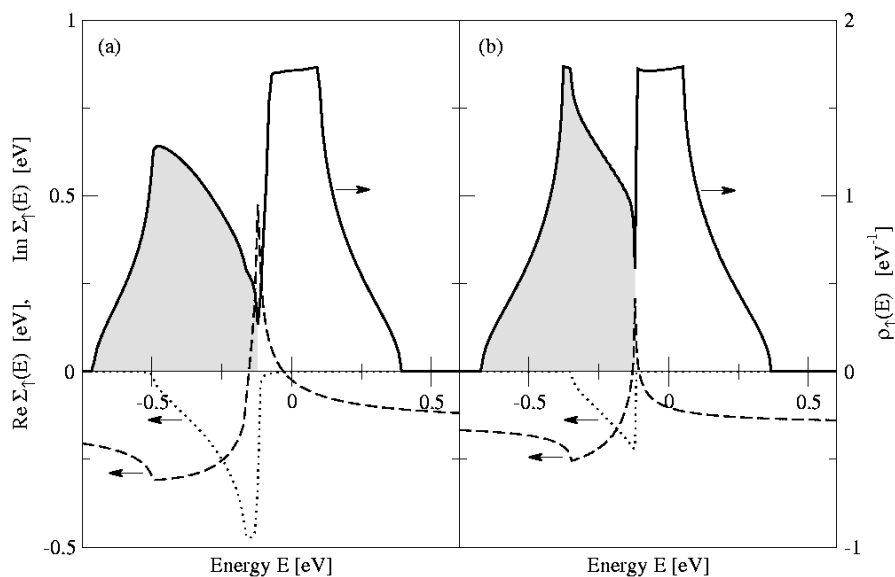


Figure 4.5: Comparison of conventional SOPT (a) and SOPT relative to Hartree-Fock (b) at $T = 0$ K for \uparrow -electrons. In both cases the real (dashed lines) and the imaginary part (dotted lines) of the self-energy is plotted. It determines the QDOS, which is also given (solid lines). The parameters are (as in Fig. 4.2): $J = 0.6$ eV, $\mu = -0.12$ eV, $S = \langle S^z \rangle = 0.5$ and $W = 1.0$ eV for a simple-cubic lattice. The resulting difference in the band-occupation is small: $n = 0.80$ (a) and $n = 0.79$ (b). The difference is larger for the polarization: 20% (a) and 29% (b).

Therefore, we would like to know how a SOPT relative to Hartree-Fock alters the statements for a conventional SOPT given above. In particular for $T = 0$ K one can observe analytically as well as numerically, that the incorporation of mean-field terms in the propagators yields a reduction of the non-linear contributions to the self-energy²¹. This is demonstrated in Fig. 4.5, where we have compared both concepts for \uparrow -electrons. One can see that the imaginary and the real part of the self-energy are closer to the mean-field values ($\Im \Sigma_{\uparrow} \equiv 0$, $\Re \Sigma_{\uparrow} = -0.15$ eV) in the SOPT relative to Hartree-Fock. Nevertheless, the principle structure is unchanged, e.g., $\Im \Sigma_{\uparrow}$ is still zero above the Fermi energy. According to (4.87) the quantitative changes of the self-energy directly influence the QDOS. The broadening of the band-width observed in conventional SOPT (compare Fig. 4.2) is now reduced. The same is true for the opening of a gap: Much larger coupling strengths are necessary, to separate the upper from the lower part of the QDOS.

However, there are also qualitative differences between these two concepts. They are related to the important question, whether or not the KLM allows for a complete polarization of the conduction band. For conventional SOPT we have shown two possibilities in Fig. 4.3. The most promising strategy was the choice of sufficiently small values for the band occupation and the coupling strength. One can show rigorously²², that the same does not work for SOPT relative to Hartree-Fock. Even for $n \rightarrow 0$ and $J \rightarrow 0$ eV

²¹In perturbation theory usually the n th order contribution diminishes the effect of the previous order $n - 1$.

²²For an analytical prove see appendix E.

there will always be a depolarization in the conduction band. Hence, the two concepts illustrated in Fig. 4.5 are not identical even for small J .

There is still the second strategy in Fig. 4.3 to obtain complete polarization. For SOPT relative to Hartree-Fock this corresponds to a coupling strength J which is large enough to shift the \downarrow -QDOS into an energy region above the \uparrow -QDOS. Then a chemical potential in the intermediate energy region ($W_e - \tilde{J}S\hbar < \mu < W_a + \tilde{J}S\hbar$) is appropriate for complete polarization, also for SOPT relative to Hartree-Fock. However, in contrast to Fig. 4.3 the situation now implies, that the \uparrow -band is completely filled ($n_\uparrow = 1$). This is a very special situation²³, which Irkhin and Katsnelson [58], do not have in mind, when referring to complete polarization. For any $n < 1$ our investigations indicate, that a complete polarization of the conduction band of the KLM is not possible.

A study of the temperature dependence of SOPT relative to Hartree-Fock does not produce new insights. The higher the temperature the smaller is the difference of the QDOS as compared to conventional SOPT. Finally, for $\langle S^z \rangle = 0$, both concepts are identical.

4.4 The modified perturbation theory

The result (4.85) is not our final answer to the question of a proper self-energy for the itinerant electrons in the KLM. The POM should be improved in order to incorporate more of the known exact features, in particular the limit of a ferromagnetically saturated semiconductor. Experiences with approximations for similar many-body Hamiltonians serve as another motivation for a refinement of SOPT. Our method of choice is similar to the modified perturbation theory [63, 129], which has turned out to be the most promising analytical approach to the Hubbard model [130]. This part has been published in [50].

Generalization of experiences with a limiting case

The ferromagnetically saturated semiconductor, which contains the magnetic polaron as a special quasiparticle, is a fundamental limit of the KLM. It is all the more unfortunate, that SOPT is not correct in this limit. By adjusting the expectation values in (4.84) accordingly, one instead obtains the \mathbf{k} -independent self-energy

$$\Sigma_\sigma = -\tilde{J} z_\sigma S\hbar + \tilde{J}^2 2S\hbar \frac{1}{N} \sum_{\mathbf{q}} G_{\mathbf{q}-\sigma}^{(0/\text{MF})} \delta_{\sigma\downarrow}, \quad (4.94)$$

which has been identified before as the weak-coupling approximation (4.18). The discussion of Sec. 4.1 showed that the next step in the continued fraction expansion of the POM yields the right memory matrix (4.52) for the exact self-energy

$$\Sigma_\sigma = -\tilde{J} z_\sigma S\hbar + \tilde{J}^2 \frac{2S\hbar \frac{1}{N} \sum_{\mathbf{q}} G_{\mathbf{q}-\sigma}^{(\text{MF})}(\omega)}{1 - \tilde{J} \frac{1}{N} \sum_{\mathbf{q}} G_{\mathbf{q}-\sigma}^{(\text{MF})}(\omega)} \delta_{\sigma\downarrow}. \quad (4.95)$$

²³Note again that a condition like $J > W/S\hbar$ is not compatible with a perturbation theory in J .

The second order result (4.94) appears in (4.95) in the numerator as well as in the denominator.

The *modified perturbation theory* (MPT) is a straightforward generalization of the analytical structure of this result to arbitrary band configurations:

$$\Sigma_\sigma(E) = -\tilde{J} z_\sigma \langle S^z \rangle + \tilde{J}^2 \frac{a_\sigma \gamma_\sigma(E)}{1 - \tilde{J} b_\sigma \gamma_\sigma(E)}, \quad (4.96)$$

where γ_σ is the SOPT result (4.85). The ansatz has the advantage to retain the benefits of SOPT (e.g. being exact to order J^2), but allows the freedom to choose the parameters a_σ and b_σ such that further criteria are fulfilled.

Following this philosophy, the values $a_\sigma \equiv 1$ and $b_\sigma \equiv 1/2S\hbar$ would be sufficient to ensure the correctness of the ferromagnetically saturated semiconductor. However, there is no reason why a choice that is designed for a certain limit, should be justified for other parameter regions, too. Indeed, these values produce some physically questionable features for $n > 0$. As explained on page 13, a fit to the spectral moments (2.17) of the Green's function is a more general approach. In addition to the expansion in powers of J , it introduces the notion of a high-energy expansion of the self-energy.

In the context of the POM the high-energy expansion of the self-energy is given by the geometric series representation of the memory matrix

$$\Sigma_{\mathbf{k}\sigma}(\omega) = -\tilde{J} z_\sigma \langle S^z \rangle + \sum_{m=0}^{\infty} \frac{\hbar}{\omega^{m+1}} \left(\mathcal{Q}\mathcal{L} c_{\mathbf{k}\sigma}^\dagger \left| (\mathcal{Q}\mathcal{L}\mathcal{Q})^m \right| \mathcal{Q}\mathcal{L} c_{\mathbf{k}\sigma}^\dagger \right). \quad (4.97)$$

In our approximation (4.77) the Liouvillian in the middle has been replaced by some $\hat{\mathcal{L}}$. This does not affect the orders ω^0 and ω^{-1} of the energy-expansion. In other words: SOPT automatically produces the exact expressions for the first three moments of the Green's function. To ensure correctness to the same order for the MPT ansatz (4.96) the parameter a_σ has to be chosen as 1. For the next order the equality

$$C_{\mathbf{k}\sigma}^{(2)} \equiv \left(\mathcal{Q}\mathcal{L} c_{\mathbf{k}\sigma}^\dagger \left| \mathcal{L} \right| \mathcal{Q}\mathcal{L} c_{\mathbf{k}\sigma}^\dagger \right) \stackrel{!}{=} \left(\mathcal{Q}\mathcal{L} c_{\mathbf{k}\sigma}^\dagger \left| \hat{\mathcal{L}} \right| \mathcal{Q}\mathcal{L} c_{\mathbf{k}\sigma}^\dagger \right) + \frac{b_\sigma \hbar}{\tilde{J}} \left(\mathcal{Q}\mathcal{L} c_{\mathbf{k}\sigma}^\dagger \left| \mathcal{Q}\mathcal{L} c_{\mathbf{k}\sigma}^\dagger \right. \right)^2 \quad (4.98)$$

is required. This determines the second parameter:

$$b_\sigma = \frac{\tilde{J}}{\hbar} \frac{\left(\mathcal{Q}\mathcal{L} c_{\mathbf{k}\sigma}^\dagger \left| \mathcal{L} - \hat{\mathcal{L}} \right| \mathcal{Q}\mathcal{L} c_{\mathbf{k}\sigma}^\dagger \right)}{\left(\mathcal{Q}\mathcal{L} c_{\mathbf{k}\sigma}^\dagger \left| \mathcal{Q}\mathcal{L} c_{\mathbf{k}\sigma}^\dagger \right. \right)^2}. \quad (4.99)$$

The explicit expression for b_σ therefore depends on the actual choice of $\hat{\mathcal{L}}$, as will be discussed in more detail below. It is also worth mentioning, that b_σ formally carries a \mathbf{k} -dependence, which vanishes identically in our calculations.

If $\hat{\mathcal{L}}$ is the Liouvillian \mathcal{L}_0 of a conventional SOPT, all terms except the J^3 contributions cancel in the numerator and b_σ becomes J -independent. More precisely,

$$b_\sigma = \frac{[\hbar^2 S(S+1) - z_\sigma \hbar \langle S^z \rangle - \langle S^z \rangle^2] (z_\sigma \langle S^z \rangle + \hbar) + 2\hbar(2z_\sigma \langle S^z \rangle + \hbar)p_\sigma - 2\hbar x_\sigma}{\tilde{J} [\hbar^2 S(S+1) - z_\sigma \hbar \langle S^z \rangle - \langle S^z \rangle^2 + 2\hbar p_\sigma]^2} \quad (4.100)$$

where $p_\sigma = z_\sigma \langle S^z \hat{n}_{-\sigma} \rangle - \langle S^{-\sigma} c_{\sigma}^\dagger c_{-\sigma} \rangle$ and x_σ are sets of further correlation functions, which have the property to vanish in the limit $n \rightarrow 0$. Combined with the additional constraint of ferromagnetic saturation $\langle S^z \rangle = \hbar S$ one obtains a b_\downarrow which corresponds to the result (4.51) of Sec. 4.1. Hence, the magnetic polaron is not exactly included.

If $\hat{\mathcal{L}}$ is the Liouvillian \mathcal{L}_{MF} of a SOPT relative to Hartree-Fock, then (4.99) contains an additional term according to the mean-field contribution $\hat{\Sigma}_\sigma = -\tilde{J} z_\sigma \langle S^z \rangle$ in the self-energy. This yields a correction

$$\Delta b_\sigma = \frac{\hat{\Sigma}_\sigma [\langle (S^z)^2 \rangle - \langle S^z \rangle^2] + \hat{\Sigma}_{-\sigma} [\langle S^{-\sigma} S^\sigma \rangle + 2\hbar z_\sigma \langle S^z \rangle \langle \hat{n}_{-\sigma} \rangle]}{\tilde{J} [\hbar^2 S(S+1) - z_\sigma \hbar \langle S^z \rangle - \langle S^z \rangle^2 + 2\hbar p_\sigma]^2} \quad (4.101)$$

to the former result (4.100). Considered again in the limit of a ferromagnetically saturated semiconductor with this correction one obtains indeed the value $b_\downarrow - \Delta b_\downarrow = 1/2S\hbar$, which corresponds to the exact result (4.52) in this limit. In this sense, the high-energy expansion is a more general approach than a fit to the magnetic polaron.

The zero bandwidth limit is the second limit considered in the context of the POM (see Sec. 4.2). It is immediately apparent²⁴ that the MPT (4.96) is not appropriate for an exact representation of the atomic-limit self-energy in its most general form (4.73). Nevertheless, at least its correctness can be checked for the case $n \rightarrow 0$. It turns out that $\hat{\mathcal{L}} \equiv \mathcal{L}_0$ yields the exact $n = 0$ self-energy, with the parameter b_σ as obtained in (4.100). That is again an improvement compared to the bare SOPT. On the other hand, at first glance the correction Δb_σ seems to be wrong. However, one should note [49] that the atomic limit is only consistent with $\langle S^z \rangle = 0$, where the correction does vanish.

In the discussion so far we have tested the MPT (4.96) in the limit $n \rightarrow 0$. One can repeat the same transformations for the opposite case $n \rightarrow 2$. By doing this one will notice that the same formulae are obtained. The only difference is the change of the sign of σ and of b_σ . This is due to particle-hole symmetry in the system [49]. Therefore, in the same sense as for $n = 0$ our MPT ansatz (4.96) fulfils the limit of the magnetic polaron and the zero-bandwidth limit for $n = 2$.

In this context it is worth mentioning that our approach seems to be related to the interpolating self-energy approach (ISA) published by Nolting *et al.* (p. 14). There, a structure of the self-energy has been concluded from a systematic study of all known exact statements on the KLM. The result looks similar to (4.96). However, their analysis is focused on the low-density limit and ensures the correctness of these statements only for $n = 0$ (or $n = 2$). In contrast, the weak-coupling theory presented in this work fulfils second-order perturbation theory and the high-energy expansion independent of the occupation number. The wider range of physical applicability is ensured by a larger set of contributing correlation functions. Additionally, we can fulfil the same criteria for $n \rightarrow 0$ as given in the ISA. Nevertheless, the two approaches are not identical even for $n = 0$, but otherwise arbitrary parameters. The major difference is the fact that in SOPT the excess electron scatters with \uparrow - and \downarrow -electrons, whereas in the ISA electrons of the same spin-direction do not influence each other.

²⁴This is due to the required four-pole structure of its Green's function. In contrast to that, the Hubbard model allows a fit of the parameters a_σ and b_σ to the atomic limit result [63]. To obtain the structure of the zero-bandwidth limit also for the KLM one could extend the ansatz (4.96) by an alloy-analogy as done in [117].

Review of experiences with other models

Even if the formulae provided are clear, the formulation of a proper MPT strategy in the case of the KLM is still a complex and cumbersome task. One reason is the above mentioned ambiguity: the results depend on the choice of $\hat{\mathcal{L}}$ in (4.99). Whenever a perturbation theory is performed in many-body theory there are principally even three different ways of treating emerging propagators: the *conventional* SOPT uses the free propagators, a SOPT *relative to Hartree-Fock* (SOPT-HF) replaces these propagators by the corresponding mean-field expressions and a *self-consistent* treatment of SOPT replaces all propagators by (functionals of) the full propagators as obtained in the previous step of iteration. A priori it is usually not known which version yields the most reliable results for SOPT. Things do not become easier if a MPT is performed.

Of course, the *self-consistent* version includes a summation of more diagrams than the other methods. However, since only a partial class of diagrams is summed, it is unclear which important diagrams are being missed out or cancelled, double-counted or even taken wrongly. There are more profound considerations as put forward by Kadanoff and Baym [8] arguing that the self-consistent approach is a conserving approximation which automatically satisfies the Luttinger theorem [84] and Fermi-liquid properties. However, it is uncertain to which degree this applies to a model which is not exclusively composed of fermions.

For a number of models the question of the most appropriate version has been discussed intensively in the literature. The Falicov-Kimball model has the advantage of being exactly soluble in infinite dimensions [14]²⁵. For this model it can be shown that a not fully self-consistent SOPT treatment does reproduce exact results qualitatively, whereas the self-consistent SOPT does not [147].

For the periodic Anderson model (PAM) Yamada and Yosida [173, 172, 174] were among the first to point out the importance of SOPT. They already considered deviations from a non-magnetic Hartree-Fock solution. Later Schweitzer and Czycholl [147] were able to numerically compare this approach with a self-consistent SOPT. Even though this version obeys more of the Luttinger sum rules [84], the self-consistent version (in contrast to SOPT-HF) failed to show the one-particle peaks near E_f and $E_f + U$ in the f -electron spectral function. Nevertheless, a definite statement on the quality cannot be given, since both versions do not fulfil the corresponding limiting cases exactly.

An ansatz similar to (4.96) has been suggested for the single-impurity Anderson model [87] and exploited by Meyer et al. [93, 94] for the PAM. For the asymmetric impurity model the MPT yields more reasonable results, in particular with respect to the Friedel sum rule [35, 78], than the bare SOPT [95]. Here, SOPT-HF has been used as input for the MPT. However, Meyer et al. reported a resulting ambiguity in the choice of the chemical potential. Instead of using a single μ for the whole theory, they considered an additional $\tilde{\mu}$ as a parameter to ensure an identical electron concentration for the Hartree-Fock and the full calculation. They did not use $\tilde{\mu}$ to fulfil the Friedel sum rule [63], as this would limit their considerations to $T = 0$ K. The ambiguity of choosing the chemical potential is discussed in more detail in [129].

²⁵An interesting combination of DMFT and POM for the Falicov-Kimball model has been suggested in [98].

For the Hubbard model there exist a large number of perturbational approaches. Many of them are evaluated in [130], where the importance of the spectral moment $m_{\mathbf{k}\sigma}^{(3)}$ for the calculation of magnetic phase boundaries and critical temperatures is emphasized. First investigations indicated that a self-consistent SOPT has the advantage of reproducing the quasiparticle subbands of the strong-coupling limit [16]. Nevertheless, the same can be obtained with a SOPT-HF, if the \mathbf{k} -dependence of the self-energy is not neglected [148]. Later Wernbter and Czycholl showed that SOPT-HF does not yield a metal-insulator transition and does not show a breakdown of the Fermi-liquid behaviour [169]. On the other hand, a straightforward application of a self-consistent SOPT does not reproduce the Hubbard bands in the atomic limit [104]. More sophisticated methods such as the interpolation scheme of Edwards and Hertz [26, 169] (a version relative to HF) or the iterative perturbation theory (IPT) of Georges and Kotliar [41] (a self-consistent version) are required to remove these drawbacks.

The IPT is based on the self-consistency cycle of dynamical mean-field theory. The impurity problem is again the single-impurity Anderson model. It has been solved by quantum Monte-Carlo and exact diagonalization methods [181, 135, 136] and shows a good interpolation between the Brinkman-Rice (small coupling strength) and the Hubbard III (large coupling strength) approach. However, the excellence of the IPT is apparently limited to half-filling. This limitation has been removed by Kajueter, Kotliar [63] and Potthoff, Wegner, Nolting [129] with a modified perturbation theory analogous to (4.96). In a comparison Potthoff et al. [130] come to the conclusion that the MPT is probably the most convincing analytic approach to the Hubbard model.

According to this literature review and due to the similarities of the Hubbard model and the KLM [124], the performance of a MPT for the KLM seems to be a natural as well as promising thing to do. However, the analysis presented above does not immediately suggest an appropriate version of SOPT to be used for the calculations. In order to clarify this point further work is required.

Variations of a MPT approach to the KLM

The particular problem of finding a MPT strategy for the KLM is the small number of clear criteria to judge the quality of different approaches.²⁶ Therefore, in some cases we are forced to draw on rather vague arguments, such as the physical plausibility and our experience with other approximations. Finally however, we shall be able to make some clear statements.

The philosophy of the MPT is as follows: We start with a SOPT expression $\gamma_{\mathbf{k}\sigma}$ that is taken from the memory matrix (4.77) without further approximations. This enters the MPT ansatz (4.96) and gives rise to the expressions (4.99) for b_σ and (4.101) for Δb_σ , respectively. Thereafter reasonable assumptions are considered for expectation values .

From the analytical considerations given above it is clear that a SOPT relative to Hartree-Fock should be preferred compared to one based on a conventional SOPT. This is because the former correctly incorporates the important limiting case of the ferromagnetically saturated semiconductor, whereas the latter does only reproduce, in this limit,

²⁶For instance, the Luttinger theorem, often used for the Hubbard model, does not necessarily hold for non-fermionic systems and finite temperatures.

the less accurate expression (4.51). Nevertheless there are still several variations possible:

1. For consistency reasons the usage of a SOPT-HF implies that the expectation values are also evaluated using mean-field Green's functions. However, learning from the experiences with the single-impurity Anderson model [129, 95] one can also introduce an additional parameter $\tilde{\mu}$ to ensure that $\langle \hat{n}_\sigma \rangle$ is identical to the value obtained using the full Green's function.
2. The MPT parameter b_σ contains the correlation function p_σ , which can be given as a function of the single electron Green's function $G_{\mathbf{k}\sigma}(E)$. This follows from a modification of the spectral theorem, using the Heisenberg equation of motion [117]:

$$p_\sigma = \frac{1}{\tilde{J}} \frac{1}{N} \sum_{\mathbf{k}} \left(-\frac{1}{\pi \hbar} \right) \int_{-\infty}^{\infty} dE \frac{\Im G_{\mathbf{k},-\sigma}(E)}{e^{\beta(E-\mu)} + 1} [E - \varepsilon_{\mathbf{k}}] \quad (4.102)$$

Also the correlation function x_σ can be treated more accurately than is done using mean-field decoupling. This is possible with the help of the exact relation (2.23). However, correlation functions such as (4.82) can only be evaluated if a decoupling is performed. Therefore, an application of (4.102) has the potential for inconsistencies.

3. For a self-consistent treatment all propagators $G_{\mathbf{k}\sigma}^{(\text{MF})}(E)$ in the MPT expression of the self-energy can be replaced by full propagators $G_{\mathbf{k}\sigma}(E)$. There are two general philosophies behind this step. It is, on the one hand, a renormalization of the self-energy, guided by the intention to include effects of higher order in the coupling strength. On the other hand, within the procedure of the POM an iterated partitioning of the Hamiltonian [16] has the same effect.
4. Furthermore, one has to clarify in which order these strategies are to be applied. The actual value of the contribution $\hat{\Sigma}_\sigma$ in (4.101) depends on the question whether or not the MPT is based on a SOPT-HF (with a subsequently performed renormalization) or alternatively it is already based on a self-consistent SOPT. In the former case, $\hat{\Sigma}_\sigma$ is the mean-field energy shift $-\tilde{J}z_\sigma \langle S^z \rangle$, which is not altered afterwards. In the latter case, the full self-energy has to be inserted to ensure the correct high-energy expansion.

All these variations have been checked carefully. The last point mentioned above can even be discussed analytically. For example, when considering the atomic limit ($W \rightarrow 0$ eV, $n \rightarrow 0$, $\langle S^z \rangle \rightarrow 0$) we are confronted with three types of self-energy:

$$\tilde{J}^2 \frac{S(S+1) \frac{1}{E-T_0}}{1 - \tilde{J} \frac{1}{E-T_0}}, \quad \tilde{J}^2 \frac{S(S+1) \frac{1}{E-T_0-\hat{\Sigma}}}{1 - \tilde{J} \frac{1}{E-T_0-\hat{\Sigma}}}, \quad \tilde{J}^2 \frac{S(S+1) \frac{1}{E-T_0-\hat{\Sigma}}}{1 - (\tilde{J} - \hat{\Sigma}) \frac{1}{E-T_0-\hat{\Sigma}}}. \quad (4.103)$$

The expression on the left corresponds to the exact result, as it is obtained with a MPT based on SOPT-HF. If in this result propagators are replaced by full Green's functions, the expression in the middle is obtained. Since it is not identical to the first one, the atomic limit is not fulfilled anymore even for $n = 0$. However, if already the determination of

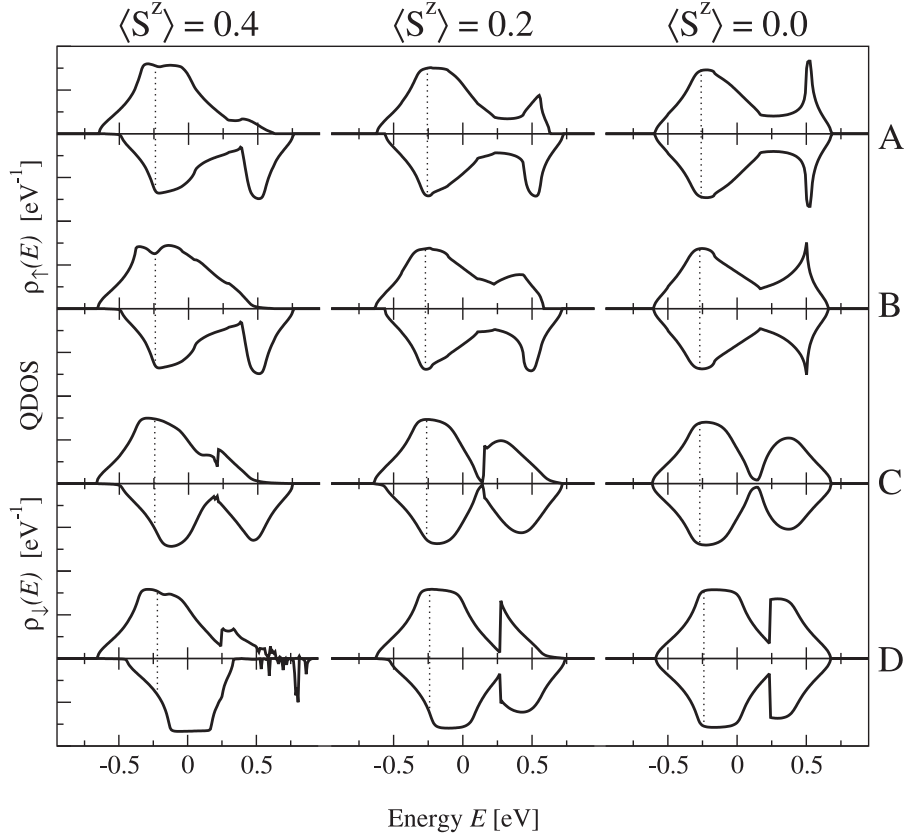


Figure 4.6: Comparison of the MPT strategies A-D as explained in the text for moderate coupling strength. The QDOS displayed is evaluated for temperatures $T = 218.4$ K, $T = 283.8$ K and $T = T_C = 300$ K, which correspond to the magnetization given at the top of the figure. The parameters are: $J = 0.6$ eV, $n = 0.5$, $S = 1/2$ and $W = 1.0$ eV for a simple-cubic lattice.

the parameters a_σ and b_σ is based on a self-consistent SOPT, this results in the self-energy given on the right hand side. It is easy to show, that the latter is identical to the expression on the left.²⁷ For this and other reasons, the choice of propagators should always happen before the parameter b_σ is fixed.

Using these considerations the variations above can be combined to for possible approaches:

A: The MPT is based on SOPT-HF. The mean-field self-energy is used for Δb_σ in the MPT ansatz. All correlation functions are treated within mean-field approximation.

B: The MPT is based on SOPT-HF. The mean-field self-energy is used for Δb_σ in the MPT ansatz. The correlation functions are treated within mean-field approximation. However, the expectation value of the electron density operator is adapted to

²⁷A similar discussion for the ferromagnetically saturated semiconductor is redundant, since the \downarrow -Green's function is uniquely determined by \uparrow -propagators, which have the iteration-independent self-energy $\Sigma_\uparrow \equiv -\tilde{J}Sh$.

the full self-energy.

- C: The MPT is based on a self-consistent SOPT. The full self-energy is used for Δb_σ in the MPT ansatz. All correlation functions are mean-field decoupled, but the expectation value of the electron density operator is adapted to the full self-energy.
- D: The MPT is based on a self-consistent SOPT. The full self-energy is used for Δb_σ in the MPT ansatz. Only for a few correlation functions a mean-field decoupling is performed. The expectation value of the electron density operator is adapted to the full self-energy. The correlation function p_σ is determined using (4.102).

All these strategies have a self-energy that is exact to order J^2 . They also share the correct behaviour in the limit of the ferromagnetically saturated semiconductor and the empty atomic limit. All of them fulfil the same moments of the Green's function. However, one should note, that strategy D is inconsistent in the sense, that not all correlation functions are treated on the same footing. This is probably also the reason, why the numerical evaluation shows a rather pure convergence, in particular for low temperatures.

The strategies are compared in Fig. 4.6 for different temperatures. The positive message is that in principle all strategies yield the same qualitative shape of the respective QDOS. For low temperatures there is a broad band in the \uparrow -QDOS, the \downarrow -QDOS consists of a scattering part and the remainder of the magnetic-polaron band. As temperature rises the spectral weight is redistributed for both spin directions. In the \uparrow -QDOS a second band is formed. This two-band structure still exists in the paramagnetic regime, where \uparrow - and \downarrow -QDOS are identical. Note, that $J = 0.6$ eV already corresponds to moderate coupling strengths. For lower values of J the differences are even smaller.

Nevertheless, the existence of differences between the strategies cannot be neglected. Close to saturation the mean-field approaches A and B exhibit energy regions, where only one kind of spin-direction is allowed for the conduction electrons. However, this does not imply a complete polarization, rather it indicates that for some electrons spin-flip processes are prohibited. There seems to be no physical justification for such a restriction, since all chosen $\langle S^z \rangle$ -values are sufficiently far from saturation. In contrast, a (asymptotically small) QDOS exists for in the approaches C and D in the whole energy region where the QDOS of the opposite spin direction is finite.

Another remarkable difference is the tendency to form a gap between the two subbands in both spin directions. It is much larger for the self-consistent approaches C and D, in approach D it is connected with an unexpected sharp increase in the QDOS. For the mean-field approaches, although yielding sharper structures in the QDOS, the gap for \downarrow -electrons always seems to close. Instead a strange peak in the unoccupied part of the QDOS is observed for high temperatures.

For large coupling strength and/or smaller bandwidths these features can be clearly observed. Even though SOPT is not designed for this limit, the fit to the ferromagnetically saturated semiconductor, atomic limit and high-energy expansion via MPT should extend the range of its applicability. This is considered in Fig. 4.7. On the right a coupling constant $J = 1.0$ eV has been chosen. For strategies C and D one can see, that this value of J is sufficient to ensure a clear separation of the two subbands. This is also the kind of

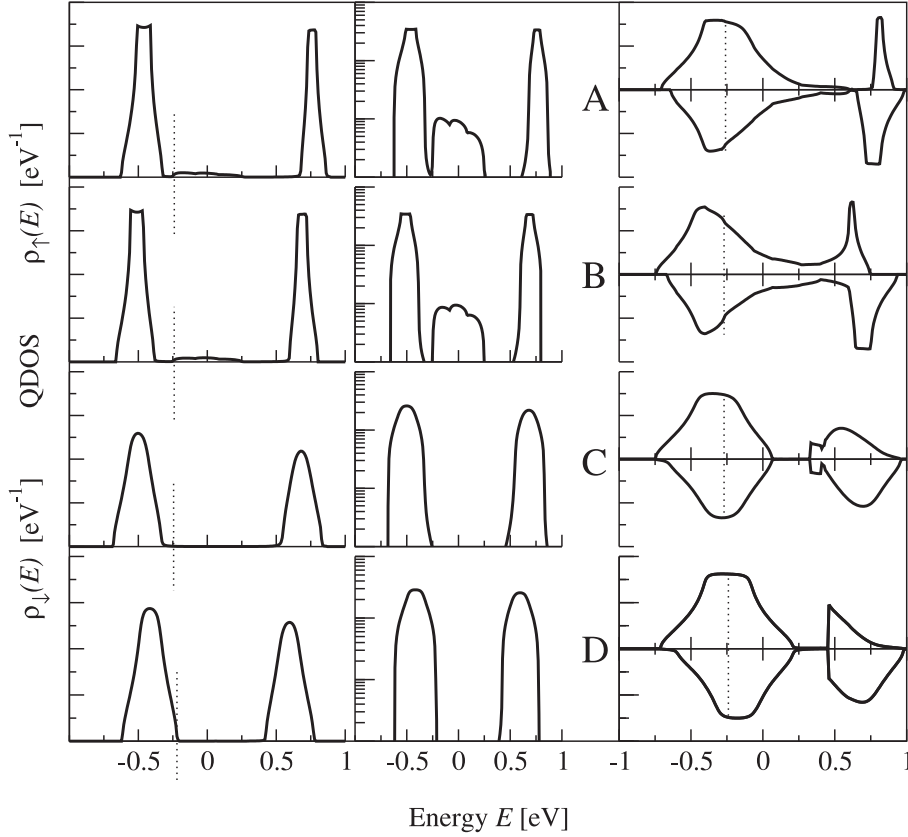


Figure 4.7: Comparison of the MPT strategies A-D mentioned in the text (rows) in the strong coupling regime. **First column:** The band width of the free DOS is reduced such ($W = 0.5$ eV), that the situation is close to the zero-bandwidth limit. The other parameters are: $J = 0.6$ eV, $T = T_C = 300$ K, $\langle S^z \rangle = 0$, $S = 3/2$ and $n = 0.4$. **Second column:** Same as first column, but with a logarithmic scale for the y -axis. **Third column:** The coupling strength is chosen large enough to separate the subbands in the QDOS ($J = 1.0$ eV). The other parameters are: $n = 0.4$, $T = 283.8$ K, $T_C = 300$ K, $\langle S^z \rangle = 0.2$, $S = 1/2$ and $W = 1.0$ eV for a simple-cubic lattice.

behaviour, which is expected from other theories such as MCDA. Nevertheless, strategies A and B tend to close this gap by a broad QDOS which is spread over the whole energy range.

On the other hand, the bandwidth W has decreased to approximate more closely the situation of the zero-bandwidth limit. Since for the paramagnetic region the \uparrow - and \downarrow -QDOS are identical, only the former is plotted on the left hand side of Fig. 4.7. Independent of the strategy we obtain two peaks in the QDOS which are close to the correct positions $-\tilde{J}\hbar S = -0.45$ eV and $\tilde{J}\hbar(S+1) = 0.75$ eV. The finite band occupation ($n = 0.4$) prohibits an exact solution within the MPT even for $W = 0$ eV. Anyhow, the appearance of a small but broad structure between these two bands is hard to explain physically. It is only observed in the MPT strategies based on SOPT-HF (it is more clearly seen in the logarithmic plot of the second column). In contrast it vanishes (slowly) during the iteration process, if a self-consistent SOPT is used as input for the MPT.

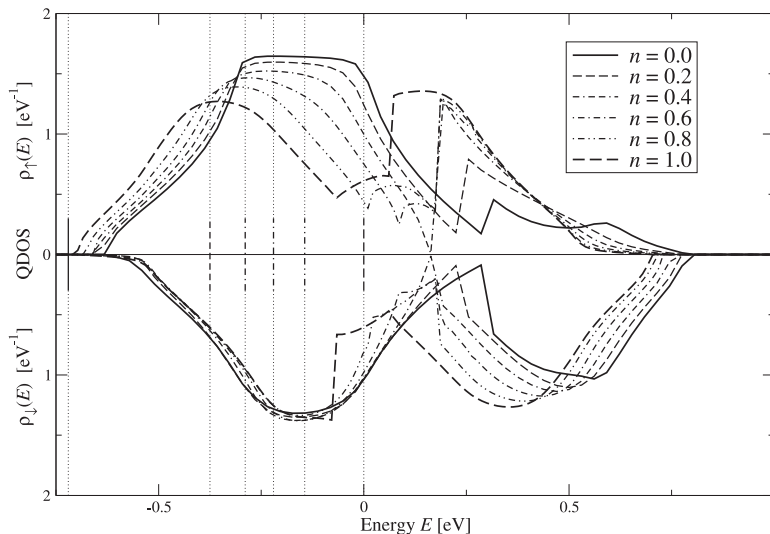


Figure 4.8: Variation of the QDOS with band occupation n for a self-consistent MPT. The vertical lines indicate the positions of the chemical potential determined self-consistently. The other parameters are: $J = 0.6$ eV, $S = 1/2$, $\langle S^z \rangle = 0.3$, $T = 259.1$ K, $T_C = 300$ K and $W = 1.0$ eV for a simple-cubic lattice.

Based on these considerations we draw the following conclusion: The most promising weak-coupling approach to the Kondo-lattice model is the MPT C, which is based on a *self-consistent* SOPT. This is in contrast to the single-impurity Anderson model, where a SOPT-HF has been chosen [63, 129, 95]. Instead we conclude that the SOPT result (4.84) dressed with full propagators $G_{\mathbf{k}\sigma}(E)$ should be used in the MPT ansatz (4.96). Only then should the parameters a_σ and b_σ be determined such that the high-energy expansion is fulfilled to power E^{-2} . This implies that b_σ depends on the full self-energy. For the correlation functions entering b_σ it is necessary that they are all treated on the same footing. This only permits a mean-field decoupling of higher correlation functions such as p_σ . The band occupation $\langle \hat{n}_\sigma \rangle$ is adapted to the full self-energy.

Discussion of the MPT results

We discuss the results again in terms of the quasiparticle densities of states (QDOS). According to our ansatz the QDOS is correct for $n = 0$, $\langle S^z \rangle = \hbar S$, however its variation as these parameters are changed is of particular interest.

Fig. 4.8 shows the variation of the QDOS when changing the band occupation n . The clear dependence on the filling of the conduction band suggests strong correlation effects, induced by the coupling J . For $n = 0$ the structure of the QDOS is closely related to the ferromagnetically saturated semiconductor. In particular the \uparrow -spectrum has the shape of the free DOS and the scattering part of the \downarrow -spectrum can be seen clearly. Only the polaron subband shows a deformation, due to finite-lifetime effects. Excited spin- \uparrow electrons can enter the energy region of the polaron, flip their spin and absorb a magnon since we are not close to saturation.

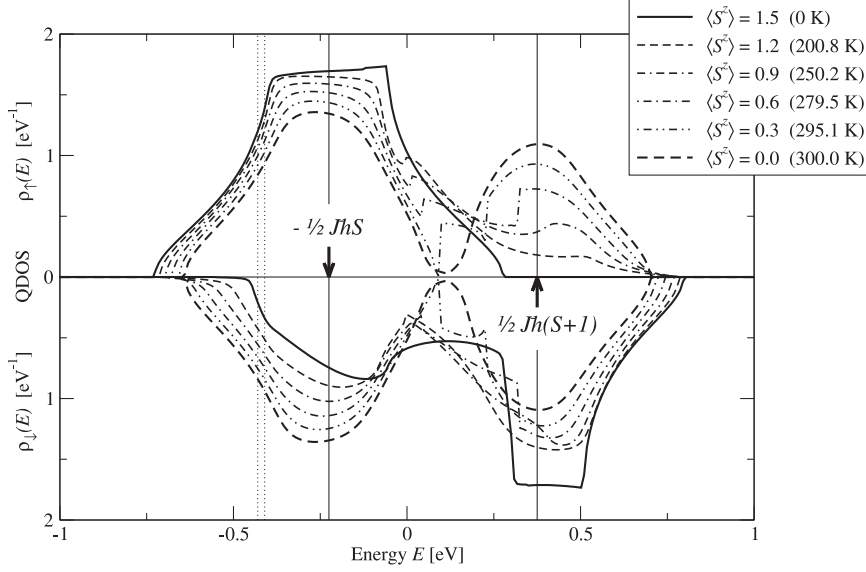


Figure 4.9: Variation of the QDOS with temperature for a self-consistent MPT. The dotted vertical lines indicate the range for the chemical potential determined self-consistently. The solid vertical lines give the position of the bands in the zero-bandwidth limit. The other parameters are: $J = 0.3$ eV, $S = 3/2$, $n = 0.2$, $T_C = 300$ K and $W = 1.0$ eV for a simple-cubic lattice.

If the chemical potential (and accordingly the band occupation) is increased, the spectral weight is redistributed between both subbands. For the chosen set of parameters the changes with n are most noticeable in the \uparrow -QDOS, where the upper subband steadily increases in importance at the expense of the lower subband. A sharp jump in the QDOS close to the pseudo-gap remains a striking feature for all values of n . It is also interesting to note, that the lower band edge is shifted by some 0.1 eV in the \uparrow -QDOS, whereas it remains at almost the same position for the \downarrow -QDOS. This behaviour is very different compared to the MPT relative to HF [52]. It is an indication that in the self-consistent MPT it are mainly the majority-spin electrons that experience strong correlations.

As the band occupation approaches half filling ($n = 1$), the point-symmetric form of the QDOS nicely illustrates the particle-hole symmetry of the system. The character of the upper \downarrow -subband becomes identical to the lower \uparrow -subband, since the latter is the polaron band for $n = 2$. For the same reason we omit the presentation of plots for $n > 1$, they can be obtained from the band occupations $2 - n$.

The dependence of the QDOS on the magnetization is given in Fig. 4.9. Here, the spin quantum number is taken as $S = 3/2$. For the implementation the Callen formulae (4.93) have been used in addition to the Brillouin function (4.90). The value for the coupling strength J , on the other hand, is chosen such that the scattering and the polaron subband are almost separated. The clear minimum becomes more dominant for higher temperatures. There are only small changes of the position of the bands as a function of the magnetization. They are fixed at the positions given by the energies E_1 and E_2 of the zero-bandwidth-limit (2.8).

Nevertheless, the edge of the lower \uparrow -subband shifts to lower energies if the temperature

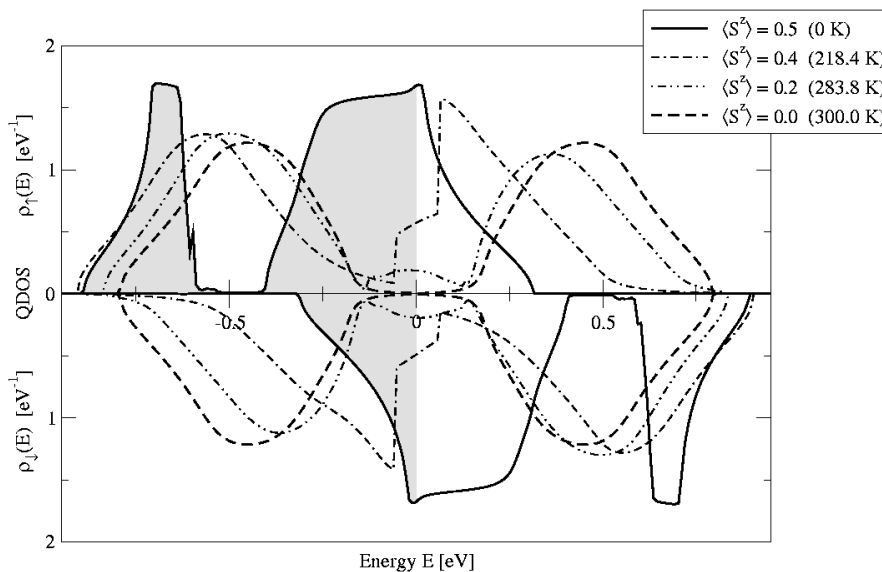


Figure 4.10: Variation of the QDOS with temperature for a MPT at half-filling. Due to the band occupation $n = 1$ the chemical potential is temperature independent ($\mu = 0$ eV). The hatched area displays the occupied part at $T = 0$ K. As in Fig. 4.4 the parameters are: $J = 1.0$ eV, $n = 1.0$, $\mu = 0.0$ eV, $S = 0.5$, $T_C = 300$ eV and $W = 1.0$ eV for a simple-cubic lattice.

is lowered from $T = T_C$ ($\langle S^z \rangle = 0$) to smaller values $T \rightarrow 0$ K (maximum $\langle S^z \rangle$). For semiconductors such an effect is known as the red shift of the optical absorption edge. In metals, since the lower \downarrow -subband is shifted in the opposite direction, it leads to a polarization of the conduction electrons of over 60%. For increasing band-occupation the existence of energy regions well below the Fermi edge occupied entirely by majority-spin electrons remains a remarkable result. For the parameters chosen in Fig. 4.9 the chemical potential is always adjusted such that the conduction electrons are not 100% polarized. This confirms depolarization effects which we observed in the SOPT-HF (see discussion in appendix E). However, we have also noticed the opposite trend within the MPT. For large coupling constants the depolarization is suppressed. Then, a completely polarized conduction band is again possible, similar to the situation in the conventional SOPT.

The situation at the lower edge of the upper subband appears to be not very systematic. When lowering temperature a sharp jump emerges for $\langle S^z \rangle \approx 0.9$ in the \uparrow -spectrum, which disappears again close to saturation. A detailed analysis of this effect is difficult, since the numerical effort to obtain convergence is substantially increased in this energy region.²⁸

The distribution of the spectral weight in Fig. 4.9 follows the transition from the ferromagnetically saturated configuration (solid lines), which even for $n = 0.2$ clearly displays the features of the exact magnetic polaron solution, to the paramagnetic regime (dashed lines), for which the QDOS has to be symmetric with respect to the x -axis. Again the more profound changes are observed for the majority-spin electrons. The increasing

²⁸This is a drawback of choosing a parameter b_σ , which explicitly depends on the self-energy.

spectral weight of the upper \uparrow -subband can be explained with higher magnon-numbers in this regime.

In Fig. 4.10 the temperature dependence is again plotted for a larger coupling constant ($J = 1.0$ eV) and a half-filled conduction band ($n = 1.0$). The parameters are chosen such that a comparison is possible with the SOPT-result in Fig. 4.4. One notices, that the QDOS has a completely different shape in the whole temperature range. In the MPT one can clearly see, that the transition from the ferromagnetic to the paramagnetic regime is connected with a metal-insulator transition.

Another feature, not known from decoupling approaches such as the moment-conserving approximation of Nolting et al. [114], is the formation of the lower subband in the \uparrow -QDOS as the magnetization $\langle S^z \rangle$ approaches saturation.²⁹ It corresponds to the polaron peak of the KLM with a completely filled conduction band ($n=2$) and therefore fulfils the particle-hole symmetry. A more detailed study of the formation of this peak can be found in Fig. 4.11a. Here, the magnetization is kept at its saturation value and the band-occupation is changed from the exact semiconductor limit ($n=0$) to half-filling ($n=1$). For the empty band, the magnetic polaron is located at the energy $E_2 = \tilde{J}\hbar(S+1)$, known from the atomic limit (2.8). Symmetrically, the peak considered in the \uparrow -spectrum is located at the energy $E_3 = -\tilde{J}\hbar(S+1)$ and is connected with double occupancy. A consideration of its spectral weight confirms this interpretation. According to the atomic limit result, $\alpha_{3\uparrow} = \frac{2S}{2S+1}\langle \hat{n}_\downarrow \rangle$. For $n=0$ the peak is not visible in Fig. 4.11a, but with increasing n and $\langle \hat{n}_\downarrow \rangle$ it becomes more and more apparent. In this context it is worth repeating our exact result for the ferromagnetically saturated KLM (p. 14) that each minority electron is sitting on a doubly occupied site. As mentioned above, $\langle \hat{n}_\downarrow \rangle$ can vanish for finite n , if a sufficiently large coupling is chosen.³⁰ Such a situation is plotted in Fig. 4.11b. Here, we can nicely convince ourselves that for $\langle \hat{n}_\downarrow \rangle = 0$ no second subband exists in the \uparrow -QDOS.

Some other methods, such as an interpolating self-energy approach [117], sometimes obtain three separated bands for a certain spin direction. The explanation is also based on atomic-limit calculations, where for finite band-occupations always three out of four subbands have a non-vanishing spectral weight. It needs further modifications of our method to retain these features. At the present stage the atomic limit of the MPT is only correct for $n=0$ and $n=2$. By construction, the existence of more than three bands is ruled out in our approach. This yields the behaviour illustrated in Fig. 4.12. For band occupations $0 < n < 2$ the two peaks move continuously from one exact position to the other (vertical lines in Fig. 4.12). Accordingly their positions at half filling ($n=1$) have to be $E_\pm = \pm\tilde{J}(2S+1)/2$, as seen in the figure. Also the redistribution of the spectral weight takes place in a similar way.

4.5 Possibility of ferromagnetic order

The calculations in this chapter are devoted to the subsystem of itinerant carriers. However, the question of a possible ferromagnetic order is not solely determined by this system.

²⁹A similar feature has been observed in calculations of Meyer et al. [96] using DMFT.

³⁰ Since the coupling of the KLM actually goes with JS , it is also sufficient to increase the value of S .

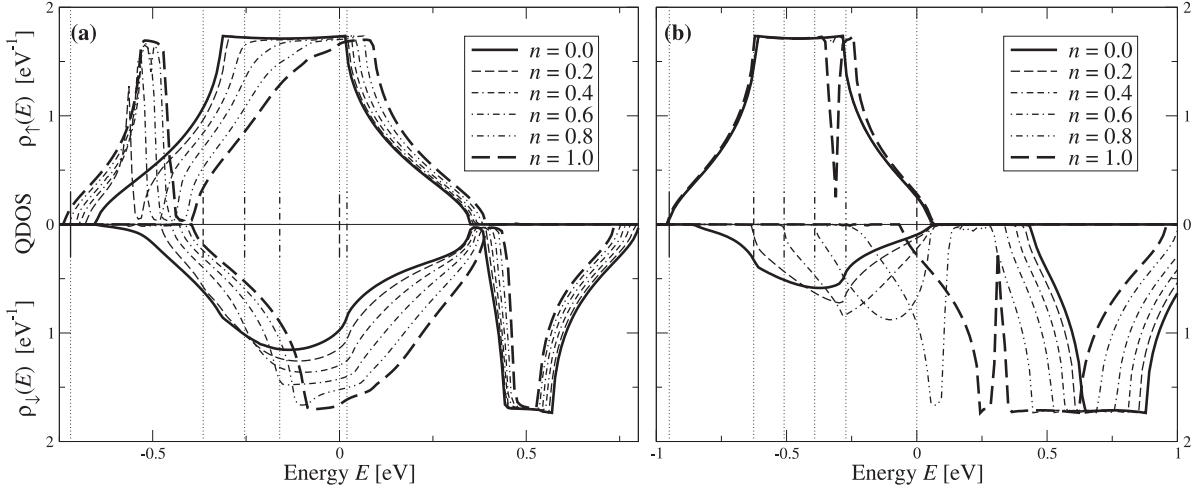


Figure 4.11: Behaviour of the QDOS for the ferromagnetically saturated KLM. The changing parameter is the band occupation n , adjusted by the chemical potential (vertical lines). For $n = 0$ the theory is exact. The spin quantum numbers $S = 1/2$ (a) and $S = 3/2$ (b) have been chosen. For **both** figures: $\langle S^z \rangle = \hbar S$, $J = 0.6$ eV, $T = 0$ K, $W = 1.0$ eV for a simple-cubic lattice.

It is decisively influenced by the local moments. In previous considerations we have used the Brillouin function (4.91) in order to model the temperature dependence of the magnetization. However, although the itinerant carriers will act according to the nature of the specified magnetic order, it is unknown, whether or not the assumed values of the magnetization are consistent with the KLM. We will use this section for an investigation of this point using some basic assumptions.

Considerations on the ground state energy

At first, we would like to clarify if the assumption of a saturated local moment system yields energetically stable results for SOPT and the MPT. For this purpose the ground state energy belonging to these self-energies is calculated. The free energy at $T = 0$ K is identical to the inner energy and is given by the expectation value of the Hamiltonian. For convenience we write the KLM in a mixture of Bloch and Wannier representations and obtain

$$U = \langle H \rangle = \sum_{\mathbf{k}} \sum_{\sigma} \varepsilon_{\mathbf{k}} \langle \hat{n}_{\mathbf{k}\sigma} \rangle - \tilde{J} \sum_i \sum_{\sigma} \underbrace{(z_{\sigma} \langle S_i^z \hat{n}_{i\sigma} \rangle + \langle S_i^{\sigma} c_{i-\sigma}^{\dagger} c_{i\sigma} \rangle)}_{-p_{-\sigma}}. \quad (4.104)$$

Therefore, the kinetic energy per lattice-site is determined by the averaged Bloch occupation number, which is easily accessible using the spectral theorem:

$$u_{\text{kin}} = \frac{1}{N} \langle H_s \rangle = \frac{1}{N} \sum_{\mathbf{k}, \sigma} \varepsilon_{\mathbf{k}} \left(-\frac{1}{\pi \hbar} \right) \int_{-\infty}^{\infty} dE \frac{\Im G_{\mathbf{k}, \sigma}(E)}{e^{\beta(E-\mu)} + 1}. \quad (4.105)$$

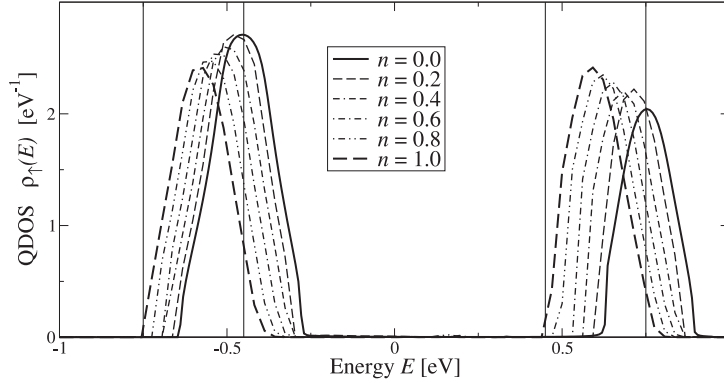


Figure 4.12: Behaviour of the QDOS close to the atomic limit. For this purpose a small bandwidth ($W = 0.5$ eV) and paramagnetic configuration ($\langle S^z \rangle = 0$) is chosen. The vertical lines indicate the exact excitation energies for this limit. The other parameters are: $J = 0.6$ eV, $S = 3/2$, $T = 300$ K and a simple-cubic lattice.

The potential energy, on the other hand, contains a sum of correlation functions, which has previously been abbreviated as p_σ . Using the modified spectral theorem (4.102), it can again be obtained from the one-electron Green's function:

$$u_{\text{pot}} = \frac{1}{N} \langle H_{sf} \rangle = \frac{1}{N} \sum_{\mathbf{k}, \sigma} \left(-\frac{1}{\pi \hbar} \right) \int_{-\infty}^{\infty} dE \frac{\Im m G_{\mathbf{k}, \sigma}(E)}{e^{\beta(E-\mu)} + 1} [E - \varepsilon_{\mathbf{k}}]. \quad (4.106)$$

Summing (4.105) and (4.106) the kinetic energy contribution of conduction electrons cancels. Making use of some relations in many-body theory and the fact that at $T = 0$ K the Fermi distribution reduces to a step function, one finds the following compact expression for the total inner energy per lattice site [140]:

$$u_{\text{tot}} = \frac{1}{N} \langle H \rangle = \sum_{\sigma} \int_{-\infty}^{\mu} dE E \rho_{\sigma}(E). \quad (4.107)$$

It is a remarkable result that u_{tot} is uniquely determined by the quasi-particle density of states.

In order to make a statement on the possibility of ferromagnetism, one has to compare the ground state energy (4.107) for an assumed ferromagnetic saturation ($\langle S^z \rangle = \hbar S$) to the energy of other assumptions for the local-moment subsystem. Here, we use as a reference system the paramagnetic configuration ($\langle S^z \rangle = 0$). Of course, this is not sufficient for an exhaustive study of the phase diagram, since antiferromagnetism [46] or phase separation [178] might occur. However, one can at least make a definite statement for which parameters a ferromagnetic order is instable.

The inner energy belonging to a ferromagnetic and a paramagnetic spin configuration is shown in Fig. 4.13 for a certain set of parameters. On the left hand side we have plotted u_{kin} and u_{pot} separately. The order of magnitude as well as the qualitative

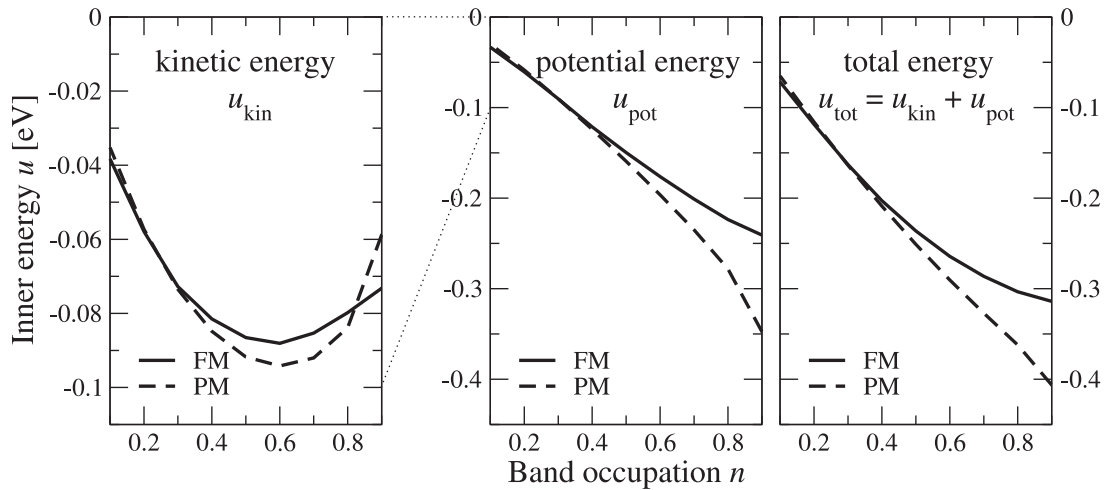


Figure 4.13: Dependence of the ground state energy on the band occupation. First, the contribution of the kinetic and potential energy to the inner energy is plotted separately. Note that the energy scales differ. On the right hand side, the sum of both contributions is presented. In all cases the ferromagnetic (solid lines) and the paramagnetic (dashed lines) configuration are compared for the MPT self-energy. The parameters are: $T = 0$ K, $J = 0.4$ eV, $S = 3/2$ and $W = 1.0$ eV for a simple-cubic lattice.

dependence on the band occupation is similar to the results of the moment-conserving decoupling approach (MCDA) investigated by Santos [140]. Both energy contributions show a small dependence on the configuration of the subsystem of localized spins for small band occupations and stronger deviations towards half-filling. Although it is hardly visible in Fig. 4.13, the energy belonging to the ferromagnetic configuration is lower than that of the paramagnetic configuration for $n < 0.2$. The band occupation for which the energy lines intersect is not identical for the kinetic ($n_{\text{kin}}^{(i)} \approx 0.25$) and the potential ($n_{\text{pot}}^{(i)} \approx 0.30$) energy. However, for a decision, which spin configuration is energetically preferred, one has to compare the total energies u_{tot} . This is done on the right hand side of Fig. 4.13. It turns out, that ferromagnetism is possible for $n < n_{\text{tot}}^{(i)} \approx 0.28$. According to Santos [140], $n_{\text{kin}}^{(i)} < n_{\text{tot}}^{(i)}$ is a typical feature of the weak-coupling regime, whereas in the double-exchange regime the phase transition is predominantly driven by the kinetic energy ($n_{\text{kin}}^{(i)} = n_{\text{tot}}^{(i)}$).

The message of Fig. 4.13 is not changed, if different parameters are chosen. We always obtain lower energies of the ferromagnetic configuration for band occupations n below some critical $n_{\text{tot}}^{(i)}$. According to these results, a spontaneous ferromagnetic order is allowed within the MPT approximation. The fact that ferromagnetism is not possible close to half-filling ($n = 1$) is in agreement with the findings of other approximations for the KLM [178, 19, 46].

The static magnetic susceptibility

In order to check the consistency of our assumptions for the local-moment subsystem, we can also make use of universal properties of phase transitions.³¹ In statistical mechanics (see textbooks such as [106, 176]) they are classified into first order and continuous phase transitions. The transition from ferromagnetic to paramagnetic order, relevant in our investigations, belongs to the latter class, since the magnetization is a continuous function of temperature. However, the second derivative of the potential, the static susceptibility $\chi(T)$, diverges at T_C . This fact will be exploited in the following.

Since we have a theory for the one-electron Green's function, the Pauli susceptibility of the itinerant electrons can be calculated. For this purpose the Hamiltonian (2.4) has to be extended by a Zeemann interaction with an external magnetic field B , defining the z -direction:

$$H = H_{\text{KLM}} - \sum_i \mu_B B (g_{\text{it}} s_i^z + g_{\text{loc}} S_i^z). \quad (4.108)$$

Here, μ_B is the Bohr magneton; $g_{\text{it}} = 2$ and g_{loc} are the Landé factors of the itinerant (spin s_i^z) and the local (spin S_i^z) electrons, respectively. The additional terms are relevant for all steps of the POM. For brevity we will only show how it enters the results of SOPT. The effect of B on the itinerant electrons can be taken into consideration by modifying the energy dispersion to $\varepsilon_{\mathbf{k}\sigma} = \varepsilon_{\mathbf{k}} - z_{\sigma} \mu_B B$. In this way, it enters the frequency and the memory matrix. The effect of B on the local moments can be understood as part of the mean-field Liouvillian, leading to a modification of the second line in (4.79). In analogy to (4.85), we obtain for the self-energy

$$\begin{aligned} \Sigma_{\sigma}(E, B) = & -\tilde{J} z_{\sigma} \langle S^z \rangle + \tilde{J}^2 \frac{1}{N} \sum_{\mathbf{k}} \frac{\langle (S^z)^2 \rangle - \langle S^z \rangle^2}{E - \varepsilon_{\mathbf{k}} + z_{\sigma} \mu_B B + \tilde{J} z_{\sigma} \langle S^z \rangle + i0^+} \\ & + \tilde{J}^2 \frac{1}{N} \sum_{\mathbf{k}} \frac{\langle S^{-\sigma} S^{\sigma} \rangle + 2\hbar z_{\sigma} \langle S^z \rangle \langle \hat{n}_{\mathbf{k}, -\sigma} \rangle}{E - \varepsilon_{\mathbf{k}} + z_{-\sigma} \mu_B B (1 + g_{\text{loc}}) + \tilde{J} z_{-\sigma} \langle S^z \rangle + i0^+}. \end{aligned} \quad (4.109)$$

Based on this result, the polarization of the conduction band is given by:

$$\langle s^z \rangle = -\frac{\hbar}{2\pi} \sum_{\sigma} z_{\sigma} \int_{-\infty}^{\infty} dE f_{-}(E) \Im \frac{1}{N} \sum_{\mathbf{k}} \frac{1}{E - \varepsilon_{\mathbf{k}} + z_{\sigma} \mu_B B - \Sigma_{\sigma}(E, B) + i0^+}. \quad (4.110)$$

This is the necessary prerequisite for a determination of the static susceptibility of the itinerant electron subsystem:

$$\chi_{\text{it}}(T) = \left. \frac{\partial \langle s^z \rangle}{\partial B} \right|_{T > T_C}^{B \rightarrow 0}. \quad (4.111)$$

In order to observe a divergence of the susceptibility, the external magnetic field has to be set to zero. Furthermore, we approach the phase transition from the paramagnetic

³¹ We have extensively studied this strategy in context of diluted magnetic semiconductors [118, 119]. There, the interpolating self-energy approach (p. 14) and a CPA (coherent potential approximation) have been used. The remarkable results make an application to the SOPT result promising. However, since the ansatz does not perfectly fit into the scope of the thesis, we will keep this discussion short.

side, what implies the vanishing of the magnetization $\langle S^z \rangle$. However, since (for $S = 1/2$) the principle structure of Eq. (4.110) is of the form $\langle s^z \rangle = g(\langle S^z \rangle, B)$, the local-moment subsystem still enters the expression for

$$\chi_{\text{it}}(T) = \left. \frac{\partial}{\partial B} g(\langle S^z \rangle, B) \right|_{T > T_C}^{B \rightarrow 0} + \left. \frac{\partial}{\partial \langle S^z \rangle} g(\langle S^z \rangle, B) \right|_{T > T_C}^{B \rightarrow 0} \cdot \underbrace{\left. \frac{\partial \langle S^z \rangle}{\partial B} \right|_{T > T_C}^{B \rightarrow 0}}_{\chi_{\text{loc}}(T)} \quad (4.112)$$

via the last term, being identical to the susceptibility of the local-moment subsystem.

The essential argument of our approach is the fact that the two response functions $\chi_{\text{it}}^{(i)}$, $\chi_{\text{loc}}^{(i)}$ are not independent of each other. Not only do they become critical at the same temperature, since the corresponding correlation functions $\langle s^z \rangle$ and $\langle S^z \rangle$ are mutually conditional. The susceptibilities also diverge with the same critical exponent γ as a function of the reduced temperature $(T - T_C)/T_C$. This is due to the fact that both subsystems belong to the same universality class. Or in other words: It is due to the fact, that at $T = T_C$ all physical quantities of the system scale with the same correlation length (scaling hypothesis), which in turn is related to the susceptibilities (fluctuation-dissipation theorem). Hence, there is no doubt that the response functions are proportional in a (very small) vicinity of the critical point :

$$\chi_{\text{loc}}(T) = \eta \cdot \chi_{\text{it}}(T) \quad \iff \quad \left. \frac{\partial \langle S^z \rangle}{\partial B} \right|_{T > T_C}^{B \rightarrow 0} = \eta \cdot \left. \frac{\partial \langle s^z \rangle}{\partial B} \right|_{T > T_C}^{B \rightarrow 0}. \quad (4.113)$$

By exploiting this proportionality the magnetization can be eliminated from Eq. (4.111). After some straightforward transformations one obtains for $S = 1/2$:

$$\chi_{\text{it}}(T) = \frac{\frac{\partial}{\partial B} g(\langle S^z \rangle, B)}{1 - \eta \cdot \frac{\partial}{\partial \langle S^z \rangle} g(\langle S^z \rangle, B)} = \mu_B \frac{\frac{1}{\pi} \int dE f_-(E) \Im m(G_2(E)A(E))}{1 - \tilde{J} \eta \frac{1}{\pi} \int dE f_-(E) \Im m(G_2(E)B(E))}, \quad (4.114)$$

$$G_2(E) = \frac{1}{N} \sum_{\mathbf{k}} \frac{1}{[E - \varepsilon_{\mathbf{k}} - \Sigma_{\sigma}(E, 0) + i0^+]^2},$$

$$A(E) = 1 - \frac{1}{2} \tilde{J} (1 + g_{\text{loc}}) \frac{1}{N} \sum_{\mathbf{k}} \frac{1}{[E - \varepsilon_{\mathbf{k}} + i0^+]^2},$$

$$B(E) = 1 + \frac{3\tilde{J}^2}{4N} \sum_{\mathbf{k}} \frac{1}{[E - \varepsilon_{\mathbf{k}} + i0^+]^2} + \frac{\tilde{J}}{N} \sum_{\mathbf{k}} \frac{1}{E - \varepsilon_{\mathbf{k}} + i0^+} - \frac{2\tilde{J}}{N} \sum_{\mathbf{k}} \frac{\langle \hat{n}_{\mathbf{k}} \rangle}{E - \varepsilon_{\mathbf{k}} + i0^+}.$$

From the singularities of the paramagnetic susceptibility, that is from the zeros of the denominator in (4.114), we find the Curie temperature T_C as a function of the model parameters. The derivation of T_C is independent of the non-specified value of g_{loc} , since it only enters the numerator of (4.114). However, the result does depend on the choice of η .

Apart from the fact that it is a constant with respect to temperature, the theory of phase transitions does not provide any information on the nature of the proportionality

constant η . Certainly, the proportionality (4.113) can be traced back to a proportionality of the expectation values $\langle S^z \rangle$ and $\langle s^z \rangle$. Additionally, we neglect the dependence of η on the energy scales W , $J\hbar$ and $k_B T_C$. Then the following equivalence of the normalized magnetization of the local-moment subsystem and the polarization of the itinerant subsystem,

$$\frac{\langle S^z \rangle}{S} \Leftrightarrow \frac{\langle \hat{n}_\uparrow - \hat{n}_\downarrow \rangle}{n}, \quad (4.115)$$

is plausible. It corresponds to $\eta = 2S/n$.

Of course, the ansatz (4.115) has to be improved in order to obtain reliable phase diagrams. In essence, we perform a combination of two theories. The first theory is the SOPT, which provides the relation $\langle s^z \rangle = g(\langle S^z \rangle, B)$ given by Eq. (4.110). The second theory is the ansatz for η , which enters the exact relation $\langle S^z \rangle = \eta \langle s^z \rangle$. It would yield a circular argument if SOPT were also used for the second relation. Instead, η could be based on, e.g., results of mean-field approaches (see Eq. (5.9)), semiclassical theories [157] or DMFT [34]. However, we want to check, whether or not the approximations within SOPT are consistent with the assumption of a ferromagnetic order. Therefore, an intermixing with other theories should be avoided, and the ansatz for η should be as simple as possible.

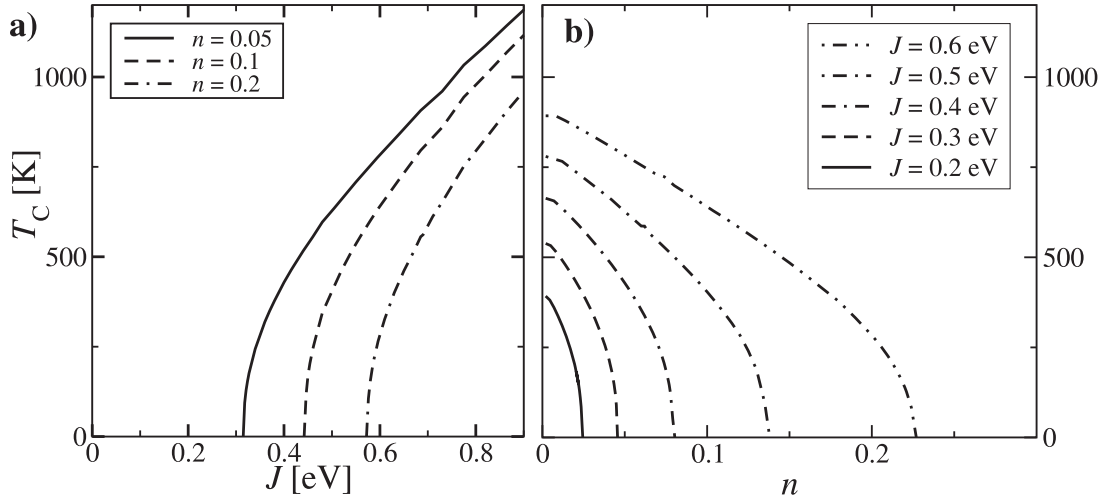


Figure 4.14: Curie temperatures obtained by exploiting the static magnetic susceptibility using a self-energy as obtained by SOPT. **a)** For several band occupations n the dependence on coupling strength J is plotted. **b)** For several coupling strengths J the dependence on the band occupation n is plotted. Other parameters: $S = 1/2$, $W = 1.0$ eV for a simple-cubic lattice.

The evaluation of Eq. (4.114) with $\eta = 2S/n$ yields reasonable results for the paramagnetic susceptibility. For sufficiently high temperatures and almost all parameter constellations, a Curie-Weiß behaviour can be recognized. The inverse susceptibility has clear intersections with the zero axis that can be associated with the respective Curie temperatures. The results, plotted in Fig. 4.14, demonstrate that ferromagnetism does exist for a large range of parameters. The principle dependence of T_C on the coupling strength J

and the band occupation n is similar to the results of the modified RKKY theory (Fig. 2.1 on p. 18). In particular, the limitation of ferromagnetism to small band occupations is confirmed by our theory.

However, three remarkable features of Fig. 4.14 are worth mentioning. Firstly, even for low band occupations a critical $J = J_c(n)$ is apparently needed to switch on ferromagnetism. Hence, we do not observe a J^2 -dependence of the Curie temperature as predicted by conventional RKKY. Secondly, for the J values presented in Fig. 4.14a a saturation cannot be observed. In this context, one should have in mind that SOPT is not reliable for large values of J . Thirdly, one concludes from Fig. 4.14b that for a fixed value of the coupling strength a reduction of the number of conduction electrons favours the possibility of ferromagnetism. Arbitrarily small band occupations are sufficient to create a ferromagnetic order. This is surprising, since a collective order is solely mediated by the interband exchange. Of course, the Curie temperature is zero at $n = 0$. It was, however, numerically not possible to decide whether or not there is a steep but continuous increase to finite values.

We also want to point out clear similarities to results obtained with a different self-energy [118]. If the derivation of (4.114) is based on the interpolating self-energy approach of Nolting et al. (see p. 14f) the qualitative dependence of the Curie temperature on J and n is identical to that in Fig. 4.14. This allows two kinds of interpretations. Either both self-energies have the same quality with respect to the properties responsible for ferromagnetism, or the assumption (4.115) has a dominant influence on the Curie temperatures. It needs further investigations to clarify this point.

Conclusion

The considerations of this section confirm the possibility of ferromagnetism within the KLM. The approximations of the POM, yielding to the self-energy of SOPT and of the MPT, are consistent with a finite value for the magnetization $\langle S^z \rangle$. The investigation of the ground-state properties and the paramagnetic susceptibility predict ferromagnetism for small band occupations. However, both results are insufficient for a quantitative analysis of the phase diagram at finite temperatures.

Chapter 5

The subsystem of local moments

In chapter 4 the projection-operator method has been successfully applied to the subsystem of conduction-electrons. We have obtained the MPT self-energy. Subsequently, in Sec. 4.5 we concluded from the response of itinerant electrons that ferromagnetism is likely to occur in certain regions of the phase diagram. Nevertheless, a ferromagnetic order is to a large extent an effect of localized moments. Therefore, we will now focus our considerations on this subsystem. We intend to apply the same methods as in Chap. 4 in order to obtain a self-consistent theory.

5.1 Application of the projection-operator method

The essential quantity related to the local-moment subsystem is the magnetization $\langle S^z \rangle$. For $S = 1/2$ all local correlation functions, which are solely related to localized moments, can be expressed by $\langle S^z \rangle$. For larger spin quantum numbers S the Callen formulae (4.93), though derived for the Heisenberg model, provide a valuable tool for approximations. However, to focus on the effects of the POM we restrict ourselves to $S = 1/2$.

The restriction to $S = 1/2$ allows the determination of the magnetization $\langle S^z \rangle$ from the one-magnon Green's function. For this purpose one combines the spin-operator relation

$$z_\sigma \hbar \langle S^z \rangle = \hbar^2 S(S+1) - \langle S^{-\sigma} S^\sigma \rangle - \langle (S^z)^2 \rangle \stackrel{S=1/2}{=} \hbar^2 S - \langle S^{-\sigma} S^\sigma \rangle \quad (5.1)$$

with the spectral theorem for commutator Green's functions

$$\langle S^{-\sigma} S^\sigma \rangle = \frac{1}{N^2} \sum_{\mathbf{k}} \left(-\frac{1}{\hbar\pi} \right) \int_{-\infty}^{\infty} dE f_+(E) \Im \langle \langle S_{-\mathbf{k}}^\sigma; S_{\mathbf{k}}^{-\sigma} \rangle \rangle_E. \quad (5.2)$$

Here, $f_+(E)$ is the Bose-Einstein distribution function, which carries the temperature dependence via $\beta = [k_B T]^{-1}$. For the determination of $\langle \langle S_{-\mathbf{k}}^\sigma; S_{\mathbf{k}}^{-\sigma} \rangle \rangle_E$ one can now apply the POM.

First order: The frequency matrix

A natural starting point is a Liouville subspace formed by single magnon excitations $|S_{\mathbf{k}}^{-\sigma}\rangle$ and a Liouville scalar product (3.3) using commutators. In this basis the susceptibility

matrix

$$\chi_{\mathbf{k}\sigma} = (S_{\mathbf{k}}^{-\sigma} | S_{\mathbf{k}}^{-\sigma}) = 2\hbar z_{\sigma} \langle S_{\mathbf{0}}^z \rangle = 2N\hbar z_{\sigma} \langle S^z \rangle \quad (5.3)$$

is proportional to the magnetization $\langle S^z \rangle$. As discussed below this unavoidable property results in problems for the evaluation of a phase transition to a paramagnetic regime.

For an evaluation of the other matrices within the POM the action of the Liouvillian on the chosen basis state needs to be known. Using the Hamiltonian (4.74) one obtains an expression

$$\mathcal{L} | S_{\mathbf{k}}^{-\sigma} \rangle = -\frac{J}{2N} \sum_{\mathbf{q}, \mathbf{p}} \left\{ \left| S_{\mathbf{q}+\mathbf{k}}^{-\sigma} c_{\mathbf{p}, -\sigma}^{\dagger} c_{\mathbf{p}-\mathbf{q}, -\sigma} \right\rangle - \left| S_{\mathbf{q}+\mathbf{k}}^{-\sigma} c_{\mathbf{p}, \sigma}^{\dagger} c_{\mathbf{p}-\mathbf{q}, \sigma} \right\rangle + 2z_{\sigma} \left| S_{\mathbf{q}+\mathbf{k}}^z c_{\mathbf{p}, -\sigma}^{\dagger} c_{\mathbf{p}-\mathbf{q}, \sigma} \right\rangle \right\} \quad (5.4)$$

that contains three additional states. Their component parallel to the level of description yields the correlation functions of the frequency matrix:

$$\Omega_{\mathbf{k}\sigma} = (S_{\mathbf{k}}^{-\sigma} | \mathcal{L} | S_{\mathbf{k}}^{-\sigma}) = -\frac{J\hbar}{N} \sum_{\mathbf{q}, \mathbf{p}} \left\langle z_{\sigma} S_{\mathbf{q}}^z \left(c_{\mathbf{p}, -\sigma}^{\dagger} c_{\mathbf{p}-\mathbf{q}, -\sigma} - c_{\mathbf{p}, \sigma}^{\dagger} c_{\mathbf{p}-\mathbf{q}, \sigma} \right) - S_{\mathbf{q}}^{\sigma} c_{\mathbf{p}, -\sigma}^{\dagger} c_{\mathbf{p}-\mathbf{q}, \sigma} \right\rangle \quad (5.5)$$

$$= -J\hbar N \left\{ z_{\sigma} \langle S^z \hat{n}_{-\sigma} \rangle - z_{\sigma} \langle S^z \hat{n}_{\sigma} \rangle - \langle S^{\sigma} c_{-\sigma}^{\dagger} c_{\sigma} \rangle \right\}. \quad (5.6)$$

The last step implies the assumption of a translational invariant spin system. Hence, we do not consider antiferromagnetism and non-collinear spin configurations.

Combining Eqs. (5.3) and (5.6) one gets a result for the magnon Green's function

$$\langle\langle S_{-\mathbf{k}}^{\sigma}; S_{\mathbf{k}}^{-\sigma} \rangle\rangle_E = \frac{2N\hbar z_{\sigma} \langle S^z \rangle}{\omega + \frac{1}{2}J \left\{ \langle S^z \hat{n}_{-\sigma} \rangle - \langle S^z \hat{n}_{\sigma} \rangle - z_{\sigma} \langle S^{\sigma} c_{-\sigma}^{\dagger} c_{\sigma} \rangle \right\} / \langle S^z \rangle}, \quad (5.7)$$

which is supposed to be correct to first order in the coupling constant J . This becomes more apparent, if one neglects the implicit J -dependence of the correlation functions in (5.7) by performing a mean-field decoupling. Then the magnon Green's function becomes

$$\langle\langle S_{-\mathbf{k}}^{\sigma}; S_{\mathbf{k}}^{-\sigma} \rangle\rangle_E = 2N\hbar^2 \frac{z_{\sigma} \langle S^z \rangle}{E - J z_{\sigma} \langle s^z \rangle + i0^+} \quad \text{with} \quad \langle s^z \rangle = \frac{\hbar}{2} [\langle \hat{n}_{\uparrow} \rangle - \langle \hat{n}_{\downarrow} \rangle]. \quad (5.8)$$

One notes, that the excitation energies in the denominator are real and do not depend on the wave vector \mathbf{k} . This allows a straightforward application of the spectral theorem (5.2). A subsequent exploitation of the spin-operator relation (5.1) yields an implicit equation for the magnetization $\langle S^z \rangle$ that can be transformed¹ to

$$\langle S^z \rangle = \hbar S \cdot \tanh [\beta J \langle s^z \rangle / 2]. \quad (5.9)$$

This is the well-known mean-field result for the magnetization of a system with Ising type interactions. It is also obtained for the KLM if spin-flip processes are neglected [57].

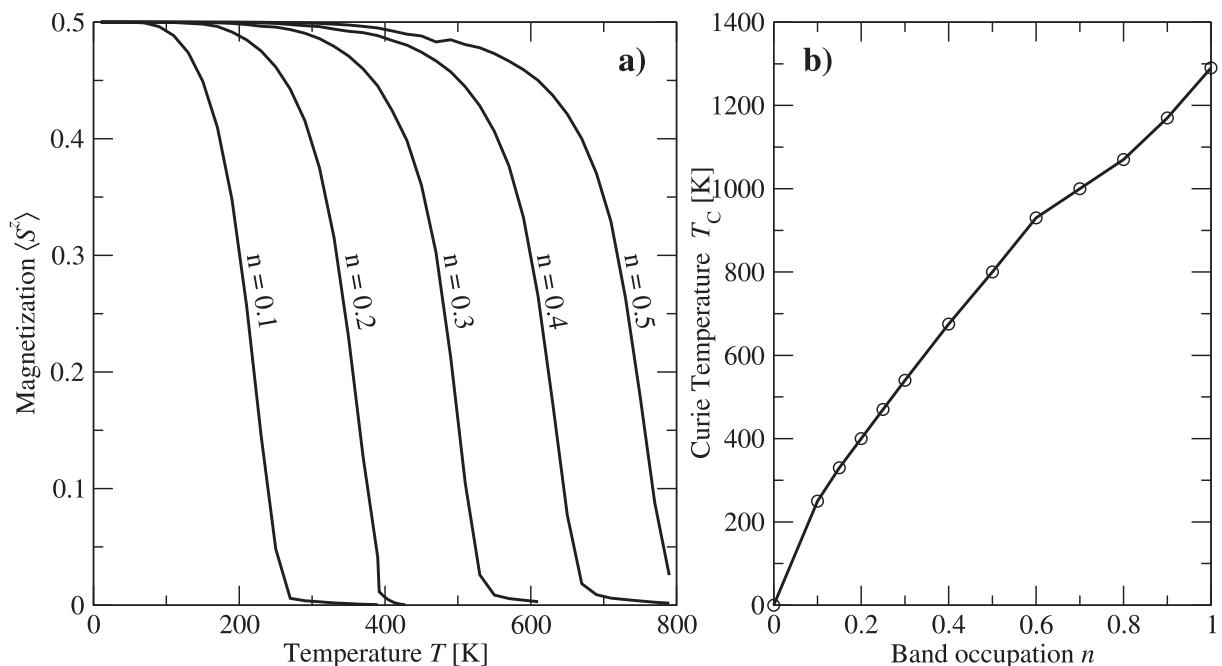


Figure 5.1: **a)** Temperature dependence of the spontaneous magnetization $\langle S^z \rangle$ for various band occupations. **b)** Phase transition temperature as a function of the band occupation. The conduction electron subsystem is solved with the MPT. For the subsystem of localized moments the mean-field result is used. The parameters are: $J = 1.0$ eV, $S = 1/2$ and $W = 1.0$ eV for a simple-cubic lattice.

Obviously, the localized magnetic moments experience the polarization of the conduction band like an effective field.

As a first step towards the desired self-consistent theory one can combine the result (5.9) with the modified perturbation theory derived in Chap. 4. The magnetization curves obtained are displayed in Fig. 5.1a. They show the expected functional dependence on temperature, which is similar to that of a Brillouin function. From the intersection with the zero temperature axis one can read off the transition temperatures T_C . Their dependence on the band occupation is plotted in Fig. 5.1b. According to this theory ferromagnetism is possible for all band-occupations for the whole parameter regime. A maximum value for the Curie temperature is observed for a half-filled conduction band ($n = 1.0$).

$$\hbar^2 S = z_\sigma \hbar \langle S^z \rangle \left\{ 1 + \frac{2}{\exp[\dots] - 1} \right\} = z_\sigma \hbar \langle S^z \rangle \left\{ \frac{\exp[\dots] + 1}{\exp[\dots] - 1} \right\} = z_\sigma \hbar \langle S^z \rangle \coth[\dots/2]$$

Second order: The memory matrix

The memory matrix incorporates parts of the orthogonal complement of the Liouville subspace spanned by $|S_{\mathbf{k}}^{-\sigma}\rangle$. The corresponding projection operator is given by

$$\mathcal{Q} = 1 - |S_{\mathbf{k}}^{-\sigma}\rangle \frac{1}{\langle S_{\mathbf{k}}^{-\sigma} | S_{\mathbf{k}}^{-\sigma} \rangle} \langle S_{\mathbf{k}}^{-\sigma}| \quad (5.10)$$

Out of the various possibilities to evaluate the memory matrix, we choose here the same procedure, (4.77)-(4.80), as in the case of conduction electrons:

$$M_{\mathbf{k}\sigma}(\omega) \approx (\mathcal{Q}\mathcal{L}S_{\mathbf{k}}^{-\sigma} | \frac{1}{\omega - \mathcal{Q}\mathcal{L}_{\text{MF}}\mathcal{Q}} | \mathcal{Q}\mathcal{L}S_{\mathbf{k}}^{-\sigma}) = \sum_{m=0}^{\infty} \frac{1}{\omega^{m+1}} (\mathcal{Q}\mathcal{L}S_{\mathbf{k}}^{-\sigma} | (\mathcal{Q}\mathcal{L}_{\text{MF}}\mathcal{Q})^m | \mathcal{Q}\mathcal{L}S_{\mathbf{k}}^{-\sigma}) \quad (5.11)$$

We exploit the fact that already the Liouville state $|\mathcal{Q}\mathcal{L}S_{\mathbf{k}}^{-\sigma}\rangle$ is proportional to the coupling J . Hence, an approximation of \mathcal{L} by its free part \mathcal{L}_s in the denominator of the memory matrix would correspond to neglecting contributions of order J^3 or higher orders in J . This simplification allows the determination of the complete geometric series given in (5.11). A typical summand is given by

$$\begin{aligned} & (\mathcal{Q}\mathcal{L}_s\mathcal{Q})^m \mathcal{Q}\mathcal{L} | S_{\mathbf{k}}^{-\sigma} \rangle \quad (5.12) \\ &= \frac{J}{2\hbar^m N} \sum_{\mathbf{q}\mathbf{p}} (\varepsilon_{\mathbf{p}} - \varepsilon_{\mathbf{p}-\mathbf{q}})^m \left\{ \frac{\langle z_{\sigma} S_{\mathbf{q}}^z (c_{\mathbf{p},-\sigma}^{\dagger} c_{\mathbf{p}-\mathbf{q},-\sigma} - c_{\mathbf{p},\sigma}^{\dagger} c_{\mathbf{p}-\mathbf{q},\sigma}) - S_{\mathbf{q}}^{\sigma} c_{\mathbf{p},-\sigma}^{\dagger} c_{\mathbf{p}-\mathbf{q},\sigma} \rangle}{z_{\sigma} \langle S_{\mathbf{0}}^z \rangle} | S_{\mathbf{k}}^{-\sigma} \rangle \right. \\ & \quad \left. - | S_{\mathbf{q}+\mathbf{k}}^{-\sigma} c_{\mathbf{p},-\sigma}^{\dagger} c_{\mathbf{p}-\mathbf{q},-\sigma} \rangle + | S_{\mathbf{q}+\mathbf{k}}^{-\sigma} c_{\mathbf{p},\sigma}^{\dagger} c_{\mathbf{p}-\mathbf{q},\sigma} \rangle - 2z_{\sigma} | S_{\mathbf{q}+\mathbf{k}}^z c_{\mathbf{p},-\sigma}^{\dagger} c_{\mathbf{p}-\mathbf{q},\sigma} \rangle \right\}. \end{aligned}$$

The conventional perturbation theory is generalized to a perturbation around the Hartree-Fock solution if instead of \mathcal{L}_s the Liouvillian \mathcal{L}_{MF} is chosen. The latter corresponds to the mean-field Hamiltonian (2.6) of the conduction electrons. In this case, some of the terms carry the mean-field self-energy in the m -dependent factor.² This implies different denominators in the resulting expression for the memory matrix³

$$\begin{aligned} M_{\mathbf{k}\sigma}(\omega) &= \frac{J^2}{4N^2} \sum_{\mathbf{q}\mathbf{p}\hat{\sigma}} \frac{\langle S_{\mathbf{q}+\mathbf{k}}^{-\sigma} S_{-\mathbf{q}-\mathbf{k}}^{\sigma} (\hat{n}_{\mathbf{p}-\mathbf{q},\hat{\sigma}} - \hat{n}_{\mathbf{p},\hat{\sigma}}) \rangle + 2z_{\sigma} \hbar \langle S_{\mathbf{0}}^z \hat{n}_{\mathbf{p}-\mathbf{q},\hat{\sigma}} (1 - \hat{n}_{\mathbf{p},\hat{\sigma}}) \rangle}{\omega - \frac{1}{\hbar} (\varepsilon_{\mathbf{p}} - \varepsilon_{\mathbf{p}-\mathbf{q}})} \\ &+ \frac{J^2}{N^2} \sum_{\mathbf{q}\mathbf{p}} \frac{\langle S_{\mathbf{q}+\mathbf{k}}^z S_{-\mathbf{q}-\mathbf{k}}^z (\hat{n}_{\mathbf{p}-\mathbf{q},\sigma} - \hat{n}_{\mathbf{p},-\sigma}) \rangle}{\omega - \frac{1}{\hbar} (\varepsilon_{\mathbf{p}} - \varepsilon_{\mathbf{p}-\mathbf{q}} + Jz_{\sigma} \langle S^z \rangle)} - \frac{2z_{\sigma} \hbar}{\omega \langle S_{\mathbf{0}}^z \rangle} \left[\frac{J}{2N} \sum_{\mathbf{p}\hat{\sigma}} z_{\hat{\sigma}} \langle S_{\mathbf{0}}^z \hat{n}_{\mathbf{p},\hat{\sigma}} \rangle \right]^2 \\ &+ z_{\sigma} \frac{J^2 \hbar}{2N^2} \sum_{\mathbf{q}\mathbf{p}} \frac{\langle S_{\mathbf{0}}^z (\hat{n}_{\mathbf{q},-\sigma} \hat{n}_{\mathbf{p},-\sigma} - 2\hat{n}_{\mathbf{q},-\sigma} \hat{n}_{\mathbf{p},\sigma} + \hat{n}_{\mathbf{q},\sigma} \hat{n}_{\mathbf{p},\sigma}) \rangle}{\omega} \quad (5.13) \end{aligned}$$

²This affects the second sum in (5.13). If the term $Jz_{\sigma} \langle S^z \rangle$ in the denominator is removed, one returns to conventional SOPT.

³ Details of the derivation of the memory matrix can be found in appendix F.

The result (5.13) is the exact J^2 contribution to the memory matrix of the magnon Green's function. Nevertheless, the displayed correlation functions are already a result of an approximation. Those expectation values, which vanish if the trace is performed with Bloch states (the eigenstates of a system with an energy independent self-energy) are not considered. This is in accordance with the notion of second-order perturbation theory for the memory matrix.

Despite this simplification Eq. (5.13) incorporates several correlation functions, which cannot be expressed by single-particle Green's functions. A mean-field decoupling further reduces the complexity of the formulae. The question is, to what extent one makes use of this possibility. If one decouples Ising terms such as

$$\langle S_0^z \hat{n}_{\mathbf{q},\sigma} \hat{n}_{\mathbf{p},\sigma} \rangle \approx \langle S_0^z \rangle \cdot \langle \hat{n}_{\mathbf{q},\sigma} \rangle \cdot \langle \hat{n}_{\mathbf{p},\sigma} \rangle, \quad (5.14)$$

the last two sums in (5.13) cancel each other. If, in addition, the spin and Fermi operators are decoupled in the remaining correlation functions, the following expression for the memory matrix is obtained:

$$\begin{aligned} M_{\mathbf{k}\sigma}(\omega) &= \frac{J^2}{4N^2} \sum_{\mathbf{q}\mathbf{p}\hat{\sigma}} \langle S_{\mathbf{q}+\mathbf{k}}^{-\sigma} S_{-\mathbf{q}-\mathbf{k}}^{\sigma} \rangle \frac{\langle \hat{n}_{\mathbf{p}-\mathbf{q},\hat{\sigma}} \rangle - \langle \hat{n}_{\mathbf{p},\hat{\sigma}} \rangle}{\omega - \frac{1}{\hbar}(\varepsilon_{\mathbf{p}} - \varepsilon_{\mathbf{p}-\mathbf{q}})} \\ &+ \frac{J^2}{4N^2} 2z_{\sigma} \hbar \langle S_0^z \rangle \sum_{\mathbf{q}\mathbf{p}\hat{\sigma}} \frac{\langle \hat{n}_{\mathbf{p}-\mathbf{q},\hat{\sigma}} \rangle (1 - \langle \hat{n}_{\mathbf{p},\hat{\sigma}} \rangle)}{\omega - \frac{1}{\hbar}(\varepsilon_{\mathbf{p}} - \varepsilon_{\mathbf{p}-\mathbf{q}})} \\ &+ \frac{J^2}{N^2} \sum_{\mathbf{q}\mathbf{p}} \langle S_{\mathbf{q}+\mathbf{k}}^z S_{-\mathbf{q}-\mathbf{k}}^z \rangle \frac{\langle \hat{n}_{\mathbf{p}-\mathbf{q},\sigma} \rangle - \langle \hat{n}_{\mathbf{p},-\sigma} \rangle}{\omega - \frac{1}{\hbar}(\varepsilon_{\mathbf{p}} - \varepsilon_{\mathbf{p}-\mathbf{q}} + Jz_{\sigma} \langle S^z \rangle)} \end{aligned} \quad (5.15)$$

The result consists of three sums, which have, on the first glance, a similar structure. All terms are of second order in the coupling constant J . Hence, they describe different aspects of an indirect exchange interaction between localized moments. The transfer of magnetic information is mediated by itinerant conduction electrons. That explains the appearance of the Bloch dispersion and the band occupation, as well as the factor J^2 .

In the first and the third line, respectively, the \mathbf{p} -summation is of the form of a Lindhard function [82]. In the first sum it has the classical form as it appears e.g. in the susceptibility of a non-interacting electron gas [40]. The last \mathbf{p} -summation is characterized by an additional self-energy in the denominator and a different spin-direction of the band-occupation operators in the numerator. More important for the physical behaviour is the difference in the \mathbf{p} -independent prefactor of both sums. The correlation function $\langle S_{\mathbf{k}}^{-\sigma} S_{-\mathbf{k}}^{\sigma} \rangle$ can be determined via the spectral theorem (5.2) from the one-magnon Green's function. However, $\langle S_{\mathbf{k}}^z S_{-\mathbf{k}}^z \rangle$ cannot be obtained in the same way.

In accordance with the weak-coupling approach mentioned above (5.14) one could think of a mean-field decoupling of the spin-spin correlation functions by inserting a complete set of eigenstates of the electronic mean-field Hamiltonian (2.6). As a consequence, the prefactor of the first sum gives zero and this contribution to the memory matrix vanishes. For the prefactor of the third sum, such a decoupling yields

$$\langle S_{\mathbf{q}+\mathbf{k}}^z S_{-\mathbf{q}-\mathbf{k}}^z \rangle \approx \langle S_0^z \rangle \cdot \langle S_0^z \rangle \delta_{\mathbf{q}+\mathbf{k},\mathbf{0}}. \quad (5.16)$$

This moves the \mathbf{k} -dependence to the Lindhard fraction. The resulting expression is identical to that of a random phase approximation, discussed in Sec. 5.3.

Besides the analytical possibilities one also has to consider the numerical effort for an evaluation of these formulae. The memory matrix $M_{\mathbf{k}\sigma}(\omega)$ enters the Green's function

$$\langle\langle S_{-\mathbf{k}}^\sigma; S_{\mathbf{k}}^{-\sigma} \rangle\rangle_E = \frac{4\hbar^2 z_\sigma \langle S_{\mathbf{0}}^z \rangle}{2\hbar\omega - \Omega_{\mathbf{k}\sigma}/z_\sigma \langle S_{\mathbf{0}}^z \rangle - M_{\mathbf{k}\sigma}(\omega)/z_\sigma \langle S_{\mathbf{0}}^z \rangle} \quad (5.17)$$

This Green's function forms the input of the spectral theorem (5.2), which is used to derive a self-consistency equation for the magnetization. For a single iteration cycle of $\langle S^z \rangle$ the most expensive numerical effort is therefore given by

- a procedure to determine the electronic self-energy for given $\langle S^z \rangle$ (which in case of the MPT is already connected with a time consuming iteration),
- an energy integration to determine the expectation values $\langle \hat{n}_{\mathbf{p}\sigma} \rangle$ and $\langle S_{\mathbf{q}+\mathbf{k}}^\alpha S_{-\mathbf{q}-\mathbf{k}}^\beta \rangle$ (which, for a few cases, can be replaced by a Sommerfeld expansion),
- two summations (\mathbf{p}, \mathbf{q}) over the Brillouin zone (only one of them can be reduced to the irreducible part of the Brillouin zone),
- an energy integration to obtain $\langle S_{\mathbf{k}}^{-\sigma} S_{-\mathbf{k}}^\sigma \rangle$ (which reduces to a root finding problem, if the magnon self-energy is real) and
- another summation (\mathbf{k}) over the Brillouin zone to obtain the local result $\langle S^{-\sigma} S^\sigma \rangle$

In particular the threefold summation over the Brillouin zone (this corresponds to 9 convoluted integrations!) is beyond the capability of conventional PCs. The situation becomes even worse due to the fact that some of these integrations include singularities. Already for these reasons simplifications of the correlation functions in (5.15) are unavoidable. The effects will be discussed in Sec. 5.3.

Before considering alternative approaches in Sec. 5.2, an additional remark on the representation (5.17) of the Green's function is worth making. We have pointed out before, that (5.13) is the exact second order result for the memory matrix. In this sense, the suggested procedure is equivalent to the SOPT for conduction band electrons. However, this does not imply a similar statement for the magnon self-energy. Due to the fact that the memory matrix has to be divided by the susceptibility matrix, we cannot claim that it is exact to order J^2 . The susceptibility matrix in the denominator is proportional to the magnetization $\langle S^z \rangle$, which in turn carries an implicit J dependence. Hence, definite statements about the correctness in terms of powers of J are not possible for the magnon self-energy.

5.2 Alternative POM for the subsystem of local moments

Although it is compatible with an expansion of the self-energy in powers of J , a mean-field decoupling of all contributing correlation functions is a crude approximation.

- In the subsystem of itinerant conduction electrons mainly the Ising term $\langle S^z \hat{n}_\sigma \rangle$ and the spin-flip term $\langle S^\sigma c_{-\sigma}^\dagger c_\sigma \rangle$ are affected. Other theories, such as the MCDA [114], predict that even at the Curie temperature these two correlation functions do not vanish. On the other hand, their sum is apparently important, since it is a major contribution to the potential energy at zero temperature (see p. 73).
- In the local-moment subsystem the expectation values $\langle S_{\mathbf{k}}^{-\sigma} S_{-\mathbf{k}}^\sigma \rangle$ and $\langle S_{\mathbf{k}}^z S_{-\mathbf{k}}^z \rangle$ are included. At least, their local part is definitely larger than zero. The exact limiting value for $T \geq T_C$ is $2\hbar^2 S(S+1)/3$ for $\langle S^{-\sigma} S^\sigma \rangle$ and $\hbar^2 S(S+1)/3$ for $\langle (S^z)^2 \rangle$. Since this is a J -independent result, its neglect is hard to justify.

Hence, an alternative approach, that treats the correlation functions more accurately or one that reduces the number of involved correlation functions to a minimum, is desirable.

The usage of a two-dimensional basis $\{|A\rangle, |B\rangle\}$ for the original Liouville subspace is a possible modification. We have successfully applied this strategy to the limit of a ferromagnetically saturated semiconductor (p. 47) and to the zero-bandwidth limit (p. 49). If the calculations are restricted to the evaluation of the frequency matrix, it yields concise expressions for the Green's function, which allow a clear interpretation. Again, we consider $|A\rangle \equiv |S_{\mathbf{k}}^{-\sigma}\rangle$. Then the two-dimensional frequency matrix corrects the mean-field contribution (5.5) to the magnon self-energy in the following way:⁴

$$\Sigma_{\mathbf{k}\sigma}^{(\text{mag})}(\omega) = \hbar \left\{ \Omega_{\mathbf{k}\sigma} + \frac{(S_{\mathbf{k}}^{-\sigma} | \mathcal{L} | B) (B | \mathcal{L} | S_{\mathbf{k}}^{-\sigma}) (B | B)^{-1}}{\omega - (B | \mathcal{L} | B) (B | B)^{-1}} \right\} (S_{\mathbf{k}}^{-\sigma} | S_{\mathbf{k}}^{-\sigma})^{-1} \quad (5.18)$$

The quality of this correction depends on the choice of the second basis state $|B\rangle$, for which we have much more freedom than in the one-dimensional case. In the following we will discuss some possibilities, but will eventually return to the result (5.15).

A generic choice for a two-dimensional basis

Within the philosophy of the POM the generic choice is $|B\rangle \equiv \mathcal{QL} |S_{\mathbf{k}}^{-\sigma}\rangle$, hence

$$\begin{aligned} |B\rangle &= \frac{J}{2\langle S^z \rangle} \left\{ \langle S^z (\hat{n}_{-\sigma} - \hat{n}_\sigma) \rangle - z_\sigma \langle S^\sigma c_{-\sigma}^\dagger c_\sigma \rangle \right\} |S_{\mathbf{k}}^{-\sigma}\rangle \\ &- \frac{J}{2N} \sum_{\mathbf{qp}} \left\{ |S_{\mathbf{q}+\mathbf{k}}^{-\sigma} (c_{\mathbf{p},-\sigma}^\dagger c_{\mathbf{p}-\mathbf{q},-\sigma} - c_{\mathbf{p},\sigma}^\dagger c_{\mathbf{p}-\mathbf{q},\sigma}) \rangle + 2z_\sigma |S_{\mathbf{q}+\mathbf{k}}^z c_{\mathbf{p},-\sigma}^\dagger c_{\mathbf{p}-\mathbf{q},\sigma} \rangle \right\}. \end{aligned} \quad (5.19)$$

This is because it allows a compact notation of the result (5.18) for the self-energy that would also be obtained in the next step of the continued fraction expansion with an

⁴Detailed explanations can be found in appendix G.

initially one-dimensional basis $|S_{\mathbf{k}}^{-\sigma}\rangle$. For the latter one had to consider $M_{\mathbf{k}\sigma}(\omega)$ as a resolvent, apply the POM and neglect the higher order memory matrix

$$M_{\mathbf{k}\sigma}(\omega) = (B| \frac{1}{\omega - \mathcal{Q}\mathcal{L}\mathcal{Q}} |B) \approx \frac{(B|B)}{\omega - (B| \mathcal{Q}\mathcal{L}\mathcal{Q} |B) (B|B)^{-1}} \quad (5.20)$$

to obtain (5.18). The concept can be generalized. A larger basis at the beginning corresponds a longer continued fraction. To completely neglect the memory matrix at a certain point in the series expansion is a remarkable alternative to our approximation (5.11) for the memory matrix, where we still considered the summation of an infinite series. It can be used to incorporate higher orders of the coupling constants J . However, one should note the similarities with the high energy expansion. The entity $(B| \mathcal{L} |B)$ is essentially the third moment of the spectral density belonging to the one-magnon Green's function. It needs considerable analytical effort to derive it. The result contains dozens of a priori unknown correlation functions and thus it renders qualitative discussions difficult. For these reasons this approach does not fit in the purpose of the present analysis, even though it is probably worthwhile to be considered in a different context.

A symmetric choice for a two-dimensional basis

We would like to reduce the complexity of the previous suggestion by limiting ourselves to essential aspects only. For spin exchange systems the primary contribution to the temperature dependence of magnetic properties is given by collective spin excitations [137]. In (5.19) the state $|B\rangle$ is a mixture of spin-wave and spin-density / magnetization operators. If we freeze the latter class of operators, we are essentially left with the operators $S_{\mathbf{k}}^{-\sigma}$ and $c_{\mathbf{p},-\sigma}^\dagger c_{\mathbf{p}-\mathbf{q},\sigma}$. With choosing $|A\rangle \equiv |S_{\mathbf{k}}^{-\sigma}\rangle$ we already consider a single-magnon excitation in the local moment subsystem. Using state $|B\rangle$ we will now describe the corresponding spin wave excitations in the conduction band. Symmetrically to $|A\rangle$ we define

$$|B\rangle \equiv |s_{\mathbf{k}}^{-\sigma}\rangle = \hbar \sum_i \left(c_{i-\sigma}^\dagger c_{i\sigma} \right) e^{-i\mathbf{k}\mathbf{R}_i} = \hbar \sum_{\mathbf{q}} \left(c_{\mathbf{q}-\mathbf{k},-\sigma}^\dagger c_{\mathbf{q},\sigma} \right). \quad (5.21)$$

As a combination of two Fermi operators, $|B\rangle$ is a bosonic state. Therefore, for the Liouville scalar product we choose the commutator and, after a straightforward calculation, obtain:

$$(A|A) = 2\hbar z_\sigma \langle S_0^z \rangle = 2N\hbar z_\sigma \langle S^z \rangle \quad (5.22)$$

$$(B|B) = N\hbar^2 \{ \langle \hat{n}_\sigma \rangle - \langle \hat{n}_{-\sigma} \rangle \} = 2N\hbar z_\sigma \langle s^z \rangle \quad (5.23)$$

$$(S_{\mathbf{k}}^{-\sigma} | \mathcal{L} | B) = (B | \mathcal{L} | S_{\mathbf{k}}^{-\sigma}) = - (S_{\mathbf{k}}^{-\sigma} | \mathcal{L} | S_{\mathbf{k}}^{-\sigma}) = -\Omega_{\mathbf{k}\sigma} \quad (5.24)$$

$$(B | \mathcal{L} | B) = \hbar \sum_{\mathbf{q}} (\varepsilon_{\mathbf{q}-\mathbf{k}} - \varepsilon_{\mathbf{q}}) (\langle \hat{n}_{\mathbf{q}\sigma} \rangle - \langle \hat{n}_{\mathbf{q}-\mathbf{k},-\sigma} \rangle) + \Omega_{\mathbf{k}\sigma} \quad (5.25)$$

Here, $\Omega_{\mathbf{k}\sigma}$ is the mean-field expression obtained in (5.6), which is actually \mathbf{k} -independent. It is noteworthy that in the spin channel the four results of the frequency matrix are (apart from a sign) all identical. This is due to the symmetry of the KLM Hamiltonian

with respect to the operators $S_{\mathbf{k}}^{-\sigma}$ and $s_{\mathbf{k}}^{-\sigma}$. As a consequence, the correction to the energy poles of the magnon Green's function are of the same order of magnitude as the mean-field result itself. This will be discussed below.

The \mathbf{k} -dependence of the frequency matrix is solely carried by its element given in (5.25). The sum

$$f_{\sigma}(\mathbf{k}) = \frac{\hbar}{N} \sum_{\mathbf{q}} (\varepsilon_{\mathbf{q}-\mathbf{k}} - \varepsilon_{\mathbf{q}}) (\langle \hat{n}_{\mathbf{q}\sigma} \rangle - \langle \hat{n}_{\mathbf{q}-\mathbf{k},-\sigma} \rangle) \quad (5.26)$$

essentially describes the response of a free electron system on spin excitations in the conduction band. The fact that it does not have the usual shape of a Lindhard function, a textbook-result e.g. for plasmon excitations in a free electron system [107, 32], is already a hint towards indicating the insufficient quality of the approximation. Nevertheless, it contains some physical properties that are worth discussing.

If the scalar products (5.23)-(5.25) are inserted into the expression for the magnon self-energy (5.18), one can evaluate the correction of the Green's function as compared to the mean field result. This correction has again the structure of a memory matrix. The calculations yield the expression

$$M_{\mathbf{k}\sigma}(\omega) = \frac{\Omega_{\mathbf{k}\sigma}^2/N}{\omega \cdot 2\hbar z_{\sigma} \langle s^z \rangle - f_{\sigma}(\mathbf{k}) - \Omega_{\mathbf{k}\sigma}/N}, \quad (5.27)$$

which has to be inserted into the Green's function (5.17). Hence, the contribution to the magnon self-energy is essentially proportional to J^2 . This is not surprising. The term is multiplied by a factor such as $\langle S^z s^z \rangle / \langle S^z \rangle \cdot \langle s^z \rangle$. Since this is an implicit function of J , too, a definite statement on the J -dependence of the magnon self-energy is not possible.

Besides the influence of J , the energy dependence of the memory matrix is most important. Due to the structure of $M_{\mathbf{k}\sigma}$ a two-pole structure of the Green's function is favourable:⁵

$$\langle\langle S_{-\mathbf{k}}^{\sigma}; S_{\mathbf{k}}^{-\sigma} \rangle\rangle_E = \frac{\langle S^z \rangle / \langle s^z \rangle}{\omega_{\text{II}}(\mathbf{k}) - \omega_{\text{I}}(\mathbf{k})} \cdot \left(\frac{N f_{\sigma}(\mathbf{k}) + \Omega_{\mathbf{k}\sigma} - \omega_{\text{I}}(\mathbf{k}) \cdot 2N\hbar z_{\sigma} \langle s^z \rangle}{\omega - \omega_{\text{I}}(\mathbf{k})} - \frac{N f_{\sigma}(\mathbf{k}) + \Omega_{\mathbf{k}\sigma} - \omega_{\text{II}}(\mathbf{k}) \cdot 2N\hbar z_{\sigma} \langle s^z \rangle}{\omega - \omega_{\text{II}}(\mathbf{k})} \right) \quad (5.28)$$

In this representation one clearly notes two branches in the magnon dispersion:

$$\begin{aligned} \omega_{\text{I}, \text{II}}(\mathbf{k}) &= \frac{1}{2} \left[\frac{\Omega_{\mathbf{k}\sigma}}{2N\hbar} \left(\frac{1}{z_{\sigma} \langle S^z \rangle} + \frac{1}{z_{\sigma} \langle s^z \rangle} \right) + \frac{f_{\sigma}(\mathbf{k})}{2\hbar z_{\sigma} \langle s^z \rangle} \right] \\ &\pm \frac{1}{2} \sqrt{\left[\frac{\Omega_{\mathbf{k}\sigma}}{2N\hbar} \left(\frac{1}{z_{\sigma} \langle S^z \rangle} + \frac{1}{z_{\sigma} \langle s^z \rangle} \right) + \frac{f_{\sigma}(\mathbf{k})}{2\hbar z_{\sigma} \langle s^z \rangle} \right]^2 - \frac{\Omega_{\mathbf{k}\sigma} \cdot f_{\sigma}(\mathbf{k})}{N\hbar^2 \langle S^z \rangle \langle s^z \rangle}} \end{aligned} \quad (5.29)$$

They can be distinguished by their \mathbf{k} -dependence. We are particularly interested in the behaviour at the Γ -point, where $f_{\sigma}(\mathbf{k}=\mathbf{0}) = 0$.

⁵Details of the derivation can be found in appendix G.

One can readily see that $\omega_I(\mathbf{k})$ represents an optical branch of the magnon dispersion, since

$$\omega_I(\mathbf{k}=\mathbf{0}) = \frac{\Omega_{\mathbf{k}\sigma}}{2N\hbar} \left(\frac{1}{z_\sigma \langle S^z \rangle} + \frac{1}{z_\sigma \langle s^z \rangle} \right). \quad (5.30)$$

Apparently, the first part of $\omega_I(\mathbf{k})$ corresponds to the mean-field result (5.7) of the magnon Green's function. The fact, that (5.30) includes another term proportional to $\langle s^z \rangle^{-1}$ is already a generalization of this previous result, which accommodates the symmetry of the two (itinerant and local) spin subsystems. Furthermore, the magnon-excitation energy of the mean-field calculation did not show any \mathbf{k} -dependence in contrast to the result for the optical branch presented here.

The energy $\omega_{II}(\mathbf{k})$ represents an acoustic branch of the magnon dispersion, since it vanishes at the Γ -point. For its physical properties the spin-wave stiffness constant is most important. It is determined by the functional dependence of the function $f_\sigma(\mathbf{k})$ - and therefore the free Bloch dispersion $\varepsilon_{\mathbf{k}}$ - on the wave-vector \mathbf{k} . If, for example, a tight-binding Bloch dispersion with next-neighbour hopping

$$\varepsilon_{\mathbf{k}} = -\frac{W}{6} \{ \cos k_x + \cos k_y + \cos k_z \}, \quad W = 1 \text{ eV} \quad (5.31)$$

is assumed, one can separate \mathbf{k} and \mathbf{q} in (5.26). Then, the \mathbf{k} -dependence of $f_\sigma(\mathbf{k})$ is given by

$$f_\sigma(\mathbf{k}) = \left(1 - \frac{12}{zW}(-\varepsilon_{\mathbf{k}}) \right) \left(\frac{1}{N} \sum_{\mathbf{q}} (-\varepsilon_{\mathbf{q}}) \langle \hat{n}_{\mathbf{q}\sigma} \rangle + \frac{1}{N} \sum_{\mathbf{q}} (-\varepsilon_{\mathbf{q}}) \langle \hat{n}_{\mathbf{q}-\sigma} \rangle \right) \geq 0, \quad (5.32)$$

where z is the coordination number.⁶ With assumption (5.31) a Taylor expansion of the energy dispersion of the acoustic branch then yields a spin wave stiffness constant

$$D \sim \frac{\langle s^z \rangle}{\langle S^z \rangle + \langle s^z \rangle} \cdot \frac{1}{N} \sum_{\mathbf{q}} (-\varepsilon_{\mathbf{q}}) (\langle \hat{n}_{\mathbf{q}\sigma} \rangle + \langle \hat{n}_{\mathbf{q}-\sigma} \rangle). \quad (5.33)$$

This number is always positive.

It is interesting to note, that an extension of the KLM by a superexchange interaction $\sum_{\mathbf{q}} J_{\mathbf{q}} \mathbf{S}_{\mathbf{q}} \cdot \mathbf{S}_{-\mathbf{q}}$ can change this property. Such an extension solely affects the element

$$(S_{\mathbf{k}}^{-\sigma} | \mathcal{L} | S_{\mathbf{k}}^{-\sigma}) = \Omega_{\mathbf{k}\sigma} + \frac{2\hbar^2}{N} \sum_{\mathbf{q}} (J_{\mathbf{q}+\mathbf{k}} - J_{\mathbf{q}}) \langle 2S_{\mathbf{q}}^z S_{-\mathbf{q}}^z + S_{\mathbf{q}}^+ S_{-\mathbf{q}}^- \rangle =: \Omega_{\mathbf{k}\sigma} + h_\sigma(\mathbf{k}). \quad (5.34)$$

of the frequency matrix. Compared to the previous result (5.6) the superexchange yields an extra term $h_\sigma(\mathbf{k})$. Its sign depends on the question, if an ferromagnetic or antiferromagnetic Heisenberg coupling $J_{\mathbf{q}}$ is assumed. Since the stiffness D is proportional to the sum $f_\sigma(\mathbf{k}) + h_\sigma(\mathbf{k})$ in the extended version, it might also become negative. Furthermore, Perkins and Plakida [127] showed for the extended KLM that self-energy corrections calculated in the self-consistent Born approximation result in a similar renormalization of the

⁶Note that the same kind of \mathbf{k} -dependence dominates the magnon-dispersion of a KLM with $J \rightarrow \infty$ [38, 124]. This might be a hint, that the results of the POM are not limited to weak coupling only.

stiffness of the acoustic spin wave branch. However, quantitative statements are missing, since no numerical evaluations have been provided in their paper.

The sign of the spin wave stiffness is important for the possibility of a phase transition from ferromagnetism to paramagnetism. The order parameter $\langle S^z \rangle$ is mainly determined by the spectral theorem (5.2). For the two-pole Green's function (5.28) with spectral weights $g_{\text{I}}(\mathbf{k})$ and $g_{\text{II}}(\mathbf{k})$ the energy integration can be performed analytically and leads to

$$\langle S^{-\sigma} S^{\sigma} \rangle = \frac{1}{N\hbar} \sum_{\mathbf{k}} \left\{ \frac{g_{\text{I}}(\mathbf{k})}{e^{\beta\hbar\omega_{\text{I}}(\mathbf{k})} - 1} + \frac{g_{\text{II}}(\mathbf{k})}{e^{\beta\hbar\omega_{\text{II}}(\mathbf{k})} - 1} \right\}. \quad (5.35)$$

Due to the appearance of the Bose distribution function, small excitation energies yield particularly large contributions. Therefore, the behaviour of the acoustic branch of the magnon dispersion close to the Γ -point determines the magnetism of the KLM. However, for a numeric evaluation of the magnon spectra the mean-field result $\Omega_{\mathbf{k}\sigma}$ is particularly important. A new suggestion for a determination of its correlation functions is presented in the next subsection.

A closed system of correlation functions

The mean-field result $\Omega_{\mathbf{k}\sigma}$, which enters the expression (5.28), is essentially a combination of the correlation functions $\langle S^z \hat{n}_{\sigma} \rangle$ and $\langle S^{\sigma} c_{-\sigma}^{\dagger} c_{\sigma} \rangle$, which are not derivable from the one-electron Green's function.⁷ To avoid a mean-field decoupling of the expectation values, one has to determine each of these entities independently. This is only possible if additional Green's functions are considered.

To be logically consistent, we apply the same idea of a two-dimensional basis to the fermionic subsystem. Again, we have a certain degree of freedom for the choice of the second Liouville state. Using our experience with the limit of a ferromagnetically saturated semiconductor, we choose, in agreement with (4.53), the basis elements

$$|A\rangle = |c_{\mathbf{k},\sigma}^{\dagger}\rangle \quad \text{and} \quad |B\rangle = \frac{1}{\hbar N} \sum_{\mathbf{q}} |S_{-\mathbf{q}}^{\sigma} c_{\mathbf{k}-\mathbf{q},-\sigma}^{\dagger}\rangle. \quad (5.36)$$

As will be shown now, this choice is sufficient to obtain a closed system of correlation functions. Furthermore, the orthogonality of $|A\rangle$ and $|B\rangle$ allows the application of the results in appendix G. Hence, the following expression for the electronic self-energy has to be evaluated:

$$\Sigma_{\mathbf{k}\sigma}^{(\text{el})}(\omega) = \varepsilon_{\mathbf{k}} - \frac{J}{2} z_{\sigma} \langle S^z \rangle + \hbar \frac{\left| (c_{\mathbf{k}\sigma}^{\dagger} | \mathcal{L} | B) \right|^2}{\omega (B | B) - (B | \mathcal{L} | B)}. \quad (5.37)$$

⁷The spectral theorem of the form (4.102) does not yield the correct combination of correlation functions.

It contains the three anticommutator scalar products

$$(B|B) = \frac{1}{\hbar^2} \langle S^{-\sigma} S^\sigma \rangle + \frac{2}{\hbar} z_\sigma \langle S^z \hat{n}_{-\sigma} \rangle, \quad (5.38)$$

$$(c_{\mathbf{k}\sigma}^\dagger | \mathcal{L} | B) = -\frac{J}{2\hbar^2} \langle S^{-\sigma} S^\sigma \rangle + \frac{J}{2\hbar} \langle S^\sigma c_{-\sigma}^\dagger c_\sigma \rangle - \frac{J}{\hbar} z_\sigma \langle S^z \hat{n}_{-\sigma} \rangle, \quad (5.39)$$

$$(B | \mathcal{L} | B) = \frac{1}{N^2} \sum_{\mathbf{q}} \varepsilon_{\mathbf{q}} \langle S_{\mathbf{k}-\mathbf{q}}^{-\sigma} S_{-(\mathbf{k}-\mathbf{q})}^\sigma \rangle + 2z_\sigma \frac{1}{N} \sum_{\mathbf{q}} \varepsilon_{\mathbf{q}} \left\{ \frac{1}{N} \sum_{\mathbf{p}} \langle S_{\mathbf{p}}^z c_{\mathbf{q},-\sigma}^\dagger c_{\mathbf{q}-\mathbf{p},-\sigma} \rangle \right\} \\ + \frac{J}{2} \left\{ z_\sigma \langle S^z S^{-\sigma} S^\sigma \rangle + \hbar \langle S^{-\sigma} S^\sigma \rangle - \hbar \langle S^{-\sigma} S^\sigma \hat{n}_{-\sigma} \rangle - \hbar \langle S^{-\sigma} S^\sigma \hat{n}_\sigma \rangle \right. \\ \left. + 2\hbar \langle (S^z)^2 \hat{n}_{-\sigma} \rangle - 2z_\sigma \hbar^2 \langle S^z \hat{n}_\sigma \hat{n}_{-\sigma} \rangle \right\}, \quad (5.40)$$

which can be obtained after a straightforward calculation.

Eqs. (5.38)-(5.40) contain a large variety of correlation functions. On the other hand, the extended basis of the Liouville subspace provides a large variety of Green's functions, too. The (generalized) spectral theorem

$$\langle (\mathcal{L}^s Y) X^+ \rangle = \left(-\frac{1}{\pi\hbar} \right) \int_{-\infty}^{\infty} \frac{dE \cdot E^s}{e^{\beta E} \pm 1} \Im G_{XY} =: \left(-\frac{1}{\pi\hbar} \right) \int_{-\infty}^{\infty} dE f_{\mp}^{(s)}(E) \Im G_{XY}. \quad (5.41)$$

can be applied to each of them⁸. Even though there is no limitation for the number s , Eq. (5.41) provides the most sensitive information for $s = 0$. An application to two of the bosonic Green's functions related to the local-moment subsystem yields equations for

$$\langle S_{\mathbf{k}}^{-\sigma} S_{-\mathbf{k}}^\sigma \rangle \xrightarrow{\Sigma_{\mathbf{k}}} \langle S^{-\sigma} S^\sigma \rangle \quad \text{and} \quad \sum_{\mathbf{q}} \langle S_{-\mathbf{k}}^\sigma c_{\mathbf{q}-\mathbf{k},-\sigma}^\dagger c_{\mathbf{q},\sigma} \rangle \xrightarrow{\Sigma_{\mathbf{k}}} \langle S^\sigma c_{-\sigma}^\dagger c_\sigma \rangle. \quad (5.42)$$

In addition, the application of the spectral theorem ($s = 0$) to two of the fermionic Green's functions based on the basis (5.36) yields equations for

$$\langle \hat{n}_{\mathbf{k},\sigma} \rangle \xrightarrow{\Sigma_{\mathbf{k}}} \langle \hat{n}_\sigma \rangle \quad \text{and} \quad \frac{1}{N^2} \sum_{\mathbf{q},\mathbf{p}} \langle S_{-\mathbf{q}}^\sigma S_{\mathbf{p}}^{-\sigma} c_{\mathbf{k}-\mathbf{q},-\sigma}^\dagger c_{\mathbf{k}-\mathbf{p},-\sigma} \rangle \xrightarrow{\Sigma_{\mathbf{k}}} \langle S^\sigma S^{-\sigma} \hat{n}_{-\sigma} \rangle. \quad (5.43)$$

However, these equations are not sufficient to determine all correlation functions in Eqs. (5.38)-(5.40). To fill the gap, the spectral theorem (5.41) for $s = 1$ is indeed very useful. It allows the determination of⁹

$$\frac{1}{N} \sum_{\mathbf{q}} \langle S_{\mathbf{q}}^z c_{\mathbf{k},-\sigma}^\dagger c_{\mathbf{k}-\mathbf{q},-\sigma} \rangle \xrightarrow{\Sigma_{\mathbf{k}}} \langle S^z \hat{n}_{-\sigma} \rangle \quad \text{and} \quad \langle S^z \hat{n}_{-\sigma} \hat{n}_\sigma \rangle. \quad (5.44)$$

Note, that the application of the spectral theorem with $s = 1$ to the itinerant Green's function $\langle\langle c_{\mathbf{k}\sigma}; c_{\mathbf{k}\sigma}^\dagger \rangle\rangle_E$ alone, only provides a sum of the Ising and the spin-flip correlation

⁸Due to the two-pole structure of the Green's functions with real energy poles E_I and E_{II} and spectral weights g_I and g_{II} the energy integration can be performed analytically: $\langle (\mathcal{L}^s Y) X^+ \rangle = \frac{1}{\hbar} \left\{ g_I f_{\mp}^{(s)}(E_I) + g_{II} f_{\mp}^{(s)}(E_{II}) \right\}$.

⁹For $\langle S^z \hat{n}_{-\sigma} \hat{n}_\sigma \rangle$ one actually has to use $\frac{1}{N^2} \sum_{\mathbf{k},\mathbf{q}} \left\{ \langle\langle S_{\mathbf{q}}^{-\sigma} c_{\mathbf{k}-\mathbf{q},-\sigma}; c_{\mathbf{k}\sigma}^\dagger \rangle\rangle_E - \langle\langle c_{\mathbf{k}-\sigma}^\dagger; S_{-\mathbf{q}}^{-\sigma} c_{\mathbf{k}-\mathbf{q},\sigma} \rangle\rangle_E \right\}$.

function. The challenge is the independent determination of both contributions. This is, for example, possible if the information (5.42) of the local-moment subsystem is also used. Hence, one sees the necessity to treat the itinerant as well as the local-moment subsystem beyond the mean-field approximation. More importantly we stress again, that we now treat both subsystems with the same method and accuracy. This meets our criterion of a balanced approximation.

An attentive reader will recognize that with $\langle S^z \rangle$ and $\langle S^z S^{-\sigma} S^\sigma \rangle$ two correlation functions are still not determined. If we assume $S = 1/2$, both can be derived from $\langle S^{-\sigma} S^\sigma \rangle$. It will become clear below, that the system of correlation functions can also be solved for an arbitrary spin quantum number. However, for the following evaluation of the obtained formulae we will use this assumption.

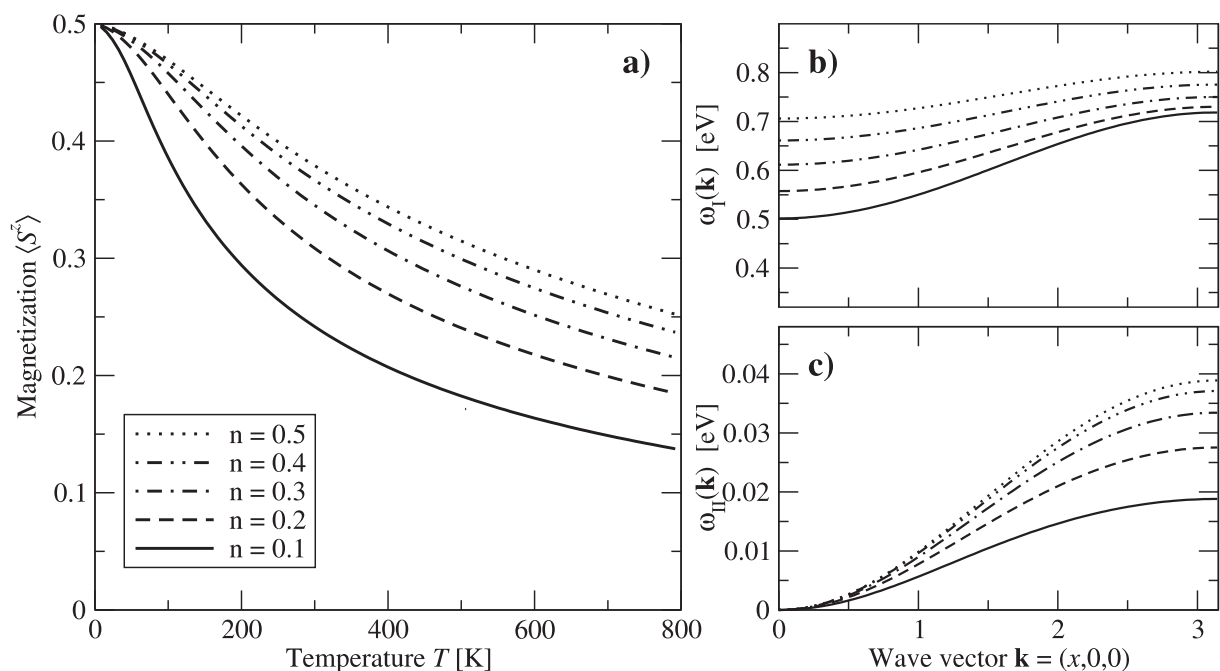


Figure 5.2: Self-consistent solution for the correlation functions included in a two-dimensional relevant Liouville subspace of the itinerant and of the local-moment subsystem. **a)** Temperature dependence of the magnetization $\langle S^z \rangle$ for various band occupations. **b)** Magnon dispersion of the optical magnon branch $\omega_I(\mathbf{k})$ at $T = 100\text{K}$. **c)** Magnon dispersion of the acoustic magnon branch $\omega_{II}(\mathbf{k})$ at $T = 100\text{K}$. The parameters are: $J = 1.0$ eV, $S = 1/2$ and $W = 1.0$ eV for a simple-cubic lattice.

The set of equations indicated in (5.42) - (5.44) is too complex to provide explicit expressions for the correlation functions involved. Instead, the system has to be solved self-consistently. Fig. 5.2 is a typical result of such a numerical evaluation. Part a) shows the temperature-dependence of the magnetization. For better comparison the same parameters are used as in Fig. 5.1. One readily notices great deviations from the mean-field treatment (5.9). Already for low temperatures we do not observe a wide region of nearly saturated magnetization, as described by the Brillouin function. In contrast a rather fast decrease of $\langle S^z \rangle$ is observed as a function of temperature for $T < 100\text{K}$. The situation

is much different in the high-temperature regime. Here, the magnetization approaches the value $\langle S^z \rangle = 0$ asymptotically. However, a definite phase transition temperature T_C cannot be observed.

There are several aspects for an explanation of this kind of behaviour. A principle problem can already be observed in the treatment with a one-dimensional Liouville subspace on page 82. If a mean-field decoupling is avoided, one is confronted with the expression

$$\langle S^z \rangle = \hbar S \cdot \tanh \left[\frac{\beta \Omega_{\mathbf{k}\sigma}}{4z_\sigma \langle S_0^z \rangle} \right] = \hbar S \cdot \tanh \left[\beta J \left\{ 2\langle S^z s^z \rangle + \hbar \langle S^\sigma c_{-\sigma}^\dagger c_\sigma \rangle \right\} / 4 \langle S^z \rangle \right] \quad (5.45)$$

for the magnetization. According to our experience with the POM and the MCDA a self-consistent determination of the expectation values $\langle S^z s^z \rangle$ and $\langle S^\sigma c_{-\sigma}^\dagger c_\sigma \rangle$ always yields non-zero values. An assumed phase transition to a paramagnetic regime with $\langle S^z \rangle = 0$ therefore implies a divergence in the argument of tanh. Hence, the right hand side of Eq. (5.45) becomes $\pm \hbar S$, which is a contradiction to the former assumption of $\langle S^z \rangle$ on the left hand side.

This kind of problem persists, if the improved two-dimensional basis is used. Then the magnon dispersions

$$\begin{aligned} \omega_{\text{I, II}}(\mathbf{k}) &= \frac{1}{2} \left[\frac{\Omega_{\mathbf{k}\sigma}}{2N\hbar} \left(\frac{1}{z_\sigma \langle S^z \rangle} + \frac{1}{z_\sigma \langle s^z \rangle} \right) + \frac{f_\sigma(\mathbf{k})}{2\hbar z_\sigma \langle s^z \rangle} \right] \\ &\pm \frac{1}{2} \sqrt{\left[\frac{\Omega_{\mathbf{k}\sigma}}{2N\hbar} \left(\frac{1}{z_\sigma \langle S^z \rangle} + \frac{1}{z_\sigma \langle s^z \rangle} \right) + \frac{f_\sigma(\mathbf{k})}{2\hbar z_\sigma \langle s^z \rangle} \right]^2 - \frac{\Omega_{\mathbf{k}\sigma} \cdot f_\sigma(\mathbf{k})}{N\hbar^2 \langle S^z \rangle \langle s^z \rangle}} \end{aligned} \quad (5.46)$$

contains again the fraction $\Omega_{\mathbf{k}\sigma} / \langle S^z \rangle$. Since the numerator $\Omega_{\mathbf{k}\sigma}$ is a positive number in all our calculations, an assumed paramagnetic configuration yields a divergence of magnon excitations. However, this does not imply a diverging susceptibility, as it is necessary for a phase transition. Instead, negative magnon excitations are a prerequisite for an instability of the ferromagnetic phase at a transition temperature T_C .

In Figs. 5.2b and 5.2c the magnon dispersion of the optical and acoustic branch is plotted, respectively. The former magnons are too high in energy to be important for our considerations. We have realized before, that the stiffness of the acoustic magnons is always positive.¹⁰ The dispersion remains positive throughout the whole Brillouin zone. An anomalous softening, as reported by Vogt et al. [163], is not observed within the approach presented here. Again, the analytical reason for this property is the positive value of $\Omega_{\mathbf{k}\sigma}$. Since $f_\sigma(\mathbf{k})$ is also positive for all \mathbf{k} , the expression in the second line of (5.46) has always a smaller absolute value than the one in the first line. Hence, $\omega_{\text{II}}(\mathbf{k}) > 0 \quad \forall \mathbf{k}$, what prevents a phase transition.

Another aspect is important for the evaluation of the presented approach, to close the system of correlation functions. The suggested methodology for a determination of the correlation functions (5.42) - (5.44) is not unique. The spectral theorem can also be

¹⁰The gapless excitation energy at $\mathbf{k}=\mathbf{0}$ is a diverging contribution to the susceptibility. However, in the case of a positive stiffness constant, this divergence is integrable in spherical coordinates. Hence, the summation over the three-dimensional Brillouin zone yields a finite value.

applied to the Green's functions, which are automatically available due to the choice of our basis, but not used until now. Each of these applications yields another relation between the expectation values involved. This can be combined into a large system of equations¹¹. It turns out, that this system of equations is over-determined. As foreshadowed above, this fact can be used to fix the values for the correlation functions $\langle S^z \rangle$ and $\langle S^z S^{-\sigma} S^\sigma \rangle$. However, for $S = 1/2$, where these entities can be expressed by $\langle S^{-\sigma} S^\sigma \rangle$, contradictions are obtained.¹²

In this context, a paper of Mancini et al. [86] is worth mentioning. In the bosonic sector their equation-of-motion approach is comparable to our ansatz, but the proposal for the fermionic sector corresponds to a Liouville basis formed by $|c_\sigma^\dagger\rangle$ and $|\hat{n}_{-\sigma} c_\sigma^\dagger\rangle$. With this choice the authors were not able to obtain a closed self-consistent scheme. They got questionable results for the magnon dispersions, too.

In summary, the method of a two-dimensional Liouville subspaces seems to be an excellent possibility to treat the itinerant and the local-moment subsystem on the same footing. However, we are confronted with three serious drawbacks: (A) the insufficient description of the free-electron susceptibility in (5.26), (B) the absence of a critical temperature due to the finite value of $\Omega_{\mathbf{k}\sigma}$ and (C) the over-determination of the system of correlation functions. We believe, that despite the shortcomings it is worth to continue further investigations in this direction. Within this thesis we will focus on an improvement of aspect (A) in the following.

A further extension of the symmetric two-dimensional basis

The insufficient \mathbf{k} -dependence (5.26) of the frequency matrix is a consequence of the relevant Liouville subspace. Apparently, the description of the electronic degree of freedom has to be extended to obtain a Lindhard-type susceptibility. In (5.21) the spin operator $s_{\mathbf{k}}^{-\sigma}$ has been used, to incorporate spin-flip processes in the conduction band. Expressed in terms of Fermi operators, this is identical to a sum of Liouville states. In contrast to that, we define the basis

$$|A\rangle = |S_{\mathbf{k}}^{-\sigma}\rangle \quad \text{and} \quad |B_{\mathbf{k}'}\rangle = \hbar |c_{\mathbf{k}'-\mathbf{k},-\sigma}^\dagger c_{\mathbf{k}',\sigma}\rangle. \quad (5.47)$$

Due to the omission of the sum the corresponding level of description has $N+1$ dimensions. Therefore, it includes many more physical processes than with the previous choice of a basis.

The price for this advantage is the large number of entities that appear in the Mori equations. Due to the high dimensionality of the problem the compact matrix notation (3.26) is less appropriate for the solution than a set of scalar Mori equations, as given in

¹¹An example for an extensive treatment of such systems of equations can be found in [49].

¹²In particular, this affects the correlation function $\langle S^\sigma c_{-\sigma}^\dagger c_\sigma \rangle$.
It can be obtained from $\sum_{\mathbf{k},\mathbf{q}} \langle\langle S_{-\mathbf{k}}^\sigma; c_{\mathbf{q}-\mathbf{k},-\sigma}^\dagger c_{\mathbf{q},\sigma} \rangle\rangle_E$ as well as from $\sum_{\mathbf{k},\mathbf{q}} \langle\langle c_{\mathbf{k},\sigma}; S_{-\mathbf{q}}^\sigma c_{\mathbf{k}-\mathbf{q},-\sigma}^\dagger \rangle\rangle_E$.

(3.23). Again, we neglect the effect of the memory matrix. Therefore, the equations

$$\omega \left(A_i \left| \frac{1}{\omega - \mathcal{L}} \right| A_j \right) \approx (A_i | A_j) + (A_i | \mathcal{L} | A_l) \chi_{lm}^{-1} \left(A_m \left| \frac{1}{\omega - \mathcal{L}} \right| A_j \right) \quad (5.48)$$

$$= (A_i | A_j) + \left(\mathcal{L} A_i \left| \mathcal{P} \frac{1}{\omega - \mathcal{L}} \right| A_j \right), \quad (5.49)$$

have to be considered¹³. Eq. (5.49) clearly demonstrates the equivalence to the procedure in decoupling approaches. In the latter, the equations of motion

$$\omega \left(A_i \left| \frac{1}{\omega - \mathcal{L}} \right| A_j \right) = (A_i | A_j) + \left(\mathcal{L} A_i \left| \frac{1}{\omega - \mathcal{L}} \right| A_j \right) \quad (5.50)$$

have to be simplified somehow such, that the higher Green's functions at the right hand side are expressed in terms of known Green's functions on the left. The same is done in a POM which is restricted to the frequency matrix. However, the vague formulation "somehow" is now replaced by the clear instruction $|\mathcal{L} A_i\rangle \rightarrow \mathcal{P} |\mathcal{L} A_i\rangle$. The approximation consists of neglecting the memory matrix. Since the memory matrix involves only terms which are of order J^2 or higher orders in J , the approximation is controlled in the sense of a perturbation theory.

For the considerations of this section, we have to use the projector

$$\mathcal{P} = |A\rangle \frac{1}{(A|A)} \left(A | + \sum_{\mathbf{k}', \mathbf{k}''} |B_{\mathbf{k}''}\rangle \right) \frac{1}{(B_{\mathbf{k}''} | B_{\mathbf{k}'})} (B_{\mathbf{k}'} |. \quad (5.51)$$

As mentioned above, its action on the time derivative of the basis states (5.47) needs to be evaluated. Making use of the orthogonality of this basis¹⁴ we formally obtain

$$\mathcal{P} |\mathcal{L} A\rangle = \frac{(A | \mathcal{L} | A)}{(A | A)} |A\rangle + \sum_{\mathbf{k}'} \frac{(B_{\mathbf{k}'} | \mathcal{L} | A)}{(B_{\mathbf{k}'} | B_{\mathbf{k}'})} |B_{\mathbf{k}'}\rangle \quad (5.52)$$

$$\mathcal{P} |\mathcal{L} B_{\mathbf{k}'}\rangle = \frac{(A | \mathcal{L} | B_{\mathbf{k}'})}{(A | A)} |A\rangle + \sum_{\mathbf{k}''} \frac{(B_{\mathbf{k}''} | \mathcal{L} | B_{\mathbf{k}'})}{(B_{\mathbf{k}''} | B_{\mathbf{k}'})} |B_{\mathbf{k}''}\rangle. \quad (5.53)$$

The results have to be inserted into Eq. (5.49). Still, one is confronted with $(N+1) \times (N+1)$ equations. A detailed analysis shows that the \mathbf{k}'' -summation in (5.53) in particular renders the solution of this system difficult.

The relevant matrix element of the frequency matrix is given by

$$\begin{aligned} (B_{\mathbf{k}''} | \mathcal{L} | B_{\mathbf{k}'}) &= \hbar(\varepsilon_{\mathbf{k}' - \mathbf{k}} - \varepsilon_{\mathbf{k}'}) (\langle \hat{n}_{\mathbf{k}'\sigma} \rangle - \langle \hat{n}_{\mathbf{k}' - \mathbf{k}, -\sigma} \rangle) \delta_{\mathbf{k}', \mathbf{k}''} \\ &+ \frac{J\hbar}{2N} \sum_{\mathbf{q}} \left\{ \left\langle S_{\mathbf{q}}^{-\sigma} c_{\mathbf{k}'+\mathbf{k}+\mathbf{q}, \sigma}^\dagger c_{\mathbf{k}' - \mathbf{k}, -\sigma} \right\rangle + \left\langle S_{\mathbf{q}}^{-\sigma} c_{\mathbf{k}', \sigma}^\dagger c_{\mathbf{k}' - \mathbf{q}, -\sigma} \right\rangle \right. \\ &\quad \left. z_\sigma \left\langle S_{\mathbf{q}}^z c_{\mathbf{k}', \sigma}^\dagger c_{\mathbf{k}' - \mathbf{q}, \sigma} \right\rangle - z_\sigma \left\langle S_{\mathbf{q}}^z c_{\mathbf{k}'+\mathbf{k}+\mathbf{q}, -\sigma}^\dagger c_{\mathbf{k}' - \mathbf{k}, -\sigma} \right\rangle \right\} \delta_{\mathbf{k}', \mathbf{k}''} \\ &+ \frac{J\hbar}{2N} \left\{ z_\sigma \left\langle S_{\mathbf{k}'' - \mathbf{k}}^z c_{\mathbf{k}'', \sigma}^\dagger c_{\mathbf{k}', \sigma} \right\rangle - z_\sigma \left\langle S_{\mathbf{k}'' - \mathbf{k}}^z c_{\mathbf{k}'', -\sigma}^\dagger c_{\mathbf{k}' - \mathbf{k}, -\sigma} \right\rangle \right\}. \quad (5.54) \end{aligned}$$

¹³ For clarity we have used a general basis $\{|A_i\rangle\}_i$.

¹⁴ Note, that $(B_{\mathbf{k}''} | B_{\mathbf{k}'}) = \hbar^2 \langle \hat{n}_{\mathbf{k}'\sigma} - \hat{n}_{\mathbf{k}' - \mathbf{k}, -\sigma} \rangle \delta_{\mathbf{k}', \mathbf{k}''}$.

Apart from the last line, all terms in (5.54) are multiplied with $\delta_{\mathbf{k}',\mathbf{k}}$. Additionally, a mean-field decoupling of the last two expectation values yields the proportionality to $\delta_{\mathbf{k}',\mathbf{k}}$ for these cases, too. As a consequence, the \mathbf{k}' -summation in (5.53) vanishes and an explicit expression is obtained for the mixed Green's function $(B_{\mathbf{k}} | \frac{1}{\omega - \mathcal{L}} | A)$. In turn, this result can be inserted into the Mori equation for $(A | \frac{1}{\omega - \mathcal{L}} | A)$. In this way, the complex set of equations is reduced to a single equation for the magnon Green's function, which can be solved analytically. The identical choice of the basis element $|S_{\mathbf{k}}^{-\sigma}\rangle$ implies the structure of this Green's function to be again of the familiar form (5.17). Now, the correction in terms of the memory matrix is given by

$$M_{\mathbf{k}\sigma}(\omega) = \sum_{\mathbf{k}'} \frac{|(B_{\mathbf{k}'} | \mathcal{L} | A)|^2}{\omega (B_{\mathbf{k}'} | B_{\mathbf{k}'}) - (B_{\mathbf{k}'} | \mathcal{L} | B_{\mathbf{k}'})}. \quad (5.55)$$

Actually, this result is quite similar to expression (5.27) obtained with the symmetric two-dimensional basis. However, the decisive difference is the position of the \mathbf{k}' -summation. Previously included in the function $f_{\sigma}(\mathbf{k})$, the summation now affects the denominator as well as the numerator of the memory matrix. This has a strong effect on the magnon dispersions.

As mentioned above, a prerequisite for this strategy is the mean-field decoupling of only two correlation functions. In accordance with other calculations in this thesis one could go one step further by treating all involved correlation functions in a mean-field manner. Then the memory matrix (5.55) can be specified:

$$M_{\mathbf{k}\sigma}(\omega) = J^2 \sum_{\mathbf{k}'} \langle S^z \rangle^2 \frac{\langle \hat{n}_{\mathbf{k}'\sigma} \rangle - \langle \hat{n}_{\mathbf{k}'-\mathbf{k},-\sigma} \rangle}{\omega - \frac{1}{\hbar} (\varepsilon_{\mathbf{k}'-\mathbf{k}} - \varepsilon_{\mathbf{k}'} + Jz_{\sigma} \langle S^z \rangle)}. \quad (5.56)$$

This result has the structure of a Lindhard function, as desired. One can conclude, that the extension of the level of description to $N + 1$ dimensions is a promising concept for a proper incorporation of conduction electrons.

Expression (5.56) is identical to the result of a random phase approximation (RPA) of the one-magnon Green's function [167]. The RPA is a standard equation-of-motion approach for local-moment systems. Within this concept, all emerging Green's functions are mean-field decoupled, and only a single higher-order Green's function is retained.¹⁵ Due to the equivalence of (5.49) and (5.50) discussed above the similarity of our calculations with the RPA result is not surprising.

From the perspective of the POM the RPA result is based on two kinds of simplifications: On the one hand, the level of description is limited to the Liouville subspace spanned by (5.47). Since the memory matrix is neglected, no contribution of the orthogonal complement of this subspace is considered. On the other hand, the mean-field

¹⁵A very different result is obtained, if the equations are decoupled at the same stage in Wannier representation [137]. This is a hint for the arbitrariness of this approach.

decoupling of the Green's function is equivalent to a mean-field treatment of all correlation functions. We would like to stress again, that the disappearance of challenging divergencies such as

$$\Omega_{\mathbf{k}\sigma} / \langle S^z \rangle = JN \left\{ 2\langle S^z s^z \rangle + \hbar \langle S^\sigma c_{-\sigma}^\dagger c_\sigma \rangle \right\} / \langle S^z \rangle \approx 2JN \langle s^z \rangle \quad (5.57)$$

is due to this mean-field treatment. Perhaps, this treatment is even more adequate for the KLM than others, which avoid a mean-field decoupling. This would explain the otherwise surprising success of the RPA. Before discussing generalizations, we should therefore investigate the properties of the RPA more thoroughly. This will be done in the next section.

5.3 The random-phase approximation

We formulate our result (5.17)+(5.56) for the one-magnon Green's function for $\sigma = \uparrow$:

$$\begin{aligned} \langle\langle S_{-\mathbf{k}}^+; S_{\mathbf{k}}^- \rangle\rangle_E &= \frac{2N\hbar^2 \langle S^z \rangle}{E - J \langle s^z \rangle + \frac{1}{2}J^2\hbar \langle S^z \rangle \chi_0(\mathbf{k}, E) + i0^+}, \\ \chi_0(\mathbf{k}, E) &= \frac{1}{N} \sum_{\mathbf{q}} \frac{\langle \hat{n}_{\mathbf{q},\downarrow} \rangle - \langle \hat{n}_{\mathbf{q}+\mathbf{k},\uparrow} \rangle}{E - J \langle S^z \rangle - (\varepsilon_{\mathbf{q}} - \varepsilon_{\mathbf{q}+\mathbf{k}}) + i0^+}. \end{aligned} \quad (5.58)$$

This result is in agreement with earlier investigations of magnon excitations in the KLM. Already in 1962 an expression similar to (5.58) was obtained by Vonskovsky and Izyumov [164] for $\langle S^z \rangle \equiv \hbar S$. Decades later Woolsey and White [171] as well as Babenco and Cottam [6] derived (5.58) diagrammatically from a single electron-hole Green's function loop. Similarly to Vonskovsky et al. the former work is limited to $\langle S^z \rangle = \hbar S$, although they used a more profound diagrammatical perturbation theory developed by Giovannini et al. [43]. Also Babenco et al. did not determine $\langle S^z \rangle$ self-consistently. A temperature dependent calculation with equations of motion has, e.g., been provided by Sigrist et al. [153] and Wang [167].

Furthermore, it is worth mentioning, that the Lindhard function $\chi_0(\mathbf{k}, E)$ is almost identical to the transverse susceptibility, obtained in a Hartree-Fock approximation of the Hubbard model [40, 101]. To obtain this Stoner result, one essentially has to replace $J \langle S^z \rangle$ by $U \langle s^z \rangle$. The Hubbard model differs from the KLM in the position where this expression appears. In fermionic models it forms the first order contribution, whereas in the KLM $\chi_0(\mathbf{k}, E)$ is part of the memory matrix.

Despite its familiar structure, a numerical evaluation of the result (5.58) is very rare. Most of the analytical discussions end with the determination of the spin wave stiffness [167]. Quantitative approximations are limited to parabolic conduction bands [6, 153], for which the $T = 0$ K Lindhard function can be simplified analytically [40]. The absence of derived magnetization curves in the literature is certainly a consequence of numerical

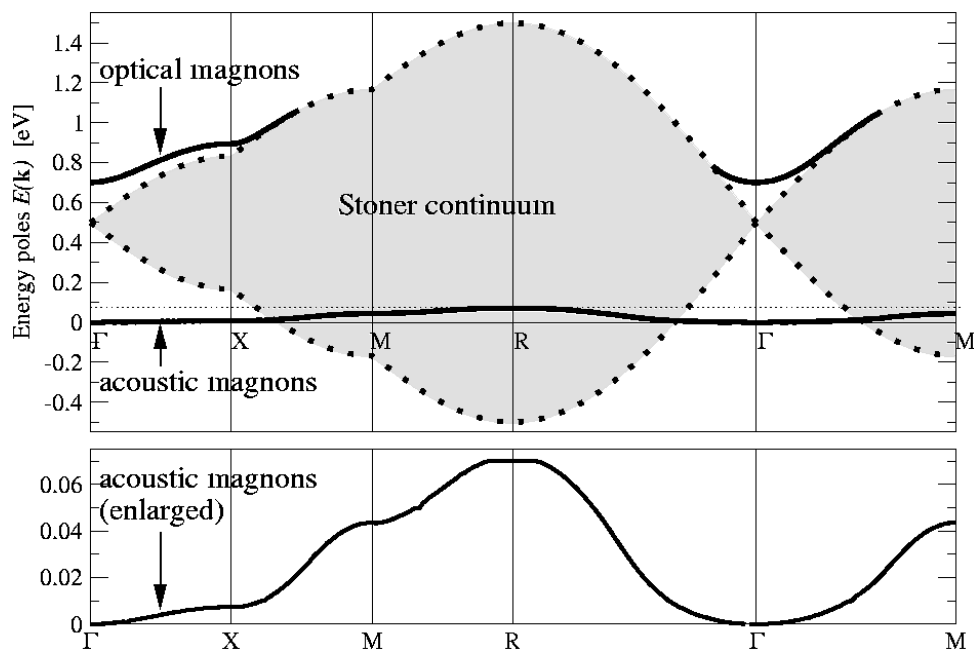


Figure 5.3: Energy poles of the one-magnon Green's function. The hedged area displays the region of the Stoner continuum. The acoustic branch is plotted in the whole Brillouin zone (in the lower part of the figure for an enlarged energy scale), whereas the optical branch vanishes when it enters the continuum. The parameters are: $J = 1.0$ eV, $n = 0.4$, $\langle S^z \rangle = S = 1/2$ and $W = 1.0$ eV for a simple-cubic lattice.

difficulties [162] related to the integration (5.2)

$$\langle S^z \rangle = \hbar S - \frac{1}{\hbar^2 N^2} \sum_{\mathbf{k}} \left(-\frac{1}{\pi} \right) \int_{-\infty}^{\infty} dE f_+(E) \Im \langle \langle S_{-\mathbf{k}}^+; S_{\mathbf{k}}^- \rangle \rangle_E. \quad (5.59)$$

The magnetic behaviour is determined by the energy poles of the Green's function (5.58), called magnons. They are given by the implicit equation

$$E(\mathbf{k}) = J \langle s^z \rangle - \frac{J^2}{2} \langle S^z \rangle \Re \chi_0(\mathbf{k}, E(\mathbf{k})). \quad (5.60)$$

One readily observes, that the magnon spectrum consists of three distinct parts (see Fig. 5.3). Similarly to the previous Green's function (5.28), Eq. (5.60) is quadratic in energy. One of the solution composes an optical magnon branch [$E_I(\mathbf{k}=\mathbf{0}) = J(\langle S^z \rangle + \langle s^z \rangle)$] and the other an acoustic branch [$E_{II}(\mathbf{k}=\mathbf{0}) = 0$]. Both have a quadratic dispersion in the vicinity of the Γ -point. The shape along the high-symmetry directions of the first Brillouin zone is strongly influenced by the band structure, for which the tight-binding Bloch dispersion (5.31) has been used.

A qualitatively new feature, not observed in the case of the memory matrix (5.27), is the appearance of a Stoner continuum. Mathematically, this is the energy region of a non-vanishing magnon spectral density, due to a finite

$$\Im \chi_0(\mathbf{k}, E_S) = \frac{-\pi}{N} \sum_{\mathbf{q}} \{ \langle \hat{n}_{\mathbf{q},\downarrow} \rangle - \langle \hat{n}_{\mathbf{q}+\mathbf{k},\uparrow} \rangle \} \delta(E_S - J \langle S^z \rangle + \varepsilon_{\mathbf{q}+\mathbf{k}} - \varepsilon_{\mathbf{q}}). \quad (5.61)$$

For a simple cubic lattice this energy interval is given by $[E_S^{(\min)}, E_S^{(\max)}]$ with

$$E_S^{(\min)}(\mathbf{k}) = J \langle S^z \rangle - \frac{W}{3} \left\{ \left| \sin \frac{k_x}{2} \right| + \left| \sin \frac{k_y}{2} \right| + \left| \sin \frac{k_z}{2} \right| \right\}, \quad (5.62)$$

$$E_S^{(\max)}(\mathbf{k}) = J \langle S^z \rangle + \frac{W}{3} \left\{ \left| \sin \frac{k_x}{2} \right| + \left| \sin \frac{k_y}{2} \right| + \left| \sin \frac{k_z}{2} \right| \right\}. \quad (5.63)$$

Physically, the energy region is characterized by those spin wave excitations in the local-moment part, which can be converted to a particle-hole pair excitation in the conduction band. In this process the hole and the electron have opposite spin and their wave vectors differ by \mathbf{q} . Since it is connected with the disappearance of the spin wave in the local-moment part, the Stoner continuum yields a damping of magnon excitations.

The optical magnon branch enters the Stoner continuum tangentially. Within the continuum (5.60) yields no solution for this branch. In contrast the acoustic magnons can also be observed within the continuum, both theoretically and experimentally [59, 56]. However, they experience a gradually increasing damping. Details of the intersection of the acoustic branch with the continuum are discussed more fully below.

Evaluations for $T = 0$ K

To avoid numerical difficulties, several authors treated the result (5.58) in a spin wave approximation, $\langle S^z \rangle = \hbar S$. Furukawa [38] considers only the lowest order of a $1/S$ expansion in this approximation. In the limit $J/W \rightarrow \infty$ he obtained a magnon dispersion relation, identical to a ferromagnetic Heisenberg model with nearest-neighbour spin exchange. A decrease of J yields a reduction of the stiffness constant D and the band width of the spin wave dispersion.

Qualitatively similar results have been obtained by Vogt et al. [163]. These authors focused on the dependence of the magnetic properties on the band occupation n . An increase of n up to quarter filling extends the band width of the spin wave dispersion. With a further increase of n the magnon energies decrease again. For very small J Vogt et al. observed an anomalous softening of the acoustic magnons at the zone boundary of the Brillouin zone. This behaviour is not reproduced in a Heisenberg model with nearest-neighbour interaction [56].

The presented results can partly explain the magnetic dynamics of maganites measured in neutron scattering experiments. Furukawa [38] was successful in fitting the spin wave data for $\text{La}_{0.7}\text{Pb}_{0.3}\text{MnO}_3$ [128]. A zone boundary softening has been measured in $\text{Pr}_{0.63}\text{Sr}_{0.37}\text{MnO}_3$ [56] and $\text{Ni}_{0.7}\text{Sr}_{0.3}\text{MnO}_3$ [31]. Although other theoretical [155, 67] and experimental [20] explanations have been suggested, it could well be associated with the effects reported by Vogt et al. [163]. Therefore, the claim of Hwang et al. [56] that their experiments are “inconsistent with double exchange models” has been disproven successfully.

However, the spin wave approximation has shortcomings in explaining the temperature dependence of neutron scattering data. First of all, the damping of high-frequency spin waves [128, 56, 20] is not correctly described with this theory. Secondly, an explanation of the reduction of the spin wave stiffness [31] and an additional zone boundary softening [56] with increasing temperature is missing.

Despite the limited applicability to finite temperatures ($\langle S^z \rangle = \hbar S$ is assumed), Vogt et al. [163] used the spin wave approximation for the determination of the Curie temperature, too. According to their approach¹⁶, the critical temperature is reached, if the number of magnons equals the spin quantum number S . To count spin excitation one has to transform the problem to Bose operators, using the Holstein-Primakoff transformation [53]. The transformed Green's function differs from its pendant in terms of spin operators by a factor $1/2S$. Hence,

$$S \stackrel{!}{=} \frac{1}{N} \sum_{\mathbf{k}} \langle \hat{n}_{\mathbf{k}}^{(\text{Mag})} \rangle = \frac{1}{N} \sum_{\mathbf{k}} \left(-\frac{1}{\hbar N \pi} \right) \int_{-\infty}^{\infty} dE f_+(E) \frac{\Im \langle \langle S_{-\mathbf{k}}^+; S_{\mathbf{k}}^- \rangle \rangle_E}{2S \hbar^2}. \quad (5.64)$$

If damping effects due to the Stoner pair excitations are neglected, the imaginary part in the integrand reduces to a δ -function. Furthermore, if $k_B T_C$ is much higher than the magnon energies, one can linearize the exponential in the Bose distribution function $f_+(E)$. A combination of these assumptions yields

$$S \approx \frac{1}{N} \sum_{\mathbf{k}} \frac{1}{\beta_C E(\mathbf{k})} \iff k_B T_C \approx \left\{ \frac{1}{NS} \sum_{\mathbf{k}} \frac{1}{E(\mathbf{k})} \right\}^{-1}. \quad (5.65)$$

This T_C -formula is formally identical to the result of a spin wave approximation of the Heisenberg model [110]. Therefore, similarities of the obtained results as compared to the modified RKKY (see p. 16) are not surprising. In particular the dependence of the Curie temperature on the band occupation as displayed in Fig. 5.4a is in good qualitative agreement with Fig. 2.1b. The spin wave approximation also predicts an impossibility of ferromagnetism around half-filling and a parabolic dependence of the Curie temperature as a function of band occupation. Since the upper n -limit for a finite T_C depends on the coupling constant, there exists a critical J below which ferromagnetism is not possible.

Evaluations for finite temperatures

The temperature enters the RPA formula via expectation values. Now $\langle S^z \rangle$, which was taken as constant above, is the decisive parameter. It does not only appear explicitly in Eqs. (5.58). If, as is common in the literature, a mean-field input of the conduction-band subsystem is used, then $\langle S^z \rangle$ is also responsible for the temperature-dependence of $\langle \hat{n}_{\mathbf{k}\sigma} \rangle$. In turn, the T -dependence of $\langle S^z \rangle$ is given by the Bose function in (5.59).

A value of $\langle S^z \rangle$ smaller than the saturation value $\hbar S$ has two main consequences for the magnetization spectra: On the one hand, one can read off the Eq. (5.62) that the lowest energy of the Stoner continuum is proportional to $\langle S^z \rangle$. In the spin wave approximation of Vogt et al. [163] the parameters S and J were chosen sufficiently high to avoid an intersection of the acoustic magnon branch with the continuum. A similar strategy is impossible if one considers temperatures close to T_C . On the other hand, we learn from

¹⁶We have used another formalism for the derivation of Eq. (5.65) than the one provided in [163]. It allows a physical understanding of the approximation without adapting formulae from a different model. For $S = 1/2$ the situation is even more transparent, since Eq. (5.64) is identical to Eq. (5.59) with $\langle S^z \rangle = 0$.

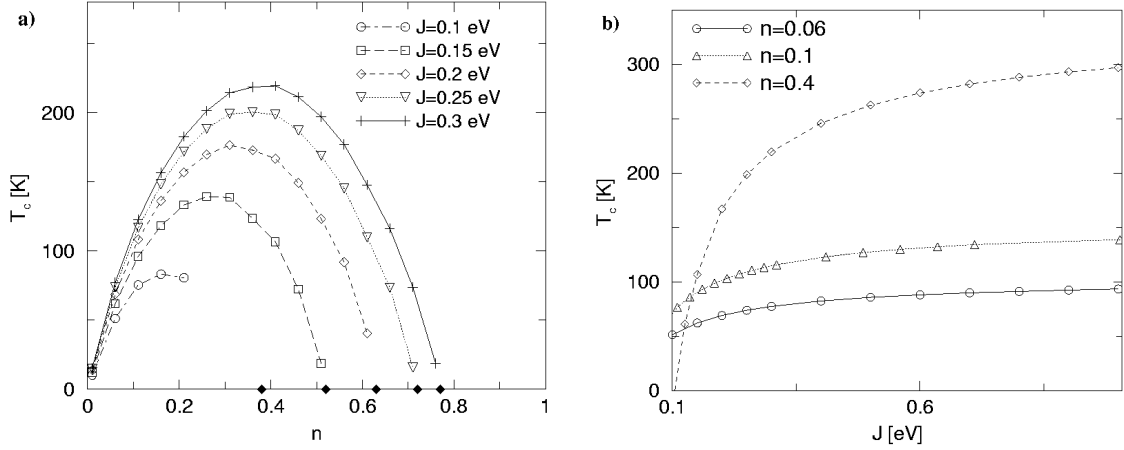


Figure 5.4: Curie temperatures obtained for the spin wave approximation of the RPA. **a)** T_C as a function of the band occupation n for different coupling constants. **b)** T_C as a function of the coupling constant J for different band occupations. The expectation value $\langle \hat{n}_{\mathbf{k}\sigma} \rangle$ is treated in a mean-field approximation. The other parameters are: $\langle S^z \rangle = S = 7/2$, $T = 0$ K and $W = 1.0$ eV for a simple-cubic lattice. [163]

Eq. (5.60) that the energies of acoustic magnons have also a strong $\langle S^z \rangle$ -dependence. Both effects will be discussed below.

Fig. 5.3 already demonstrates that an intersection of the acoustic magnon branch with the Stoner continuum cannot be avoided. However, the value of the imaginary part of the Lindhard function differs a lot in the energy interval given by (5.62) and (5.63). There are also parameter constellations (E_S, \mathbf{k}) where it is negligible small. For example, one can rigorously show that

$$\lim_{E_S \rightarrow 0} \Im \chi_0(\mathbf{k}, E_S) = 0, \quad (5.66)$$

provided that a mean-field electronic self-energy is used. For these parameters there is effectively no damping. Therefore, the way the magnon dispersion is affected does depend very much on the constellation of \mathbf{k} , $E(\mathbf{k})$ and $\langle S^z \rangle$, too.

A possible evolution of the intersection of the acoustic branch with the continuum is illustrated in Fig. 5.5. For magnetizations close to saturation the Stoner continuum is still too high in energy to have an effect on the magnon branch in the $[x, 0, 0]$ -direction. If $\langle S^z \rangle$ is decreased below 0.45 an intersection takes place and results in a deformation of the dispersion line. The lower the value of $\langle S^z \rangle$ the more pronounced this deformation becomes. For $\langle S^z \rangle = 0.4$ the deformation takes on the form of a jump in the functional dependence $E(\mathbf{k})$. A more detailed investigation of this feature (see magnified part in Fig. 5.5b shows that Eq. (5.60) has three low energy solutions within the vicinity of $\mathbf{k}^* = (\pi, 0, 0)/\sqrt{2}$. However, the damping is too large for an observation of a three-peak structure experimentally as well as in the spectral density

$$A_{\mathbf{k}}(E) = -\frac{1}{\pi} \Im \langle \langle S_{-\mathbf{k}}^+; S_{\mathbf{k}}^- \rangle \rangle_E. \quad (5.67)$$

Fig. 5.6 demonstrates that the magnon dispersion for a simple-cubic lattice is not

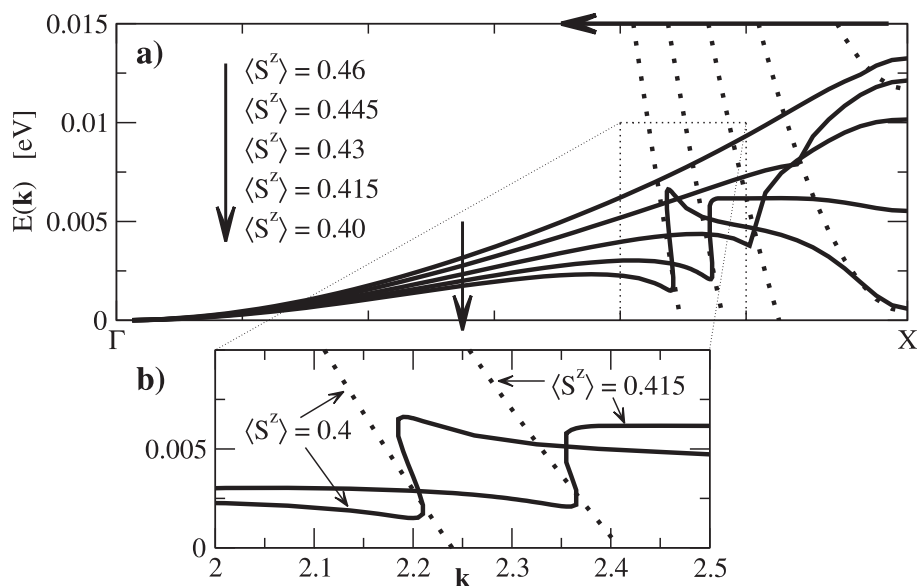


Figure 5.5: Variation of the magnon dispersion with magnetization (temperature). The excitation energy of the acoustic branch (solid lines) and the lower edge of the Stoner continuum (dotted lines) are shown. With decreasing magnetization (indicated by arrows) the acoustic magnons enter the continuum. In part b the deformation of two magnon dispersions is magnified. The parameters are: $J = 0.75$ eV, $S = 1/2$, $n = 0.2$, $T = 30$ K and $W = 1.0$ eV for a simple-cubic lattice.

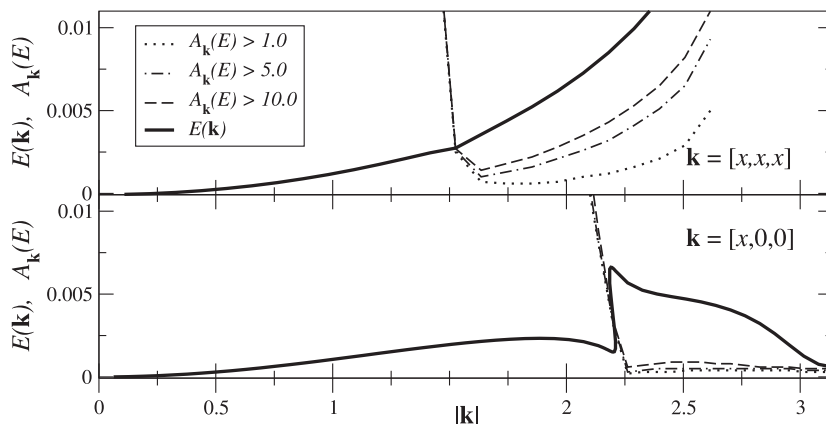


Figure 5.6: Effect of the Stoner continuum on the acoustic magnon branch in the high-symmetry directions $[x, 0, 0]$ and $[x, x, x]$. The strength of the Stoner damping is indicated by lines of equal spectral density. The same parameters are chosen as in Fig. 5.5, $\langle S^z \rangle = 0.4$.

isotropic. For the chosen set of parameters the behaviour in the directions $[x, x, 0]$ and $[x, x, x]$ is similar, but the jump in the dispersion is only observed in the $[x, 0, 0]$ direction. The distance of the intersection from the Γ -point is also not the same for $[x, 0, 0]$ and $[x, x, x]$. Furthermore, Fig. 5.6 sketches the damping effect of the Stoner continuum by providing lines of equal spectral density. This can well explain the heavy damping

effects observed in neutron scattering experiments [128, 56, 20]. In particular, the strong increase of the magnon linewidth with temperature can be understood. For the $[x, 0, 0]$ direction the obtained broadening is so strong, that one might even have difficulties to experimentally determine an energy that can be associated with an acoustic magnon excitation.

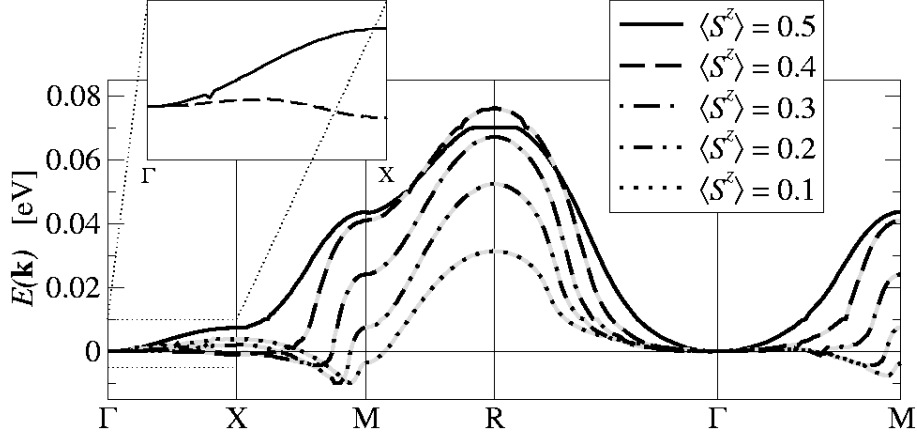


Figure 5.7: Spin waves along the high-symmetry directions of the Brillouin zone for different magnetizations (temperatures). The parameters are: $J = 1.0$ eV, $S = 1/2$, $n = 0.4$ and $W = 1.0$ eV for a simple-cubic lattice.

In Fig. 5.7 the dispersion of the acoustic magnons is plotted for all high-symmetry directions in the Brillouin zone. In this figure we do not consider damping effects. Instead the parameters chosen allow the discussion of another feature: the appearance of negative magnon energies. As long as the magnetization is equal to its saturation value, the dispersion is very similar to published calculations with spin-wave approximations [38] and neutron scattering data [128]. A determination of the Curie temperature based on Eq. (5.65) yields a finite value. However, if the magnetization is lowered, as it happens in a self-consistent calculation for finite temperatures based on Eq. (5.59), the dispersion becomes negative in some regions of the Brillouin zone. The effect is most pronounced along the path $X \rightarrow M$, but the enlarged inset points out that even for small demagnetizations ($\langle S^z \rangle = 0.4$) the dispersion crosses the line of zero energy in the vicinity of the X-point.

Usually negative excitation energies are associated with an instability of the system. This is certainly correct if they are observed for the ground-state configuration $\langle S^z \rangle = \hbar S$. Then, whenever connected with a gain in energy, magnons will be emitted and thereby the magnetization will be reduced. In principle, the situation is not that clear, if $\langle S^z \rangle$ is smaller than $\hbar S$. In this case an emission of magnons does not contradict the assumption for the magnetization.¹⁷ Instead, there will be a balance of magnon emissions and absorptions in a non-collinearly ordered system. The magnetization $\langle S^z \rangle$ is just an average over the varying behaviour in different regions of the Brillouin zone.

¹⁷Note, that a negative magnon energy is a positive excitation in terms of the Green's function $\langle\langle S_{-\mathbf{k}}^-; S_{\mathbf{k}}^+ \rangle\rangle_E$.

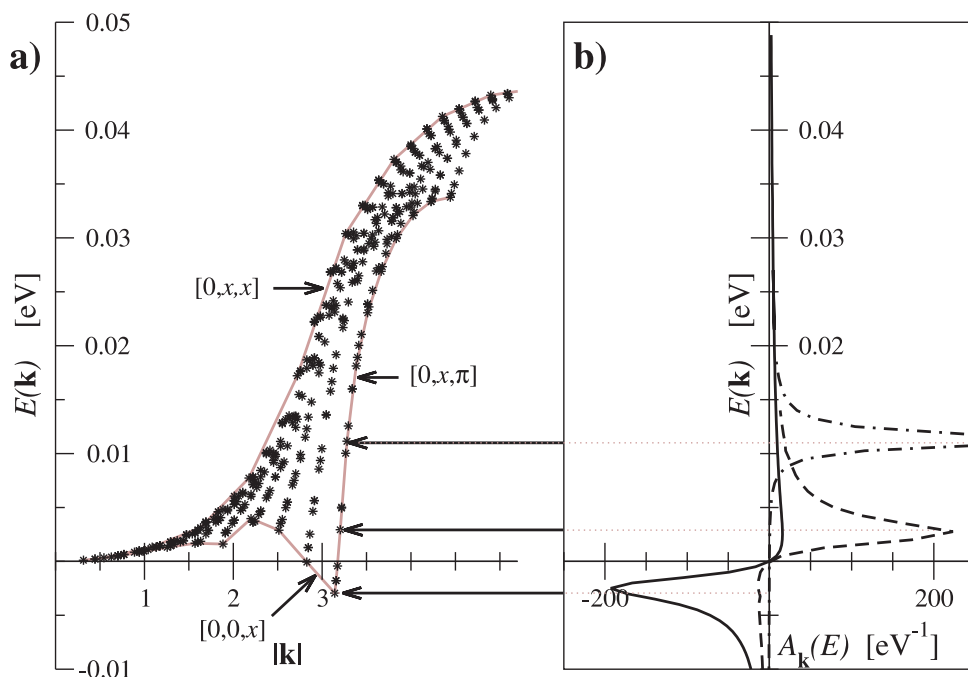


Figure 5.8: **a)** Excitations energies of the acoustic magnon branch at equidistant points throughout the whole Brillouin zone. The horizontal axis shows the distance of these points from the Γ -point. Certain high-symmetry directions are indicated. **b)** For three points of the $[0,x,\pi]$ direction (indicated by arrows) the energy-dependence of the spectral density is plotted. The same parameters as in Fig. 5.5 are chosen, $\langle S^z \rangle = 0.38$.

However, within the RPA negative magnon energies always cause inconsistencies. The reason can be seen in Fig. 5.8. On the left hand side the excitation energy $E(\mathbf{k})$ is given for an equidistant grid of \mathbf{k} -points throughout the whole (irreducible) Brillouin zone.¹⁸ We have chosen three of these \mathbf{k} -points to plot the associated spectral density (5.67) in Fig. 5.8b. If $E(\mathbf{k})$ is sufficiently high (dash-dotted line), the spectral density has the expected behaviour. Also for negative $E(\mathbf{k})$ (solid line) there is a clear peak in the functional dependence of $A_{\mathbf{k}}(E)$. However, this peak has negative spectral weight. In addition we have plotted the spectral density for a positive, but small $E(\mathbf{k})$ (dashed line). In this case, most of the spectral weight is positive, however a small negative contribution can also be observed.

The obtained numerical result can readily be confirmed analytically. According to Eq. (5.61) an energy E_S within the Stoner continuum implies the existence of a wave-vector \mathbf{q} such that $E_S = J \langle S^z \rangle - \varepsilon_{\mathbf{q}+\mathbf{k}} + \varepsilon_{\mathbf{q}}$. Hence,

$$E_S < 0 \quad \iff \quad \varepsilon_{\mathbf{q}} + \frac{1}{2}J \langle S^z \rangle < \varepsilon_{\mathbf{q}+\mathbf{k}} - \frac{1}{2}J \langle S^z \rangle. \quad (5.68)$$

If, as in all our current considerations, a mean-field input from the itinerant subsystem is assumed, then the factor in front of the Kronecker δ in (5.61) has the following form

$$-\pi \left\{ \langle \hat{n}_{\mathbf{q},\downarrow} \rangle - \langle \hat{n}_{\mathbf{q}+\mathbf{k},\uparrow} \rangle \right\} = -\pi \left\{ f_-(\varepsilon_{\mathbf{q}} + \frac{1}{2}J \langle S^z \rangle) - f_-(\varepsilon_{\mathbf{q}+\mathbf{k}} - \frac{1}{2}J \langle S^z \rangle) \right\}. \quad (5.69)$$

¹⁸In contrast to Fig. 5.7 this presentation is not restricted to the high-symmetry directions.

Since the Fermi distribution function is monotonically decreasing, a combination of (5.68) and (5.69) yields a negative sign for $\Im \chi_0(\mathbf{k}, E_S)$. Finally, one concludes from (5.58) and (5.67) that the sign of $A_{\mathbf{k}}(E)$ is the same as that of $\Im \chi_0(\mathbf{k}, E_S)$.

There is no doubt, that a negative spectral density is in contrast to rigorous analytical properties of retarded Green's functions. This limits the applicability of the RPA. As long as a mean-field input is used for $\langle \hat{n}_{\mathbf{q},\sigma} \rangle$, negative magnon excitations cannot be considered. For positive but small $E(\mathbf{k})$ one has to accept the violation of sum rules when integrating over positive energies only. Since the RPA enjoys a wide range of applications, it is surprising that this fact has, to best of our knowledge, not been reported in the literature.

It is certainly possible to evaluate the RPA for low temperatures. In particular for large values of $\langle S^z \rangle$ and J a mutual interference of the acoustic magnons and the Stoner continuum can be avoided. Furthermore, we found, that the problem of negative spectral densities is very much reduced for small band occupations. Therefore, typical magnetization curves for $n = 0.1$ are provided in Fig. 5.9a. The differences compared to the mean-

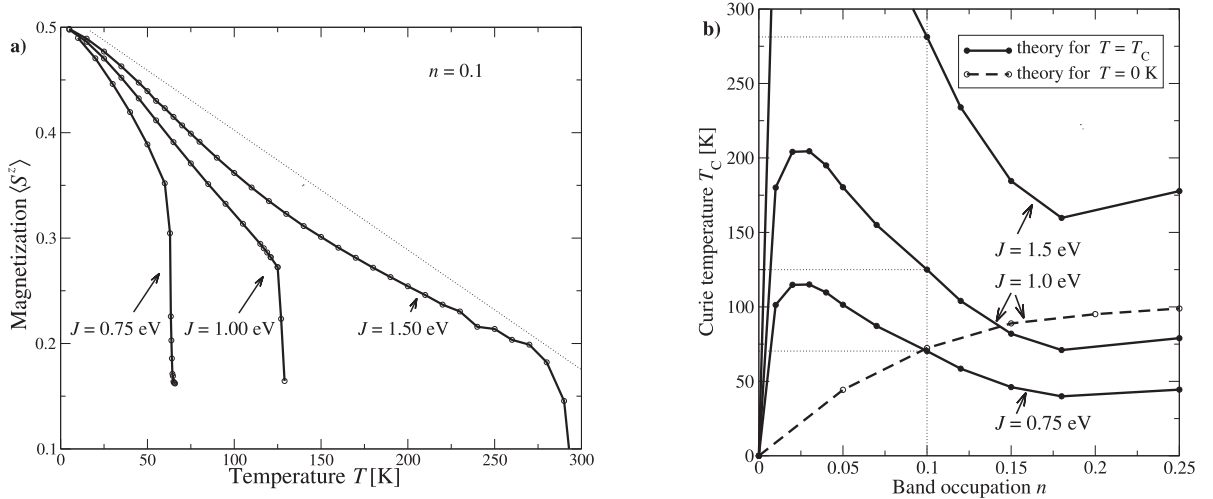


Figure 5.9: **a)** Temperature dependence of the spontaneous magnetization $\langle S^z \rangle$ calculated with the RPA Green's function. The dotted line has been inserted to realize the convexity of the magnetization. **b)** Dependence of the Curie temperature on the band occupation. An evaluation of the RPA formula for $T = T_C$ is compared to the spin wave approximation at $T = 0$ K. In both figures the expectation value $\langle \hat{n}_{\mathbf{k}\sigma} \rangle$ is treated in a mean-field approximation. The parameters are: $S = 1/2$ and $W = 1.0$ eV for a simple-cubic lattice.

field results displayed in Fig. 5.1 are remarkable. In contrast to the Brillouin function there is no wide temperature range, where $\langle S^z \rangle$ -values are close to saturation. Instead, the magnetization decreases rapidly. Close to the Curie temperature the descent is particularly steep. For stronger coupling another striking trend is the existence of magnetization curves with convex curvature as a function of temperature. A similar feature has already been observed in Fig. 5.2. This illustrates the fact that with increasing J the difference between the levels of description for choices (5.21) and (5.47) becomes less important.

We have not plotted the magnetization close to the Curie temperature. The reason is the low accuracy in this region. Apart from the appearance of negative spectral weights, the small magnon energies yield a divergence of the Bose distribution function. In the vicinity of the Γ -point it is possible to perform an analytical integration to master this problem. However, low excitation energies in other parts of the Brillouin zone are numerically much more challenging.¹⁹

Despite the fact, that the calculation for low magnetizations is difficult, one can estimate the Curie temperature from Fig. 5.9a. Nevertheless, a more accurate determination is desirable. One could use the spin-wave formula (5.65). The result for $J = 1.0$ eV is plotted in Fig. 5.9b as a dashed line. We have discussed the shortcomings of this formula above. They are related to the fact that properties at $T = 0$ K are used to determine a finite transition temperature. A more accurate T_C formula would be based on properties at $T = T_C$. Indeed, one can exploit the fact (e.g., see Eq. (5.60) and Fig. 5.7), that the magnon energies $E(\mathbf{k})$ become infinitesimally small when approaching T_C . Due to (5.66), the imaginary part of $\chi_0(\mathbf{k}, E)$ can be neglected in this limit. Hence, for $T = T_C$ Eq. (5.59) reads:

$$\hbar S = \frac{1}{N} \sum_{\mathbf{k}} \int_{-\infty}^{\infty} dE f_+(E) 2 \langle S^z \rangle \delta(E - J \langle s^z \rangle + \frac{1}{2} J^2 \hbar \langle S^z \rangle \Re \chi_0(\mathbf{k}, E)) \quad (5.70)$$

Since it describes higher order effects in the magnetization $\langle S^z \rangle$, the E -dependence of $\chi_0(\mathbf{k}, E)$ within the δ -function can also be neglected. Finally, the fact that $k_B T_C$ is much higher than the magnon energies²⁰, allows a linearization of the exponential in the Bose distribution function $f_+(E)$. In combination one obtains the following expression for T_C :

$$k_B T_C = J^2 \hbar^2 \left\{ \frac{4}{NS} \sum_{\mathbf{k}} \frac{1}{\Re \chi_0(\mathbf{k}, 0) - \Re \chi_0(\mathbf{0}, 0)} \right\}^{-1}, \quad (5.71)$$

where $\langle s^z \rangle$ has been given in terms of $\Re \chi(\mathbf{0}, 0)$ and all contributions are understood to be taken for $\langle S^z \rangle = 0$. Since it does not include any further approximation, (5.71) is apparently the exact expression for the Curie temperature within the RPA. The same expression has been derived, but not evaluated, by Sigrist et al. [153].²¹ Furthermore, it is worth mentioning, that a structurally identical result is obtained with the Rudermann-Kittel-Kasuya-Yosida (RKKY) theory (2.35). The second order perturbation theory for the ground state energy yields Heisenberg exchange parameters (2.35), which are essentially given by $\chi(\mathbf{k}, 0)$ [110].

¹⁹A lot of effort has been invested in an optimization of numerical algorithms for the manifold integrations. This includes adaptive integrations, Cramers-Kronig relations, Sommerfeld expansions, regula falsi etc.. However, due to the analytic character of this work, we have decided not to present these details.

²⁰In contrast to the derivation of (5.65) this is now a rigorous result.

²¹The derivation in [153] is not identical to our formalism and surprisingly their final formula (13) differs by a factor 2 from our result.

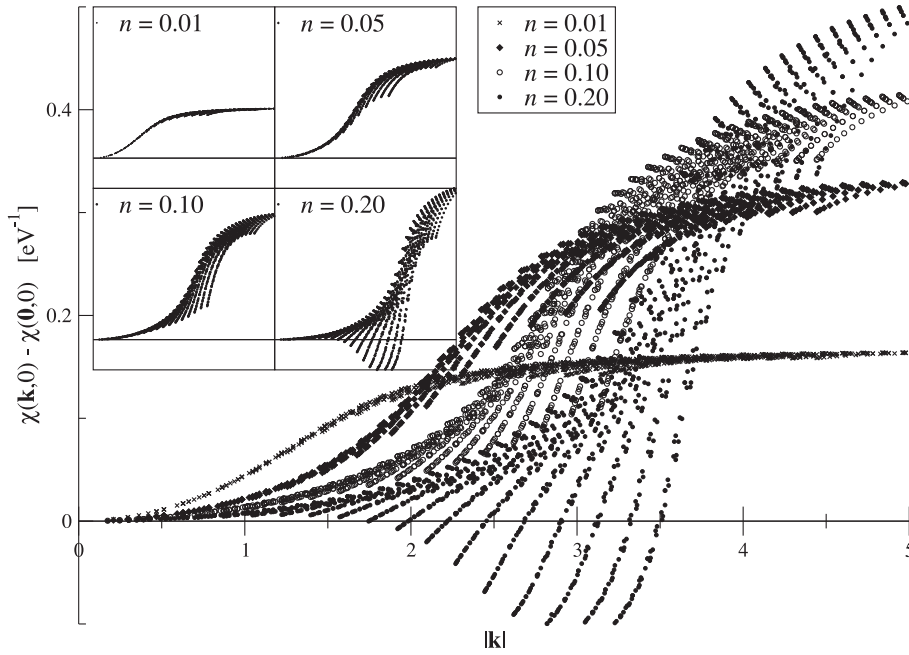


Figure 5.10: Dispersion of $\chi_0(\mathbf{k}, 0)$ as given in the denominator of Eq. (5.71). The \mathbf{k} -dependence for several band occupations has been plotted on top of each other. The insets show the same dispersions separately. The same display format as in Fig. 5.8 has been chosen. The parameters are: $J = 1.0$ eV, $S = 1/2$ and $W = 1.0$ eV for a simple-cubic lattice.

Although a numerical evaluation of Eq. (5.71) includes one energy integration less than the calculation of the magnetization $\langle S^z \rangle$ based on (5.59), the twofold summation over the whole Brillouin zone remains challenging. Fig. 5.10 displays the \mathbf{k} -dependence of the Lindhard function for several band occupations. For $n = 0.01$ the spectrum is almost isotropic. With increasing n the stiffness constant decreases; for \mathbf{k} further away from the Γ -point the Lindhard function increases and the dispersion becomes less isotropic. The last point is the reason why for $n > 0.12$ the value of $\chi_0(\mathbf{k}, 0)$ becomes negative in the vicinity of the X-point.²² As a consequence the sum (5.71) has diverging contributions.

In Fig. 5.9b the Curie temperature obtained with Eq. (5.71) is plotted as a function of the band occupation (solid lines). In the region of small n we note a steep increase of T_C . The maximum Curie temperature is obtained at $n \approx 0.03$. If the number of conduction electrons is increased further, a fast reduction of the phase transition temperature is observed. The behaviour shows strong deviations from the n -dependence of T_C as obtained using Eq. (5.65) based on spin wave theory (dashed line in Fig. 5.9b). This observation seems to be in particular relevant in the current discussion of diluted magnetic semiconductors, where some authors [175, 13] rely on the T_C -formula (5.65).

Furthermore, Fig. 5.9b can be compared to results obtained for the conventional RKKY theory by Santos et al. [116]. For small band occupations there is an excellent qualitative agreement. However, for values of n above the maximum T_C there are consider-

²²Contrary to the discussion on negative spectral densities (p. 106) the negative values reported here are not in conflict with analytical requirements for the Green's function.

able differences. Calculations for the conventional RKKY theory predict a J -independent critical band occupation $n_c \approx 0.13$ above which ferromagnetism is not allowed. This result is not confirmed by our calculations. The discrepancy is certainly due to different numerical techniques. Santos et al. evaluated the RKKY theory in real space. Heisenberg exchange integrals $J_{ij}^{(\text{RKKY})}$ for many shells of neighbours were implemented in the program. However, the number of shells has to be truncated and the question of convergence cannot be answered. Such a truncation is not necessary for a \mathbf{k} -summation over the whole Brillouin zone. Instead the above mentioned divergencies, limit the accuracy of the integrations. This is also the reason, why results for $n > 0.25$ are not presented in Fig. 5.9b.

Nevertheless, at least for $n < 0.12$ the numerical evaluation of (5.71) does yield reliable results. An impressive argument in favour of this remark comes from a comparison of Figs. 5.9a and 5.9b. The figure on the left hand side has been calculated for $n = 0.1$. This band occupation has been marked by a dotted line in the figure on the right hand side. One can readily convince oneself, that the obtained Curie temperatures, based on Eq. (5.71) are in very good agreement with the estimated values from magnetization curves based on (5.59). This is true for all J considered. In turn one concludes, that also the magnetization curves yield a J^2 -dependence of the Curie temperature.

Combination with results for the itinerant subsystem

Within the language of the POM the RPA formula can be derived based on a one-dimensional basis for the level of description, a memory matrix where the dynamics is governed by the mean-field Liouvillian and consequent mean-field decoupling of all correlation functions. The application of exactly the same procedure to the itinerant subsystem has lead to the expression for the second order perturbation theory (4.85). Hence, we were successful in developing a formalism, that can treat both subsystems on the same footing.

A further step would be a combination of these two theories into a self-consistent iteration scheme. The itinerant Green's function enters the RPA formula via $\langle \hat{n}_{\mathbf{q}\sigma} \rangle$. In all previous calculations of this section, this expectation value has been evaluated by applying the spectral theorem to a mean-field Green's function. It is a natural extension to use the SOPT Green's function instead. Going one step further, one could even apply the result of the MPT.

The outcome of this procedure is illustrated in Fig. 5.11. For comparison, the density of states and the spin wave dispersion obtained using a mean-field self-energy are presented again in the first row. The magnetization $\langle S^z \rangle$ varies from saturation to $\langle S^z \rangle = 0.1$. In contrast to Fig. 5.7 the set of parameters has been chosen such that the spin excitation energies remain positive. As a consequence the dispersion lines are smooth throughout the whole Brillouin zone. The most pronounced effects appear at the Γ -point.

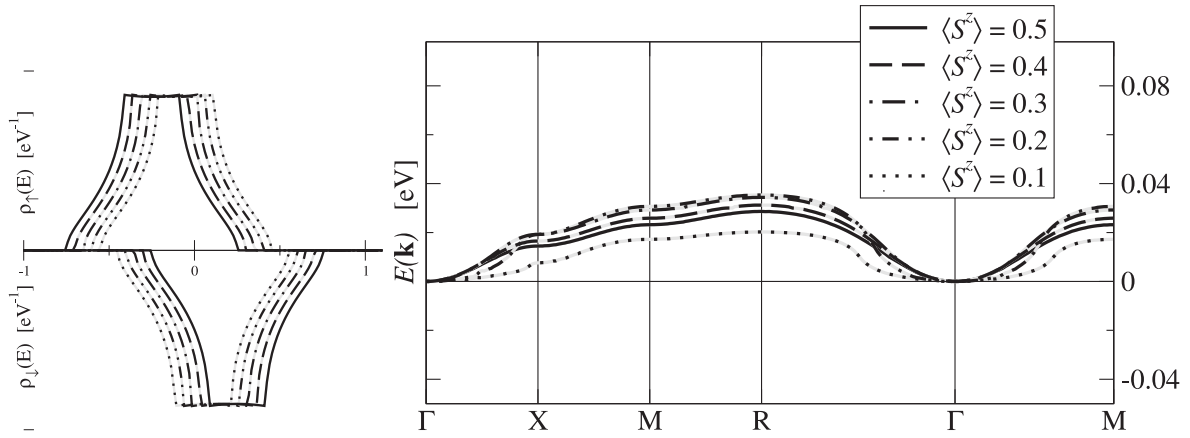
In the second row the results of a self-consistent SOPT are presented for exactly the same set of parameters. The spin wave dispersions differ a lot from those above. Already for $\langle S^z \rangle = 0.5$ the modified QDOS, in particular the scattering part for \downarrow -electrons, has a strong influence on magnon dispersions. Within a wide region centered around the Γ -point a harmonic behaviour is observed. The stiffness constant is much larger than for the mean-field input. This yields rather large magnon excitation energies, which are not

relevant for the thermodynamics of the system. Between the local minima at the Γ -point, the M -point and the R -point the dispersion shows sharp peaks. If the magnetization is lowered, the principle structure of the dispersion remains unchanged. The harmonic region is reduced and the excitations energies are shifted to lower values in the remaining part of the Brillouin zone. A qualitatively new and decisive characteristic is the large region of the Brillouin zone for which we observe negative excitation energies. This feature is not any more limited to certain parameter configurations. On the contrary, as soon as the magnetization is sufficiently low, we observe negative magnon energies for all coupling strengths and band occupations.

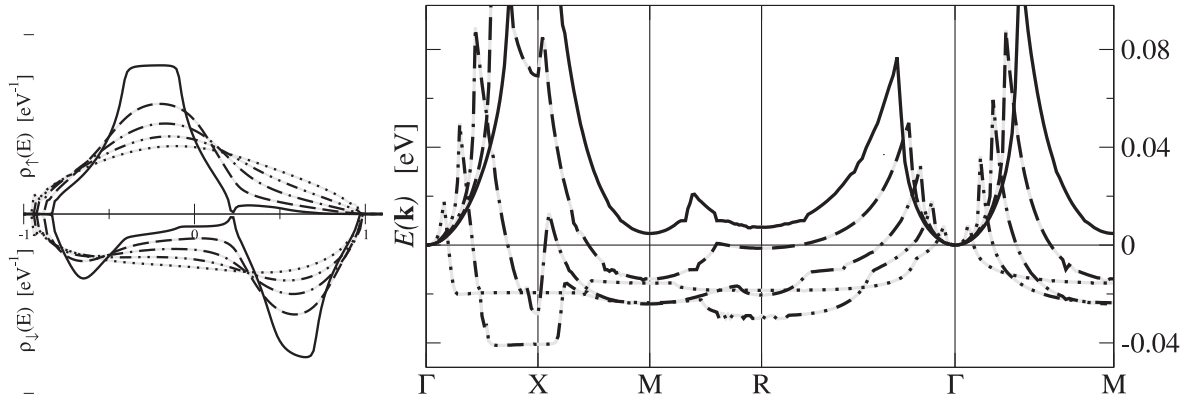
The usage of the MPT instead of SOPT (third row in Fig. 5.11) does not yield significant differences in the spin wave dispersion. For $n = 0.1$ the latter is determined by the lower edge of the QDOS. Here, the differences between MPT and SOPT are negligible as compared to the mean-field QDOS. Only for $\langle S^z \rangle = 0.5$ does the MPT show small deviations from the SOPT, which result in much lower peaks in the spin wave dispersion. The MPT also shows large regions of the Brillouin zone with negative magnon energies.

As discussed above, such a behaviour is not consistent with analytical properties of the RPA. However, for the proof of negative spectral densities relation (5.69) is based on the condition of a mean-field self-energy. This seems to be a general property of the RPA: It is designed for a mean-field input from the conduction electron subsystem. The spin wave dispersion reacts very sensitively to a change of this self-energy. Since the derivation of the RPA with the POM revealed the necessity of a mean-field decoupling of all correlation functions, this observation is perhaps not surprising. A more advanced expression for the self-energy for $\langle \hat{n}_{\mathbf{k}\sigma} \rangle$ would imply, that not all correlations functions are treated on the same footing. In chapter 4 we have already noticed that such an inconsistency yields unphysical results. In conclusion, it can be stated that an improvement of a decoupling theory, which only affects a few correlation functions, does also not work for the RPA.

RPA with mean-field self-energy (4.76):



RPA with self-energy of second order perturbation theory (4.85):



RPA with self-energy of modified perturbation theory (4.96):

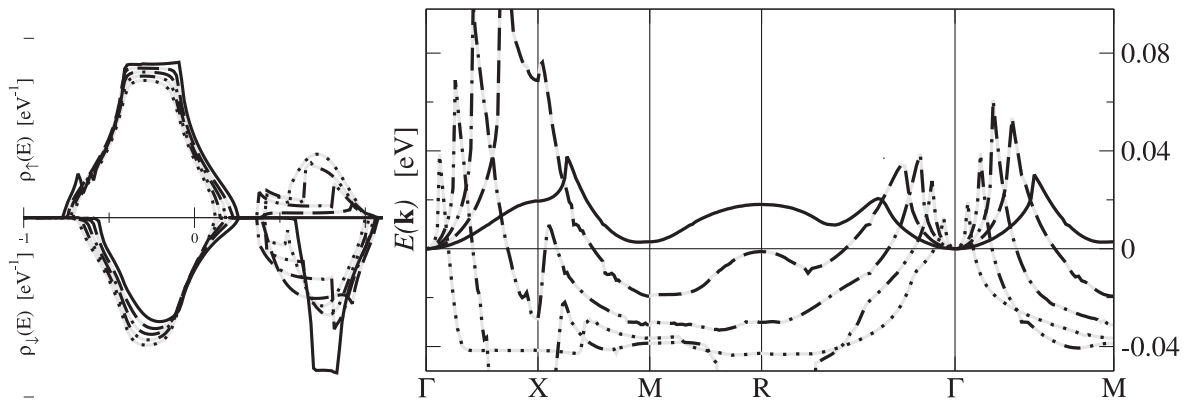


Figure 5.11: Comparison of the spin wave dispersion for several electronic self-energies. The left column shows the densities of states related to the approximation of the itinerant subsystem. In the right column the corresponding spin excitation energies are displayed. For both cases $\langle S^z \rangle$ has been varied. The parameters are: $J = 1.0$ eV, $n = 0.1$, $S = 1/2$ and $W = 1.0$ eV for a simple-cubic lattice.

Chapter 6

Concluding remarks

In the first chapter, we have stated the twofold intention of our research. On the one hand, we were interested in an assessment of the projection-operator method as a new approach to the Kondo-lattice model. On the other hand, we wanted to investigate analytical properties of this model. After explaining the model (Chap. 2) and the method (Chap. 3), we applied the POM to the subsystem of itinerant carriers (Chap. 4) and the subsystem of local moments (Chap. 5). Throughout this thesis all considerations were guided by the intentions mentioned above. Therefore, the conclusions, which are drawn in this chapter, are also given from these two perspectives. Afterwards, suggestions for further investigations in this field will be given.

6.1 Assessment of the POM

The projection-operator method (POM) fulfills almost all expectations, which have been raised at the beginning of this thesis. First of all, we wanted to have a controllable approximation scheme. This requirement is automatically met by the philosophy of mapping the dynamics of the system under investigation onto a relevant Liouville subspace, called the level of description. It ensures, that all dynamic ingredients of the model are treated equally. This is an advantage as compared to decoupling techniques such as the MCDA (p. 15f), which apply different approximations to different types of higher-order Green's functions. Furthermore, we have shown (p. 52ff), that a straightforward choice of subspace basis elements yields an expression for the self-energy, which is exact to second order in the coupling constant.

Since the focus of the POM is the memory matrix, this method directly addresses the self-energy rather than the Green's function itself. The POM shares this property with diagrammatic perturbation theory, but it is not a feature of decoupling techniques. An advantage can be seen most clearly in the context of our modified perturbation theory (p. 60ff). By construction, any approximation of the memory matrix automatically fulfills the first three moments of the spectral density. This is due to the fact that each coefficient of the high-energy expansion of the self-energy, provided in (2.22), already contains a sum of spectral moments. The property is similar to cumulant expansions and the linked cluster theorem for Feynman diagrams.

Another advantage of the POM has been demonstrated in the context of the ferromagnetically saturated semiconductor (Sec. 4.1): One has a variety of possibilities to apply the POM. This includes the choice of a level of description, its extension in several steps and also the determination of expressions within a level of description. For the exactly soluble limit mentioned above we have first presented a strategy (p. 41f) without any approximations. Secondly, we were able to provide a Taylor expansion of the exact self-energy by rearranging sums (p. 41ff). Furthermore, the restriction of the full Liouvillian in the denominator of the memory matrix to its mean-field part has been introduced (p. 45f). Finally, the concept of a two-dimensional basis of the relevant Liouville subspace has been explained (p. 47). In particular, the approximations suggested in strategies III and IV are important for the investigation of arbitrary parameter configurations.

Within this thesis we have mainly presented calculations, that apply the strategy of a restricted Liouvillian to the full Kondo lattice. The reason for this choice is our interest in a weak-coupling theory. The neglect of the interaction part of the Liouvillian in its denominator (p. 52f and p. 84f), guarantees that the memory matrix is exact to second order in the coupling strength. Since this strategy implies the summation of an infinite geometric series, it is not the simplest approach. For the subsystem of itinerant electrons it has the advantage, that a lot of the dynamics of the KLM is included in the self-energy via (energy-dependent) propagators. This feature lead us to hope that the importance of correlation functions, involved in the expression for the Green's function, is reduced.

Of course, instead of summing up an infinite geometric series, one could evaluate many terms of the infinite continued fraction for the memory matrix. Within the POM this is an alternative strategy and is, similar to the evaluation of spectral moments (in a spectral density approach), always possible, at least in principle. As a consequence, many more correlation functions have to be considered and the dynamics cannot be expressed in terms of propagators any more. For these reasons, our calculations based on this strategy were not very promising and did not enter this thesis. Nevertheless, it is worthwhile to perform further investigations in this direction.

The discussion brings us to a decisive conceptual difficulty of the POM: The susceptibility matrix, the frequency matrix and the memory matrix contain correlation functions. The POM does not provide an inherent recipe for determining these static quantities. One has the possibility to increase the basis such that the spectral theorem can be applied to several Green's functions. If this is not wanted, the correlation functions have to be evaluated independently. The POM shares this feature with all other equation-of-motion approaches for Green's functions, since it is based on the Mori equations (3.13). We have mentioned an approach by Becker and Fulde to overcome this shortcoming by treating static values in the same way as dynamic entities, using Liouville scalar products in terms of cumulants (p. 30). The application goes beyond the scope of this thesis, but it is recommended as for further research. For consistency and simplicity, we have mainly used mean-field expectation values in our considerations. Furthermore, an extended version based on the spectral theorem (Sec. 5.2) has been evaluated.

Our goal of treating both subsystems of the Kondo-lattice model similarly is connected to the issue of correlation functions. This is due to the fact that the itinerant subsystem is strongly influenced by the magnetization of localized electrons $\langle S^z \rangle$. In turn, the localized subsystem depends on the band occupation $\langle \hat{n}_\sigma \rangle$. Hence, the one-electron and the one-

magnon Green's function need to be evaluated. It is an important advantage of the POM, that its application is not restricted to one of the subsystems.

Indeed, performing the same kind of restriction of the Liouvillian within the memory matrix we successfully obtained non-trivial results for the one-electron Green's function (Sec. 4.3) as well as for the one-magnon Green's function (Sec. 5.1). Consequently, the quality of the memory-matrix with respect to the coupling strength is the same for both. The interesting physical properties derived from these results will be summarized in Sec. 6.2.

A shortcoming of the approach is related to the fact that the correlation functions $\langle S^z \hat{n}_\sigma \rangle$ and $\langle S^\sigma c_{-\sigma}^\dagger c_\sigma \rangle$ appear separately in the equations. Therefore, the determination of their sum, accessible from the one-particle Green's function, is not sufficient. This is in contrast, e.g., to the interpolating self-energy approach of Nolting et al. (p. 14).

However, a more serious problem is an apparent inconsistency in using at the same time a decoupling procedure for several correlation functions and an advanced theory for $\langle \hat{n}_\sigma \rangle$. We were confronted with this fact in the context of the random-phase approximation (p. 109f). The decoupling is necessary for managing the emerging expressions. On the other hand, the correlation function $\langle \hat{n}_\sigma \rangle$ is the only possibility for incorporating higher-order coupling effects of the conduction band into the physics of local moments. The combination has led to negative magnon dispersions. We argue, that this feature is an artifact of the applied theory, rather than being related to physical properties of the KLM.

In Sec. 5.2 we have suggested a modification of the POM, that allows for an advanced evaluation of correlation functions. By extending the basis of the level of description to two dimensions, we were able to derive all correlation functions self-consistently from the respective Green's functions, using the spectral theorem. This demonstrates that the POM is capable of treating correlation functions as accurate as standard equation-of-motion approaches. In fact, we have highlighted the close relationship to decoupling techniques (p. 96), if the contribution of the two-dimensional memory matrix is neglected. It is worth mentioning that, even with an enlarged level of description, we have always treated the itinerant and the local-moment subsystem separately and obtained a combination of the subsystems via the correlation functions. This is due to the fact that the most convenient choice for the Liouville scalar product differs in both subsystems, since the one-particle excitations belong to different (Fermi and Bose) statistics. Nevertheless, for further investigations it is worthwhile to study an approach that resorts to a single level of description, despite of these differences.

When applying the POM to the KLM, we obtained the impression that it is a very compact formalism, as compared to the decoupling techniques for example. Despite all variety, this limits the diversity of treating certain dynamical functions within the formalism. At the beginning of this section we have mentioned this property as an advantage in terms of controllability. At the same time, it complicates the adjustment to physical situations. Therefore, it is much more difficult to obtain the exact solution of the limit of the ferromagnetically saturated semiconductor within the POM compared to solving the eigenvalue problem, for example.

To summarize this part, we can state that the POM comes into its own when being applied to the KLM. It combines advantages of the decoupling techniques and the diagrammatic perturbation theory. Therefore, it allows insight into the physics of the KLM,

which has not been possible before with other methods. However, the major problem of treating the static quantities within the same theory has not been resolved by this method. This drastically limits the success of an application of the POM.

6.2 Weak-coupling results for the KLM

Since diluted magnetic semiconductors became a hot topic in solid state physics, the Kondo-lattice model has been used in hundreds of publications for a theoretical explanation of magnetic phenomena in these materials. However, in most of these works the physics of the model is either mapped onto the Heisenberg model using a conventional RKKY theory, or it is treated in a mean-field approximation. Both approaches are weak-coupling theories. With this thesis we have addressed the same limit, but we go beyond these theories. The corrections obtained are highly relevant for physical properties of materials concerned.

For the itinerant subsystem the mean-field result is just the first step of the POM. Higher order effects are included in the memory matrix (4.84), which has been constructed such that it is exact to second order in the coupling strength. The analytic structure of this expression revealed a strong influence of these higher-order contributions. In contrast to a mean-field theory, the one-electron excitations depend on the current state of all other electrons. Moreover, the magnon dispersions of the subsystem of localized spins are relevant for conduction electrons, too.

Accordingly, strong correlation effects have been observed in the quasiparticle density of states (p. 55). Already for moderate values of the coupling strength, we have noticed a substantial broadening and a two-peak structure of the QDOS for \downarrow -electrons. For non-zero band occupations also \uparrow -electrons experience correlation effects. With rising temperature a considerable deformation of the QDOS and a redistribution of spectral weight have been obtained (p. 57). The results have very little in common with a mean-field shift of the free density of states. However, there are qualitative similarities to the MCDA (p. 15ff). This holds even without using a fit to limiting cases such as the magnetic polaron or the atomic limit. Therefore, we can conclude that the essential physics predicted by this decoupling approach is confirmed by second-order perturbation theory (SOPT).

We have also addressed the question of 100% polarized conduction electrons (p. 57f), which is interesting for spintronics applications. From conventional SOPT one cannot exclude situations for which all electrons carry the same spin. However, for the more reliable perturbation theory around the Hartree-Fock solution a complete polarization is not allowed for sensible values of the coupling strength (p. 143).

We have not only pointed out that the propagators within the SOPT expression should be refined, we also argued that the structure of the self-energy can be modified in order to incorporate additional physical properties (p. 60ff). The construction of our modified perturbation theory (MPT) is strongly influenced by the limit of the ferromagnetically saturated semiconductor. The atomic limit is included for $n = 0$ and $n = 2$. Furthermore, the high-energy expansion is fulfilled to power E^{-2} . Studying several versions we were able to make an informed statement, which of all approaches is the most reliable one.

In particular, we showed that the calculations have to be performed self-consistently. Furthermore, we mentioned the necessity to treat all correlation functions on the same footing.

All of the suggested approaches had in common that they are correct up to second order in the coupling parameter J . Nevertheless, our improvements are of a non-perturbative nature in the sense that no Taylor series expansion is provided. This is not predominantly due to technical reasons. A pure perturbation theory can probably not explain discontinuities in the physical properties of the model as J changes sign. Additionally, we have pointed out (p. 44) that in the limit of a ferromagnetically saturated semiconductor the J^3 -contribution to the exact self-energy diverges although the sum over all orders yields a finite result.

We have discussed (p. 69ff) several features of the QDOS for the MPT. The crossover from the ferromagnetic to the paramagnetic situation as well as the crossover from an empty conduction band to half-filling has been considered. The results are consistent and sound. Most remarkable, as compared to the MCDA, are strong correlation effects for majority-spin electrons. Even at $T = 0$ K we observed for some parameter constellations a two-band structure for \uparrow -electrons, deviating from a mean-field density of states. This aspect is particularly relevant for combinations of many-body calculations with ab-initio results based on a density functional theory.

Furthermore, we have investigated the subsystem of localized magnetic moments of the KLM without making use of a mapping onto the Heisenberg model. Instead, the magnetization was determined by the magnon dispersion relations, as obtained from the one-magnon Green's function. The POM has been applied for this purpose. The calculations revealed a couple of analytical peculiarities of the KLM, which, to the best of our knowledge, have not been addressed before. We consider the points mentioned below to be essential in order to understand the behaviour of this model and the possibility of ferromagnetic order.

Already the first-order result, the frequency matrix (p. 82), contains the expression $\{2\langle S^z s^z \rangle + \hbar\langle S^\sigma c_{-\sigma}^\dagger c_\sigma \rangle\} / \langle S^z \rangle$, which gives rise to question marks. By definition, the denominator $\langle S^z \rangle$ vanishes at the Curie temperature. By contrast, approximations such as the MCDA in combination with the modified RKKY theory (p. 17f), predict the numerator $2\langle S^z s^z \rangle + \hbar\langle S^\sigma c_{-\sigma}^\dagger c_\sigma \rangle$ to remain finite within the paramagnetic regime. We have shown that within a simple mean-field approach the resulting divergence contradicts the possibility of a phase transition (p. 94). The evaluation of a more advanced approach, using a closed system of correlation functions (p. 91ff), supported this result.

If the local-moment subsystem of the KLM is considered in the literature, the random-phase approximation (RPA) is usually employed (p. 19). Due to the Tyablikov decoupling the sum of correlation functions mentioned above does not cause problems anymore. It remains an open question, whether or not this procedure is a proper physical answer to the difficulties mentioned above or if the RPA circumvents these difficulties by using unjustified assumptions.

The application of the POM does inevitably lead to the RPA formulae, too. This was the result of two different approaches. The evaluation of a two-dimensional frequency matrix (p. 95ff) most clearly illustrated the assumptions on which the RPA is based: It

reduces the relevant dynamics to the excitations $|S_{\mathbf{k}}^{-\sigma})$ and $|c_{\mathbf{q}-\mathbf{k},-\sigma}^\dagger c_{\mathbf{q},\sigma})$, and it mean-field decouples all static expectation values. However, an approach which also includes the memory matrix (p. 81) demonstrates more clearly the drastic simplifications inherent in the RPA. Within this approach the RPA formulae can only be obtained from (5.15), if in addition the correlation functions $\langle S_{\mathbf{q}+\mathbf{k}}^{-\sigma} S_{-\mathbf{q}-\mathbf{k}}^\sigma \rangle$ and $\langle S_{\mathbf{q}+\mathbf{k}}^z S_{-\mathbf{q}-\mathbf{k}}^z \rangle$ are also decoupled into products of two expectation values. Furthermore, one \mathbf{k} -independent contribution to the memory matrix has to be neglected. Due to numerical constraints, these simplifications were also required in our investigations (p. 98ff). It turned out that the computation of the resulting magnon dispersions remains demanding, if one does not resort to a harmonic approximation.

The magnetization curves obtained (p. 106) show clear deviations from a Brillouin function and yield finite transition temperatures. We were able to show that a calculation of the Curie temperature based on spin waves at $T = 0$ K is insufficient. Instead, our T_C -formula has a structure similar to the one obtained from conventional RKKY theory.

Within our approach, a temperature-dependent deformation of magnon dispersions and the influence of the Stoner continuum is incorporated. Both effects reduce the possibility of a ferromagnetic order. More importantly, they are both related to negative magnon energies which arise within the RPA. The existence of negative excitation energies in a spin-wave theory is not surprising. However, we found out that within RPA these energies also imply a negative spectral density. Such a behaviour contradicts analytical properties of retarded Green's functions. Hence, the applicability of the RPA formulae is questionable, at least for certain parameter constellations. Reliable statements on the magnetic behaviour can be made for small band occupations, where softening effects are less important.

Finally, we have investigated the possibility of an extension of the RPA. In the literature the RPA theory is always discussed using uncorrelated conduction electrons. We tried to understand the effect of the electronic self-energy on the local-moment subsystem using the expectation value $\langle \hat{n}_{\mathbf{k}\sigma} \rangle$ for a connection of both subsystems. We observed a dramatic influence of correlations in the conduction band on the magnon dispersion. Using the self-energy of the SOPT and the MPT instead of a mean-field expression leads to clear changes of the spin-wave excitation energies. As a matter of fact, negative magnon energies become a dominant feature for these self-energies. Due to the reason mentioned above, this excludes a further usage of the results. Even worse, it is our impression that the inevitable mean-field decoupling, necessary for the derivation of the RPA, is not consistent with any input which goes beyond a mean-field description. Since the RPA is probably the most advanced theory for a treatment of the localized subsystem of the KLM, which does not resort to the Heisenberg model, which uses quantum-mechanical spins and is still numerically manageable, this is an unwelcomed message for attempts to combine advanced theories for the itinerant and the local-moment subsystem.

6.3 Perspectives

The Kondo-lattice model with its two subsystems of electrons is a challenge from a physical and mathematical point of view. This remains true, even if a very compact and powerful tool such as the projection-operator method is used. This thesis is aimed at presenting a complete overview of the potential of this method in the context of the KLM. However, it is not meant to be an exhaustive study of all many-body effects of the KLM. By contrast, our research has raised new questions, which have not been addressed before.

We believe that it is worthwhile to expend upon some of these questions. From our perspective, the crux of a deeper understanding of the magnetism in materials as described by the KLM is a proper combination of the two subsystems of the Kondo-lattice model. Therefore, an improvement of the RPA theory is essential. A good starting point is our derivation of the one-magnon Green's function based on an infinite series for the memory matrix (5.15). A proper approximation of the two terms, not considered within RPA should be performed in order to study their influence.

Furthermore, our method of obtaining a closed system of Green's functions (p. 91) can definitely be improved by a more systematic handling of the correlation functions and by taking the memory matrix into consideration. It is desirable to treat the two-dimensional basis in the same way as it has been done for the one-dimensional basis of the SOPT. This would resolve the problem of a proper determination of the correlation functions $\langle S^z \hat{n}_{-\sigma} \rangle$ and $\langle S^\sigma c_{-\sigma}^\dagger c_\sigma^\dagger \rangle$, which are essential for the physics of the KLM, since these expressions contribute to the ground state energy. To extend the list of wishes, the two-dimensional basis should be treated such that the two important limits of ferromagnetic saturation and zero bandwidth are automatically included, without using workarounds such as the MPT. Our study of these limits (p. 47 and p. 49f) was very promising, but a straightforward implementation turned out to be not successful. Some new ideas for an effective treatment of the cumbersome equations are required.

We believe that a comprehensive understanding of the Kondo-lattice model implies an understanding of the magnetism in many materials. Nevertheless, there is no doubt that the model has to be adapted to certain experimental situations by incorporating a superexchange interaction or a Hubbard term. For a consideration of the currently highly topical diluted magnetic semiconductors the dilution and disorder of localized spins has to be implemented. Interesting suggestions, how this can be done on the basis of the RPA theory, have been recently put forward by Berciu et al. [65].

Hence, there remains a lot of work to be done for a full understanding of the fascinating physical and mathematical properties of the Kondo-lattice model. For this reason, we would like to conclude this discussion with the same wish which we expressed at the beginning of this work: A greatest success of this thesis would be to inspire someone else by the work presented here into continuing the investigations and answering the outstanding questions.

Bibliography

- [1] W. Ameling. *Laplace-Transformation*. Studienbücher in Naturwissenschaft und Technik. Vieweg, Braunschweig, 1984.
- [2] P. W. Anderson. Localized magnetic states in metals. *Phys. Rev.*, 124:41, 1961.
- [3] P. W. Anderson and H. Hasegawa. Considerations on double exchange. *Phys. Rev.*, 100:675, 1955.
- [4] M. Ya. Antimirov, A. A. Kolyshkin, and R. Vaillancourt. *Applied Integral Transforms*, volume 2 of *CRM monograph series*. Am. Math. Soc. , Providence, Rhode Island, 1993.
- [5] A. Avella, F. Mancini, and R. Hayn. The composite operator method for impurity models. *Acta Phys. Pol. B*, 34:1345, 2003.
- [6] A. Babcenco and M. G. Cottam. Theory of elementary excitations in ferromagnetic semiconductors. *J. Phys. C*, 14:5347, 1981.
- [7] R. A. Bari. Narrow-band expansions in the Hubbard model: A comment. *Phys. Rev. B*, 2:2260, 1970.
- [8] G. Baym and L. P. Kadanoff. Conservation laws and correlation functions. *Phys. Rev.*, 124:287, 1961.
- [9] K. W. Becker and W. Brenig. Cumulant approach to dynamical correlation functions. *Z. Phys. B*, 79:195, 1990.
- [10] K. W. Becker and P. Fulde. Ground-state energy of strongly correlated electronic systems. *Z. Phys. B*, 72:423, 1988.
- [11] K. W. Becker, H. Won, and P. Fulde. Application of a new projection technique to the 2D Heisenberg Hamiltonian. *Z. Phys. B*, 75:335, 1989.
- [12] N. N. Bogoliubov and S. V. Tyablikov. . *Dokl. Akad. Nauk. USSR*, 126:53, 1959.
- [13] G. Bouzerar and T. P. Pareek. Carrier-induced ferromagnetism in diluted magnetic semiconductors. *Phys. Rev. B*, 65:153203, 2002.
- [14] U. Brandt and C. Mielsch. Thermodynamics and correlation functions of the Falicov-Kimball model in large dimensions. *Z. Phys. B*, 75:365, 1989.

- [15] G. Bulk and R. J. Jelitto. A modified perturbation theory: Iterative partitioning of the hamiltonian. *Phys. Lett. A*, 133:231, 1988.
- [16] G. Bulk and R. J. Jelitto. Perturbational treatment of correlation effects in the Hubbard model. *Phys. Rev. B*, 41:413, 1990.
- [17] H. B. Callen. Green function theory of ferromagnetism. *Phys. Rev.*, 130:890, 1963.
- [18] A. Chattopadhyay, A. J. Millis, and S. Das Sarma. Optical spectral weights and the ferromagnetic transition temperature of colossal-magnetoresistance manganites: Relevance of double exchange to real materials. *Phys. Rev. B*, 61:10738, 2000.
- [19] A. Chattopadhyay, A. J. Millis, and S. Das Sarma. T=0 phase diagram of the double-exchange model. *Phys. Rev. B*, 64:012416, 2001.
- [20] P. Dai, H. Y. Hwang, J. Zhang, J. A. Fernandez-Baca, S-W. Cheong, C. Kloc, Y. Tomioka, and Y. Tokura. Magnon damping by magnon-phonon coupling in manganese perovskites. *Phys. Rev. B*, 61:9553, 2000.
- [21] S. Das Sarma, E.H. Hwang, and A. Kaminski. Temperature-dependent magnetization in diluted magnetic semiconductors. *Phys. Rev. B*, 67:155201, 2003.
- [22] R. A. de Groot, F. M. Mueller, P. G. van Engen, and K. H. J. Buschow. New class of materials: Half-metallic ferromagnets. *Phys. Rev. B*, 50:2024, 1983.
- [23] M. Van den Bergh and G. Vertogen. Absence of magnetic phase transition in one- and two-dimensional s-d interaction models. *Phys. Lett. A*, 50:85, 1974.
- [24] T. Dietl, H. Ohno, F. Matsukura, J. Cibert, and D. Ferrand. Zener model description of ferromagnetism in zinc-blende magnetic semiconductors. *Science*, 287:1019, 2000.
- [25] D. M. Edwards. Ferromagnetism and electron-phonon coupling in the manganites. *Adv. Phys.*, 51:1259, 2002.
- [26] D. M. Edwards and J. A. Hertz. The breakdown of Fermi liquid theory in the Hubbard model. *Physica B*, 163:527, 1990.
- [27] D. M. Edwards, A. C. M. Green, and K. Kubo. Electronic structure and resistivity of the double exchange model. *J. Phys. C*, 11:2791, 1999.
- [28] D. M. Esterling. Hubbard model near the atomic limit. *Phys. Rev. B*, 2:4686, 1970.
- [29] D. M. Esterling and R. V. Lange. Degenerate mass operator perturbation theory of the Hubbard model. *Rev. Mod. Phys.*, 40:796, 1968.
- [30] A. J. Fedro and R. S. Wilson. New self-consistent many-body perturbation theory: Application to the Hubbard model. *Phys. Rev. B*, 11:12148, 1975.
- [31] J. A. Fernandez-Baca, P. Dai, H. Y. Hwang, C. Kloc, and S-W. Cheong. Evolution of the low-frequency spin dynamics in ferromagnetic manganites. *Phys. Rev. Lett.*, 80:4012, 1998.

-
- [32] A. L. Fetter and J. D. Walecka. *Quantum Field Theory of Many-Particle Systems*. Mc Graw-Hill, New York, 1971.
- [33] E. Fick and G. Sauermann. *The Quantum Statistics of Dynamic Processes*. Springer, Berlin, 1990.
- [34] R. S. Fishman and M. Jarrell. Magnetic susceptibility of the double-exchange model. *Phys. Rev. B*, 67:100403, 2003.
- [35] J. Friedel. On some electrical and magnetic properties of metallic solid solutions. *Can. J. Phys.*, 34:1190, 1956.
- [36] H. Fröhlich. Electrons in lattice fields. *Adv. Phys.*, 3:325, 1954.
- [37] P. Fulde. *Electron Correlations in Molecules and Solids*, volume 100 of *Solid-State Science*. Springer, Berlin, Heidelberg, 1991.
- [38] N. Furukawa. Spin excitation spectrum of $\text{La}_{1-x}\text{A}_x\text{MnO}_3$. *J. Phys. Soc. Jpn.*, 65:1174, 1996.
- [39] N. Furukawa. Thermodynamics of the double exchange system. In T. Kaplan and S. Mahanti, editors, *Physics of Manganites*. Plenum Publishing, New York, 1999.
- [40] W. Gasser, E. Heiner, and K. Elk. *Greensche Funktionen in Festkörper- und Vielteilchenphysik*. Wiley-VCH, Berlin, 2001.
- [41] A. Georges and G. Kotliar. Hubbard model in infinite dimensions. *Phys. Rev. B*, 45:6479, 1992.
- [42] A. Georges, G. Kotliar, W. Krauth, and M. J. Rozenberg. Dynamical mean-field theory of strongly correlated fermion systems and the limit of infinite dimensions. *Rev. Mod. Phys.*, 68:13, 1996.
- [43] B. Giovannini, M. Peter, and S. Koidé. Dynamic effects in paramagnetic resonance of magnetic ions in metals. *Phys. Rev.*, 149:251, 1966.
- [44] N. Grewe and F. Steglich. Heavy fermions. In K. A. Schneider and L. Eyring, editors, *Handbook on the Physics and Chemistry of Rare Earth*, volume 14. Elsevier Science Publishing, Amsterdam, 1991.
- [45] K. Held and D. Vollhardt. Electronic correlations in manganites. *Phys. Rev. Lett.*, 84:5168, 2000.
- [46] J. Hennig. *Grundzustandsphasendiagramm des s-f-Modells*. Diploma thesis, Humboldt-Universität zu Berlin, 2005.
- [47] T. Herrmann and W. Nolting. Magnetism in the single-band Hubbard model. *J. Magn. Magn. Mat.*, 170:253, 1997.
- [48] A. C. Hewson. *The Kondo Problem to Heavy Fermions*. Cambridge University Press, Cambridge, 1993.

- [49] T. Hickel. *Exakte Aussagen zum korrelierten Kondo-Gitter-Modell*. Diploma thesis, Humboldt-Universität zu Berlin, 2001.
- [50] T. Hickel and W. Nolting. Proper weak-coupling approach to the periodic s-d(f) exchange model. *Phys. Rev. B*, 69:085110, 2004.
- [51] T. Hickel, J. Röseler, and W. Nolting. Exact solution of the two-site correlated Kondo-lattice model. *Act. Phys. Pol. B*, 34:1291, 2003.
- [52] T. Hickel, C. Santos, and W. Nolting. The projection-operator approach to the Kondo-lattice model. *J. Magn. Magn. Mat.*, 272:e263, 2004.
- [53] T. Holstein and H. Primakoff. Field dependence of the intrinsic domain magnetization of a ferromagnet. *Phys. Rev.*, 58:1098, 1940.
- [54] J. Hubbard. Electron correlations in narrow energy bands. *Proc. Roy. Soc. A*, 276:238, 1963.
- [55] J. Hubbard. Electron correlations in narrow energy bands, III. an improved solution. *Proc. Roy. Soc. A*, 281:401, 1964.
- [56] H. Y. Hwang, P. Dai, S-W. Cheong, G. Aeppli, D. A. Tennant, and H. A. Mook. Softening and broadening of the zone boundary magnons in $\text{Pr}_{0.63}\text{Sr}_{0.37}\text{MnO}_3$. *Phys. Rev. Lett.*, 80:1316, 1998.
- [57] V. Yu Irkhin and M. I. Katsnelson. On the mean-field theory of magnetically ordered Kondo lattices. *J. Phys. : Condens. Matter*, 2:8715, 1989.
- [58] V. Yu Irkhin and M. I. Katsnelson. Half-metallic ferromagnets. *Phys. Uspekhi*, 37:659, 1994.
- [59] Y. Ishikawa, G. Shirane, and J. A. Tarvin. Magnetic excitations in the weak itinerant ferromagnet MnSi. *Phys. Rev. B*, 16:4956, 1977.
- [60] Yu. A. Izyumov and Yu. N. Skryabin. *Statistical Mechanics of Magnetically Ordered Systems*. Springer, New York, 1988.
- [61] S. Mathi Jaya and W. Nolting. Quasiparticle bandstructure of antiferromagnetic EuTe. *J. Phys. C*, 9:10439, 1997.
- [62] S. Jin, T. H. Tiefel, M. McCormack, R. A. Fastnacht, R. Ramesh, and L. H. Chen. Thousandfold change in resistivity in magnetoresistive La-Ca-Mn-O films. *Science*, 264:413, 1994.
- [63] H. Kajueter and G. Kotliar. New iterative perturbation scheme for lattice models with arbitrary filling. *Phys. Rev. Lett.*, 77:131, 1996.
- [64] Y. Kakehashi and P. Fulde. Coherent potential approximation and projection operators. *Phys. Rev. B*, 69:045101, 2004.

-
- [65] A. Kassaian and M. Berciu. Magnetic susceptibility of diluted magnetic semiconductors at low carrier densities. *Phys. Rev. B*, 71:125203, 2005.
- [66] T. Kasuya. A theory of metallic ferro- and antiferromagnetism on Zener's model. *Prog. Theor. Phys.*, 16:45, 1956.
- [67] G. Khaliullin and R. Kilian. Theory of anomalous magnon softening in ferromagnetic manganites. *Phys. Rev. B*, 61:3494, 2000.
- [68] J. Kienert, C. Santos, and W. Nolting. The correlated Kondo-lattice model. *phys. stat. sol. (b)*, 236:515, 2003.
- [69] R. Kishore. Quasiparticle spectrum of the Hubbard model. *Phys. Rev. B*, 35:6854, 1987.
- [70] E. Kogan and M. Auslender. Paramagnetic-ferromagnetic transition in a double-exchange model. *Phys. Rev. B*, 67:132410, 2003.
- [71] H. Köhler, M. Vojta, and K. Becker. Cumulant approach to the low-temperature thermodynamics of many-body systems. *Phys. Rev. B*, 56:6603, 1997.
- [72] W. Koller, A. Prüll, H. G. Evertz, and W. von der Linden. Uniform hopping approach to the ferromagnetic Kondo model at finite temperature. *Phys. Rev. B*, 67:104432, 2003.
- [73] J. Kondo. Resistance minimum in dilute magnetic alloys. *Progr. Theor. Phys. (Kyoto)*, 32:37, 1964.
- [74] J. König, J. Schliemann, T. Jungwirth, and A. H. MacDonald. Ferromagnetism in (iii,mn)v semiconductors. In D. J. Singh and D. A. Papaconstantopoulos, editors, *Electronic Structure and Magnetism of Complex Materials*. Springer Verlag, Berlin, Heidelberg, 2002.
- [75] J. Kübler, A. R. William, and C. B. Sommers. Formation and coupling of magnetic moments in Heusler alloys. *Phys. Rev. B*, 28:1745, 1983.
- [76] K. Kubo and N. Ohata. A quantum theory of double exchange. i. *J. Phys. Soc. Jpn.*, 33:21, 1972.
- [77] R. Kubo. Generalized cumulant expansion method. *J. Phys. Soc. Jpn.*, 17:1100, 1962.
- [78] D. Langreth. Friedel sum rule for anderson's model of localized impurity states. *Phys. Rev.*, 150:516, 1966.
- [79] S. Legfold. in *Ferromagnetic Materials*, ed. E. P. Wohlfarth, volume 1. North Holland, Amsterdam, 1980.
- [80] P. W. Leung, Z. Liu, E. Manousakis, M. A. Novotny, and P. E. Oppenheimer. Density of states of the two-dimensional Hubbard model on a 4 x 4 lattice. *Phys. Rev. B*, 46:11779, 1992.

- [81] E. H. Lieb. Two theorems on the Hubbard model. *Phys. Rev. Lett.*, 62:1201, 1989.
- [82] J. Lindhard. On the properties of a gas of charged particles. *Medd. Dan. Vid. Selsk.*, 28:No. 8, 1954.
- [83] H.-G. Luo and S.-J. Wang. Moment-conserving decoupling approach for many-body systems. *Phys. Rev. B*, 60:15480, 1999.
- [84] J. M. Luttinger and J. C. Ward. Ground-state energy of a many-fermion system. II. *Phys. Rev.*, 118:1417, 1960.
- [85] G. D. Mahan. *Many-Particle Physics*. Plenum Press, New York and London, 1990.
- [86] F. Mancini, N. B. Perkins, and N. M. Plakida. Spin-wave dispersion softening in the ferromagnetic Kondo lattice model for manganites. *Phys. Lett. A*, 284:286, 2001.
- [87] A. Martin-Rodero, E. Louis, F. Flores, and C. Tejedor. Interpolative solution for the periodic Anderson model of mixed-valence compounds. *Phys. Rev. B*, 33:1814, 1986.
- [88] N. Matsumoto and F. J. Ohkawa. Kondo-lattice in infinite dimensions. *Phys. Rev. B*, 51:4110, 1995.
- [89] B. Mehlig, H. Eskes, R. Hayn, and M. B. J. Meinders. Single-particle spectral density of the Hubbard model. *Phys. Rev. B*, 52:2463, 1995.
- [90] N. D. Mermin and H. Wagner. Absence of ferromagnetism or antiferromagnetism in one- or two-dimensional isotropic heisenberg models. *Phys. Rev. Lett.*, 17:1133, 1966.
- [91] W. Metzner and D. Vollhardt. Correlated lattice fermions in $d = \infty$ dimensions. *Phys. Rev. Lett.*, 62:324, 1989.
- [92] D. Meyer. *Electron correlation effects in ferromagnetic local-moment and intermediate-valence systems*. Dissertation, Humboldt-Universität zu Berlin, 2001.
- [93] D. Meyer and W. Nolting. Dynamical mean-field study of ferromagnetism in the periodic Anderson model. *Phys. Rev. B*, 62:5657, 2000.
- [94] D. Meyer and W. Nolting. Ferromagnetism in the periodic Anderson model: A comparison of spectral density approximation, modified alloy analogy and modified perturbation theory. *Europ. Phys. J. B*, 18:385, 2000.
- [95] D. Meyer, T. Wegner, M. Potthoff, and W. Nolting. The asymmetric single-impurity Anderson model - the modified perturbation theory. *Physica B*, 270:225, 1999.
- [96] D. Meyer, C. Santos, and W. Nolting. Quantum effects in the quasiparticle structure of the (ferromagnetic) Kondo lattice model. *J. Phys. : Condens. Matter*, 13:2531, 2001.

-
- [97] B. Michaelis and A. J. Millis. Dynamical mean-field theory for transition temperature and optics of pseudocubic manganites. *Phys. Rev. B*, 68:115111, 2003.
- [98] T. Minh-Tien. Nonlocal dynamical correlations in the Falicov-Kimball model. *Phys. Rev. B*, 58:R15965, 1998.
- [99] H. Mori. Transport, collective motion, and Brownian motion. *Prog. Theor. Phys.*, 33:432, 1965.
- [100] H. Mori. A continued-fraction representation of the time-correlation functions. *Prog. Theor. Phys.*, 34:399, 1965.
- [101] T. Moriya. *Spin Fluctuations in Itinerant Electron Magnetism*, volume 56 of *Solid-State Sciences*. Springer, Berlin, 1985.
- [102] W. Müller and W. Nolting. Ferromagnetic EuS films: Magnetic stability, electronic structure and magnetic surface states. *Phys. Rev. B*, 69:155425, 2004.
- [103] E. Müller-Hartmann. Correlated fermions on a lattice in high dimensions. *Z. Phys. B*, 74:507, 1989.
- [104] E. Müller-Hartmann. The Hubbard model at high dimensions: some exact results and weak coupling theory. *Z. Phys. B*, 76:211, 1989.
- [105] S. Nakajima. On quantum theory of transport phenomena. *Prog. Theor. Phys.*, 20:948, 1958.
- [106] W. Nolting. *Statistische Physik*, volume 6 of *Grundkurs Theoretische Physik*. Springer, Berlin, Heidelberg, 2002.
- [107] W. Nolting. *Viel-Teilchen-Theorie*, volume 7 of *Grundkurs Theoretische Physik*. Springer, Berlin, Heidelberg, 2002.
- [108] W. Nolting. Methode der Spektralmomente für das Hubbard-Modell eines schmalen s-Bandes. *Z. Phys.*, 225:25, 1972.
- [109] W. Nolting. Theory of ferromagnetic semiconductors. *phys. stat. sol. (b)*, 96:11, 1979.
- [110] W. Nolting. *Quantentheorie des Magnetismus 1+2*. B. G. Teubner, Stuttgart, 1986.
- [111] W. Nolting and W. Borgiel. Band magnetism in the Hubbard model. *Phys. Rev. B*, 39:6962, 1989.
- [112] W. Nolting and M. Matlak. Complete analytical solution for the zero bandwidth s-f model. *phys. stat. sol. (b)*, 123:155, 1984.
- [113] W. Nolting, S. Mathi Jaya, and S. Rex. Magnetic polaron in ferro- and antiferromagnetic semiconductors. *Phys. Rev. B*, 54:14455, 1996.

- [114] W. Nolting, S. Rex, and S. Mathi Jaya. Magnetism and electronic structure of a local moment ferromagnet. *J. Phys. : Condens. Matter*, 9:1301, 1997.
- [115] W. Nolting, G. G. Reddy, A. Ramakanth, and D. Meyer. Low-density approach to the Kondo-lattice model. *Phys. Rev. B*, 64:155109, 2001.
- [116] W. Nolting, W. Müller, C. Santos, and P. Sinjukow. Local moment systems: magnetism and electronic correlations. In A. Avella, R. Citro, C. Noce, and M. Salerno, editors, *Highlights in Condensed Matter Physics*, volume 695. AIP Conference Proceedings, Melville, New York, 2003.
- [117] W. Nolting, G. G. Reddy, A. Ramakanth, D. Meyer, and J. Kienert. Self-energy approach to the correlated Kondo lattice model. *Phys. Rev. B*, 67:024426, 2003.
- [118] W. Nolting, T. Hickel, A. Ramakanth, G. G. Reddy, and M. Lipowczan. Carrier induced ferromagnetism in concentrated and diluted local-moment systems. *Phys. Rev. B*, 70:075207, 2004.
- [119] W. Nolting, T. Hickel, and C. Santos. Carrier induced ferromagnetism in concentrated and diluted local-moment systems. In M. Donath and W. Nolting, editors, *Lecture Notes on Physics* (to be printed). Springer, Berlin, 2005.
- [120] H. Ohno. Toward functional spintronics. *Science*, 291:840, 2001.
- [121] H. Ohno. Making nonmagnetic semiconductors ferromagnetic. *Science*, 281:951, 1998.
- [122] H. Ohno. Properties of ferromagnetic III-V semiconductors. *J. Magn. Magn. Mat.*, 200:110, 1999.
- [123] H. Ohno, D. Chiba, F. Matsukura, T. Omiya, E. Abe, T. Dietl, Y. Ohno, and K. Ohtani. Electric-field control of ferromagnetism. *Nature*, 408:944, 2000.
- [124] T. Okabe. Spin wave and stability of the double exchange ferromagnet. *Prog. Theor. Phys.*, 97:21, 1997.
- [125] S. Onoda and M. Imada. Operator projection method applied to the single-particle Green's function in the Hubbard model. *J. Phys. Soc. Jpn.*, 70:632, 2001.
- [126] J.-H. Park, E. Vescovo, H.-J. Kim, C. Kwon, R. Ramesh, and T. Venkatesan. Direct evidence for a half-metallic ferromagnet. *Nature*, 392:794, 1998.
- [127] N. B. Perkins and N. M. Plakida. Spin dynamics in the generalized ferromagnetic Kondo model for manganites. *Theor. Math. Phys.*, 120:1182, 1999.
- [128] T. G. Perring, G. Aeppli, S. M. Hayden, S. A. Carter, J. P. Remeika, and S-W. Cheong. Spin waves throughout the Brillouin zone of a double-exchange ferromagnet. *Phys. Rev. Lett.*, 77:711, 1996.

-
- [129] M. Potthoff, T. Wegner, and W. Nolting. Interpolating self-energy of the infinite-dimensional Hubbard model: Modifying the iterative perturbation theory. *Phys. Rev. B*, 55:16132, 1997.
- [130] M. Potthoff, T. Herrmann, T. Wegner, and W. Nolting. The moment sum rule and its consequences for ferromagnetism in the Hubbard model. *phys. stat. sol. (b)*, 210:199, 1998.
- [131] T. Pruschke, M. Jarrell, and J. K. Freericks. Anomalous normal-state properties of high- t_c superconductors: intrinsic properties of strongly correlated electron systems? *Adv. Phys.*, 44:187, 1995.
- [132] J. Rau and B. Müller. From reversible quantum microdynamics to irreversible quantum transport. *Phys. Rep.*, 272:1, 1996.
- [133] S. Rex, V. Eyert, and W. Nolting. Temperature-dependent quasiparticle bandstructure of ferromagnetic gadolinium. *J. Magn. Magn. Mat.*, 192:529, 1999.
- [134] L. M. Roth. Electron correlation in narrow energy bands. i. the two-pole approximation in a narrow s band. *Phys. Rev.*, 184:451, 1969.
- [135] M. J. Rozenberg, G. Kotliar, and X. Y. Zhang. Mott-hubbard transition in infinite dimensions. II. *Phys. Rev. B*, 49:10181, 1994.
- [136] M. J. Rozenberg, G. Kotliar, H. Kajueter, G. A. Thomas, D. H. Rapkine, J. M. Honig, and P. Metcalf. Optical conductivity in Mott-Hubbard-systems. *Phys. Rev. Lett.*, 75:105, 1995.
- [137] Yu. Rudavsky, G. Ponedilok, and L. Dorosh. Long-wave spin excitations of crystalline s - d models. *Cond. Matt. Phys.*, 1:145, 1998.
- [138] M. A. Rudermann and C. Kittel. Indirect exchange coupling of nuclear magnetic moments by conduction electrons. *Phys. Rev.*, 96:99, 1954.
- [139] C. Santos. *private communication*, 2004.
- [140] C. Santos. *Temperaturabhängige elektronische Struktur und Magnetismus von metallischen Systemen mit lokalisierten Momenten: Anwendung auf Gadolinium*. Dissertation, Humboldt-Universität zu Berlin, 2005.
- [141] C. Santos and W. Nolting. Ferromagnetism in the Kondo-lattice model. *Phys. Rev. B*, 65:144419, 2002.
- [142] C. Santos and W. Nolting. Erratum: Ferromagnetism in the Kondo-lattice model. *Phys. Rev. B*, 66:019901(E), 2002.
- [143] C. Santos, V. Eyert, and W. Nolting. Ferromagnetism and temperature-dependent electronic structure of hcp gadolinium. *Phys. Rev. B*, 69:214412, 2004.

- [144] R. Schiller and W. Nolting. Temperature-dependent band structure of bulk EuO. *Solid State Commun.*, 118:173, 2001.
- [145] R. Schiller and W. Nolting. Prediction of a surface state and a related surface insulator-metal transition for the (100) surface of stoichiometric EuO. *Phys. Rev. Lett.*, 86:3847, 2001.
- [146] J. R. Schrieffer and P. A. Wolff. Relation between the Anderson and Kondo hamiltonians. *Phys. Rev.*, 149:491, 1966.
- [147] H. Schweitzer and G. Czycholl. Selfconsistent perturbational approach to the heavy fermion problem in high dimensions. *Z. Phys. B*, 79:377, 1990.
- [148] H. Schweitzer and G. Czycholl. Weak-coupling treatment of the Hubbard model in one, two and three dimensions. *Z. Phys. B*, 83:93, 1991.
- [149] B. S. Shastry and D. C. Mattis. Theory of the magnetic polaron. *Phys. Rev. B*, 24:5340, 1981.
- [150] S. Q. Shen. Total spin and antiferromagnetic correlation in the Kondo model. *Phys. Rev. B*, 53:14252, 1996.
- [151] M. Sigrist, H. Tsunetsugu, and K. Ueda. Rigorous results for the one-electron Kondo-lattice model. *Phys. Rev. Lett.*, 67:2211, 1991.
- [152] M. Sigrist, H. Tsunetsugu, K. Ueda, and T. M. Rice. Ferromagnetism in the strong-coupling regime of the one-dimensional Kondo-lattice model. *Phys. Rev. B*, 46:13838, 1992.
- [153] M. Sigrist, K. Ueda, and H. Tsunetsugu. Ferromagnetism of the Kondo lattice in the low-carrier concentration limit. *Phys. Rev. B*, 46:175, 1992.
- [154] P. Sinjukow and W. Nolting. Exact mapping of periodic Anderson model to Kondo lattice model. *Phys. Rev. B*, 65:212303, 2002.
- [155] I. V. Solovyev and K. Terakura. Zone boundary softening of the spin-wave dispersion in doped ferromagnetic manganites. *Phys. Rev. Lett.*, 82:2959, 1999.
- [156] H. Tasaki. The Hubbard model - an introduction and selected rigorous results. *J. Phys. : Condens. Matter*, 10:4353, 1998.
- [157] C. Timm, F. von Oppen, and F. Höfling. Magnetic susceptibilities of diluted magnetic semiconductors and anomalous Hall-voltage noise. *Phys. Rev. B*, 69:115202, 2004.
- [158] H. Tsunetsugu. Rigorous results for half-filled Kondo lattices. *Phys. Rev. B*, 55:3042, 1997.
- [159] H. Tsunetsugu, M. Sigrist, and K. Ueda. The ground-state phase diagram of the one-dimensional Kondo lattice model. *Rev. Mod. Phys.*, 69:809, 1997.

-
- [160] A. M. Tsvelik. Semiclassical solution of one dimensional model of Kondo insulator. *Phys. Rev. Lett.*, 72:1048, 1994.
- [161] D. Villani, E. Lange, A. Avella, and G. Kotliar. Two-scale analysis of the $SU(N)$ Kondo model. *Phys. Rev. Lett.*, 85:804, 2000.
- [162] M. Vogt. *Magnonen im ferromagnetischen Kondo-Gitter Modell*. Diploma thesis, Department of Physics, Humboldt University Berlin, 1999.
- [163] M. Vogt, C. Santos, and W. Nolting. Magnons in the ferromagnetic Kondo-lattice model. *phys. stat. sol. (b)*, 223:679, 2001.
- [164] S. V. Vonsovskij and Yu. A. Izyumov. Electronic theory of transition metals II. . *Usp. Fiz. Nauk*, 78:3, 1962.
- [165] P. Wachter. Europium chalcogenides: EuO, EuS, EuSe and EuTe. In K. A. Schneider and L. Eyring, editors, *Handbook on the Physics and Chemistry of Rare Earth*, volume 2. Elsevier Science Publishing, Amsterdam, 1979.
- [166] D. F. Wang and C. Gruber. Exactly solvable Kondo-lattice model. *Phys. Rev. B*, 51:7476, 1995.
- [167] X. Wang. Theory of spin waves in a ferromagnetic Kondo lattice model. *Phys. Rev. B*, 57:7427, 1998.
- [168] P. J. Webster, K. R. A. Ziebeck, S. L. Town, and M. S. Peak. Magnetic order and phase transformation in Ni_2MnGa . *Phil. Mag.*, 49:295, 1984.
- [169] S. Wermbter and G. Czycholl. The metal-insulator transition and Fermi-liquid behaviour in the infinite-dimensional Hubbard model. *J. Phys. : Condens. Matter*, 6:5439, 1994.
- [170] S. A. Wolf, D. D. Awschalom, R. A. Buhrmann, J. M. Daughton, S. von Molnár, M. L. Roukes, A. Y. Chtchelkanova, and D. M. Treger. Spintronics: A spin-based electronics vision of the future. *Science*, 294:1488, 2001.
- [171] R. B. Woolsey and R. M. White. Electron-magnon interaction in ferromagnetic semiconductors. *Phys. Rev. B*, 1:4474, 1970.
- [172] K. Yamada. Perturbation expansion for the Anderson Hamiltonian II. *Prog. Theor. Phys.*, 53:970, 1975.
- [173] K. Yamada and K. Yosida. Perturbation expansion for the Anderson Hamiltonian. *Prog. Theor. Phys. Suppl.*, 46:244, 1970.
- [174] K. Yamada and K. Yosida. Perturbation expansion for the Anderson Hamiltonian III. *Prog. Theor. Phys.*, 53:12, 1975.
- [175] M.-F. Yang, S.-J. Sun, and M.-C. Chang. Comment on "theory of diluted magnetic semiconductor ferromagnetism". *Phys. Rev. Lett.*, 86:5636, 2001.

- [176] J. M. Yeomans. *Statistical Mechanics of Phase Transitions*. Clarendon, Oxford, 1992.
- [177] K. Yosida. Magnetic properties of Cu-Mn alloys. *Phys. Rev.*, 106:893, 1957.
- [178] S. Yunoki, J. Hu, A. L. Malvezzi, A. Moreo, N. Furukawa, and E. Dagotto. Phase separation in electronic models for manganites. *Phys. Rev. Lett.*, 80:845, 1998.
- [179] C. Zener. Interaction between the d shells in the transition metals. *Phys. Rev.*, 81:440, 1951.
- [180] C. Zener. Interaction between the d shells in the transition metals. II. ferromagnetic compounds of manganese with perovskite structure. *Phys. Rev.*, 82:403, 1951.
- [181] X. Y. Zhang, M. J. Rozenberg, and G. Kotliar. Mott transition in the $d = \infty$ Hubbard model at zero temperature. *Phys. Rev. Lett.*, 70:1666, 1993.
- [182] R. Zwanzig. Ensemble method in the theory of irreversibility. *J. Chem. Phys.*, 33:1338, 1960.
- [183] R. Zwanzig. Memory effects in irreversible thermodynamics. *Phys. Rev.*, 124:983, 1961.

Appendix A

Basic operator relations

Some of the results of this thesis are based on cumbersome calculations with operators in second quantization and quantum spin operators. In many cases straightforward transformations between certain steps have not been given. Since the reader might wish to fill some of the gaps themselves, we provide in this appendix basic operator relations used in our calculations.

Fourier transformation

The Fourier transformation is provided, since different versions are used in some papers.

$$\begin{aligned} S_{\mathbf{k}}^{\alpha} &= \sum_{i=1}^N S_i^{\alpha} e^{-i\mathbf{k}\mathbf{R}_i}, & S_i^{\alpha} &= \frac{1}{N} \sum_{\mathbf{k}}^{\text{BZ}} S_{\mathbf{k}}^{\alpha} e^{i\mathbf{k}\mathbf{R}_i}, \\ c_{\mathbf{k}\sigma} &= \frac{1}{\sqrt{N}} \sum_i c_{i\sigma} e^{-i\mathbf{k}\mathbf{R}_i}, & c_{i\sigma} &= \frac{1}{\sqrt{N}} \sum_{\mathbf{k}} c_{\mathbf{k}\sigma} e^{i\mathbf{k}\mathbf{R}_i}, \\ \varepsilon_{\mathbf{k}} &= \frac{1}{N} \sum_{(i-j)} T_{ij} e^{-i\mathbf{k}(\mathbf{R}_i - \mathbf{R}_j)}, & T_{ij} &= \frac{1}{N} \sum_{\mathbf{k}} \varepsilon_{\mathbf{k}} e^{i\mathbf{k}(\mathbf{R}_i - \mathbf{R}_j)}, \\ \delta_{\mathbf{q},\mathbf{p}} &= \frac{1}{N} \sum_i e^{i(\mathbf{q}-\mathbf{p})\mathbf{R}_i}, & \delta_{i,j} &= \frac{1}{N} \sum_{\mathbf{k}} e^{i\mathbf{k}(\mathbf{R}_i - \mathbf{R}_j)}, \\ G_{\mathbf{k}\sigma} &= \frac{1}{N} \sum_{(i-j)} G_{ij\sigma} e^{-i\mathbf{k}(\mathbf{R}_i - \mathbf{R}_j)}, & G_{ij\sigma} &= \frac{1}{N} \sum_{\mathbf{k}} G_{\mathbf{k}\sigma} e^{i\mathbf{k}(\mathbf{R}_i - \mathbf{R}_j)}. \end{aligned}$$

Due to translational invariance only the distance of two sites is relevant for the double sums of $\varepsilon_{\mathbf{k}}$ and $G_{\mathbf{k}\sigma}$. This is expressed by the notation “ $(i-j)$ ”.

Fundamental commutation relations

Based on the Fourier transformation one can also transform the commutation relations to momentum space. $[\cdot, \cdot]_+$ and $[\cdot, \cdot]_-$ denote the anticommutator and the commutator,

respectively.

$$\begin{aligned}
 [c_{i\sigma}, c_{j\sigma}^\dagger]_+ &= \delta_{ij} & \iff & [c_{\mathbf{k}_1\sigma}, c_{\mathbf{k}_2\sigma}^\dagger]_+ = \delta_{\mathbf{k}_1, \mathbf{k}_2} \\
 [S_i^z, S_j^\sigma]_- &= z_\sigma \hbar S^\sigma \delta_{ij} & \iff & [S_{\mathbf{k}_1}^z, S_{\mathbf{k}_2}^\sigma]_- = z_\sigma \hbar S_{\mathbf{k}_1 + \mathbf{k}_2}^\sigma \\
 [S_i^\sigma, S_j^{-\sigma}]_- &= 2z_\sigma \hbar S^z \delta_{ij} & \iff & [S_{\mathbf{k}_1}^\sigma, S_{\mathbf{k}_2}^{-\sigma}]_- = 2z_\sigma \hbar S_{\mathbf{k}_1 + \mathbf{k}_2}^z
 \end{aligned}$$

Commutation relations of more than two operators

If more than two operators A, B, C, D are involved, the following rules are helpful. In particular, the transformation from commutators to anticommutators and vice versa is often needed.

$$\begin{aligned}
 [A, BC]_- &= B [A, C]_- + [A, B]_- C \\
 [A, BC]_- &= [A, B]_+ C - B [A, C]_+ \\
 [AB, C]_- &= A [B, C]_+ - [A, C]_+ B \\
 [A, BC]_+ &= [A, B]_- C + B [A, C]_+ \\
 [A, BCD]_+ &= [A, B]_+ CD - B [A, C]_+ D + BC [A, D]_+ \\
 [AB, CD]_+ &= C [A, D]_+ B + CA [B, D]_- + [A, C]_- BD + A [B, C]_- D \\
 [AB, CD]_- &= A [B, C]_+ D - AC [B, D]_+ + [A, C]_+ DB - C [A, D]_+ B \\
 [AB, CD]_- &= A [B, C]_- D + AC [B, D]_- + [A, C]_- DB + C [A, D]_- B \\
 &= A [B, C]_- D + CA [B, D]_- + [A, C]_- BD + C [A, D]_- B
 \end{aligned}$$

Relation between spin operators

An often used relation, that is particularly helpful for $S = 1/2$ is given by

$$S^\sigma S^{-\sigma} = \hbar^2 S(S+1) + z_\sigma \hbar S^z - (S^z)^2$$

Appendix B

A remarkable equality

The goal of this appendix is the proof of the equality (2.23) on p. 14. Although this equation contains an unusual combination of correlation functions, it seems to be an intrinsic property of the KLM. There are several possibilities for a proof, of which we are going to present two. Both are based on quite fundamental concepts.

Theorem B1: For any arbitrary operator A the expectation value $\langle \mathcal{L}A \rangle$ vanishes, if \mathcal{L} is the Liouvillian corresponding to the Hamiltonian of the system.

Proof: The theorem is related to the observation that expectation values are static entities. Another straightforward proof uses the definition of the canonical average

$$\langle AH \rangle = \frac{\text{Tr}(e^{\beta H} AH)}{\text{Tr}(e^{\beta H})} = \frac{\text{Tr}(e^{\beta H} HA)}{\text{Tr}(e^{\beta H})} = \langle HA \rangle \quad \implies \quad \langle [A, H]_- \rangle = 0 \quad (\text{B.1})$$

and the cyclic invariance of the trace. □

Based on the Hamiltonian (2.5) of the KLM one can now apply the theorem to several operators A . For most cases the results are trivial. For $A = S^z$, e.g., we obtain the identity $\langle S^\sigma c_{-\sigma}^\dagger c_\sigma \rangle = \langle S^{-\sigma} c_\sigma^\dagger c_{-\sigma} \rangle$. However, for our purpose we use $A = S_i^\sigma c_{i-\sigma}^\dagger c_{i\sigma}$. Then the necessary commutators are:

$$\begin{aligned} [A, H_s]_- &= \sum_{jk} \sum_{\sigma'} T_{jk} \left[S_i^\sigma c_{i-\sigma}^\dagger c_{i\sigma}, c_{j\sigma'}^\dagger c_{k\sigma'} \right]_- \\ &= S_i^\sigma \sum_{jk} \sum_{\sigma'} T_{jk} \left(c_{i-\sigma}^\dagger c_{k\sigma'} \delta_{ij} \delta_{\sigma\sigma'} - c_{j\sigma'}^\dagger c_{i\sigma} \delta_{ik} \delta_{-\sigma\sigma'} \right) \\ &= \sum_j T_{ij} \left(S_i^\sigma c_{i-\sigma}^\dagger c_{j\sigma} - S_i^\sigma c_{j-\sigma}^\dagger c_{i\sigma} \right) \end{aligned} \quad (\text{B.2})$$

$$\begin{aligned} \sum_{\sigma'} z_{\sigma'} [A, S_j^z \hat{n}_{j\sigma'}]_- &= \sum_{\sigma'} z_{\sigma'} \left\{ S_i^\sigma S_i^z \left[c_{i-\sigma}^\dagger c_{i\sigma}, \hat{n}_{i\sigma'} \right]_- + \hat{n}_{i\sigma'} c_{i-\sigma}^\dagger c_{i\sigma} [S_i^\sigma, S_i^z]_- \right\} \delta_{ij} \\ &= \left\{ z_\sigma S_i^\sigma S_i^z \left(c_{i-\sigma}^\dagger c_{i\sigma} + c_{i-\sigma}^\dagger c_{i\sigma} \right) - \sum_{\sigma'} z_{\sigma'} z_\sigma \hbar S_i^\sigma \hat{n}_{i\sigma'} c_{i-\sigma}^\dagger c_{i\sigma} \right\} \delta_{ij} \\ &= \left(2z_\sigma S_i^\sigma S_i^z c_{i-\sigma}^\dagger c_{i\sigma} + \hbar S_i^\sigma c_{i-\sigma}^\dagger c_{i\sigma} \right) \delta_{ij} \end{aligned} \quad (\text{B.3})$$

$$\begin{aligned}
 \sum_{\sigma'} \left[A, S_j^{\sigma'} c_{j-\sigma'}^\dagger c_{j\sigma'} \right]_- &= \left[S_i^\sigma c_{i-\sigma}^\dagger c_{i\sigma}, S_i^{-\sigma} c_{i\sigma}^\dagger c_{i-\sigma} \right]_- \delta_{ij} \\
 &= \left(S_i^\sigma S_i^{-\sigma} c_{i-\sigma}^\dagger c_{i\sigma} c_{i\sigma}^\dagger c_{i-\sigma} - S_i^{-\sigma} S_i^\sigma c_{i\sigma}^\dagger c_{i-\sigma} c_{i-\sigma}^\dagger c_{i\sigma} \right) \delta_{ij} \\
 &= \left(S_i^\sigma S_i^{-\sigma} \hat{n}_{i-\sigma} (1 - \hat{n}_{i\sigma}) - S_i^{-\sigma} S_i^\sigma \hat{n}_{i\sigma} (1 - \hat{n}_{i-\sigma}) \right) \delta_{ij} \\
 &= \left([S_i^{-\sigma}, S_i^\sigma]_- \hat{n}_{i-\sigma} \hat{n}_{i\sigma} + S_i^\sigma S_i^{-\sigma} \hat{n}_{i-\sigma} - S_i^{-\sigma} S_i^\sigma \hat{n}_{i\sigma} \right) \delta_{ij} \\
 &= \left(-2z_\sigma \hbar S_i^z \hat{n}_{i-\sigma} \hat{n}_{i\sigma} + S_i^\sigma S_i^{-\sigma} \hat{n}_{i-\sigma} - S_i^{-\sigma} S_i^\sigma \hat{n}_{i\sigma} \right) \delta_{ij} \quad (\text{B.4})
 \end{aligned}$$

$$\begin{aligned}
 \implies [A, H_{sf}]_- &= -\frac{J}{2} \left(\hbar S_i^\sigma c_{i-\sigma}^\dagger c_{i\sigma} + 2z_\sigma S_i^\sigma S_i^z c_{i-\sigma}^\dagger c_{i\sigma} \right. \\
 &\quad \left. - 2z_\sigma \hbar S_i^z \hat{n}_{i-\sigma} \hat{n}_{i\sigma} + S_i^\sigma S_i^{-\sigma} \hat{n}_{i-\sigma} - S_i^{-\sigma} S_i^\sigma \hat{n}_{i\sigma} \right) \quad (\text{B.5})
 \end{aligned}$$

If theorem B1 is applied to the sum of (B.2) and (B.5), Eq. (2.23) is obtained. \square

Theorem B2: For arbitrary Liouville states $|A\rangle$ and $|B\rangle$ the frequency matrix is Hermitian

$$(A | \mathcal{L} | B) = (B | \mathcal{L} | A)^*, \quad (\text{B.6})$$

if \mathcal{L} is the Liouvillian corresponding to the Hamiltonian of the system. A real frequency matrix is therefore symmetric.

Proof: We implement the definition of the Liouville scalar product to obtain

$$\begin{aligned}
 (A | \mathcal{L} | B) &= \langle A^+ H B \rangle - \langle A^+ B H \rangle + \langle H B A^+ \rangle - \langle B H A^+ \rangle \\
 &= \langle B^+ H A \rangle^* - \langle H B^+ A \rangle^* + \langle A B^+ H \rangle^* - \langle A H B^+ \rangle^* \\
 &= \langle B^+ H A \rangle^* - \langle B^+ A H \rangle^* + \langle H A B^+ \rangle^* - \langle A H B^+ \rangle^* = (B | \mathcal{L} | A)^*. \quad \square
 \end{aligned}$$

Theorem B2 is a generalization of B1, since $\langle \mathcal{L} A \rangle = \frac{1}{2} (\mathbf{1} | \mathcal{L} | A)$. It is closely related to the POM, applied in this work. This also motivates the choice of the Liouville states $|A\rangle$ and $|B\rangle$. For the evaluation of the atomic limit we have used the basis

$$\left| c_{l\sigma}^\dagger \right\rangle, \left| \hat{n}_{l-\sigma} c_{l\sigma}^\dagger \right\rangle, \left| z_\sigma S_l^z c_{l\sigma}^\dagger + S_l^\sigma c_{l-\sigma}^\dagger \right\rangle \text{ and } \left| z_\sigma S_l^z \hat{n}_{l-\sigma} c_{l\sigma}^\dagger + S_l^\sigma \hat{n}_{l\sigma} c_{l-\sigma}^\dagger \right\rangle. \quad (\text{B.7})$$

There are 6 possible combinations of these basis elements. For 3 cases trivial results are obtained. For the other 3 cases, however (these are the combination of the first and the last, of the second and the third as well as of the second and the fourth) theorem B2 yields equality (2.23). This is a clear indication of the relevance of this property. There is no need to give detailed calculations here, as similar calculations are performed for the atomic limit.

Appendix C

The Laplace transformation

The dynamics of the retarded Green's function is determined by the Heaviside step function. Hence, this function vanishes for all times before a certain starting point t_0 which, without a loss in generality, can be set to 0. The Laplace transform has been invented for such functions and, therefore, is often used in the context of strongly correlated electron systems. Within this appendix we will explain this transformation and properties which are necessary to show the equivalence of the Mori equations (3.13) and (3.23).

C.1 A special Fourier transformation

For a function $G(t) = \Theta(t)f(t)$ the Fourier transformation can be formulated such that the effect of the step function is already exploited:

$$\tilde{f}(E) = \int_0^{\infty} d\tau f(\tau) e^{-iE\tau/\hbar} \longleftrightarrow \frac{1}{2\pi\hbar} \int_{-\infty}^{+\infty} dE \tilde{f}(E) e^{iEt/\hbar} = \begin{cases} f(t), & t \geq 0 \\ 0, & t < 0 \end{cases}. \quad (\text{C.1})$$

To ensure the convergence of these integrals the function $f(t)$ is multiplied by an additional factor $e^{-\delta t}$, with a conveniently chosen parameter $\delta > 0$. For the obtained function $f^*(t) = f(t) e^{-\delta t}$ the transformation formulae are

$$\tilde{f}^*(E) = \int_0^{\infty} d\tau f(\tau) e^{-(\delta+iE/\hbar)\tau} = \tilde{f}(E - i\hbar\delta), \quad (\text{C.2})$$

$$f^*(t) = \frac{1}{2\pi\hbar} \int_{-\infty}^{+\infty} dE \tilde{f}^*(E) e^{iEt/\hbar} \Rightarrow f(t) = \frac{1}{2\pi\hbar} \int_{-\infty}^{+\infty} dE \tilde{f}(E - i\hbar\delta) e^{(\delta+iE/\hbar)t}. \quad (\text{C.3})$$

It is customary to define the new parameter $s := \delta + iE/\hbar$ and to neglect the factor $i\hbar$ in the argument of \tilde{f} to obtain the *Laplace transformation*:

$$\tilde{f}(s) = \int_0^{\infty} d\tau f(\tau) e^{-s\tau} \longleftrightarrow f(t) = \frac{1}{2\pi i\hbar} \int_{\delta-i\infty}^{\delta+i\infty} ds \tilde{f}(s) e^{st}. \quad (\text{C.4})$$

If instead of s the definition $\omega = E/\hbar - i\delta$ is used, the transformation is usually called the one-sided Fourier transformation. In the context of Green's functions the convergence parameter δ be chosen infinitesimally small ($\delta = 0^+$).

C.2 Application to the Mori equation

There are several books [1, 4] on advantages and properties of Laplace transformations. Out of this material, only two theorems are necessary for the solution of the Mori integro-differential equation (3.13). These are

The Differentiation Theorem: The Laplace transform of a derivative $f(t) = \frac{dg}{dt}$ is given by

$$\tilde{f}(s) = s\tilde{g}(s) - g(0) \quad (\text{C.5})$$

The Convolution Theorem: The Laplace transform of a convolution

$$f(t) = \int_0^t d\tau g(t - \tau)h(\tau) \quad (\text{C.6})$$

is given by the product of Laplace transforms $\tilde{f}(s) = \tilde{g}(s)\tilde{h}(s)$.

With the help of these theorems the integro-differential equation (3.13) can be readily simplified. First of all, the *dynamical correlation function*

$$\Xi_{\gamma\nu}(t) = i(A_\gamma | A_\nu(t)) \quad (\text{C.7})$$

is introduced. Its equation of motion is given by

$$\frac{d}{dt} \Xi_{\gamma\nu}(t) = i\Xi_{\gamma\mu}(t)\chi_{\mu\rho}^{-1}\Omega_{\rho\nu} - \int_0^t dt' \Xi_{\gamma\mu}(t - t')\chi_{\mu\rho}^{-1}M_{\rho\nu}(t'). \quad (\text{C.8})$$

Due to the fact, that the residual force $f_\mu(t)$ belongs to the orthogonal complement of the level of description, it has no influence on the dynamical correlation function.

Then we perform a Laplace transformation on both sides of (C.8).

$$s\tilde{\Xi}_{\gamma\nu}(s) = i\chi_{\gamma\nu} + i\tilde{\Xi}_{\gamma\mu}(s)\chi_{\mu\rho}^{-1}\Omega_{\rho\nu} - \tilde{\Xi}_{\gamma\mu}(s)\chi_{\mu\rho}^{-1}\tilde{M}_{\rho\nu}(s). \quad (\text{C.9})$$

Here, it has been used that $\Xi_{\gamma\nu}(0) = i\chi_{\gamma\nu}$. The result obtained has a structure which is similar to the energy representation of the Mori equations given in (3.23). The differences can be resolved by a proper definition of all contributing functions.

Appendix D

Details of calculations in Sec. 4.1

In Sec. 4.1 the explanation of the POM for the limit of the ferromagnetically saturated semiconductor was restricted such that one can follow the gist of the calculations. For the interested reader the explicit derivation of several formulae will be given here.

Derivation of (4.6)

To derive this formula one can make use of the exact relationship for $n = 0$:

$$\left\langle \left[c_i S_i, S_l c_l^\dagger \right]_+ \right\rangle = \left\langle S_i S_l \left[c_i, c_l^\dagger \right]_+ - [S_i, S_l]_- c_l^\dagger c_i \right\rangle \stackrel{n=0}{\rightarrow} \langle S_i S_l \rangle \delta_{il}. \quad (\text{D.1})$$

Based on the definition (4.78) of the Liouville state $|\mathcal{QL}c_{l\sigma}^\dagger\rangle$ one therefore obtains

$$\left(\mathcal{QL}c_{i\sigma}^\dagger \left| \mathcal{QL}c_{l\sigma}^\dagger \right. \right) = \frac{J^2}{4\hbar^2} \{ \langle [S_i^z - \langle S^z \rangle] [S_l^z - \langle S^z \rangle] \rangle + \langle S_i^{-\sigma} S_l^\sigma \rangle \} \delta_{il} \quad (\text{D.2})$$

$$\stackrel{\langle S^z \rangle = \hbar S}{=} \frac{J^2}{4} \{ 0 + S(1 - z_\sigma) \} \delta_{il} = \frac{1}{2} J^2 S \delta_{\sigma\downarrow} \delta_{il}. \quad (\text{D.3})$$

Derivation of (4.8)

We start with expression (4.7) for the action of \mathcal{L}_{sf} on the Liouville state $|\mathcal{QL}c_{l\sigma}^\dagger\rangle$. It can be simplified with the help of another exact relationship for $n = 0$, namely

$$\left[S_j c_j^\dagger c_j, S_l c_l^\dagger \right]_- = S_j S_l \left[c_j^\dagger c_j, c_l^\dagger \right]_- + [S_j, S_l]_- c_l^\dagger c_j^\dagger c_j \stackrel{n=0}{\rightarrow} S_j S_l c_l^\dagger \delta_{jl}. \quad (\text{D.4})$$

We obtain

$$\begin{aligned} \mathcal{L}_{sf} \left| \mathcal{QL}c_{l\sigma}^\dagger \right\rangle &= \frac{J^2}{4\hbar^2} \sum_i \sum_{\sigma'} \left[\left[z_{\sigma'} S_i^z \hat{n}_{i\sigma'} + S_i^{\sigma'} c_{i-\sigma'}^\dagger c_{i\sigma'}, z_\sigma \delta(S_l^z) c_{l\sigma}^\dagger + S_l^\sigma c_{l-\sigma}^\dagger \right]_- \right] \\ &= \frac{J^2}{4\hbar^2} \left[S_l^z \delta(S_l^z) c_{l\sigma}^\dagger + z_\sigma S_l^\sigma \delta(S_l^z) c_{l-\sigma}^\dagger + z_{-\sigma} S_l^z S_l^\sigma c_{l-\sigma}^\dagger + S_l^{-\sigma} S_l^\sigma c_{l\sigma}^\dagger \right] \end{aligned} \quad (\text{D.5})$$

With the help of some additional identities for spin operators, namely

$$\delta(S_l^{-\sigma} S_l^\sigma) = -z_\sigma \hbar \delta(S_l^z) - (S_l^z)^2 + \langle S^z \rangle^2 \quad (\text{D.6})$$

$$\text{and } [S_l^\sigma, S_l^z]_- = S_l^\sigma S_l^z - S_l^z S_l^\sigma = -z_\sigma \hbar S_l^\sigma, \quad (\text{D.7})$$

we can now apply the projector \mathcal{Q} on the result

$$\begin{aligned}
 \mathcal{Q}\mathcal{L}_{sf} \left| \mathcal{Q}\mathcal{L}c_{l\sigma}^\dagger \right\rangle &= \frac{J^2}{4\hbar^2} \left| S_l^z \delta(S_l^z) c_{l\sigma}^\dagger + z_\sigma S_l^\sigma \delta(S_l^z) c_{l-\sigma}^\dagger - z_\sigma S_l^z S_l^\sigma c_{l-\sigma}^\dagger + \delta(S_l^{-\sigma} S_l^\sigma) c_{l\sigma}^\dagger \right\rangle \\
 &= \frac{J^2}{4\hbar^2} \left\{ \left[\langle S^z \rangle^2 - S_l^z \langle S^z \rangle - z_\sigma \hbar \delta(S_l^z) \right] \left| c_{l\sigma}^\dagger \right\rangle - \left[z_\sigma S_l^\sigma \langle S_l^z \rangle + \hbar S_l^\sigma \right] \left| c_{l-\sigma}^\dagger \right\rangle \right\} \\
 &= -\frac{J^2}{4\hbar^2} (\hbar + z_\sigma \langle S_l^z \rangle) \left\{ z_\sigma \delta(S_l^z) \left| c_{l\sigma}^\dagger \right\rangle + S_l^\sigma \left| c_{l-\sigma}^\dagger \right\rangle \right\} \\
 &= \frac{J}{2} (1 + z_\sigma S) \left| \mathcal{Q}\mathcal{L}c_{l\sigma}^\dagger \right\rangle
 \end{aligned} \tag{D.8}$$

This is the expression given in (4.8).

Derivation of (4.16)

Before performing the Fourier transformation, the complete expression of scalar products are needed in Wannier representation. Similar to the derivation of (4.6) one obtains:

$$\begin{aligned}
 \left(\mathcal{Q}\mathcal{L}c_{i\sigma}^\dagger \left| \left(-\frac{1}{2}J\right) \left| z_\sigma \delta(S_l^z) c_{k\sigma}^\dagger + S_l^\sigma c_{k-\sigma}^\dagger \right\rangle \right. \right) &= \frac{J^2}{4\hbar^2} \langle S_i^{-\sigma} S_l^\sigma \rangle \delta_{ik} = \frac{1}{2} J^2 S \delta_{\sigma\downarrow} \delta_{il} \delta_{ik} \\
 \implies \left(\mathcal{Q}\mathcal{L}c_{i\sigma}^\dagger \left| (\mathcal{Q}\mathcal{L}_s \mathcal{Q})^m \left| \mathcal{Q}\mathcal{L}c_{l\sigma}^\dagger \right\rangle \right. \right) &\stackrel{(4.15)}{=} \frac{1}{2} J^2 S \delta_{\sigma\downarrow} [\underline{\mathbb{T}}^m]_{il} \delta_{il}.
 \end{aligned} \tag{D.9}$$

The Fourier transformation of the hopping matrix is given by

$$\begin{aligned}
 [\underline{\mathbb{T}}^m]_{il} &= \frac{1}{N^m} \sum_{k_1, \dots, k_{m-1}} \sum_{\mathbf{p}_1, \mathbf{p}_2, \dots, \mathbf{p}_m} \varepsilon_{\mathbf{p}_1} \cdots \varepsilon_{\mathbf{p}_m} e^{i\mathbf{p}_1(\mathbf{R}_i - \mathbf{R}_{k_{m-1}})} \cdots e^{i\mathbf{p}_m(\mathbf{R}_{k_1} - \mathbf{R}_l)} \\
 &= \frac{1}{N} \sum_{\mathbf{p}_1, \mathbf{p}_2, \dots, \mathbf{p}_m} \varepsilon_{\mathbf{p}_1} \cdots \varepsilon_{\mathbf{p}_m} e^{i\mathbf{p}_1 \mathbf{R}_i} \delta_{\mathbf{p}_1, \mathbf{p}_2} \cdots \delta_{\mathbf{p}_{m-1}, \mathbf{p}_m} e^{-i\mathbf{p}_m \mathbf{R}_l} \\
 &= \frac{1}{N} \sum_{\mathbf{p}} \varepsilon_{\mathbf{p}}^m e^{i\mathbf{p}(\mathbf{R}_i - \mathbf{R}_l)}.
 \end{aligned} \tag{D.10}$$

Hence,

$$\begin{aligned}
 \left(\mathcal{Q}\mathcal{L}c_{k\sigma}^\dagger \left| (\mathcal{Q}\mathcal{L}_s \mathcal{Q})^m \left| \mathcal{Q}\mathcal{L}c_{k\sigma}^\dagger \right\rangle \right. \right) &= \frac{1}{N} \sum_{il} e^{-i\mathbf{k}(\mathbf{R}_i - \mathbf{R}_l)} \left(\mathcal{Q}\mathcal{L}c_{i\sigma}^\dagger \left| (\mathcal{Q}\mathcal{L}_s \mathcal{Q})^m \left| \mathcal{Q}\mathcal{L}c_{l\sigma}^\dagger \right\rangle \right. \right) \\
 &= \frac{1}{2} J^2 S \delta_{\sigma\downarrow} \frac{1}{N} \sum_{il} e^{-i\mathbf{k}(\mathbf{R}_i - \mathbf{R}_l)} [\underline{\mathbb{T}}^m]_{il} \delta_{il} \\
 &= \frac{1}{2} J^2 S \delta_{\sigma\downarrow} \frac{1}{N^3} \sum_{il} \sum_{\mathbf{p}\mathbf{q}} e^{-i(\mathbf{k} - \mathbf{p} - \mathbf{q})(\mathbf{R}_i - \mathbf{R}_l)} \varepsilon_{\mathbf{p}}^m \\
 &= \frac{1}{2} J^2 S \delta_{\sigma\downarrow} \frac{1}{N} \sum_{\mathbf{p}\mathbf{q}} \delta_{\mathbf{p}, \mathbf{k} - \mathbf{q}} \varepsilon_{\mathbf{p}}^m \\
 &= \frac{1}{2} J^2 S \delta_{\sigma\downarrow} \frac{1}{N} \sum_{\mathbf{q}} \varepsilon_{\mathbf{k} - \mathbf{q}}^m.
 \end{aligned} \tag{D.11}$$

Derivation of (4.21)

The product in Eq. (4.21) is obtained when the operators $S_{k_i}^z$ are commuted to the left within the expectation value and thereafter ferromagnetic saturation is used:

$$\begin{aligned}
(A_{ii}|_{k_n \dots k_1} A_{lj}) &= \frac{J^2}{4} \left(\frac{J}{2} z_\sigma \right)^n \left(S_i^\sigma c_{i-\sigma}^\dagger \left| S_{k_n}^z S_{k_{n-1}}^z \cdots S_{k_2}^z S_{k_1}^z S_l^\sigma c_{j-\sigma}^\dagger \right. \right) \\
&\stackrel{(D.1)}{=} \frac{J^2}{4} \left(\frac{J}{2} z_\sigma \right)^n \delta_{ij} \langle S_i^{-\sigma} S_{k_n}^z S_{k_{n-1}}^z \cdots S_{k_2}^z S_{k_1}^z S_l^\sigma \rangle \\
&= \frac{J^2}{4} \left(\frac{J}{2} z_\sigma \right)^n \delta_{ij} (\hbar z_\sigma \delta_{ik_n} + \hbar S) \langle S_i^{-\sigma} S_{k_{n-1}}^z \cdots S_{k_2}^z S_{k_1}^z S_l^\sigma \rangle \\
&= \frac{J^2}{4} \left(\frac{J}{2} z_\sigma \right)^n \delta_{ij} \prod_{x=1}^n (\hbar z_\sigma \delta_{ik_x} + \hbar S) \langle S_i^{-\sigma} S_l^\sigma \rangle \\
&= \frac{1}{2} J^2 S \delta_{\sigma\downarrow} \delta_{ij} \delta_{il} \prod_{x=1}^n \frac{1}{2} J \hbar (\delta_{ik_x} - S) \tag{D.12}
\end{aligned}$$

Derivation of (4.28)

We have noticed in Sec. 4.1 that instead of $\mathcal{L}_s + \mathcal{L}_{s_f}$ the Liouvillian should be treated as $\mathcal{L} = \mathcal{L}_{\text{MF}} + \mathcal{L}_{\text{I}}$. For the contribution $(\mathcal{L}_{\text{MF}} + \mathcal{L}_{\text{I}})^m$ to the memory matrix, one has to consider all products of \mathcal{L}_{MF} and \mathcal{L}_{I} which contribute to the term proportional to the power m . The application of a certain power $p \leq m$ of \mathcal{L}_{I} leads to p different δ -functions (see Eqs. (4.21) and (4.22)) which are positioned in between the $\underline{\text{U}}$ -matrices such that matrix-multiplications are prevented. Instead the $\underline{\text{U}}$ -matrices can be grouped in different ways:

$$\begin{aligned}
[\underline{\text{U}}^0]^{q_0} [\underline{\text{U}}^1]^{q_1} [\underline{\text{U}}^2]^{q_2} \cdots [\underline{\text{U}}^r]^{q_r} \quad \text{with} \quad m - p &= 0 \cdot q_0 + 1 \cdot q_1 + \cdots + r \cdot q_r, \tag{D.13} \\
p + 1 &= q_0 + q_1 + \cdots + q_r.
\end{aligned}$$

To consider all groupings that only differ in the order of the $\underline{\text{U}}$ -matrices a prefactor

$$N_{\{q\}} = \frac{(p+1)!}{q_0! \cdot q_1! \cdot q_2! \cdots q_r!}, \tag{D.14}$$

needs to be used. This factor is identical to the binomial coefficient used for the polynomial theorem

$$\left(\frac{1}{\omega} \sum_{m=0}^r \left[\left(\frac{\underline{\text{U}}}{\omega} \right)^m \right]_{il} \right)^{p+1} = \frac{1}{\omega^q} \sum_{\sum q_i = p+1} \binom{p+1}{q_0, q_1, \dots, q_r} \left[\left(\frac{\underline{\text{U}}}{\omega} \right)^0 \right]_{il}^{q_0} \left[\left(\frac{\underline{\text{U}}}{\omega} \right)^1 \right]_{il}^{q_1} \cdots \left[\left(\frac{\underline{\text{U}}}{\omega} \right)^r \right]_{il}^{q_r}. \tag{D.15}$$

It is valid for any finite r . From these considerations we can conclude for the memory matrix

$$M_{il\sigma} = \frac{1}{\omega} \sum_{m=0}^{\infty} \frac{1}{\omega^m} \left(\mathcal{Q}\mathcal{L}c_{i\sigma}^\dagger \left| (\mathcal{Q}\mathcal{L}_{\text{MF}}\mathcal{Q} + \mathcal{Q}\mathcal{L}_I\mathcal{Q})^m \right| \mathcal{Q}\mathcal{L}c_{i\sigma}^\dagger \right) \quad (\text{D.16})$$

$$\stackrel{(\text{D.13})}{=} \frac{1}{2} J^2 S \delta_{\sigma\downarrow} \delta_{il} \left\{ \frac{1}{\omega} \sum_{m=0}^{\infty} \left[\left(\frac{\mathbb{U}}{\omega} \right)^m \right]_{il} + \frac{J}{2} \frac{1}{\omega^2} \left(1 + 2 \left[\left(\frac{\mathbb{U}}{\omega} \right)^1 \right]_{il} + 2 \left[\left(\frac{\mathbb{U}}{\omega} \right)^2 \right]_{il} + \left[\left(\frac{\mathbb{U}}{\omega} \right)^1 \right]_{il}^2 + 2 \left[\left(\frac{\mathbb{U}}{\omega} \right)^3 \right]_{il} + 2 \left[\left(\frac{\mathbb{U}}{\omega} \right)^2 \right]_{il} \left[\left(\frac{\mathbb{U}}{\omega} \right)^1 \right]_{il} + \dots \right) + \frac{J^2}{4} \frac{1}{\omega^3} \left(1 + 3 \left[\left(\frac{\mathbb{U}}{\omega} \right)^1 \right]_{il} + 3 \left[\left(\frac{\mathbb{U}}{\omega} \right)^2 \right]_{il} + 3 \left[\left(\frac{\mathbb{U}}{\omega} \right)^1 \right]_{il}^2 + \dots \right) + \dots \right\} \quad (\text{D.17})$$

$$\stackrel{(\text{D.15})}{=} \frac{1}{2} J^2 S \delta_{\sigma\downarrow} \delta_{il} \left\{ \left(\frac{1}{\omega} \sum_{m=0}^{\infty} \left[\left(\frac{\mathbb{U}}{\omega} \right)^m \right]_{il} \right) + \frac{J}{2} \left(\frac{1}{\omega} \sum_{m=0}^{\infty} \left[\left(\frac{\mathbb{U}}{\omega} \right)^m \right]_{il} \right)^2 + \frac{J^2}{4} \left(\frac{1}{\omega} \sum_{m=0}^{\infty} \left[\left(\frac{\mathbb{U}}{\omega} \right)^m \right]_{il} \right)^3 + \dots \right\} \quad (\text{D.18})$$

Derivation of (4.45)

The Liouville state we want to consider is given by

$$\hat{\mathcal{Q}} \mathcal{Q}\mathcal{L}\mathcal{Q} \left| \mathcal{Q}\mathcal{L}c_{i\sigma}^\dagger \right\rangle \stackrel{(\text{4.23})}{=} \hat{\mathcal{Q}} \left| A_{lk} \hat{T}_{kl} + {}_{\nu}A_{ll} \right\rangle = \hat{T}_{kl} |A_{lk}\rangle + |{}_{\nu}A_{ll}\rangle - (T_0 + \frac{1}{2} J\hbar(1-S)) |A_{ll}\rangle. \quad (\text{D.19})$$

The term $|{}_{\nu}A_{ll}\rangle$ can be simplified. It enters the scalar product

$$\left({}_{\hat{k}}A_{\hat{i}\hat{j}} |{}_{\hat{k}}A_{l\hat{j}} \right) \stackrel{(\text{4.21})}{=} \frac{1}{2} J^2 S \delta_{\hat{j}\hat{j}} \delta_{\hat{i}\hat{l}} \left(\frac{1}{2} J\hbar \delta_{\hat{i}\hat{k}} - \frac{1}{2} J\hbar S \right) \left(\frac{1}{2} J\hbar \delta_{lk} - \frac{1}{2} J\hbar S \right), \quad (\text{D.20})$$

formulated here for general indices. However, since \mathcal{L}_s will not alter the first two indices of $|{}_{\nu}A_{ll}\rangle$, they will remain identical. Hence, a state $|{}_{\alpha}A_{ab}\rangle$ enters the scalar product (D.20) always such that the δ -function gives 1 and therefore acts like $\frac{1}{2} J\hbar(1-S) |{}_{\alpha}A_{ab}\rangle$. This results in

$$\hat{\mathcal{Q}} \mathcal{Q}\mathcal{L}\mathcal{Q} \left| \mathcal{Q}\mathcal{L}c_{i\sigma}^\dagger \right\rangle \rightarrow T_{kl} |A_{lk}\rangle - T_0 |A_{ll}\rangle = T_{kl} (1 - \delta_{kl}) |A_{lk}\rangle. \quad (\text{D.21})$$

Appendix E

Depolarization effects in the conduction band

Irkhin and Katsnelson [58] have claimed that the Kondo-lattice model with $J > 0$ allows parameter constellations such that the conduction band is completely polarized. Here, we will extend the discussion in Sec. 4.3 of this issue in the context of the SOPT.

Essentially, one has to investigate the possibility of a vanishing QDOS for the minority conduction electrons below the Fermi energy. We have convinced ourselves that the special form of the self-energy in SOPT implies that $\Im \Sigma_{\downarrow}(E)$ is zero in this energy range. Hence, out of the two scenarios which, according to (4.87), yield a finite $\rho_{\downarrow}(E)$ only the first one remains. We are searching for quasi-free, undamped electrons which have an effective energy $E_{\text{eff}} = E - \Re \Sigma_{\downarrow}(E)$ such that $\rho_0(E_{\text{eff}})$ is non-zero. More precisely, if

$$W_a < E - \Re \Sigma_{\downarrow}(E) < W_e \quad (\text{E.1})$$

is fulfilled for some $E = \mu - \epsilon$ with $\epsilon > 0$ then \downarrow -electrons are present and yield a depolarization of the conduction band. For sufficiently small E the second part of the inequality can always be fulfilled. The crux is the first inequality, on which we will focus in the following.

E.1 The conventional SOPT

For the conventional SOPT a completely polarized conduction band is possible if

$$E - \Re \Sigma_{\downarrow} = E - \tilde{J}S\hbar - \tilde{J}^2 2S\hbar^2 \text{Pr} \int_{\mu}^{W_e} dx \frac{\rho_0(x)}{E-x} \stackrel{!}{<} W_a. \quad (\text{E.2})$$

One has to distinguish different regimes for the chemical potential μ or equivalently for the band occupation n . For a finite value of n_{\uparrow} we have to make sure that $\mu > W_a - \tilde{J}S\hbar$.

Regime I₁: $W_a - \tilde{J}S\hbar < \mu \leq W_a$

We set $\mu = W_a - \delta$ with $\delta \geq 0$. Then the integrand in (E.2) is always negative, the principle value is identical to the integral itself and the range of integration can be shifted

to obtain:

$$\mu - \epsilon - \tilde{J}S\hbar + \tilde{J}^2 2S\hbar^2 \int_0^W dx \frac{\rho_0(W_a + x)}{x + \delta + \epsilon} \stackrel{!}{<} \mu + \delta \quad (\text{E.3})$$

$$\iff \int_0^W dx \frac{\rho_0(W_a + x)}{x + \delta + \epsilon} \stackrel{!}{<} \frac{1}{2\tilde{J}\hbar} + \frac{\delta + \epsilon}{2\tilde{J}^2\hbar^2 S} \quad (\text{E.4})$$

For example, if we assume a rectangular DOS $\rho_0(E)$ the inequality becomes

$$\frac{1}{W} \ln \left[1 + \frac{W}{\delta + \epsilon} \right] \stackrel{!}{<} \frac{1}{2\tilde{J}\hbar} + \frac{\delta}{2\tilde{J}^2\hbar^2 S} + \frac{\epsilon}{2\tilde{J}^2\hbar^2 S}. \quad (\text{E.5})$$

For fixed $\delta > 0$ the expression on the left has its maximum value at $\epsilon = 0$. However, for a sufficiently small $\hat{J}(\delta)$ one can still fulfill (E.5). For all other values of ϵ the left hand side becomes smaller and the right hand side larger. Hence, with the determined $\hat{J}(\delta)$ the inequality is fulfilled for all relevant energies.

If $\rho_0(E)$ is the DOS of a simple cubic lattice, one can even ensure the inequality (E.4) for $\delta = 0$, although an analytical calculation is not possible. Numerical evaluation shows that the maximum of the integral on the left hand side (that is for $\delta = \epsilon = 0$) is approximately 3.03 eV^{-1} . Hence, $J < 0.33 \text{ eV}$ fulfills (E.4) for $\delta = \epsilon = 0$ and accordingly, for all other values of δ and ϵ .

One therefore has to conclude, that conventional SOPT allows a complete polarization of the conduction band to occur, if n as well as J are chosen sufficiently small.

Regime II₁: $W_a < \mu < W_e$

The same kind of argument as put forward for regime I₁ can be applied for $W_a < \mu < W_e$. The only difference is that $\mu = W_a + \delta$ with $0 < \delta < W$. Again we perform a shift of the range of integration such, that the integrand has always the same sign. This yields

$$\int_0^{W-\delta} dx \frac{\rho_0(W_a + \delta + x)}{x + \epsilon} \stackrel{!}{<} \frac{1}{2\tilde{J}\hbar} + \frac{\epsilon - \delta}{2\tilde{J}^2\hbar^2 S} \quad (\text{E.6})$$

Evaluated for a rectangular DOS one obtains

$$\frac{1}{W} \ln \left[1 + \frac{W - \delta}{\epsilon} \right] \stackrel{!}{<} \frac{1}{2\tilde{J}\hbar} - \frac{\delta}{2\tilde{J}^2\hbar^2 S} + \frac{\epsilon}{2\tilde{J}^2\hbar^2 S} \quad (\text{E.7})$$

$$\implies W - \delta \stackrel{!}{<} \epsilon \left(\exp \left[W \left(\frac{1}{2\tilde{J}\hbar} - \frac{\delta}{2\tilde{J}^2\hbar^2 S} + \frac{\epsilon}{2\tilde{J}^2\hbar^2 S} \right) \right] - 1 \right). \quad (\text{E.8})$$

It is immediately evident, that it is not always possible to fulfill this relation. For a fixed set of parameters W, J, S, δ there will always be an ϵ small enough to ensure that (E.8) is invalid.

An arbitrary free DOS can be approximated by a rectangular one. We only have to assume that there is an energy region $[W_a + \delta, W_a + \delta + A]$ with $A > 0$, where $\rho_0(E)$ is positive everywhere. This is always possible if $\rho_0(E)$ is connected and $\mu < W_e$. Then we denote the minimum of $\rho_0(E)$ in this interval by $B > 0$ and obtain

$$\int_0^A dx \frac{B}{x + \varepsilon} < \int_0^{W-\delta} dx \frac{\rho_0(W_a + \delta + x)}{x + \varepsilon} \stackrel{!}{<} \frac{1}{2\tilde{J}\hbar} + \frac{\varepsilon - \delta}{2\tilde{J}^2\hbar^2 S} \quad (\text{E.9})$$

$$\implies A \stackrel{!}{<} \varepsilon \left(\exp \left[\frac{1}{B} \left(\frac{1}{2\tilde{J}\hbar} - \frac{\delta}{2\tilde{J}^2\hbar^2 S} + \frac{\varepsilon}{2\tilde{J}^2\hbar^2 S} \right) \right] - 1 \right). \quad (\text{E.10})$$

Again, there is always an ε to contradict this statement. This defines an energy region below the Fermi edge with a non-vanishing QDOS for the minority conduction electrons.

Regime III₁: $W_e < \mu < W_a + \tilde{J}S\hbar$

This parameter regime only exists if J is sufficiently large. As a consequence the second order contribution in $\Re \Sigma_{\downarrow}$ vanishes and condition (E.2) becomes

$$\mu - \varepsilon - \tilde{J}S\hbar \stackrel{!}{<} W_a. \quad (\text{E.11})$$

Evidently, this relationship is fulfilled for all ε . This implies complete polarization.

Regime IV₁: $\max\{W_e, W_a + \tilde{J}S\hbar\} < \mu$

The condition of complete polarization is again given by (E.11). However, it is not fulfilled anymore for all ε . Depolarization will take place.

E.2 The SOPT relative to Hartree-Fock

The SOPT relative to Hartree-Fock has a slightly different \downarrow -self-energy. Accordingly, the condition (E.2) has to be modified:

$$E - \Re \Sigma_{\downarrow} = E - \tilde{J}S\hbar - \tilde{J}^2 2S\hbar^2 \text{Pr} \int_{\mu + \tilde{J}S\hbar}^{W_e} dx \frac{\rho_0(x)}{E - x + \tilde{J}S\hbar} \stackrel{!}{<} W_a. \quad (\text{E.12})$$

By writing $E = \mu - \varepsilon$ one recognizes that as far as the J^2 -contribution is concerned this modification leads only to a shift of the regime borders for the chemical potential. Due to the fact, that also

$$\Sigma_{\uparrow}(E) = -\tilde{J}S\hbar + \tilde{J}^2 2S\hbar^2 \text{Pr} \int_{W_a}^{\mu - \tilde{J}S\hbar} dx \frac{\rho_0(x)}{E - x - \tilde{J}S\hbar + i0^+} \quad (\text{E.13})$$

is affected, in some cases there are qualitative changes of the results. That is the reason why we repeat the discussion of the regimes of μ .

Regime I₂: $\mu \leq W_a - \tilde{J}S\hbar$

This situation is analogous to regime I₁ in the discussion of the conventional SOPT characterized by an integration over the full width of the free DOS $\rho_0(x)$ in (E.12). It is again possible to prove, that $n_{\downarrow} = 0$ can be enforced by a sufficiently small coupling constant J . However, at the same time the second order contribution to Σ_{\uparrow} vanishes and its mean-field contribution is too small to allow for a finite occupation of the \uparrow -conduction band. Hence, in this regime $n = 0$ and this does not allow for a non-zero polarization.

Regime II₂: $W_a - \tilde{J}S\hbar < \mu < W_e - \tilde{J}S\hbar$

Using the definition $\mu = W_a - \tilde{J}S\hbar + \delta$ with $0 < \delta < W$, one obtains an inequality

$$\int_0^{W-\delta} dx \frac{\rho_0(W_a + \delta + x)}{x + \epsilon} < \frac{1}{\tilde{J}\hbar} + \frac{\epsilon - \delta}{2\tilde{J}^2\hbar^2 S} \quad (\text{E.14})$$

as a condition for complete polarization, which is almost identical to (E.6). In analogy to the argument presented in II₁ one can prove, that an energy region does always exist below the Fermi edge with a non-vanishing QDOS for minority conduction electrons.

Regime III₂: $W_e - \tilde{J}S\hbar < \mu < W_a + \tilde{J}S\hbar$

As for the case III₁, this parameter regime requires a large value of J . Again, this has the consequence that the second order contribution to $\Re \Sigma_{\downarrow}$ vanishes and the mean-field contribution is large enough to ensure $n_{\downarrow} = 0$. It is worth studying the \uparrow -electrons, too. On the one hand the requirement $\mu < W_a + \tilde{J}S\hbar$ implies that the J^2 contribution to $\Re \Sigma_{\uparrow}$ is zero. On the other hand the requirement $W_e - \tilde{J}S\hbar < \mu$ implies that the chemical lies above the mean-field shifted \uparrow -DOS. As a consequence, we have a completely filled \uparrow -conduction band ($n_{\uparrow} = 1$). This is a somehow special situation for complete polarization.

Regime IV₂: $\max\{W_e - \tilde{J}S\hbar, W_a + \tilde{J}S\hbar\} < \mu$

Similar to regime IV₁ the mean-field contribution to $\Re \Sigma_{\downarrow}$ yields a finite n_{\downarrow} value and hence a depolarization.

E.3 Conclusion

The POM cannot be used to strictly prove that a complete polarization, as claimed by Irkhin and Katsnelson, is impossible within the KLM. With I₁ and III₁ there are two energy regimes for the chemical potential, for which $n_{\uparrow} > 0$ and $n_{\downarrow} = 0$. This result is exact in second order perturbation theory in the coupling constant J .

Out of these two regimes, the former is closest to the corresponding figures in [58]. And it is this regime which does not exist as a region of complete polarization in a SOPT relative to Hartree-Fock. The remaining regime III₂ with 100% polarization is a very special situation, which Irkhin and Katsnelson [58] did not consider.

Since all our investigations lead to the result that a SOPT relative to Hartree-Fock is more suited for an approximation of the KLM than the conventional SOPT, we therefore conclude that a complete polarization with $n < 1$ is very improbable within the KLM. However, a more definite statement cannot be provided without additional assumption on the density of states and the self-energy.

Appendix F

Details of calculations in Sec. 5.1

In Sec. 5.1 the derivation of the memory matrix of the one-magnon Green's function is restricted to a few fundamental steps. Similar to App. D we use this appendix to provide some further details for the interested reader.

We start with a consideration of contributing Liouville states. If the basis element of the initial Liouville subspace $|S_{\mathbf{k}}^{-\sigma}\rangle$ is referred to as $|B_{1\mathbf{k}\sigma}\rangle$, the additional states in (5.4) can be abbreviated as follows

$$\begin{aligned} \mathcal{L}|S_{\mathbf{k}}^{-\sigma}\rangle &= -\frac{J}{2\hbar N} \sum_{\mathbf{q}\mathbf{p}} \sum_{\sigma'} \left(z_{\sigma'} [S_{\mathbf{q}}^z, S_{\mathbf{k}}^{-\sigma}]_{-} c_{\mathbf{p},\sigma'}^{\dagger} c_{\mathbf{p}-\mathbf{q},\sigma'} + [S_{\mathbf{q}}^{\sigma'}, S_{\mathbf{k}}^{-\sigma}]_{-} c_{\mathbf{p},-\sigma'}^{\dagger} c_{\mathbf{p}-\mathbf{q},\sigma'} \right) \quad (\text{F.1}) \\ &= \frac{-J}{2N} \sum_{\mathbf{q}\mathbf{p}} \left\{ \underbrace{|S_{\mathbf{q}+\mathbf{k}}^{-\sigma} c_{\mathbf{p},-\sigma}^{\dagger} c_{\mathbf{p}-\mathbf{q},-\sigma}\rangle}_{|B_{2\mathbf{k}\mathbf{q}\mathbf{p}\sigma}\rangle} - \underbrace{|S_{\mathbf{q}+\mathbf{k}}^{-\sigma} c_{\mathbf{p},\sigma}^{\dagger} c_{\mathbf{p}-\mathbf{q},\sigma}\rangle}_{|B_{3\mathbf{k}\mathbf{q}\mathbf{p}\sigma}\rangle} + 2z_{\sigma} \underbrace{|S_{\mathbf{q}+\mathbf{k}}^z c_{\mathbf{p},-\sigma}^{\dagger} c_{\mathbf{p}-\mathbf{q},\sigma}\rangle}_{|B_{4\mathbf{k}\mathbf{q}\mathbf{p}\sigma}\rangle} \right\} \end{aligned}$$

Due to the structure of the projection operator \mathcal{Q} the scalar products

$$V_{\mathbf{q}\mathbf{p}\sigma}^{(23)} \equiv \frac{(B_{1\mathbf{k}\sigma} | B_{2\mathbf{k}\mathbf{q}\mathbf{p}\sigma}) - (B_{1\mathbf{k}\sigma} | B_{3\mathbf{k}\mathbf{q}\mathbf{p}\sigma})}{(B_{1\mathbf{k}\sigma} | B_{1\mathbf{k}\sigma})} = \frac{1}{\langle S_{\mathbf{0}}^z \rangle} \langle S_{\mathbf{q}}^z (c_{\mathbf{p},-\sigma}^{\dagger} c_{\mathbf{p}-\mathbf{q},-\sigma} - c_{\mathbf{p},\sigma}^{\dagger} c_{\mathbf{p}-\mathbf{q},\sigma}) \rangle \quad (\text{F.2})$$

$$\text{and} \quad V_{\mathbf{q}\mathbf{p}\sigma}^{(4)} \equiv \frac{(B_{1\mathbf{k}\sigma} | B_{4\mathbf{k}\mathbf{q}\mathbf{p}\sigma})}{(B_{1\mathbf{k}\sigma} | B_{1\mathbf{k}\sigma})} = \frac{1}{2 \langle S_{\mathbf{0}}^z \rangle} \langle S_{\mathbf{q}}^{\sigma} c_{\mathbf{p},-\sigma}^{\dagger} c_{\mathbf{p}-\mathbf{q},\sigma} \rangle \quad (\text{F.3})$$

are needed. Additionally, one needs to know the effect of the truncated Liouvillian on these states. In order to study renormalization effects, we consider as the unperturbed Hamiltonian the expression H_{MF} , which incorporates the mean-field self-energy of con-

duction electrons.

$$\begin{aligned}
 \mathcal{L}_{\text{MF}} |B_{2/3 \mathbf{kqp}\sigma}) &= \sum_{\mathbf{p}'} \sum_{\sigma'} \left[\frac{1}{\hbar} \varepsilon_{\mathbf{p}'} - \frac{J}{2\hbar} z_{\sigma'} \langle S^z \rangle \right] \left| S_{\mathbf{q}+\mathbf{k}}^{-\sigma} [\hat{n}_{\mathbf{p}'\sigma'}, c_{\mathbf{p},\mp\sigma}^\dagger c_{\mathbf{p}-\mathbf{q},\mp\sigma}]_- \right\rangle \\
 &= \left[\frac{1}{\hbar} \varepsilon_{\mathbf{p}} \pm \frac{J}{2\hbar} z_{\sigma} \langle S^z \rangle \right] \left| S_{\mathbf{q}+\mathbf{k}}^{-\sigma} c_{\mathbf{p},\mp\sigma}^\dagger c_{\mathbf{p}-\mathbf{q},\mp\sigma} \right\rangle - \left[\frac{1}{\hbar} \varepsilon_{\mathbf{p}-\mathbf{q}} \pm \frac{J}{2\hbar} z_{\sigma} \langle S^z \rangle \right] \left| S_{\mathbf{q}+\mathbf{k}}^{-\sigma} c_{\mathbf{p},\mp\sigma}^\dagger c_{\mathbf{p}-\mathbf{q},\mp\sigma} \right\rangle \\
 &= \frac{1}{\hbar} (\varepsilon_{\mathbf{p}} - \varepsilon_{\mathbf{p}-\mathbf{q}}) |B_{2/3 \mathbf{kqp}\sigma}) \tag{F.4}
 \end{aligned}$$

$$\begin{aligned}
 \mathcal{L}_{\text{MF}} |B_{4\mathbf{kqp}\sigma}) &= \sum_{\mathbf{p}'} \sum_{\sigma'} \left[\frac{1}{\hbar} \varepsilon_{\mathbf{p}'} - \frac{J}{2\hbar} z_{\sigma'} \langle S^z \rangle \right] \left| S_{\mathbf{q}+\mathbf{k}}^z [\hat{n}_{\mathbf{p}'\sigma'}, c_{\mathbf{p},-\sigma}^\dagger c_{\mathbf{p}-\mathbf{q},\sigma}]_- \right\rangle \\
 &= \left[\frac{1}{\hbar} \varepsilon_{\mathbf{p}} + \frac{J}{2\hbar} z_{\sigma} \langle S^z \rangle \right] \left| S_{\mathbf{q}+\mathbf{k}}^z c_{\mathbf{p},-\sigma}^\dagger c_{\mathbf{p}-\mathbf{q},\sigma} \right\rangle - \left[\frac{1}{\hbar} \varepsilon_{\mathbf{p}-\mathbf{q}} - \frac{J}{2\hbar} z_{\sigma} \langle S^z \rangle \right] \left| S_{\mathbf{q}+\mathbf{k}}^z c_{\mathbf{p},-\sigma}^\dagger c_{\mathbf{p}-\mathbf{q},\sigma} \right\rangle \\
 &= \frac{1}{\hbar} (\varepsilon_{\mathbf{p}} - \varepsilon_{\mathbf{p}-\mathbf{q}} + J z_{\sigma} \langle S^z \rangle) |B_{4\mathbf{kqp}\sigma}) \tag{F.5}
 \end{aligned}$$

Based on these prerequisite the geometric series can be handled. The following set of operators has to be evaluated:

$$\begin{aligned}
 \mathcal{Q}\mathcal{L} |S_{\mathbf{k}}^{-\sigma}) &= \frac{-J}{2N} \sum_{\mathbf{qp}} \left\{ [|B_{2\mathbf{kqp}\sigma}) - |B_{3\mathbf{kqp}\sigma}) - V_{\mathbf{qp}\sigma}^{(23)} |B_{1\mathbf{k}\sigma})] \right. \\
 &\quad \left. + 2z_{\sigma} [|B_{4\mathbf{kqp}\sigma}) - V_{\mathbf{qp}\sigma}^{(4)} |B_{1\mathbf{k}\sigma})] \right\} \\
 \mathcal{L}_{\text{MF}} \mathcal{Q}\mathcal{L} |S_{\mathbf{k}}^{-\sigma}) &= \frac{-J}{2\hbar N} \sum_{\mathbf{qp}} \left\{ (\varepsilon_{\mathbf{p}} - \varepsilon_{\mathbf{p}-\mathbf{q}}) [|B_{2\mathbf{kqp}\sigma}) - |B_{3\mathbf{kqp}\sigma})] \right. \\
 &\quad \left. + 2z_{\sigma} (\varepsilon_{\mathbf{p}} - \varepsilon_{\mathbf{p}-\mathbf{q}} + J z_{\sigma} \langle S^z \rangle) |B_{4\mathbf{kqp}\sigma}) \right\} \\
 \mathcal{Q}\mathcal{L}_{\text{MF}} \mathcal{Q}\mathcal{L} |S_{\mathbf{k}}^{-\sigma}) &= \frac{-J}{2\hbar N} \sum_{\mathbf{qp}} \left\{ (\varepsilon_{\mathbf{p}} - \varepsilon_{\mathbf{p}-\mathbf{q}}) [|B_{2\mathbf{kqp}\sigma}) - |B_{3\mathbf{kqp}\sigma}) - V_{\mathbf{qp}\sigma}^{(23)} |B_{1\mathbf{k}\sigma})] \right. \\
 &\quad \left. + 2z_{\sigma} (\varepsilon_{\mathbf{p}} - \varepsilon_{\mathbf{p}-\mathbf{q}} + J z_{\sigma} \langle S^z \rangle) [|B_{4\mathbf{kqp}\sigma}) - V_{\mathbf{qp}\sigma}^{(4)} |B_{1\mathbf{k}\sigma})] \right\} \\
 (\mathcal{Q}\mathcal{L}_{\text{MF}} \mathcal{Q})^m \mathcal{Q}\mathcal{L} |S_{\mathbf{k}}^{-\sigma}) &= \frac{-J}{2\hbar^m N} \sum_{\mathbf{qp}} \left\{ (\varepsilon_{\mathbf{p}} - \varepsilon_{\mathbf{p}-\mathbf{q}})^m [|B_{2\mathbf{kqp}\sigma}) - |B_{3\mathbf{kqp}\sigma}) - V_{\mathbf{qp}\sigma}^{(23)} |B_{1\mathbf{k}\sigma})] \right. \\
 &\quad \left. + 2z_{\sigma} (\varepsilon_{\mathbf{p}} - \varepsilon_{\mathbf{p}-\mathbf{q}} + J z_{\sigma} \langle S^z \rangle)^m [|B_{4\mathbf{kqp}\sigma}) - V_{\mathbf{qp}\sigma}^{(4)} |B_{1\mathbf{k}\sigma})] \right\}
 \end{aligned}$$

Hence, the explicit result for the memory matrix for the magnon Green's function can be

given:

$$\begin{aligned}
M_{\mathbf{k}\sigma}(\omega) &= (S_{\mathbf{k}}^{-\sigma} | \mathcal{L}Q \frac{1}{\omega - Q\mathcal{L}_0Q} Q\mathcal{L} | S_{\mathbf{k}}^{-\sigma}) = \sum_{m=0}^{\infty} \frac{1}{\omega^{m+1}} (S_{\mathbf{k}}^{-\sigma} | \mathcal{L}Q (Q\mathcal{L}_0Q)^m Q\mathcal{L} | S_{\mathbf{k}}^{-\sigma}) \\
&= \frac{J^2}{4N^2} \sum_{\mathbf{q}'\mathbf{p}'\mathbf{q}\mathbf{p}} \left\{ \begin{aligned} & \frac{[(B_{2\mathbf{k}\mathbf{q}'\mathbf{p}'\sigma} - B_{3\mathbf{k}\mathbf{q}'\mathbf{p}'\sigma}) + 2z_{\sigma}(B_{4\mathbf{k}\mathbf{q}'\mathbf{p}'\sigma})][|B_{2\mathbf{k}\mathbf{q}\mathbf{p}\sigma} - B_{3\mathbf{k}\mathbf{q}\mathbf{p}\sigma}) - V_{\mathbf{q}\mathbf{p}\sigma}^{(23)}|B_{1\mathbf{k}\sigma})|]}{\omega - \frac{1}{\hbar}(\varepsilon_{\mathbf{p}} - \varepsilon_{\mathbf{p}-\mathbf{q}})} \\ & + 2z_{\sigma} \frac{[(B_{2\mathbf{k}\mathbf{q}'\mathbf{p}'\sigma} - B_{3\mathbf{k}\mathbf{q}'\mathbf{p}'\sigma}) + 2z_{\sigma}(B_{4\mathbf{k}\mathbf{q}'\mathbf{p}'\sigma})][|B_{4\mathbf{k}\mathbf{q}\mathbf{p}\sigma}) - V_{\mathbf{q}\mathbf{p}\sigma}^{(4)}|B_{1\mathbf{k}\sigma})|]}{\omega - \frac{1}{\hbar}(\varepsilon_{\mathbf{p}} - \varepsilon_{\mathbf{p}-\mathbf{q}} + Jz_{\sigma}\langle S^z \rangle)} \end{aligned} \right\} \quad (\text{F.6})
\end{aligned}$$

The result (F.6) is the exact J^2 contribution to the memory matrix of the magnon Green's function. However, it still includes a large number of correlation functions, which are a priori unknown. If these expectation values are evaluated with the full KLM Hamiltonian, they carry an additional J dependence. This yields contributions to the memory matrix, which are of higher order than J^2 . For our purpose it is sufficient to evaluate all expectation values with the eigenstates of the free electron Hamiltonian, since this retains the second order result. As a consequence, the moment and the z -component of the spin is already conserved for the fermionic degree of freedom. This yields the following simplifications:

$$V_{\mathbf{q}\mathbf{p}\sigma}^{(23)} \approx \frac{1}{\langle S_0^z \rangle} \langle S_{\mathbf{q}}^z (\hat{n}_{\mathbf{p},-\sigma} - \hat{n}_{\mathbf{p},\sigma}) \rangle \delta_{\mathbf{q},\mathbf{0}}, \quad V_{\mathbf{q}\mathbf{p}\sigma}^{(4)} \approx 0$$

$$\begin{aligned}
(B_{2\mathbf{k}\mathbf{q}'\mathbf{p}'} | B_{2\mathbf{k}\mathbf{q}\mathbf{p}}) &= \left\langle [S_{-\mathbf{q}'-\mathbf{k}}^{\sigma} c_{\mathbf{p}'-\mathbf{q}',-\sigma}^{\dagger} c_{\mathbf{p}',-\sigma}, S_{\mathbf{q}+\mathbf{k}}^{-\sigma} c_{\mathbf{p},-\sigma}^{\dagger} c_{\mathbf{p}-\mathbf{q},-\sigma}] - \right\rangle \\
&= 2z_{\sigma}\hbar \left\langle S_{\mathbf{q}-\mathbf{q}'}^z c_{\mathbf{p}'-\mathbf{q}',-\sigma}^{\dagger} c_{\mathbf{p}',-\sigma} c_{\mathbf{p},-\sigma}^{\dagger} c_{\mathbf{p}-\mathbf{q},-\sigma} \right\rangle \\
&\quad + \left\langle S_{\mathbf{q}+\mathbf{k}}^{-\sigma} S_{-\mathbf{q}'-\mathbf{k}}^{\sigma} c_{\mathbf{p}'-\mathbf{q}',-\sigma}^{\dagger} c_{\mathbf{p}-\mathbf{q},-\sigma} \right\rangle \delta_{\mathbf{p},\mathbf{p}'} - \left\langle S_{\mathbf{q}+\mathbf{k}}^{-\sigma} S_{-\mathbf{q}'-\mathbf{k}}^{\sigma} c_{\mathbf{p},-\sigma}^{\dagger} c_{\mathbf{p}',-\sigma} \right\rangle \delta_{\mathbf{p}'-\mathbf{q}',\mathbf{p}-\mathbf{q}} \\
&\approx 2z_{\sigma}\hbar \left\langle S_{\mathbf{q}-\mathbf{q}'}^z c_{\mathbf{p}'-\mathbf{q}',-\sigma}^{\dagger} c_{\mathbf{p}',-\sigma} c_{\mathbf{p},-\sigma}^{\dagger} c_{\mathbf{p}-\mathbf{q},-\sigma} \right\rangle (\delta_{\mathbf{p},\mathbf{p}'} \delta_{\mathbf{q},\mathbf{q}'} + \delta_{\mathbf{q},\mathbf{0}} \delta_{\mathbf{q}',\mathbf{0}}) \quad (*) \\
&\quad + \left\langle S_{\mathbf{q}+\mathbf{k}}^{-\sigma} S_{-\mathbf{q}'-\mathbf{k}}^{\sigma} c_{\mathbf{p}'-\mathbf{q}',-\sigma}^{\dagger} c_{\mathbf{p}-\mathbf{q},-\sigma} \right\rangle \delta_{\mathbf{p},\mathbf{p}'} \delta_{\mathbf{q},\mathbf{q}'} - \left\langle S_{\mathbf{q}+\mathbf{k}}^{-\sigma} S_{-\mathbf{q}'-\mathbf{k}}^{\sigma} c_{\mathbf{p},-\sigma}^{\dagger} c_{\mathbf{p}',-\sigma} \right\rangle \delta_{\mathbf{p},\mathbf{p}'} \delta_{\mathbf{q},\mathbf{q}'} \\
&= 2z_{\sigma}\hbar \left\{ \langle S_0^z \hat{n}_{\mathbf{p},-\sigma} \rangle \delta_{\mathbf{q},\mathbf{0}} + \langle S_0^z \hat{n}_{\mathbf{p}-\mathbf{q},-\sigma} \rangle - \langle S_0^z \hat{n}_{\mathbf{p},-\sigma} \hat{n}_{\mathbf{p}-\mathbf{q},-\sigma} \rangle \right\} \delta_{\mathbf{p},\mathbf{p}'} \delta_{\mathbf{q},\mathbf{q}'} \\
&\quad + 2z_{\sigma}\hbar \langle S_0^z \hat{n}_{\mathbf{p}',-\sigma} \hat{n}_{\mathbf{p},-\sigma} \rangle \delta_{\mathbf{q},\mathbf{0}} \delta_{\mathbf{q}',\mathbf{0}} \\
&\quad + \left\langle S_{\mathbf{q}+\mathbf{k}}^{-\sigma} S_{-\mathbf{q}-\mathbf{k}}^{\sigma} \hat{n}_{\mathbf{p}-\mathbf{q},-\sigma} \right\rangle \delta_{\mathbf{p},\mathbf{p}'} \delta_{\mathbf{q},\mathbf{q}'} - \left\langle S_{\mathbf{q}+\mathbf{k}}^{-\sigma} S_{-\mathbf{q}-\mathbf{k}}^{\sigma} \hat{n}_{\mathbf{p},-\sigma} \right\rangle \delta_{\mathbf{p},\mathbf{p}'} \delta_{\mathbf{q},\mathbf{q}'} \\
(B_{2\mathbf{k}\mathbf{q}'\mathbf{p}'} | B_{3\mathbf{k}\mathbf{q}\mathbf{p}}) &= \left\langle [S_{-\mathbf{q}'-\mathbf{k}}^{\sigma} c_{\mathbf{p}'-\mathbf{q}',-\sigma}^{\dagger} c_{\mathbf{p}',-\sigma}, S_{\mathbf{q}+\mathbf{k}}^{-\sigma} c_{\mathbf{p},\sigma}^{\dagger} c_{\mathbf{p}-\mathbf{q},\sigma}] - \right\rangle \\
&= 2z_{\sigma}\hbar \left\langle S_{\mathbf{q}-\mathbf{q}'}^z c_{\mathbf{p}'-\mathbf{q}',-\sigma}^{\dagger} c_{\mathbf{p}',-\sigma} c_{\mathbf{p},\sigma}^{\dagger} c_{\mathbf{p}-\mathbf{q},\sigma} \right\rangle \\
&\approx 2z_{\sigma}\hbar \langle S_0^z \hat{n}_{\mathbf{p}',-\sigma} \hat{n}_{\mathbf{p},\sigma} \rangle \delta_{\mathbf{q},\mathbf{0}} \delta_{\mathbf{q}',\mathbf{0}}
\end{aligned}$$

$$\begin{aligned}
 (B_{2\mathbf{k}\mathbf{q}'\mathbf{p}'} | B_{4\mathbf{k}\mathbf{q}\mathbf{p}}) &= \left\langle [S_{-\mathbf{q}'-\mathbf{k}}^\sigma c_{\mathbf{p}'-\mathbf{q}',-\sigma}^\dagger c_{\mathbf{p}',-\sigma}, S_{\mathbf{q}+\mathbf{k}}^z c_{\mathbf{p},-\sigma}^\dagger c_{\mathbf{p}-\mathbf{q},\sigma}]_- \right\rangle \\
 &= -z_\sigma \hbar \left\langle S_{\mathbf{q}-\mathbf{q}'}^\sigma c_{\mathbf{p}'-\mathbf{q}',-\sigma}^\dagger c_{\mathbf{p}',-\sigma} c_{\mathbf{p}-\mathbf{q},\sigma}^\dagger \right\rangle + \left\langle S_{\mathbf{q}+\mathbf{k}}^z S_{-\mathbf{q}'-\mathbf{k}}^\sigma c_{\mathbf{p}'-\mathbf{q}',-\sigma}^\dagger c_{\mathbf{p}-\mathbf{q},\sigma} \right\rangle \delta_{\mathbf{p},\mathbf{p}'} \\
 &\approx 0 \\
 (B_{3\mathbf{k}\mathbf{q}'\mathbf{p}'} | B_{3\mathbf{k}\mathbf{q}\mathbf{p}}) &= \left\langle [S_{-\mathbf{q}'-\mathbf{k}}^\sigma c_{\mathbf{p}'-\mathbf{q}',\sigma}^\dagger c_{\mathbf{p}',\sigma}, S_{\mathbf{q}+\mathbf{k}}^{-\sigma} c_{\mathbf{p},\sigma}^\dagger c_{\mathbf{p}-\mathbf{q},\sigma}]_- \right\rangle \\
 &= 2z_\sigma \hbar \left\{ \langle S_0^z \hat{n}_{\mathbf{p},\sigma} \rangle \delta_{\mathbf{q},\mathbf{0}} + \langle S_0^z \hat{n}_{\mathbf{p}-\mathbf{q},\sigma} \rangle - \langle S_0^z \hat{n}_{\mathbf{p},\sigma} \hat{n}_{\mathbf{p}-\mathbf{q},\sigma} \rangle \right\} \delta_{\mathbf{p},\mathbf{p}'} \delta_{\mathbf{q},\mathbf{q}'} \\
 &\quad + 2z_\sigma \hbar \langle S_0^z \hat{n}_{\mathbf{p}',\sigma} \hat{n}_{\mathbf{p},\sigma} \rangle \delta_{\mathbf{q},\mathbf{0}} \delta_{\mathbf{q}',\mathbf{0}} \\
 &\quad + \langle S_{\mathbf{q}+\mathbf{k}}^{-\sigma} S_{-\mathbf{q}-\mathbf{k}}^\sigma \hat{n}_{\mathbf{p}-\mathbf{q},\sigma} \rangle \delta_{\mathbf{p},\mathbf{p}'} \delta_{\mathbf{q},\mathbf{q}'} - \langle S_{\mathbf{q}+\mathbf{k}}^{-\sigma} S_{-\mathbf{q}-\mathbf{k}}^\sigma \hat{n}_{\mathbf{p},\sigma} \rangle \delta_{\mathbf{p},\mathbf{p}'} \delta_{\mathbf{q},\mathbf{q}'} \\
 (B_{3\mathbf{k}\mathbf{q}'\mathbf{p}'} | B_{4\mathbf{k}\mathbf{q}\mathbf{p}}) &= \left\langle [S_{-\mathbf{q}'-\mathbf{k}}^\sigma c_{\mathbf{p}'-\mathbf{q}',\sigma}^\dagger c_{\mathbf{p}',\sigma}, S_{\mathbf{q}+\mathbf{k}}^z c_{\mathbf{p},-\sigma}^\dagger c_{\mathbf{p}-\mathbf{q},\sigma}]_- \right\rangle \\
 &= -z_\sigma \hbar \left\langle S_{\mathbf{q}-\mathbf{q}'}^\sigma c_{\mathbf{p}'-\mathbf{q}',\sigma}^\dagger c_{\mathbf{p}',\sigma} c_{\mathbf{p}-\mathbf{q},\sigma}^\dagger \right\rangle - \left\langle S_{\mathbf{q}+\mathbf{k}}^{-\sigma} S_{-\mathbf{q}'-\mathbf{k}}^\sigma c_{\mathbf{p},-\sigma}^\dagger c_{\mathbf{p}',\sigma} \right\rangle \delta_{\mathbf{p}'-\mathbf{q}',\mathbf{p}-\mathbf{q}} \\
 &\approx 0 \\
 (B_{4\mathbf{k}\mathbf{q}'\mathbf{p}'} | B_{4\mathbf{k}\mathbf{q}\mathbf{p}}) &= \left\langle [S_{-\mathbf{q}'-\mathbf{k}}^z c_{\mathbf{q}'-\mathbf{p}',\sigma}^\dagger c_{-\mathbf{p}',-\sigma}, S_{\mathbf{q}+\mathbf{k}}^z c_{\mathbf{p},-\sigma}^\dagger c_{\mathbf{p}-\mathbf{q},\sigma}]_- \right\rangle \\
 &= \left\langle S_{\mathbf{q}+\mathbf{k}}^z S_{-\mathbf{q}'-\mathbf{k}}^z c_{\mathbf{p}'-\mathbf{q}',\sigma}^\dagger c_{\mathbf{p}-\mathbf{q},\sigma} \right\rangle \delta_{\mathbf{p},\mathbf{p}'} - \left\langle S_{\mathbf{q}+\mathbf{k}}^z S_{-\mathbf{q}'-\mathbf{k}}^z c_{\mathbf{p},-\sigma}^\dagger c_{\mathbf{p}',-\sigma} \right\rangle \delta_{\mathbf{p}'-\mathbf{q}',\mathbf{p}-\mathbf{q}} \\
 &\approx \left\langle S_{\mathbf{q}+\mathbf{k}}^z S_{-\mathbf{q}-\mathbf{k}}^z \hat{n}_{\mathbf{p}-\mathbf{q},\sigma} \right\rangle \delta_{\mathbf{p},\mathbf{p}'} \delta_{\mathbf{q},\mathbf{q}'} - \left\langle S_{\mathbf{q}+\mathbf{k}}^z S_{-\mathbf{q}-\mathbf{k}}^z \hat{n}_{\mathbf{p},-\sigma} \right\rangle \delta_{\mathbf{p},\mathbf{p}'} \delta_{\mathbf{q},\mathbf{q}'}
 \end{aligned}$$

The notation in the line marked (*) is understood in the following sense: When summed over the quadruple of wavevectors there are two scenarios when the correlation function does not vanish - either $\mathbf{p} = \mathbf{p}'$, $\mathbf{q} = \mathbf{q}'$ or $\mathbf{q} = \mathbf{q}' = \mathbf{0}$. It is our convention, that the intersection of these two conditions is treated as part of the second term. It should not be counted twice.

Then the memory matrix (F.6) becomes:

$$\begin{aligned}
 M_{\mathbf{k}\sigma}(\omega) &\approx \frac{J^2}{4N^2} \sum_{\mathbf{q}\mathbf{p}} \frac{1}{\omega - \frac{1}{\hbar}(\varepsilon_{\mathbf{p}} - \varepsilon_{\mathbf{p}-\mathbf{q}})} \left\{ \langle S_{\mathbf{q}+\mathbf{k}}^{-\sigma} S_{-\mathbf{q}-\mathbf{k}}^\sigma \hat{n}_{\mathbf{p}-\mathbf{q},-\sigma} \rangle - \langle S_{\mathbf{q}+\mathbf{k}}^{-\sigma} S_{-\mathbf{q}-\mathbf{k}}^\sigma \hat{n}_{\mathbf{p},-\sigma} \rangle \right. \\
 &\quad \left. + \langle S_{\mathbf{q}+\mathbf{k}}^{-\sigma} S_{-\mathbf{q}-\mathbf{k}}^\sigma \hat{n}_{\mathbf{p}-\mathbf{q},\sigma} \rangle - \langle S_{\mathbf{q}+\mathbf{k}}^{-\sigma} S_{-\mathbf{q}-\mathbf{k}}^\sigma \hat{n}_{\mathbf{p},\sigma} \rangle \right. \\
 &\quad \left. + 2z_\sigma \hbar \left[\langle S_0^z \hat{n}_{\mathbf{p}-\mathbf{q},-\sigma} \rangle + \langle S_0^z \hat{n}_{\mathbf{p}-\mathbf{q},\sigma} \rangle - \langle S_0^z \hat{n}_{\mathbf{p},-\sigma} \hat{n}_{\mathbf{p}-\mathbf{q},-\sigma} \rangle - \langle S_0^z \hat{n}_{\mathbf{p},\sigma} \hat{n}_{\mathbf{p}-\mathbf{q},\sigma} \rangle \right] \right\} \\
 &+ \frac{J^2}{4N^2} \sum_{\mathbf{p}'\mathbf{p}} \frac{2z_\sigma \hbar}{\omega} \left\{ \langle S_0^z \hat{n}_{\mathbf{p}',-\sigma} \hat{n}_{\mathbf{p},-\sigma} \rangle - \langle S_0^z \hat{n}_{\mathbf{p}',-\sigma} \hat{n}_{\mathbf{p},\sigma} \rangle - \langle S_0^z \hat{n}_{\mathbf{p},-\sigma} \hat{n}_{\mathbf{p}',\sigma} \rangle + \langle S_0^z \hat{n}_{\mathbf{p},\sigma} \hat{n}_{\mathbf{p}',\sigma} \rangle \right. \\
 &\quad \left. - \frac{1}{\langle S_0^z \rangle} \langle S_0^z (\hat{n}_{\mathbf{p},-\sigma} - \hat{n}_{\mathbf{p},\sigma}) \rangle \langle S_0^z (\hat{n}_{\mathbf{p}',-\sigma} - \hat{n}_{\mathbf{p}',\sigma}) \rangle \right\} \\
 &\quad + \frac{J^2}{N^2} \sum_{\mathbf{q}\mathbf{p}} \frac{\langle S_{\mathbf{q}+\mathbf{k}}^z S_{-\mathbf{q}-\mathbf{k}}^z \hat{n}_{\mathbf{p}-\mathbf{q},\sigma} \rangle - \langle S_{\mathbf{q}+\mathbf{k}}^z S_{-\mathbf{q}-\mathbf{k}}^z \hat{n}_{\mathbf{p},-\sigma} \rangle}{\omega - \frac{1}{\hbar}(\varepsilon_{\mathbf{p}} - \varepsilon_{\mathbf{p}-\mathbf{q}} + Jz_\sigma \langle S^z \rangle)}
 \end{aligned}$$

This is the result (5.13) for the memory matrix, which has been provided in a more compact notation on page 84.

Appendix G

The POM with a two-dimensional basis

The Green's function

In general, the basic relation of the POM (3.26) is a matrix equation. If the relevant Liouville subspace is spanned by two basis elements $|A\rangle$ and $|B\rangle$, these matrices are of dimension 2×2 . Neglecting the contribution of the memory matrix one has to evaluate

$$\begin{aligned} & \begin{pmatrix} (A|A) & (A|B) \\ (B|A) & (B|B) \end{pmatrix} \\ &= \left\{ \begin{pmatrix} \omega & 0 \\ 0 & \omega \end{pmatrix} - \begin{pmatrix} (A|\mathcal{L}|A) & (A|\mathcal{L}|B) \\ (B|\mathcal{L}|A) & (B|\mathcal{L}|B) \end{pmatrix} \cdot \begin{pmatrix} (A|A) & (A|B) \\ (B|A) & (B|B) \end{pmatrix}^{-1} \right\} \begin{pmatrix} G_{AA} & G_{AB} \\ G_{BA} & G_{BB} \end{pmatrix} \end{aligned} \quad (\text{G.1})$$

In the context of the zero-bandwidth limit (Sec. 4.2) we have already elaborated that a diagonal susceptibility matrix, i.e. $(A|B) = 0 = (B|A)$, is desirable. This is no additional loss of generality, due to the applicability of the Gram-Schmidt orthogonalization procedure. As a consequence, the matrix multiplication in (G.1) simplifies to:

$$\begin{pmatrix} (A|A) & 0 \\ 0 & (B|B) \end{pmatrix} = \begin{pmatrix} \omega - (A|\mathcal{L}|A)(A|A)^{-1} & -(A|\mathcal{L}|B)(B|B)^{-1} \\ -(B|\mathcal{L}|A)(A|A)^{-1} & \omega - (B|\mathcal{L}|B)(B|B)^{-1} \end{pmatrix} \begin{pmatrix} G_{AA} & G_{AB} \\ G_{BA} & G_{BB} \end{pmatrix} \quad (\text{G.2})$$

In order to determine the Green's functions, another matrix inversion is necessary:

$$\begin{aligned} & \begin{pmatrix} G_{AA} & G_{AB} \\ G_{BA} & G_{BB} \end{pmatrix} \\ &= \frac{1}{D} \begin{pmatrix} \omega - (B|\mathcal{L}|B)(B|B)^{-1} & (A|\mathcal{L}|B)(B|B)^{-1} \\ (B|\mathcal{L}|A)(A|A)^{-1} & \omega - (A|\mathcal{L}|A)(A|A)^{-1} \end{pmatrix} \begin{pmatrix} (A|A) & 0 \\ 0 & (B|B) \end{pmatrix} \end{aligned} \quad (\text{G.3})$$

$$= \frac{1}{D} \begin{pmatrix} [\omega - (B|\mathcal{L}|B)(B|B)^{-1}](A|A) & (A|\mathcal{L}|B) \\ (B|\mathcal{L}|A) & [\omega - (A|\mathcal{L}|A)(A|A)^{-1}](B|B) \end{pmatrix} \quad (\text{G.4})$$

Here, the determinant D is given by:

$$D = \left(\omega - \frac{(A|\mathcal{L}|A)}{(A|A)} \right) \left(\omega - \frac{(B|\mathcal{L}|B)}{(B|B)} \right) - \frac{(A|\mathcal{L}|B)(B|\mathcal{L}|A)}{(A|A)(B|B)} \equiv (\omega - \omega_{\text{I}})(\omega - \omega_{\text{II}}) \quad (\text{G.5})$$

$$\omega_{\text{I, II}} = \frac{1}{2} \left\{ \frac{(A|\mathcal{L}|A)}{(A|A)} + \frac{(B|\mathcal{L}|B)}{(B|B)} \right\} \pm \frac{1}{2} W \quad (\text{G.6})$$

$$W = \sqrt{\left\{ \frac{(A|\mathcal{L}|A)}{(A|A)} + \frac{(B|\mathcal{L}|B)}{(B|B)} \right\}^2 + 4 \frac{(A|\mathcal{L}|B)(B|\mathcal{L}|A) - (A|\mathcal{L}|A)(B|\mathcal{L}|B)}{(A|A)(B|B)}} \quad (\text{G.7})$$

An expansion into partial fractions eventually yields:

$$G_{AA} = -\frac{(A|A)}{W} \left(\frac{(B|\mathcal{L}|B)(B|B)^{-1} - \omega_{\text{I}}}{\omega - \omega_{\text{I}}} - \frac{(B|\mathcal{L}|B)(B|B)^{-1} - \omega_{\text{II}}}{\omega - \omega_{\text{II}}} \right) \quad (\text{G.8})$$

$$G_{AB} = \frac{(A|\mathcal{L}|B)}{W} \left(\frac{1}{\omega - \omega_{\text{I}}} - \frac{1}{\omega - \omega_{\text{II}}} \right) \quad (\text{G.9})$$

$$G_{BA} = \frac{(B|\mathcal{L}|A)}{W} \left(\frac{1}{\omega - \omega_{\text{I}}} - \frac{1}{\omega - \omega_{\text{II}}} \right) \quad (\text{G.10})$$

$$G_{BB} = -\frac{(B|B)}{W} \left(\frac{(A|\mathcal{L}|A)(A|A)^{-1} - \omega_{\text{I}}}{\omega - \omega_{\text{I}}} - \frac{(A|\mathcal{L}|A)(A|A)^{-1} - \omega_{\text{II}}}{\omega - \omega_{\text{II}}} \right) \quad (\text{G.11})$$

Therefore, based on the susceptibility and the frequency matrices one has direct access to the energy poles and spectral weights of the Green's functions involved. Due to the neglect of the memory matrix, these entities are real.

The self-energy

We would like to evaluate the improvement of the result (G.8) as compared to the use of a one-dimensional Liouville subspace, spanned by $|A\rangle$. For this purpose we consider the diagonal self-energy Σ_{AA} , making use of the relation¹

$$G_{XY} = \frac{g_{\text{I}}}{\omega - \omega_{\text{I}}} + \frac{g_{\text{II}}}{\omega - \omega_{\text{II}}} = \frac{g_{\text{I}} + g_{\text{II}}}{\omega - \frac{1}{\hbar} \Sigma_{XY}} \Leftrightarrow \frac{1}{\hbar} \Sigma_{XY} = \frac{\omega(g_{\text{I}}g_{\text{I}} + \omega_{\text{II}}g_{\text{II}}) - (g_{\text{I}} + g_{\text{II}})\omega_{\text{I}}\omega_{\text{II}}}{\omega(g_{\text{I}} + g_{\text{II}}) - (\omega_{\text{I}}g_{\text{II}} + \omega_{\text{II}}g_{\text{I}})} \quad (\text{G.12})$$

One can readily check, that for G_{AA} the sum rule $g_{\text{I}} + g_{\text{II}} = (A|A)$ is fulfilled. Furthermore, we need the following relations for the energy poles (G.6)

$$\omega_{\text{I}} - \omega_{\text{II}} = W \quad (\text{G.13})$$

$$\omega_{\text{I}}^2 - \omega_{\text{II}}^2 = \left\{ \frac{(A|\mathcal{L}|A)}{(A|A)} + \frac{(B|\mathcal{L}|B)}{(B|B)} \right\} \cdot W \quad (\text{G.14})$$

$$\omega_{\text{I}}\omega_{\text{II}} = \frac{(A|\mathcal{L}|A)}{(A|A)} \cdot \frac{(B|\mathcal{L}|B)}{(B|B)} - \frac{(A|\mathcal{L}|B)(B|\mathcal{L}|A)}{(A|A)(B|B)} \quad (\text{G.15})$$

¹ For electrons the definition of the self-energy is modified such, that it includes the free Bloch energy $\varepsilon_{\mathbf{k}}$. Note, that the self-energy has the dimension of an energy in our notation.

Hence, the expression (G.12) for the self-energy gets for $X = Y = A$:

$$\frac{1}{\hbar}\Sigma_{AA} = \frac{\omega \frac{1}{W} (\omega_I^2 - \omega_{II}^2) - \omega \frac{(B|\mathcal{L}|B)}{(B|B)} - \omega_I \omega_{II}}{\omega - \frac{(B|\mathcal{L}|B)}{(B|B)}} \quad (\text{G.16})$$

$$= \left\{ (A|\mathcal{L}|A) + \frac{(A|\mathcal{L}|B)(B|\mathcal{L}|A)(B|B)^{-1}}{\omega - (B|\mathcal{L}|B)(B|B)^{-1}} \right\} (A|A)^{-1} \quad (\text{G.17})$$

Hence, the correction to the frequency matrix of the one-dimensional Liouville subspace has again the structure of a memory matrix. Apparently, the Σ_{AA} in (G.17) is identical to the total self-energy, if the Liouville space orthogonal to the subspace spanned by $|A\rangle$ and $|B\rangle$ is neglected:

$$\begin{aligned} \frac{1}{\hbar}\Sigma_{AA} &\stackrel{!}{=} \left\{ (A|\mathcal{L}|A) + (A|\mathcal{L}Q \frac{1}{\omega - Q\mathcal{L}Q} Q\mathcal{L}|A) \right\} (A|A)^{-1} \quad \Leftrightarrow \\ Q &\equiv \mathbf{1} - |A\rangle \frac{1}{(A|A)} \langle A| \stackrel{!}{=} |B\rangle \frac{1}{(B|B)} \langle B| \quad \Leftrightarrow \quad \mathbf{1} = |A\rangle \frac{1}{(A|A)} \langle A| + |B\rangle \frac{1}{(B|B)} \langle B| \end{aligned} \quad (\text{G.18})$$

Furthermore, the choice

$$|B\rangle \equiv Q\mathcal{L}|A\rangle = \left\{ \mathcal{L} - \frac{(A|\mathcal{L}|A)}{(A|A)} \right\} |A\rangle \quad (\text{G.19})$$

allows a second analogy: In this case the correction in (G.17) is the memory matrix M_{AA} as it is obtained in the next step of the POM if the higher order memory matrix is neglected:

$$M_{AA} = (A|\mathcal{L}Q \frac{1}{\omega - Q\mathcal{L}Q} Q\mathcal{L}|A) = (B| \frac{1}{\omega - Q\mathcal{L}Q} |B) \quad (\text{G.20})$$

$$= \frac{(B|B)}{\omega - (B|Q\mathcal{L}Q|B)(B|B)^{-1} - M_{BB}(B|B)^{-1}} \quad (\text{G.21})$$

$$\approx \frac{(B|B)}{\omega - (B|Q\mathcal{L}Q|B)(B|B)^{-1}} = \frac{(A|\mathcal{L}Q|B)(B|Q\mathcal{L}A)(B|B)^{-1}}{\omega - (B|\mathcal{L}|B)(B|B)^{-1}} \quad (\text{G.22})$$

Note, that $Q|B\rangle = |B\rangle$. This analogy is a consequence of the fact, that the result of the POM only depends on the level of description and not on the way this Liouville subspace is split within various steps. A similar observation has been mentioned in Sec. 4.1 and 4.2.

Abbreviations

Abbreviation	Explanation
DMFT	Dynamical mean-field theory
DMS	Diluted magnetic semiconductors
EOM	Equation of motion approach
HF	Hartree-Fock
IPT	Iterative perturbation theory
ISA	Interpolating self-energy approach
KLM	Kondo-lattice model
MCDA	Moment-conserving decoupling approach
MRAM	Magnetic random access memory
PAM	Periodic Anderson model
POM	Projection operator method
QDOS	Quasiparticle density of states
MPT	Modified perturbation theory
RKKY	Rudermann-Kittel-Kasuya-Yosida exchange interaction
RPA	Random-phase approximation
SDA	Spectral density approach
SOPT	Second order perturbation theory

Danksagung

*Die Faszination des Kondo-Gitter-Modells besteht für mich in der Reduktion des komplexen magnetischen Verhaltens vieler Materialien auf eine universelle Formel. Der Vorteil der Projektions-Operator-Methode ist die systematische Unterscheidung nach relevanten und irrelevanten Prozessen. Es wäre jedoch vollkommen unzureichend, wenn ich beim Rückblick auf die vergangenen 3-4 Jahre dieselben Prinzipien anwenden würde. Die Zeit meiner Promotion war geprägt von einer erfreulichen Vielfalt von Kontakten zu Menschen, die sich keinesfalls auf eine universelle Formel reduzieren lässt. Ich möchte hier die Gelegenheit nutzen, **allen** zu danken, die den Entstehungsprozess dieser Arbeit begleitet und direkt oder indirekt zu deren Vollendung beigetragen haben. Es ist mir zwar ein Bedürfnis, einige dieser Menschen gesondert zu nennen, doch ist diese Auswahl nicht im Sinne der Projektions-Operator-Methode zu verstehen.*

Zuallererst möchte ich Prof. Nolting nennen. Ich weiß es zu schätzen, eine Fragestellung anvertraut bekommen zu haben, die Prof. Nolting selbst über Jahre bewegt hat. Doch war Wolfgang Nolting für mich nicht einfach nur ein Betreuer. Vielmehr hatte ich immer das Gefühl, ein geachteter Kollege zu sein. Die zahlreichen gemeinsamen Aktivitäten werden mir in bester Erinnerung bleiben. Vor allem aber wird die wertvolle Erfahrung bleiben, in Prof. Nolting jemanden gehabt zu haben, der mir stets in freundschaftlicher Art mit wissenschaftlichen und menschlichen Ratschlägen zur Verfügung stand.

Am Entstehen dieser Arbeit war ebenfalls Carlos Santos maßgeblich beteiligt. Wie kein anderer hat er immer wieder das wissenschaftliche Gespräch gesucht und mir dadurch, aber auch durch seinen unerschöpflichen Vorrat an Wissen und Ideen sehr geholfen.

Auch die Diskussion mit den anderen Doktoranden, Diplomanden und Gästen des Lehrstuhls in den Freitagsrunden, Seminaren oder zwischendurch war immer erfreulich und konstruktiv. Stellvertretend seien hier vor allem Jochen Kienert, Wolf Müller, Stephan Schwieger, Anand Sharma und Peter Sinjukow genannt. Sie und viele andere haben das Leben und Arbeiten am Lehrstuhl Festkörpertheorie sehr angenehm gemacht.

Über das Leben am Lehrstuhl kann man natürlich nicht sprechen, ohne insbesondere Marion Götsch zu erwähnen. Die zahlreichen Gespräche über fröhliche und auch ernste Themen, haben dieser Zeit eine ganz besondere Note gegeben.

So analytisch diese Arbeit auch erscheinen mag, so habe ich doch die bei weitem meiste Zeit meiner Promotion vor dem Computer verbracht. Dass dies (meist) ohne technische Schwierigkeiten möglich war, verdanke ich Wolf Müller, Carlos Santos und Jochen Kienert.

Die Schwierigkeiten, einen solchen Text nicht in der Muttersprache zu schreiben, waren größer als erwartet. Außerordentlich dankbar bin ich daher Klaus Neumann für die aufwendigen Korrekturen und die, über das rein Sprachliche hinausgehenden Anmerkungen. Auch Carlos Santos, Blazej Grabowski und allen anderen, die Teile der Arbeit gelesen

und korrigiert haben, sei hiermit gedankt.

Während der Promotion habe ich die Förderung durch die Friedrich-Naumann-Stiftung genossen. Über die finanziellen Zuwendungen hinaus, empfand ich die Stipendiatenzeit als überaus bereichernd und anregend. Insbesondere möchte ich den Mitarbeiterinnen der Begabtenförderung Frau Wohleben und Frau Simon meinen Dank aussprechen.

Im gleichen Atemzug könnte ich hier die Tätigkeit von Jörg Röseler als Vertrauensdozenten der Friedrich-Naumann-Stiftung nennen. Doch die zahlreichen Gespräche mit Hinweisen und Ratschlägen waren natürlich weit mehr als das, und verdienen ein gesondertes Dankeschön.

Unbedingt erwähnt werden sollte an dieser Stelle auch Sebastian Dreßler. Seine Hilfsbereitschaft und Freundschaft habe ich nicht nur im Rahmen der Stiftung sehr schätzen gelernt.

Diese ganze Arbeit wäre nicht möglich gewesen ohne einen verlässlichen Rückhalt im Privaten. Mein Dank gilt daher meiner Lebensgefährtin Ramona, deren Liebe und Beistand mir unendlich geholfen haben. Last but definitely not least, möchte ich meinen Eltern Barbara und Giselher und meinen Geschwistern Uta und Konrad für ihre vielfältige Unterstützung und Anteilnahme danken.

Selbständigkeitserklärung

Hiermit erkläre ich, die Dissertation selbständig und nur unter Verwendung der angegebenen Hilfe und Hilfsmittel angefertigt zu haben.

Berlin, 13. Mai 2005